Report No. K-TRAN: KU-03-2
FINAL REPORT

I. CONTROLS ON ARCHITECTURE OF ARGENTINE LIMESTONE AND ASSOCIATED STRATA IN NORTHEASTERN KANSAS

II. A FIRST-CUT METHOD FOR EVALUATING LIMESTONE AGGREGATE DURABILITY USING SPECTRAL SCINTILLOMETRY

Julienne Ruth Emry
Robert H. Goldstein
The University of Kansas
Lawrence, Kansas

and

Evan K. Franseen
Kansas Geological Survey
Lawrence, Kansas

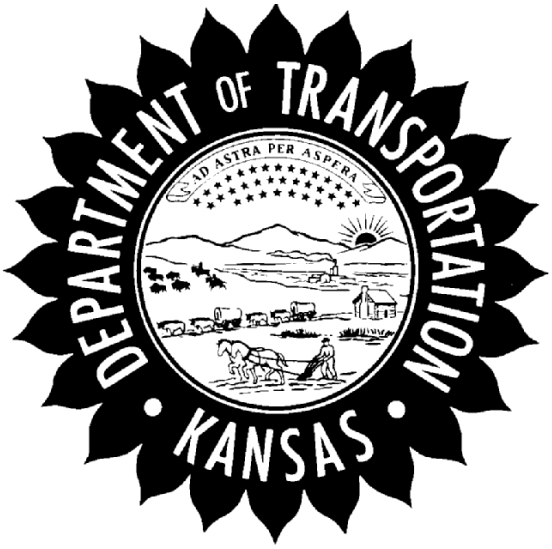

OCTOBER 2006

K-TRAN
A COOPERATIVE TRANSPORTATION RESEARCH PROGRAM BETWEEN:
KANSAS DEPARTMENT OF TRANSPORTATION
KANSAS STATE UNIVERSITY
THE UNIVERSITY OF KANSAS

1 Report No. K-TRAN: KU-03-2	**2 Government Accession No.**	**3 Recipient Catalog No.**
4 Title and Subtitle I. CONTROLS ON ARCHITECTURE OF ARGENTINE LIMESTONE AND ASSOCIATED STRATA IN NORTHEASTERN KANSAS and II. A FIRST-CUT METHOD FOR EVALUATING LIMESTONE AGGREGATE DURABILITY USING SPECTRAL SCINTILLOMETRY		**5 Report Date** October 2006 **6 Performing Organization Code**
7 Author(s) Julienne Ruth Emry, Robert H. Goldstein and Evan K. Franseen		**8 Performing Organization Report No.**
9 Performing Organization Name and Address Emry & Goldstein, both with University of Kansas Dept of Geology, 1475 Jayhawk Blvd 120 Lindley, Lawrence, Kansas 66045, and Franseen, with Kansas Geological Survey, University of Kansas, 1930 Constant Ave, Lawrence, Kansas 66045		**10 Work Unit No. (TRAIS)** **11 Contract or Grant No.** C1364
12 Sponsoring Agency Name and Address Kansas Department of Transportation Bureau of Materials and Research 700 SW Harrison Street Topeka, Kansas 66603-3754		**13 Type of Report and Period Covered** Final Report August 2002 – June 2006 **14 Sponsoring Agency Code** RE-0316-01
15 Supplementary Notes For more information write to address in block 9.		

16 Abstract

Missourian strata were studied in eastern Kansas to evaluate the build-and-fill controls on strata deposited in association with high-amplitude glacioeustatic sea-level fluctuations. Results from this study show that creation of relief in high-frequency glacioeustatic sequences can occur after falls in sea level, with deposition of lobate siliciclastics and erosion of preexisting strata. Intermediate sea-level positions after falls result in carbonate deposits that fill relief and even out topography.

In Kansas, many of these units are utilized for limestone aggregate. The Kansas Department of Transportation (KDOT) uses physical tests to determine aggregate durability. This project tests a first-cut method for evaluating aggregate durability using spectral gamma ray scintillometry. A logistic model using Kmax measurements provides the best prediction of durability. Implementation of the first-cut test uses lithologic determinations in the field and an Excel add-in that calculates the probability of an aggregate passing or failing the KDOT physical tests.

17 Key Words Aggregate, Geology, Limestone and Testing		**18 Distribution Statement** No restrictions. This document is available to the public through the National Technical Information Service, Springfield, Virginia 22161	
19 Security Classification (of this report) Unclassified	**20 Security Classification (of this page)** Unclassified	**21 No. of pages** 269	**22 Price**

Form DOT F 1700.7 (8-72)

Part I: CONTROLS ON ARCHITECTURE OF ARGENTINE LIMESTONE AND ASSOCIATED STRATA IN NORTHEASTERN KANSAS

Part II: A FIRST-CUT METHOD FOR EVALUATING LIMESTONE AGGREGATE DURABILITY USING SPECTRAL SCINTILLOMETRY

By:
Julienne Ruth Emry
Robert H. Goldstein
The University of Kansas
Lawrence, Kansas

and

Evan K. Franseen
Kansas Geological Survey
Lawrence, Kansas

A Report on Research Sponsored By

THE KANSAS DEPARTMENT OF TRANSPORTATION
TOPEKA, KANSAS

and

UNIVERSITY OF KANSAS CENTER FOR RESEARCH, INC.
LAWRENCE, KANSAS

October 2006

© Copyright 2006, **Kansas Department of Transportation**

PREFACE

The Kansas Department of Transportation's (KDOT) Kansas Transportation Research and New-Developments (K-TRAN) Research Program funded this research project. It is an ongoing, cooperative and comprehensive research program addressing transportation needs of the state of Kansas utilizing academic and research resources from KDOT, Kansas State University and the University of Kansas. Transportation professionals in KDOT and the universities jointly develop the projects included in the research program.

NOTICE

The authors and the state of Kansas do not endorse products or manufacturers. Trade and manufacturers names appear herein solely because they are considered essential to the object of this report.

This information is available in alternative accessible formats. To obtain an alternative format, contact the Office of Transportation Information, Kansas Department of Transportation, 700 SW Harrison, Topeka, Kansas 66603-3754 or phone (785) 296-3585 (Voice) (TDD).

DISCLAIMER

The contents of this report reflect the views of the authors who are responsible for the facts and accuracy of the data presented herein. The contents do not necessarily reflect the views or the policies of the state of Kansas. This report does not constitute a standard, specification or regulation.

EDITOR'S NOTE

The report references a Microsoft Excel spreadsheet. This spreadsheet is still beta testing and is not available with the distribution of this report.

ABSTRACT

Missourian strata were studied in eastern Kansas to evaluate the build-and-fill controls on strata deposited in association with high-amplitude glacioeustatic sea-level fluctuations. Results from this study show that creation of relief in high-frequency glacioeustatic sequences can occur after falls in sea level, with deposition of lobate siliciclastics and erosion of preexisting strata. Intermediate sea-level positions after falls result in carbonate deposits that fill relief and even out topography.

In Kansas, many of these units are utilized for limestone aggregate. The Kansas Department of Transportation (KDOT) uses physical tests to determine aggregate durability. This project tests a first-cut method for evaluating aggregate durability using spectral gamma ray scintillometry. A logistic model using Kmax measurements provides the best prediction of durability. Implementation of the first-cut test uses lithologic determinations in the field and an Excel add-in that calculates the probability of an aggregate passing or failing the KDOT physical tests.

EXECUTIVE SUMMARY

Part I. Controls on Architecture of Argentine Limestone and Associated Strata in Northeastern Kansas

Pennsylvanian strata in the US Midcontinent were deposited in association with high-amplitude glacio-eustatic sea-level fluctuations. Many such sequences are thin and maintain similar thickness throughout wide geographic areas. The facies both build and fill relief. Many of those that fill relief are commonly, but incorrectly ascribed to carbonate mounding. Missourian strata were studied in a 3,670 km^2 area of eastern Kansas to evaluate the controls on build-and-fill architecture.

Nine lithofacies were described in association with the Argentine Limestone, Frisbie Limestone, Quindaro Shale and Liberty Memorial Shale: (1)Phylloid Algal-Microbial Boundstone-Packstone (2) Skeletal Wackestone-Packstone, (3) Shale, Siltstone and Fine Sandstone (4) Lime Mudstone, Interbedded Mudstone and Calcareous Siltstone (5) Peloidal, Heliospongia Packstone (6) Encrusting Microbial Boundstone (7) Fossil Fragment Grainstone-Packstone (8) Shaley, Oncoid, Fusulinid Packstone (9) Microbial Mudstone-Wackestone. A sequence stratigraphic framework was established based upon lithofacies distributions and correlations in order to evaluate the controls on lithofacies distributions. Relative changes in sea level controlled the large-scale depositional architecture. Local factors such as accommodation and underlying paleotopography were the most important factors controlling which facies either built or filled depositional topography.

Lowermost strata are those of the Liberty Memorial Shale which created lobate positive topography. Shale facies changed laterally to phylloid algal and possible microbial carbonates, but no mound-like topography was built. A subsequent relative rise in sea level resulted in a

condensed section. Phylloid algal and other carbonate facies were deposited after a minor relative fall in sea level. Strata were deposited preferentially in low areas, onlapping preexisting topography. Although these lithologies are typically ascribed to carbonate buildups, geometries clearly filled topography, subduing most of the original paleotopography and resulting in a relatively flat surface. After a minor relative sea level fall, erosion created topography on the upper surface of the Argentine Limestone, which was previously misidentified as the result of mounding.

Results from this study show that the creation of relief in high-frequency glacioeustatic sequences can occur after falls in sea level, with deposition of lobate siliciclastics and erosion of preexisting strata. High or falling sea levels result in carbonate deposits which fill relief and even out topography. Understanding this mechanism of building and filling of relief is paramount to understanding the nature of deposits that are utilized as carbonate aggregate sources. Identifying lithologies that produce good aggregate and understanding how and where they form can help with quality control and aggregate resource exploration.

Part II. A First-Cut Method for Evaluating Limestone Aggregate Durability Using Spectral Scintillometry

There continues to be an increase in demand for durable carbonate aggregate resources for state and regional highway construction projects**.** The Kansas Department of Transportation has specific protocols for evaluating aggregate durability, but these tests take a minimum of six months to perform necessitating the development of faster, on-the-outcrop first-cut techniques to evaluate the potential durability of an aggregate resource.

This section evaluated the use of a spectral gamma ray scintillometer as a first-cut tool for evaluating limestone aggregate durability. Twenty ledges were sampled in nine stratigraphic

units with a spectral gamma-ray scintillometer. Five facies were described based only upon matrix lithology and clay distribution: (1) Matrix, disseminated clays and diffuse stylocumulates, (2) Matrix, disseminated clays (3) Matrix (4) Matrix, diffuse stylocumulates (5) Sparry calcite (disseminated clay-poor, diffuse stylocumulate-poor) (6) Shale/siltstone.

A previous K-TRAN study determined that the clay content and clay distribution in limestones, as disseminated clay and clay-rich seams, as well as clay minerology, appear to be important factors in the durability of limestone aggregate. Logistic models for determining the probability that an aggregate would pass or fail KDOT physical tests were developed for limestones with micritic matrices. These models were based on the relationship between the maximum measurement of the potassium contribution to the natural gamma radiation (Kmax) and the pass/fail status of a particular KDOT bed. The first model included all of the measurements for a particular KDOT bed. A second logistic model was developed because it is generally believed that shale beds and concentrated stylocumulate zones are removed from the final aggregate product by the crushing process. Therefore, the second model omitted measurements within 30 cm of shale beds and concentrated stylocumulate zones. The first model more accurately predicted the pass/fail status of the aggregate tested suggesting that such clay-rich zone are not removed during crushing.

The type of clays were determined by X-ray diffraction of the clay-sized fraction of acid insoluble residue to test for a correlation between clay mineralogy and whether an aggregate sample would pass or fail the KDOT physical tests. Results showed that the mineralogy of the clays present, and even the number of clays present did not directly correlate with whether an aggregate sample would pass or fail the KDOT physical tests. Instead, it was determined that the amount of clay present, independent of its mineralogy, may be a more important factor. A

handbook of instructions for implementation of the first cut test of aggregate durability is provided along with an Excel* add-in that will automatically calculate the probability of an aggregate passing or failing the KDOT physical tests.

*(*Please see Editor's Note on page i)*

ACKNOWLEDGEMENTS

This document is based on the Masters Thesis of Julienne Emry, completed at the University of Kansas, Department of Geology, under the direction of Robert Goldstein and Evan Franseen.

The authors would like to thank Jason Emry for a reoccurring role of field assistant, safety manager, and pack mule. Dr. Jen Roberts stepped in at a critical time with advice and, most importantly, her time. Funding for this project was provided by the Kansas Department of Transportation (KDOT). KDOT Bureau of Materials and Research's Robert Henthorne provided advice and logistical help. Also, thanks to Barb Smith for being the KDOT liaison and answering several procedural questions. Thanks to Dick Ryan for his field assistant roll, willingness to drive all the way from Chanute and support. Gary Lane helped in facilitating quarry access.

A special thanks goes out to Frank Rockers from Shawnee Rock Company. There are many who provided access to quarries in Kansas and Missouri. Don Maroney from Martin Marietta needs a special thank you for driving all over eastern Kansas and western Missouri to the MM quarries and helping in the field. Also, thanks to Ronny Bryant, J.R. Downs, Blane Foster, Jack Kagarice, James Nicholson, and Charley Reed from Martin Marietta. Thanks to Tom Degonia, Ron Stanley, and Joe Epperson from Ashgrove Aggregates. A special thanks to the Stanley's for repeated unfettered access to their quarry. Thank you to Dale Patton from APAC quarries. Thank you to Jody Crowley, Julia Ciero at the Hunt Midwest Crawford Quarry and Ramon Gonzales from Hamm Quarries.

We thank Rhonda Houser for help with GIS, John Kelly, for help with the statistics especially logistic regression, Doug Powell for help with the XRD machine, Mark Anderson for lab equipment and advice, and Gwen MacPherson for use of her lab equipment and advice on

prepping XRD samples. Thank you to Dr. Dick Berry at the University of Miami X-ray Diffraction Lab for advice and help interpreting the XRD data.

TABLE OF CONTENTS

ABSTRACT ..... **II**

EXECUTIVE SUMMARY ..... **III**

ACKNOWLEDGEMENTS ..... **VII**

TABLE OF CONTENTS ..... **IX**

LIST OF TABLES ..... **XI**

LIST OF FIGURES ..... **XII**

CHAPTER 1 ..... **1**

INTRODUCTION **1**

1.1 PURPOSE 1
1.2 ORGANIZATION 2

CHAPTER 2: **4**

PART I: CONTROLS ON ARCHITECTURE OF ARGENTINE LIMESTONE AND ASSOCIATED STRATA IN NORTHEASTERN KANSAS **4**

2.1 INTRODUCTION 4
2.2 MATERIALS AND METHODS 5
2.3 STRATIGRAPHY 6
2.4 LITHOFACIES AND DEPOSITIONAL ENVIRONMENTS 9
2.4.1 Phylloid Algal-Microbial Boundstone-Packstone Facies *9*
2.4.2 Skeletal Wackestone-Packstone Facies *14*
2.4.3 Shale, Siltstone and Fine Sandstone *15*
2.4.4 Lime Mudstone, Interbedded Mudstone and Calcareous Siltstone *16*
2.4.5 Phylloid Algal Fragment Packstone *19*
2.4.6 Peloidal, Heliospongia Packstone *20*
2.4.7 Encrusting Microbial Boundstone *21*
2.4.8 Fossil Fragment Grainstone-Packstone *25*
2.4.9 Shaley, Oncoid, Fusulinid Packstone *29*
2.4.10 Microbial Mudstone-Wackestone *29*
2.5 STRATIGRAPHY AND INTERPRETATIONS 31
2.5.1 Stratigraphic Interval A – Liberty Memorial Shale-Frisbie-Lower Argentine Interval *38*
2.5.2 Stratigraphic Interval B – Quindaro Shale *41*
2.5.3 Stratigraphic interval C—"Middle"Argentine Limestone Interval *44*
2.5.4 Stratigraphic Interval D—"Top of the Argentine" Interval *47*
2.6 DISCUSSION 52
2.7 CONCLUSIONS 57

CHAPTER 3 60

PART II: A FIRST-CUT METHOD FOR EVALUATING LIMESTONE AGGREGATE DURABILITY USING SPECTRAL SCINTILLOMETRY 60

3.1 INTRODUCTION 60
3.2 MATERIALS AND METHODS 63
3.2.1 KDOT Tests 68
3.3 RESULTS 69
3.4 DISCUSSION 128
3.4.1 Spectral Scintillometry 128
3.4.2 Clays 135
3.5 APPLICATION 137
3.6 FURTHER WORK 138
3.7 IMPLEMENTATION RECOMMENDATIONS 139
3.7.1 Step 1 139
3.7.2 Step 2 142
3.7.3 Step 3 143
3.7.4 Step 4 144
3.7.5 Step 5 145
3.7.6 Step 6 146
3.7.7 Step 7 149
3.7.8 Step 8 150
3.7.9 Step 9 150
3.7.10 Step 10 151

CHAPTER 4 152

CONCLUSIONS 152

4.1 CONTROLS ON ARCHITECTURE OF ARGENTINE LIMESTONE AND ASSOCIATED STRATA IN NORTHEASTERN KANSAS 152
4.2 A FIRST-CUT METHOD FOR EVALUATING LIMESTONE AGGREGATE DURABILITY USING SPECTRAL SCINTILLOMETRY 153

REFERENCES 156

APPENDIX 160

LIST OF TABLES

Table 2.1: Facies Attributes for the Lithofacies of the Argentine Limestone Described in this Study 11
Table 3.1: KDOT Quarry Code 4-061-08, Miami County, APAC "Reno" Quarry..... 74
Table 3.2: KDOT Quarry Code 4-054-11, Leavenworth County, Ashgrove Aggregates Lacygne Quarry 77
Table 3.3: KDOT Quarry Code 4-054-11, Leavenworth County, Ashgrove Aggregates Lacygne Quarry 79
Table 3.4: KDOT Quarry Code 1-044-01, Jefferson County, Hamm "North Lawrence" Quarry 81
Table 3.5: KDOT Quarry Code 4-061-05, Miami County, Hunt-Midwest "Crawford" Quarry .. 83
Table 3.6: KDOT Quarry Code 1-046-11, Johnson County, Hunt-Midwest "Sunflower" Quarry 84
Table 3.7: KDOT Quarry Code 1-046-11, Johnson County, Hunt-Midwest “Sunflower” Quarry 85
Table 3.8: KDOT Quarry Code 1-046-11, Johnson County, Hunt-Midwest "Sunflower" Quarry 86
Table 3.9: KDOT Quarry Code 1-046-07, Johnson County, Johnson County Aggregate/Ashgrove Aggregate "Olathe" Quarry..... 87
Table 3.10: KDOT Quarry Code 1-046-07, Johnson County, Johnson County Aggregate/Ashgrove Aggregate "Olathe" Quarry 88
Table 3.11: KDOT Quarry Code 1-046-07, Johnson County, Johnson County Aggregate/Ashgrove Aggregate "Olathe" Quarry 90
Table 3.12: KDOT Quarry Code 1-052-01, Leavenworth County, (Privately-Owned) Loring Quarry 91
Table 3.13: KDOT Quarry Code MO-021, Cass County, Martin Marietta Peculiar Quarry 94
Table 3.14: KDOT Quarry Code 1-089-05, Cass County, Martin Marietta Big Springs Quarry. 96
Table 3.15: KDOT Quarry Code 4-054-11, Leavenworth County, Martin Marietta Greenwood Quarry 97
Table 3.16: KDOT Quarry Code 4-054-11, Cass County, Martin Marietta Greenwood Quarry . 99
Table 3.17: KDOT Quarry Code 4-030-02 Franklin County, Martin Marietta Ottawa Quarry . 100
Table 3.18: KDOT Quarry Code 1-105-02 Wyandotte County, Shawnee Rock Company Bonner Springs Quarry..... 102
Table 3.19: KDOT Quarry Code 1-105-02 Wyandotte County, Shawnee Rock Company Shawnee (JCL-Meth) Quarry..... 103
Table 3.20: KDOT Quarry Code 1-046-13, Johnson County, Shawnee Rock Company "Lone Elm" Quarry..... 104
Table 3.21: KDOT Quarry Code 4-061-08, Miami County, APAC "Reno" Quarry, Upper Farley 105
Table 3.22: Results of X-Ray Diffraction Clay Mineral Analysis..... 127

LIST OF FIGURES

Figure 2.1: Index Map Showing Location and Type of Field Localities and Major Towns for Reference 5
Figure 2.2: Generalized Stratigraphic Section Showing the Relationships and Lithologies of the Liberty Memorial Shale, Frisbie Limestone Quindaro Shale and Argentine Limestone along with Underlying and Overlying Units..... 7
Figure 2.3: Polished Slab of the Phylloid Algal Microbial Packstone-Boundstone Facies..... 10
Figure 2.4: Photomicrograph of a Poorly Preserved Phylloid Algal Blade (PA) 13
Figure 2.5: Photomicrograph of Microbial Component of the Phylloid Algal Microbial Packstone-Boundstone 13
Figure 2.6: Slab Illustrating the Typical Appearance of the Skeletal Wackestone-Packstone Facies 15
Figure 2.7: Photograph of the Nature of the Shale, Siltstone and Fine Sandstone Facies in Outcrop 17
Figure 2.8: Slab Illustrating the Typical Appearance of the Lime Mudstone in the Lime Mudstone, Interbedded Mudstone and Calcareous Siltstone Facies..... 17
Figure 2.9: Slab Illustrating the Typical Appearance of the Siliciclastic Lithology in the Lime Mudstone, Interbedded Mudstone and Calcareous Siltstone Facies..... 18
Figure 2.10: Slab of Phylloid Algal Fragment Packstone Facies 20
Figure 2.11: Slab of the Peloidal *Heliospongia* Packstone..... 21
Figure 2.12: Slab Illustrating the Typical Appearance of the Encrusting Microbial Boundstone 23
Figure 2.13: Photomicrograph Showing the Clotted Appearance of Micrite in the Encrusting Microbial Boundstone Facies 24
Figure 2.14: Photomicrograph Showing the Typical Appearance of Dendritic or Arborescent Microbial Textures Common in the Encrusting Microbial Boundstone Facies 24
Figure 2.15: S. Slab of Subfacies A of the Fossil Fragment Grainstone-Packstone Facies 26
Figure 2.16: Photomicrograph of Subfacies A of the Fossil Fragment Grainstone-Packstone 26
Figure 2.17: Slab of Subfacies B of the Fossil Fragment Grainstone-Packstone 27
Figure 2.18: Photomicrograph of Subfacies B in the Fossil Fragment Grainstone-Packstone Facies 27
Figure 2.19: Slab of the Subfacies C of the Fossil Fragment Grainstone-Packstone Facies..... 28
Figure 2.20: Photomicrograph of Subfacies C in the Fossil Fragment Grainstone-Packstone Facies 28
Figure 2.21: Slab Illustrating the Typical Appearance of the Shaley, Oncoid, Fusulinid Packstone 30
Figure 2.22: Photomicrograph of Consortium of Encrusting Organisms Forming Oncoidal Coatings Commonly Found on Grains in the Shaley, Oncoid, Fusulinid Packstone 30
Figure 2.23: Photomicrograph of a Microbial-Like Microspar “Finger” from the Digitate Microbial Facies Illustrating the Micritic Encrustations Commonly Surrounding These Structures (E). 31
Figure 2.24: Reconstructed Cross-Section along Line AA-A. 33
Figure 2.25: Reconstructed Cross-Section along Line AA-B..... 34
Figure 2.26: Reconstructed Cross-Section Along Line AAA-C..... 35
Figure 2.27: Fence Diagram Viewed from the West Showing Stratigraphic Correlations in Three Dimensions 36

Figure 2.28: Reconstructed East-West Cross-Section from E to D in the Northern Part of Johnson County 37
Figure 2.29: Isopach Map of Stratigraphic Interval A 40
Figure 2.30: Outcrop Photo Showing a Lens Shaped Bed in the Frisbie at OBS that is Pinching Out within Siltstone Lithology Identical to the Liberty Memorial Shale at this Locality 41
Figure 2.31: Photograph Showing Location of Quindaro-Equivalent Surface at the OBS Locality Marked by the White Arrow 43
Figure 2.32: Reconstructed Stratigraphic Section of the Top of Stratigraphic Interval C and Stratigraphic Interval D from the SRS Locality within the Johnson County Landfill..... 50
Figure 3.1: Index Map Showing Quarry Locations in Kansas and Missouri..... 62
Figure 3.2: Photograph of Ledge at Shawnee Rock Company's Shawnee Quarry Showing Scintillometer Measuring Points at 0.3 cm (1 ft) Intervals 64
Figure 3.3: Hypothetical Illustration of Two Limestone Beds with Various Forms of Clay Distributed within Them 66
Figure 3.4: Polished Slab of the Matrix, Disseminated Clays and Diffuse Stylocumulates Facies 69
Figure 3.5: Polished Slab of the Matrix, Disseminated Clays Facies 70
Figure 3.6: Polished Slab of the Matrix Facies 70
Figure 3.7: Polished Slab of the Matrix and Diffuse Stylocumulates Facies 71
Figure 3.8: Cut Slab of the Shale Facies 71
Figure 3.9: Polished Slab of the Sparry Matrix Facies 72
Figure 3.10: Figure Legend for Each of the Measured Sections 106
Figure 3.11: Measured Section of the Captain Creek Limestone in Olathe, Kansas..... 107
Figure 3.12: Measured Section of the Ervine Creek Limestone in Big Springs, Kansas 108
Figure 3.13: Measured Section of the Bethany Falls Limestone in Greenwood, Missouri 109
Figure 3.14: Measured Section of the Bethany Falls Limestone in Greenwood, Missouri 110
Figure 3.15: Measured Section of the Bethany Falls Limestone in La Cygne, Kansas..... 111
Figure 3.16: Measured Section of the Argentine Limestone in DeSoto, Kansas 112
Figure 3.17: Measured Section of the Upper Farley Limestone in DeSoto, Kansas 113
Figure 3.18: Measured Section of the Argentine Limestone in Louisburg, Kansas 114
Figure 3.19: Measured Section of the Argentine Limestone in Louisburg, Kansas 115
Figure 3.20: Measured Section of the Spring Hill Limestone in Olathe, Kansas..... 116
Figure 3.21: Measured Section of the Bethany Falls Limestone in Peculiar, Missouri..... 117
Figure 3.22: Measured Section of the Winterset Limestone in Greenwood, Missouri..... 118
Figure 3.23: Measured Section of the Argentine Limestone in Loring, Kansas..... 119
Figure 3.24: Measured Section of the Argentine Limestone in Bonner Springs, Kansas 120
Figure 3.25: Measured Section of the Winterset Limestone in LaCygne, Kansas 121
Figure 3.26: Measured Section of the Plattsmouth Limestone in Lawrence, Kansas..... 122
Figure 3.27: Measured Section of the Stoner Limestone in Ottawa, Kansas 123
Figure 3.28: Measured Section of the Bethany Falls Limestone in Olathe, Kansas..... 124
Figure 3.29: Measured Section of the Upper Farley Limestone in Louisburg, Kansas..... 125
Figure 3.30: Measured Section of the Argentine Limestone in Lone Elm, Kansas..... 126
Figure 3.31: Graph of the Logistic Model of the Relationship between the Maximum Value for Potassium (K_{max}) and the Data from which it was Derived..... 130

Figure 3.32: Graph of the Logistic Model of the Relationship between the Maximum Value for Potassium (K_{max}) ,After Removing Points within 30 cm of a Shale/Stylolite Beds, and the Data from which it was Derived 133
Figure 3.33: Aggregate Pieces Consisting of Diffuse Stylocumulates Recovered from a Class 1 Stockpile Shown on the Left 134
Figure 3.34: Plot of Kmax versus Pass or Fail with Individual Stratigraphic Units Indicated by Different Colored Symbols 135
Figure 3.35: Graph Illustrating the Effect of Smectite on Whether a Bed will Pass or Fail the KDOT Physical Tests 136
Figure 3.36: Example of Non-Micritic Matrix Facies 140
Figure 3.37: Example of Non-Micritic Matrix Facies 141
Figure 3.38: Example of Non-Micritic Matrix Facies 142
Figure 3.39: Example of the Discoloration of Potential Limestone Aggregate Sources Due to the Presence of Iron Rich Carbonates 143
Figure 3.40: Quarry Face Being Powerwashed Using 2700 psi Gasoline-Powered Powerwasher Supplied with Water from a 50 gallon Pressurized Cement-Mixer Tank 144
Figure 3.41: Quarry Face Marked with Spray Paint for Successive Spectral Gamma Ray Scintillometer Readings Every 30 centimeters (11.8 inches) 145
Figure 3.42: Hold Detector as Flush against the Outcrop as Possible 146
Figure 3.43: Screen Shot of Excel during the First Step of Method 2 for Installing an Add-In. 147
Figure 3.44: Screen Shot of Excel during the Second Step of Method 2 for Installing an Add-In 148
Figure 3.45: Screen Shot of the Tools | Add-Ins Dialog Box after Installation is Complete 148
Figure 3.46: Screen Shot of Yellow Lightbulb Icon that Opens a New Workbook 149
Figure 3.47: Screen Shot of Method for Opening a New Data Workbook using the File Menu Option 149
Figure 3.48: Screen Shot of Workbook with an Example of Appropriately Entered Data 150
Figure 3.49: Screen Shot of the Results Sheet Produced after the Data have been Analyzed.... 151

Chapter 1

Introduction

1.1 Purpose

The demand for durable carbonate aggregate for state, county, and municipal projects is increasing in the United States. In Kansas, carbonate aggregate is an abundant resource that plays a significant role in the state's economy. The Kansas Department of Transportation has established a series of physical tests to determine aggregate durability, but the physical test procedure on aggregate requires 6 months to complete, and paving with non-Class 1 aggregate carries great expense. Moreover, as a ledge is quarried laterally, results from KDOT physical tests are known to vary without any obvious indication in change in rock type. In two recent instances, production samples failed the KDOT physical tests, indicating possible use of substandard aggregate for a substantial amount of time. In another, one section of highway was D-cracked whereas others were not, suggesting lateral variation of the aggregate which was not detected during production. As of the 1997 Pavement Management Survey about 10.5 miles of highway constructed since 1981 were identified as either possibly in the early stages of D-cracking or currently D-cracked. At a cost for repaving of $1 million/mile, prevention of such D-cracking could save well over $10 million on these projects alone.

Concerns about the use of limestone aggregate have led some Kansas municipalities to legislate the use of hard-rock aggregate from distant sources. These actions take money away from the local aggregate industry and the Kansas economy and increase costs for municipal infrastructure projects. The quality control issues, the high demand for aggregate, and the increased cost associated with using poor quality aggregate are all factors illustrating a growing need for effective first-cut techniques to evaluate aggregate durability.

There is an increasing trend in the aggregate industry toward utilizing geological studies as well as physical test parameters to evaluate carbonate aggregate durability and to better understand and predict the factors that affect aggregate quality. This project stems from a previous KTRAN research project (KU-97-1) that reported that a particular rock type, limestones with micritic matrices, tended to produce durable aggregate, and the clay content of the limestones was an important factor in aggregate durability.

The first phase of this project was to study a specific aggregate-producing unit in detail to better understand the controls on the deposition of the unit, to improve understanding of the factors that ultimately affect the distribution and quality of aggregate resources. The Argentine Limestone was chosen as a test case because it is a major aggregate-producing unit and is exposed in several quarries in eastern Kansas. In older literature, it was often referred to as the "crusher ledge" illustrating its status as a major source for limestone aggregate both then and now (Moore, 1935, Moore et al., 1936).

The second part of this project involved evaluating the validity of using a spectral gamma ray scintillometer as a first-cut tool to evaluate limestone aggregate durability. A successful methodology was established and instructions for implementation are included.

1.2 Organization

This report is divided into two stand-alone, yet related papers. The first paper, Chapter 2 discusses the factors that control the deposition of the Argentine Limestone in eastern Kansas. Topics discussed include stratigraphic descriptions and environmental interpretations of the facies of the Argentine Limestone and associated units. Some of the factors discussed include the amount of accommodation during deposition, facies relationships, and sea-level.

The second paper tests the applicability of a spectral gamma ray scintillometer as a first-cut technique for determining aggregate durability. It includes a logistic model for predicting aggregate quality based on the maximum value for the potassium contribution to the natural gamma radiation. It also illustrates several directions that further studies could take to allow for even better prediction of aggregate resources and to develop models for other rock types that are used as aggregate.

The final section, Chapter 4, presents the conclusions of the previous two chapters.

Chapter 2:

Part I: Controls on Architecture of Argentine Limestone and Associated Strata in Northeastern Kansas

2.1 Introduction

Pennsylvanian strata in the US Midcontinent were deposited in association with high-amplitude glacio-eustatic sea-level fluctuations (Heckel, 1972, McKirahan, 2003). Many of these sequences are thin and maintain similar thickness throughout wide geographic areas McKirahan, 2003). The thicknesses of sediment deposited are well below the amplitude of relative changes in sea-level which resulted in unfilled accommodation (Watney et al, 1989, Franseen and Goldstein, 2004). Facies found in these sequences both build and fill relief on a local scale, but result in low relief in overall sequence thickness. An explanation for these characteristics has been proposed and labeled build-and-fill sequence architecture, where certain sedimentary processes are responsible for building relief and other sedimentary processes are responsible for filling relief (McKirahan et al. 2003; Franseen and Goldstein, 2004). McKirahan et al. (2003) looked at controls of build-and-fill architecture in Farley Limestone (Missourian). One goal of this study is to continue to evaluate the controls on build-and-fill architecture in the Argentine Limestone in eastern Kansas, which lies stratigraphically just below the Farley Limestone. Argentine Limestone strata consist of deltaic siliciclastic, marine siliciclastic, and marine carbonate deposits.

The research completed in this study specifically evaluates the degree to which deltaic siliciclastics create positive relief and affect distribution of overlying carbonate strata. It also evaluates the effect of that topography on distribution and stratal geometries of phylloid algal

and microbial carbonates commonly interpreted as mounds. In particular, it evaluates the controls on whether such facies build relief on paleotopographic highs or fill relief in paleotopographic lows. Finally, it evaluates the effect of paleotopography on shallowing of facies and the creation of erosional topography in carbonate systems.

2.2 Materials and Methods

The field area for this study consists of approximately 3,670 square km in Johnson, Miami, Wyandotte, and Leavenworth counties in northeastern Kansas (Figure 2.1). Data consist of outcrops, quarry exposures, and drill cores and represent 24 sites within the study area.

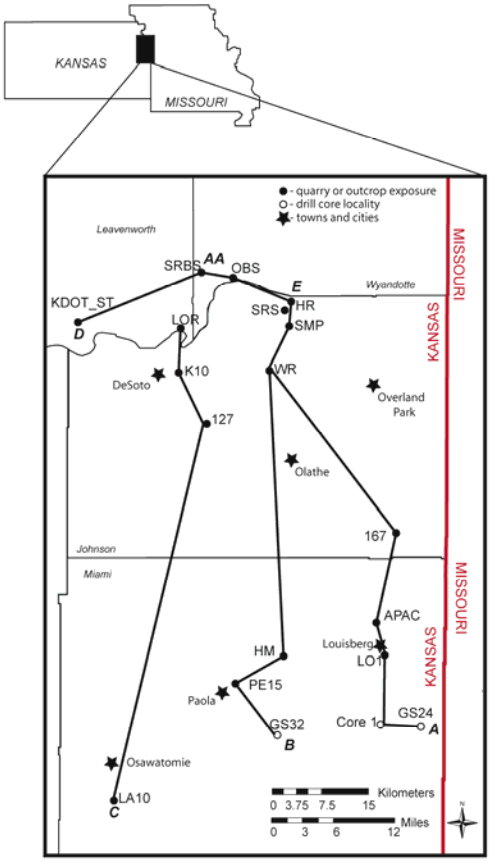

Figure 2.1: Index Map Showing Location and Type of Field Localities and Major Towns for Reference

(Reconstructed correlations are illustrated in Figures 2.24-2.28. Five sections were measured at the Shawnee Rock Company Shawnee Quarry "SRS".)

2.3 Stratigraphy

This paper employs revisions in the stratigraphic nomenclature by Arvidson (1990) and Watney and Heckel (1994) to the original stratigraphic nomenclature of Moore (1935). The Argentine Limestone was named by Newell in 1932, "after a particularly good outcrop near the town of Argentine, Kansas" and was included as the middle member of the Wyandotte Limestone Formation (Thompson, 2001). Reclassification of the overlying units established the Argentine Limestone as the uppermost and thickest limestone bed in the Wyandotte Limestone (Figure 1.2). The Liberty Memorial Shale underlies this succession. In the past the Liberty Memorial Shale has been frequently miscorrelated with the Lane Shale, which overlies the Argentine Limestone (Thompson, 1991, Arvidson, 1990.) This error came about through misidentification of the Argentine Limestone with what was likely the Lower Farley, placing it above the Lane Shale in Miami County. According to Arvidson (1990) Heckel rectified this error by reviving the name "Liberty Memorial Shale" for the shale unit that occurs below the Wyandotte Limestone. In the northern part of the study area, the Argentine Limestone is located above either the Quindaro Shale Member or, where the Quindaro Shale is absent, the Frisbie Limestone. In the southern portion of the study areas, the Frisbie Limestone and the Quindaro Shale may be absent, placing the Argentine Limestone directly on the Liberty Memorial Shale. In southwestern Miami county the Liberty Memorial Shale pinches out, and the Argentine Limestone directly overlies the Raytown Limestone Member of the Iola Formation (Arvidson, 1990).

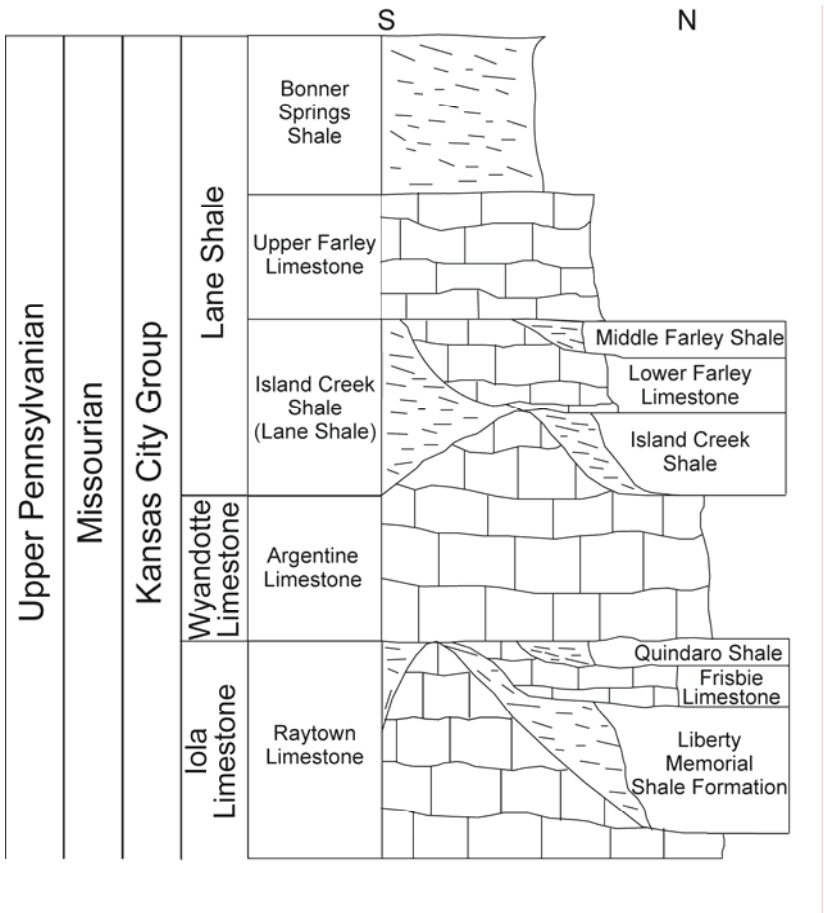

Figure 2.2: Generalized Stratigraphic Section Showing the Relationships and Lithologies of the Liberty Memorial Shale, Frisbie Limestone Quindaro Shale and Argentine Limestone along with Underlying and Overlying Units
(modified from Thompson et al., 1991)

In general, the Liberty Memorial Shale has been interpreted as being formed in nearshore deltaic and non-marine environments deposited during a stillstand or fall in sea level (Watney et al., 1989). Relief formed by the deposition of the Liberty Memorial Shale affected the deposition of the overlying Wyandotte Limestone, especially the Argentine Member (Arvidson, 1990; Heckel and Baseman, 1975*)*.

The Frisbie Limestone is a thin, very spatially restricted unit consisting of a single limestone bed, or several thin limestone beds interbedded with thin, grey shales. In north-central Johnson County it attains a thickness of 1.3 meters and contains meter-scale phylloid algal build-

ups (Watney, et al., 1989). It has been interpreted as being deposited during a regional marine incursion over the nearshore and terrestrial deposits of the Liberty Memorial Shale (Olszewski, 1996)

The overlying Quindaro Shale is also a spatially restricted unit that occurs primarily where the Frisbie Limestone is present. It ranges from 2.3 meters (7.5 feet) in northwest Johnson County to 0 meters in eastern Johnson and Miami counties in Kansas. It is composed of grey, platy shale, calcareous siltstone and small amounts of black shale in the northern part of the field area. An abundant and diverse conodont assemblage led Bisnett and Heckel (1996) to interpret the Quindaro Shale as "core" shale in his cyclothem model even though it is not a black, fissile, uranium-rich shale typical of most core shales. The distinct conodont assemblage was identified by Arvidson (1990) in most of the sections included in this paper and was used to identify the location of the Quindaro Shale-equivalent interval. As a core shale in the cyclothem model the Quindaro Shale has been interpreted as having been deposited during the maximum marine transgression for this cycle (Arvidson, 1990, Watney et al, 1989).

The most striking characteristic of the Argentine Limestone is its wide variation in thickness and lithologic character throughout the field area. The Argentine Limestone is dominantly a carbonate unit, but it does contain interbedded shale and siltstone beds. In the southern part of its range the Argentine Limestone varies in thickness from slightly over two meters (6 feet) in central Miami County to over 13.5 meters (44.3 feet) in Franklin County (Arvidson, 1990). In the northeastern part of the study area the Argentine Limestone attains a thickness of approximately 15 meters (50 feet) in eastern Johnson County and thins westward to 4 meters at the Shawnee Rock Company Quarry and then thickens again to approximately 16 meters in Leavenworth County.

2.4 Lithofacies and Depositional Environments

The Argentine Limestone and associated strata have been divided into ten lithofacies in this study. Characteristics of the lithofacies are summarized in Table 2.1. The interpretations of the depositional environments are presented below.

2.4.1 Phylloid Algal-Microbial Boundstone-Packstone Facies

Figure 2.3 is a polished slab illustrating the general appearance of the phylloid algal-microbial boundstone-packstone facies. Phylloid algae are identified by their characteristic internal microstructures visible in thin section (Baars and Torres, 1991). Phylloid algae in the Argentine Limestone are preserved by both recrystallization and the filling of molds with sparry calcite cement following dissolution of the original skeleton (Figure 2.4). These modes of preservation make the identification of the phylloid algal genera difficult. One genera identified in this study is *Archaeolithophyllum. Archaeolithophyllum* has been compared to the modern coralline red algal genus *Lithophyllum*, which typically develops in shallow, normal marine waters within the photic zone to a depth of approximately 30 m, but can be present up to depths of 100 meters (Wray, 1964). Other phylloid algae could be identified as green algae by the presence of utricles, but they are so poorly preserved that they cannot be identified to genus. Green algae are also indicative of shallow, clear, normal marine water (Baars and Torres, 1991; Kirkland, 1993). The presence of other organisms such as bryozoans, echinoids, and crinoids support the interpretation of this facies being deposited in a normal marine environment. This facies is also characterized by an abundant micritic microbial framework that encrusts phylloid algal fragments and sediment surfaces (Figure 2.5). The microbial frameworks are likely formed by "calcimicrobes" that are not necessarily photosynthetic (Riding, 2000). Good preservation of fossils, such as mostly intact phylloid algal blades and brachiopods with both valves and in some

cases, spines preserved in place, indicate little current reworking, suggesting relatively low energy conditions.

Figure 2.3: Polished Slab of the Phylloid Algal Microbial Packstone-Boundstone Facies
(Phylloid algae are the brownish wavy veins. Note that phylloid algae are generally whole, although some fragmentation occurs.)

Table 2.1: Facies Attributes for the Lithofacies of the Argentine Limestone Described in this Study

Facies Name	Rock Type and Texture	Grain types	Bedding	Prominent structures
Phylloid algal-microbial boundstone-packstone facies	Phylloid algal boundstone and packstone	More than 50% of skeletal constituents are phylloid algae;contains *Archaeolithophyllum*; contains calcareous green algae; microbial framework and encrustations abundant; associated fauna dominated by brachiopods, bryozoans, and crinoids; bivalves gastropods, foraminifera, ostracodes, rugose corals and trilobites are less common.	Medium to thick (50-100 cm) accentuated by thin shale partings commonly containing abundant crinoidal and bryozoan material; characteristic wavy bedding	Matrix is micritic; contains peloidal internal sediment; localized framework growth of phylloid algae, commonly with a brecciated texture from collapse; clotted peloidal textures, digitate microbial structures and microstromatolitic structures; phylloid algal blades are generally whole or slightly fragmented, some brachiopods are commonly preserved with both valves and in some cases have spines preserved in place attached to the valves
Skeletal wackestone-packstone	Packstone and wackestone with micritic matrix	Most common skeletal constituents are whole and fragmented brachiopods; fenestrate bryozoans and crinoid ossicles, are often disarticulated, but are unabraded and occur in little piles showing little evidence of reworking, fusulinids, trilobites and and gastropods are also present; phylloid algal fragments are less than 20 percent of total fauna	Thin-to-medium-bedded (25-50 cm); stylolites common along bedding planes	Commonly contains patches of densely packed packstone-grainstone; variable, patchy, lateral and vertical variations within individual beds in the predominance of packstone-versus wackestone lithologies; brachiopods commonly preserve both valves
Phylloid algal fragment packstone	Packstone with some zones of wackestone	Main constituents are shell fragments or phylloid algal fragments (50%) of approximately the same size (1-1.5 cm); contains crinoids, brachiopods and bryozoan fragments; rare whole brachiopods and gastropods	Medium-to-thick bedding (50-100 cm)	Patches where fossil fragments are concentrated (5-10cm); fossil fragments randomly oriented possibly resulting from burrowing
Peloidal, *Heliospongia* packstone	Packstone	Micritic matrix with abundant small fossil fragments; abundant fine-grained bryozoan fragments, *Heliospongia* commonly encrusted with bryozoans and microbial micrite; clay mineral-rich matrix; other fragments include gastropods, crinoids, foraminifera, tribloites, serpulid worm tubes, echinoid spines, and sponge spicules	Thin-bedded (10-50cm)	Dark brown in color; generally not well-laminated; *Heliopsongia* common; zones of lighter colored patches; distinctive "chalky" weathering that appears to correlate to high clay content (McKirahan, 2000)
Encrusting microbial boundstone	Distinctive alternating layers of micrite and sparry calcite, microstromatolitic textures, clotted peloidal textures	Abundant small (0.25-0.5 cm) bryozoan, crinoid, foraminifera and unidentifiable fossil fragments; less than 10% (1-3 cm) phylloid algal blades, small (1-2 cm) brachiopods with both valves, and gastropods with geopetal infills	Thin-to-medium-bedded (10-50cm)	Abundant microbial structures and sparry calcite

Table 2.1 CONTINUED

Shaley-oncoid, fusulinid packstone	Packstone	Fissile, clay-rich matrix with foraminifera, and crinoid fragments; less common brachiopod, bivalve, gastropod, trilobite and bryozoan fragments; oncoidal "osagia-like" very crinkly-looking coatings common on all fossil fragments Fish scales and fossil hash consisting of bryozoan, brachiopod and crinoid debris on upper surfaces of beds	Thin-bedded (10 cm)	Many of the foraminifera-rich zones are oriented long-axis parallel to bedding; but some foraminifera-rich zones are unoriented; iron-staining common on the upper surfaces of beds
Fossil fragment grainstone and packstone	One subfacies (A) is "*osagia*" grainstone. Second subfacies (B) is grainstone grading upwards into packstone; and third subfacies (C) is fossil fragment oolitic grainstone	The siliciclastics portion consists of silt-and-sand sized quartz and less-commonly clay particles; crinoid and echinoid fragments are most common skeletal constituents, also common are brachiopod, bryozoan, bivalve, foraminifera, gastropod, green algae, fragments of *Archaeolithyphyllum*, trilobite fragments, echinoid spines, and serpulid worm tubes; there are are abundant micritic envelopes on all grains; Subfacies A contains abundant *osagia* coatings, the highest amount of siliciclastics (approximately 15-20%, sand and silt sized) and composite grains (grapestone); Lower part of subfacies B is very similar to subfacies one, with less (>5%) siliciclastics material, upper part of subfacies B contains 1-5 cm broken phylloid algal blade molds in packstone; Subfacies C contains ooids, fewer siliciclastic grains compared to other two subfacies and *Myalinid* clams preserved in place	Medium-to-thick-bedded (10-50 cm)	Cross-bedding near the top in several localities; grains show abrasion and micrite envelopes, resulting in generally spherical grains which are generally poorly sorted; best sorting occurs in subfacies C; in subfacies B there are normally graded beds which commonly grade upwards from grainstone layers to packstone layers containing phylloid algal blades;
Lime mudstone, interbedded mudstone and calcareous siltstone	Micrite and silt-to-clay sized quartz and clay; laminations of sand-sized quartz grains	Siliceous sponge spicules, isolated crinoid ossicles, and carbonized plant fragments in carbonate mudstone; wisps of organic matter, rare crinoid ossicles and lenticular bedding in the siltstone	Carbonate mudstone is a single massive bed, the siltstones; thin-bedded	Isolated lenticular beds consisting of silt and sand-sized quartz and burrow mottling in siltstones
Microbial mudstone-wackestone	Mudstone and wackestone	This facies is characterized by micritic matrix containing centimeter-scale brownish digitate structures composed of pseudospar. Digits are encrusted with crinkly concentric and lamellar micritic and microsparitic coatings; Brachiopods are the most common; Bryozoans, crinoids, echinoids, gastropods and phylloid algal fragments are also present;	Medium-to-thick bedded (10-50 cm)	This facies is strongly overprinted with an autobreccia texture; microscopically much of the matrix and microbial-like structures have undergone recrystallization.

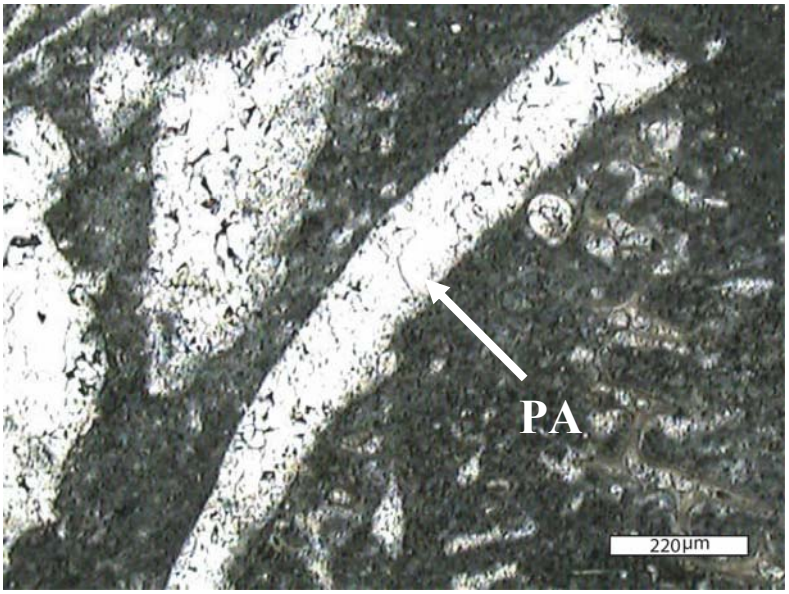

Figure 2.4: Photomicrograph of a Poorly Preserved Phylloid Algal Blade (PA)
(Note the coarse calcite crystals that have replaced the original structure of the thalli.)

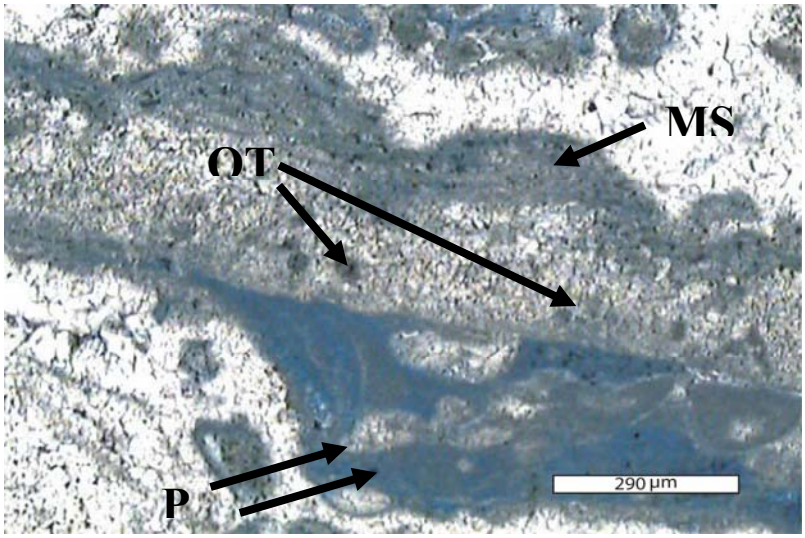

Figure 2.5: Photomicrograph of Microbial Component of the Phylloid Algal Microbial Packstone-Boundstone
*[Note the microstromatolitic structures (**MS**) on the upper surface of the blade and the micritic pendant looking structure on the underside (**P**). The lower encrustation appears to be constructed by a consortium of organisms. The micrite appears blue because the slide was impregnated and a blue filter was used to highlight the textures. Also, note that there is a small amount of original texture preserved inside the phylloid algal thalli (**OT**).]*

2.4.2 Skeletal Wackestone-Packstone Facies

This facies is dominantly composed of micrite, skeletal fossil fragments, and peloids. It ranges in texture from wackestone to packstone both vertically and laterally within individual beds. Some localities contains patches of concentrated skeletal grains that are 1-10 centimeter in diameter. This type of texture has been interpreted as being created by storm-infilling of burrow networks (Tedesco and Wanless, 1989). Alternatively, this texture could just be the result of reworking and concentration of fossils present in the sediments. It contains less than 20% phylloid algae most of which have been fragmented, showing evidence of transport. Figure 2.6 illustrates the typical appearance of the skeletal wackestone-packstone facies.

A diverse biota of unabraded crinoids, bryozoans, brachiopods, echinoids, gastropods, bivalves, fusulinids and, less commonly, trilobites and rugose corals is present. Organisms such as bryozoans, brachiopods, echinoderms and corals indicate a marine environment of normal salinity (Heckel, 1972; Scholle, et al., 1983). A diverse brachiopod fauna is characteristic of this facies and well-preserved specimens generally occur *in situ.* This facies lacks the microbial framework that stabilized and bound the phylloid algal boundstone-packstone facies. In order to contain abundant micritic matrix without a binding mechanism, this facies must have been deposited in a relatively quiet, low energy setting (Heckel, 1972; Scholle, et al., 1983). These features lead to the interpretation of this facies as being deposited under a normal marine, subtidal, relatively low energy environment that may have experienced intermittent periods of higher energy from events such as storms.

2.4.3 Shale, Siltstone and Fine Sandstone

This facies occurs exclusively in the Liberty Memorial Shale and is primarily composed of clay and quartz silt, although it can be somewhat calcareous in places. The nature of this facies in outcrop is shown in Figure 2.7.

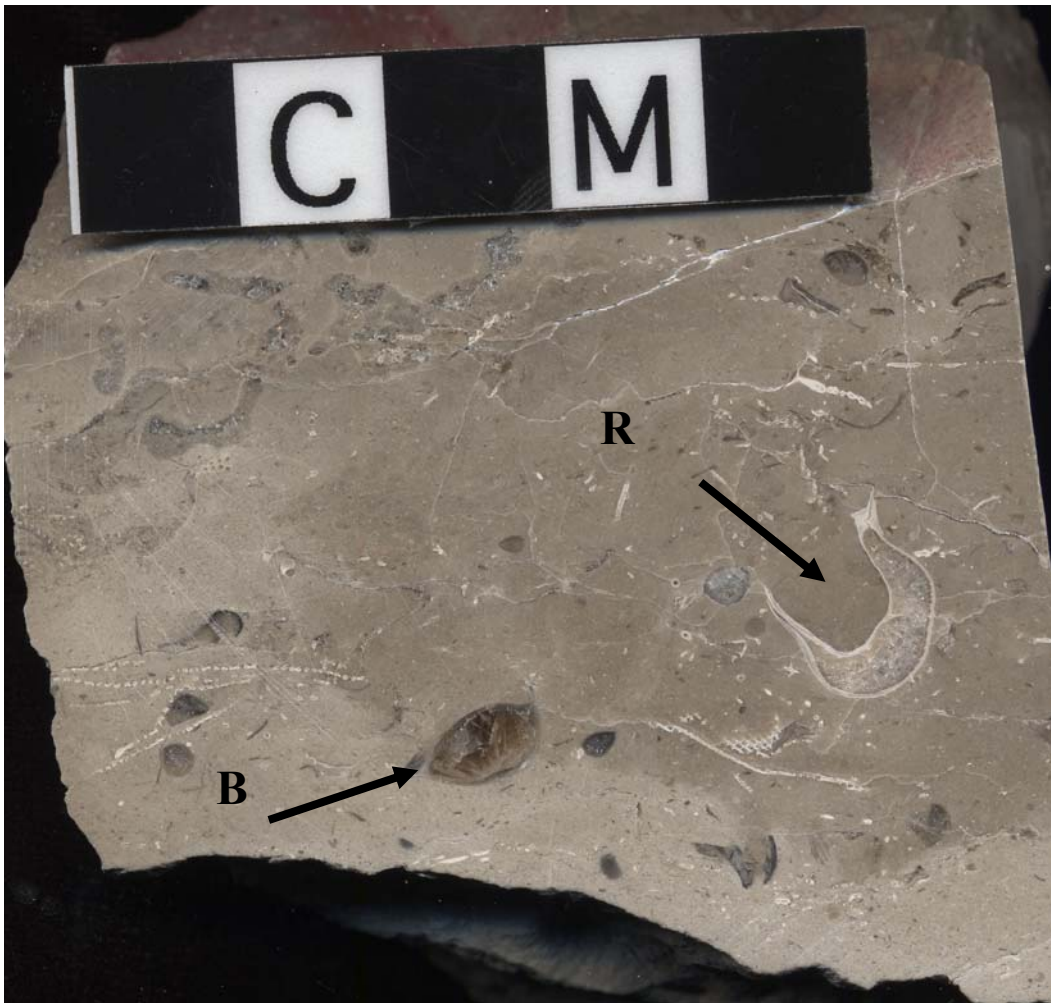

Figure 2.6: Slab Illustrating the Typical Appearance of the Skeletal Wackestone-Packstone Facies
[Note excellent preservation of the whole brachiopod (B) and the while U-shaped structure is a rugose coral (R).]

It is sparsely fossiliferous, containing normal marine organisms such as crinoids, fenestrate and ramose bryozoans, and brachiopods. Physical sedimentary structures are only rarely preserved, which could indicate a high degree of bioturbation (Reineck and Singh, 1973). Possible lenticular bedding can be found in isolated areas. The formation of lenticular bedding requires current action that deposits lenses of silt or sand alternating with the deposition of mud during slackwater conditions.

The possible presence of lenticular stratification indicates that this environment may have been at least intermittently impacted by current energy. Bisnett and Heckel (1996) defined a similar sparsely fossiliferous facies composed of sand- and silt-sized particles in Mid-continent Pennsylvanian strata in the context of Heckel's cyclothem model and interpreted them to represent prodelta environments deposited at lower sea-level stands. McKirahan et al. (2000) defined a nearly identical facies in the overlying Lane-Island Creek Shales and interpreted it to have been deposited in a tidally dominated delta front or prodelta marine environment. Deposition in a tidally dominated prodelta or delta front environment is a likely origin for this facies in the Liberty Memorial Shale.

2.4.4 Lime Mudstone, Interbedded Mudstone and Calcareous Siltstone

The lime mudstone of this facies is dark brown and massive, composed primarily of micrite, and contains abundant flecks of organic matter visible in thin section. No obvious sedimentary structures are present except for a few mottled zones that resemble burrows. It has a limited biota consisting of siliceous sponge spicules, fusulinids, and rare crinoid ossicles (Figure 2.8).

Figure 2.7: Photograph of the Nature of the Shale, Siltstone and Fine Sandstone Facies in Outcrop
(The multi-tool is 12 centimeters in length.)

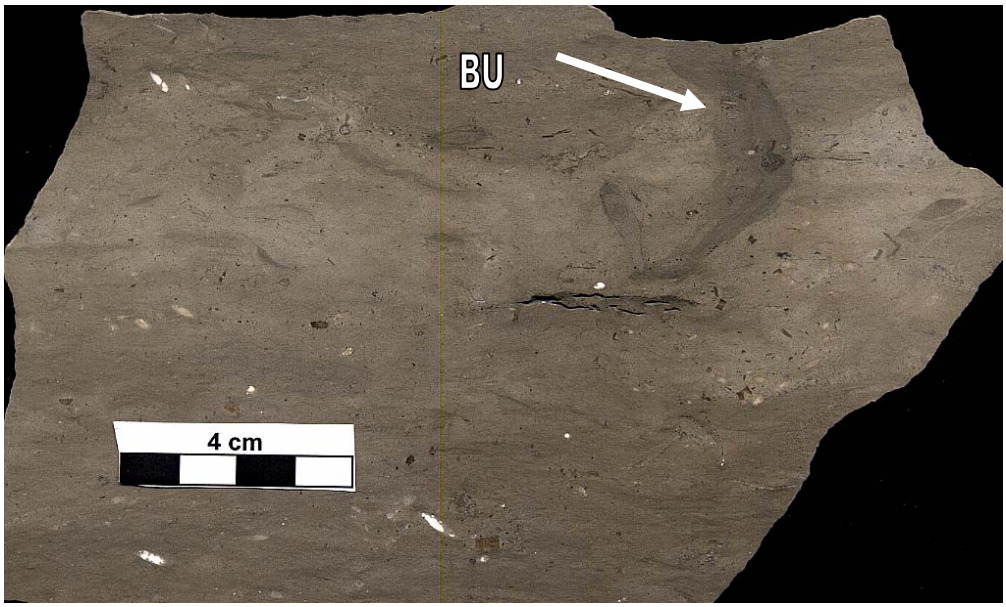

Figure 2.8: Slab Illustrating the Typical Appearance of the Lime Mudstone in the Lime Mudstone, Interbedded Mudstone and Calcareous Siltstone Facies
[Note the curved structure that may be a burrow (BU).]

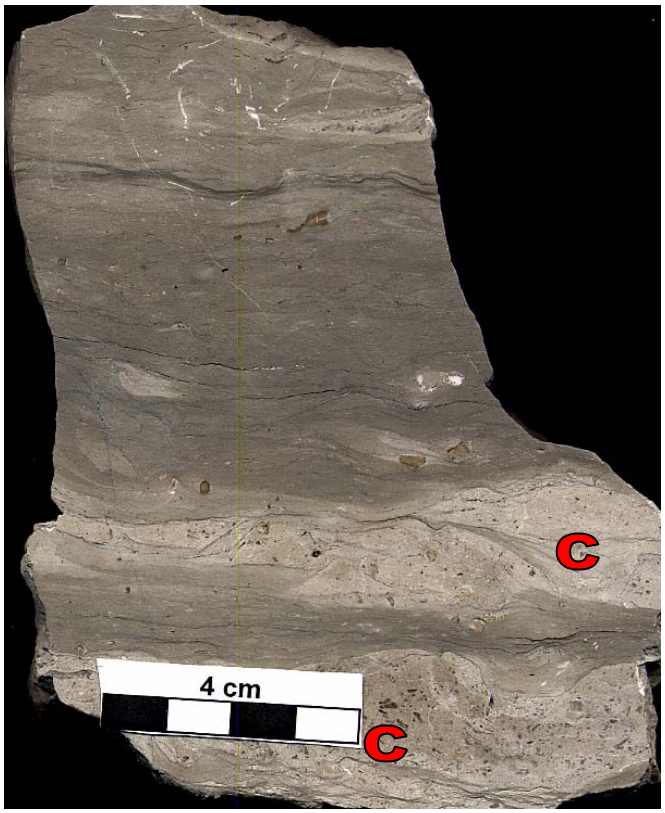

Figure 2.9: Slab Illustrating the Typical Appearance of the Siliciclastic Lithology in the Lime Mudstone, Interbedded Mudstone and Calcareous Siltstone Facies
*[The light colored portions are lenses of carbonate (**C**).]*

The siliciclastic-rich part of this facies consists of grey siltstone with lenses of peloidal carbonate wackestone and packstone (Figure 2.9). Fossils are rare and consist of crinoid ossicles and mollusc fragments. Structures similar to lenticular stratification are also present in the siltstone. This facies in the Argentine Limestone is located only in a small part of north-central to north-east Miami County. The presence of an impoverished biota can be characteristic of restricted environments (Scholle, et al., 1983). A similar facies consisting of micrite and pelleted micrite with an impoverished fauna and limited sedimentary structures has been described from the modern Great Bahama Bank. This facies is only found in water depths of 1.8-7.2 meters in the shelf lagoon on the west side of Andros Island (Purdy, 1963). The spatially limited nature of

the lime mudstone, interbedded mudstone and calcareous siltstone facies, and its similarity to lagoonal deposits of the Great Bahama Bank leads me to interpret this facies to have been deposited in a somewhat restricted setting. The siliciclastic portion of this facies also contains features such as an impoverished biota, and possible evidence of tidal influence, which also support the restricted interpretation of depositional environment (Renicke and Singh, 1973).

2.4.5 Phylloid Algal Fragment Packstone

The major constituents of this facies are fossil fragments and micritic matrix, some of which occurs in distinct patches. Figure 2.10 illustrates the typical appearance of the phylloid algal fragment facies. Identification of phylloid algal fragments is difficult because most are preserved as molds filled with sparry calcite cement. However, the shapes of the molds resemble broken phylloid algal blades and perhaps some mollusc fragments and, therefore, are interpreted as such. Other identifiable fossils include crinoid ossicles, bryozoan fragments, brachiopod fragments, and rare small whole brachiopods and gastropods.

Some of the fragments of identifiable fossils such as crinoid ossicles and brachiopod fragment show some abrasion. Some 1-5 cm patches of better sorted fossil fragments are apparent. The fragmentation, abrasion and sorting of the grains indicates that current energy was present during deposition of this facies. The co-occurrence of transported grains and micritic matrix, especially when the micrite is patchily distributed, has been interpreted as the result of incomplete winnowing or partial leaching of mud or mixing by burrowers (Dunham, 1962). This facies also lacks lamination which may be indicative of intense bioturbation destroying any prior sedimentary structures and creating micritic patches from the infilling of burrows. Brachiopods in which both valves are preserved are relatively common indicating that they probably lived in this environment and were not transported. This facies was likely deposited in an environment where energy was high enough to transport the phylloid algal and mollusk grains but not so high

as to completely winnow away the micrite and prevent organisms from thoroughly burrowing the sediment. This facies was likely deposited in a normal marine, subtidal environment that experienced some current energy located near a source for phylloid algal and mollusk fragments.

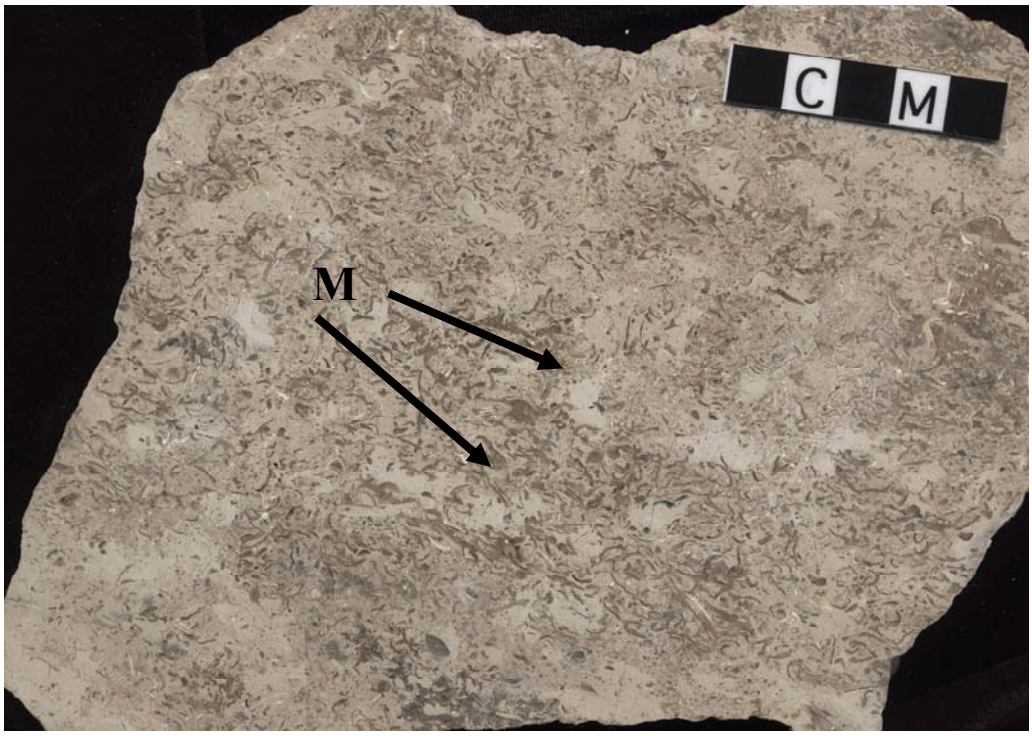

Figure 2.10: Slab of Phylloid Algal Fragment Packstone Facies
*Note the patches of white micrite (**M**) that could have formed from burrowing.*

2.4.6 Peloidal, Heliospongia Packstone

The main constituents of this facies are peloids, fossil fragments, and Heliospongia. Figure 2.11 illustrates the typical appearance of this facies. *Heliospongia* fragments are commonly encrusted with foraminifera and microbial encrustations, quartz silt and micrite. Fish scales and a hash of reworked bryozoan and brachiopod fragments are commonly present in the upper parts of beds of this facies. Little work has been published regarding the paleoenvironments that *Heliospongia* sp. occupied, but as members of the class Demospongia they are among the most numerous, diverse and widespread of all sponges. Demosponges can

tolerate, and thrive in a variety of sedimentologic conditions and environments that deviate from normal marine conditions (Finks, 2003). The matrix appears micritic in hand sample but is approximately 50% peloidal and 50% micritic in thin section. The matrix also contains abundant clay particles and quartz silt. The abundance of micrite and clay indicate relatively low energy. The facies commonly lacks lamination and appears mottled with discontinuous patches of micrite and zones of concentrated grains indicative of burrowing. The abundant siliciclastic material and the fact that this facies is often found interbedded with grey, silty shales indicate proximity to a siliciclastic source. This facies likely represents deposition in a subtidal, relatively normal marine to somewhat restricted environment near a siliciclastics source. The fossil fragment packstone lithologies found at the top of the beds in this facies may represent periodic hiatuses of deposition resulting in a concentration of grainy sediments and fish scales.

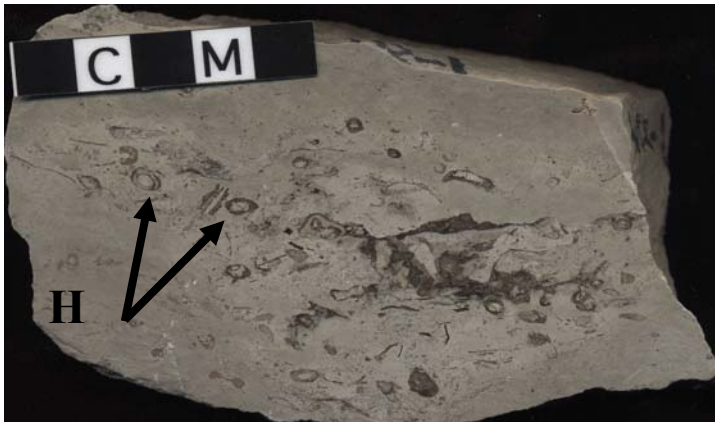

Figure 2.11: Slab of the Peloidal *Heliospongia* Packstone
*(Cross-sections of Heliospongia are the oval-shaped objects (**H**).)*

2.4.7 Encrusting Microbial Boundstone

This facies is characterized by distinctive dark and light bands of alternating micritic matrix and sparry calcite, respectively (Figure 2.12). Macrofossils, though relatively rare include bryozoans (ramose, fenestrate and encrusting) brachiopods, crinoid fragments, phylloid algal

fragments, bivalve and gastropod fragments. A *Tubiphytes*-like, organism locally encrusts fenestrate bryozoan fragments. Fabrics containing clotted peloidal microfabrics (Figure 2.13), crinkly laminated (stromatolitic) textures with domal micron-scale relief, and dendrolitic or arborescent fabrics (Figure 2.14) are interpreted to be microbial in origin (Riding, 2000; Dupraz, P.T., et al; Shen, J.W. and Webb, G. E.). Microbial textures described from a deposit in a modern crater lake in Indonesia bear a striking resemblance to the textures seen in this facies (Arp, et al., 2003). The macroorganisms present indicate a subtidal, marine environment, but the dominance of microbial textures suggests that there may have been an imbalance of nutrients or change in alkalinity away from normal marine conditions.

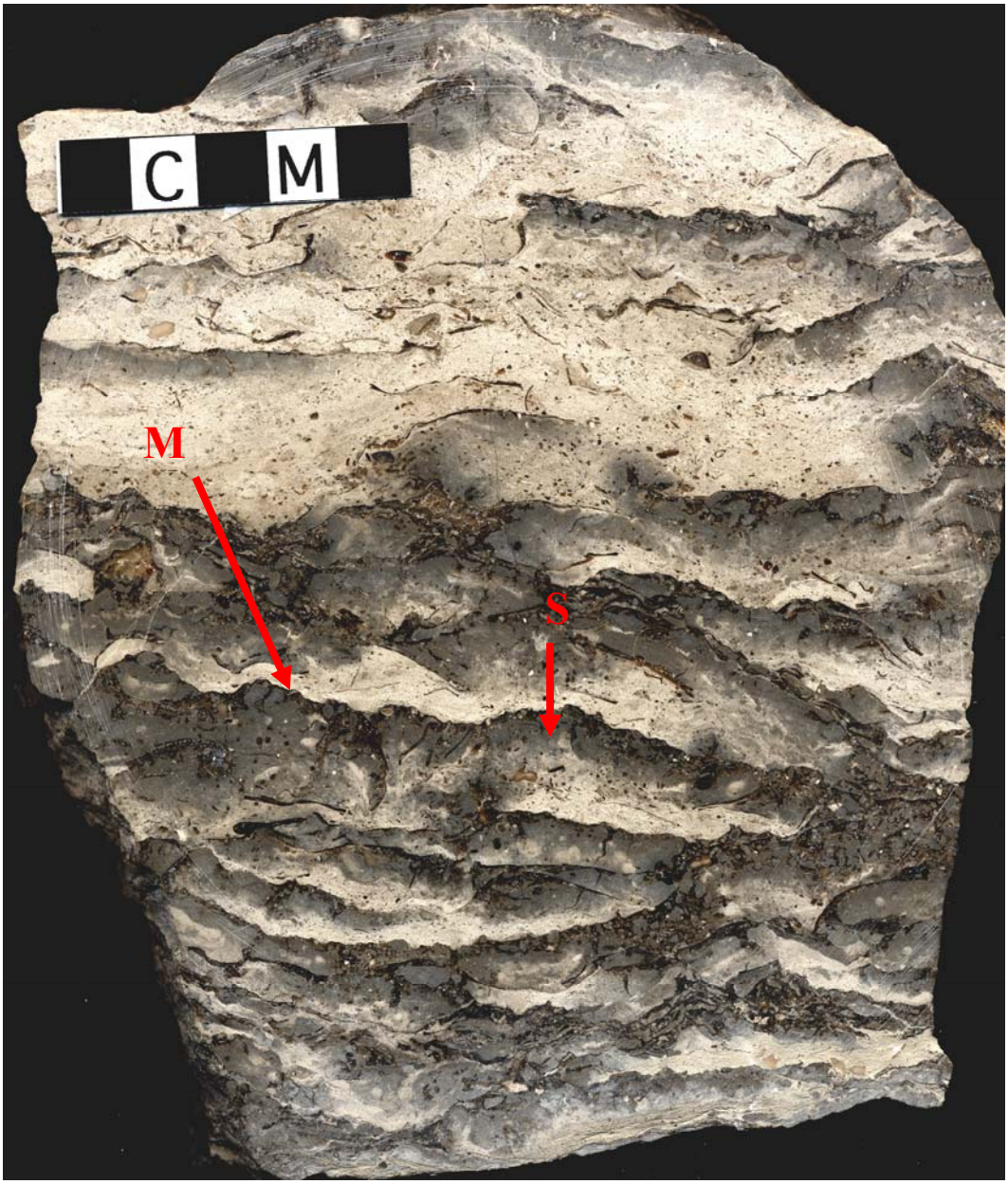

Figure 2.12: Slab Illustrating the Typical Appearance of the Encrusting Microbial Boundstone

[Note the characteristic light/dark banding formed by alternating layers of micritic matrix (M) and sparry calcite cement (S).]

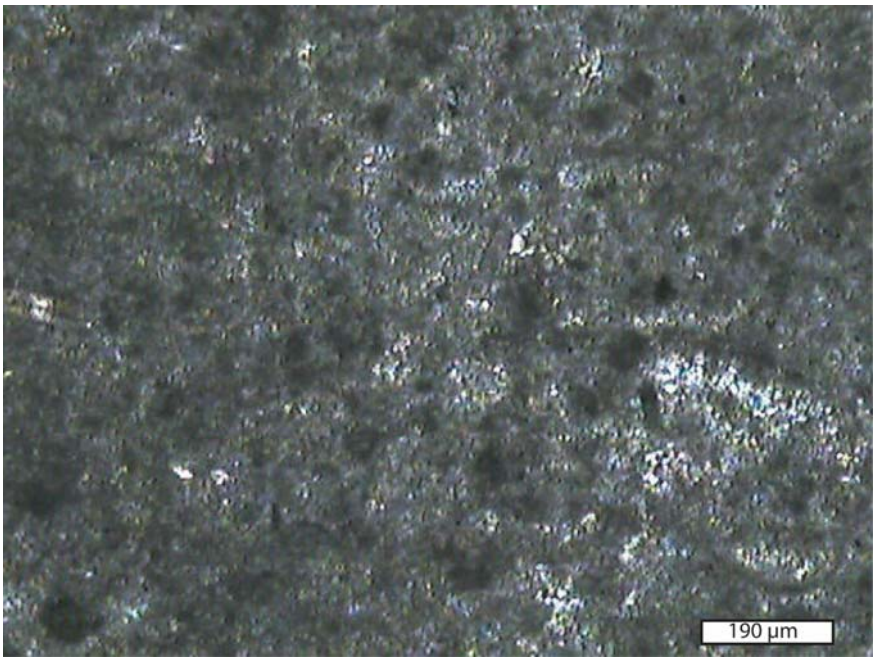

Figure 2.13: Photomicrograph Showing the Clotted Appearance of Micrite in the Encrusting Microbial Boundstone Facies

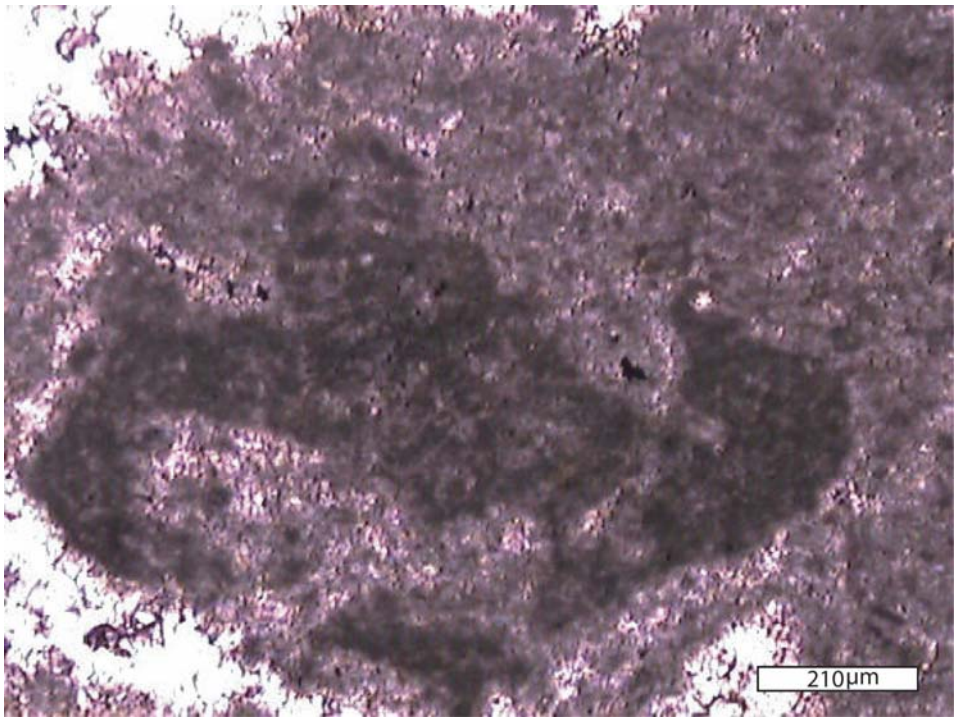

Figure 2.14: Photomicrograph Showing the Typical Appearance of Dendritic or Arborescent Microbial Textures Common in the Encrusting Microbial Boundstone Facies

2.4.8 Fossil Fragment Grainstone-Packstone

This facies consists of three sub-facies that were described in the uppermost bed of the Argentine Limestone in the Johnson County Landfill/ Shawnee Rock Company Shawnee quarry. Fossil fragments and silt-and-sand sized quartz grains are the most common grains in all three subfacies. The presence of quartz indicates deposition in an environment proximal to a siliciclastic source. The carbonate grains show significant corrosion resulting in rounded fossil fragments, but are generally not very well sorted. Sparry, equant calcite cement fills most of the spaces between grains, but significant amounts of interstitial micrite occur in one of the subfacies. Sedimentary structures such as ripples and cross-lamination are present at certain localities. The shapes and sorting of grains and presence of sedimentary structures indicating current energy suggest that this facies was deposited in a relatively high energy environment.

The first subfacies, A, is distinguished by the abundance of "*osagia*-type" coated oncoidal grains, phylloid algal fragments, rip-up clasts of the underlying phylloid algal lithology and a large percentage (15-20%) of siliciclastic material (Figures 2.15, 2.16). The second sub-facies, B, is a distinctive bed that grades from a crinoid, brachiopod grainstone upwards into a packstone with phylloid algal blades (Figure 2.17, 2.18). Subfacies B records a decrease in energy as the bed was being deposited. In one locality, the uppermost portion of subfacies B is composed of a *Composita* brachiopod packstone indicating that the upper part of this subfacies was deposited in a restricted environment (Ramsbottom, 1978). The third subfacies, C, contains less siliciclastic material (<5%), significant amounts (approximately 10-20%) of ooids and has westward-oriented unidirectional ripple marks on its upper surface (Figures 2.19, 2.20). Isolated burrows can be found and *Myalinid* clams are common in subfacies C in the Shawnee Rock Company Shawnee quarry. Myalinid clams are interpreted to have lived in shallow, high energy, possibly restricted marine environments (Moore, 1964). The characteristics found in the three

subfacies are typical of facies deposited in a high energy more normal marine environment alternating with a lower energy restricted marine environment.

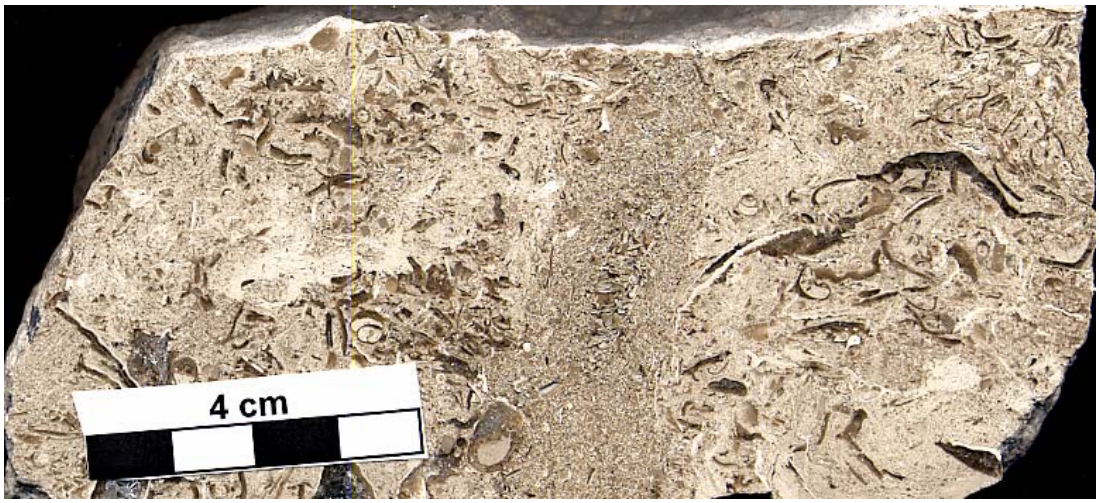

Figure 2.15: S. Slab of Subfacies A of the Fossil Fragment Grainstone-Packstone Facies
(The near-vertical linear structure in the middle is a burrow that was later filled by finer-grained sediments.)

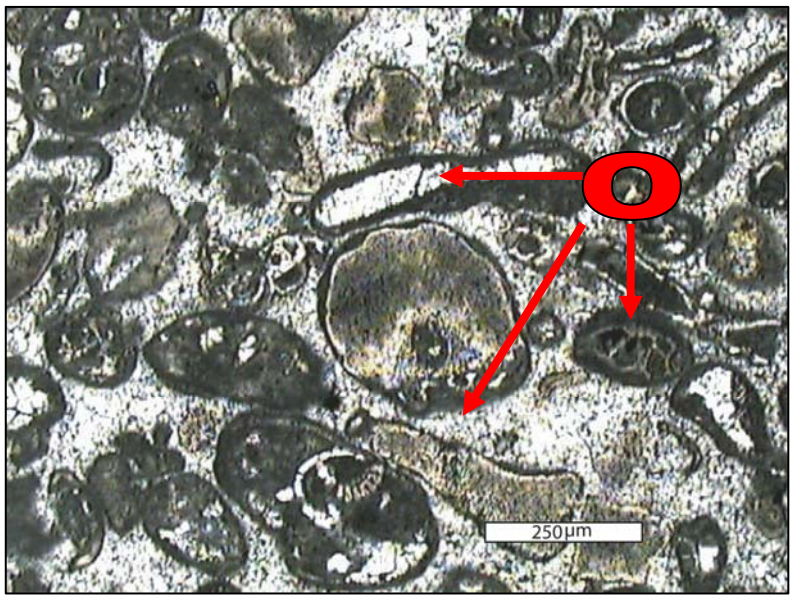

Figure 2.16: Photomicrograph of Subfacies A of the Fossil Fragment Grainstone-Packstone
[This subfacies is characterized by abundant "oncoidal" coatings which are apparent on almost all of the grains (O).]

Figure 2.17: Slab of Subfacies B of the Fossil Fragment Grainstone-Packstone
(Note how the grainy lithology sharply transitions vertically into muddier lithology with phylloid algal fragments.)

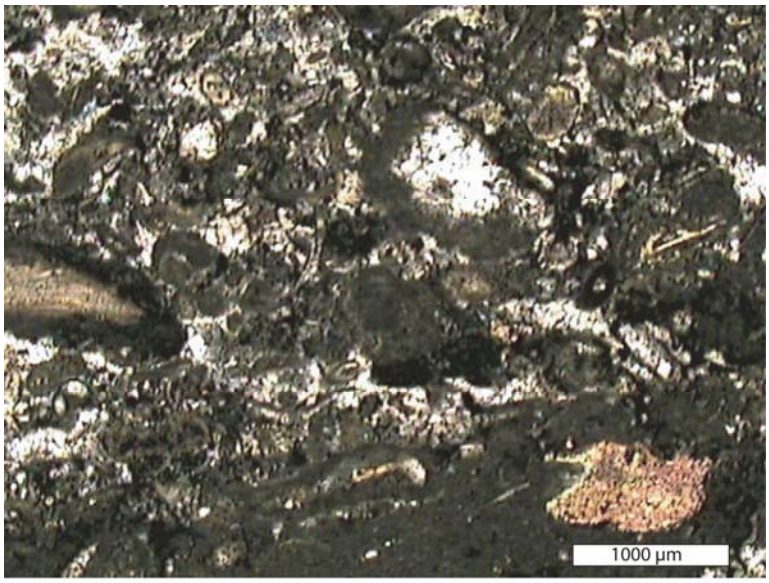

Figure 2.18: Photomicrograph of Subfacies B in the Fossil Fragment Grainstone-Packstone Facies
(Note how the grainy texture with sparry calcite cement between the grains grades into a zone with abundant micritic matrix. Photomicrograph taken with partially crossed polars.)

Figure 2.19: Slab of the Subfacies C of the Fossil Fragment Grainstone-Packstone Facies
(The cross-lamination seen here is common to wherever this subfacies was found.)

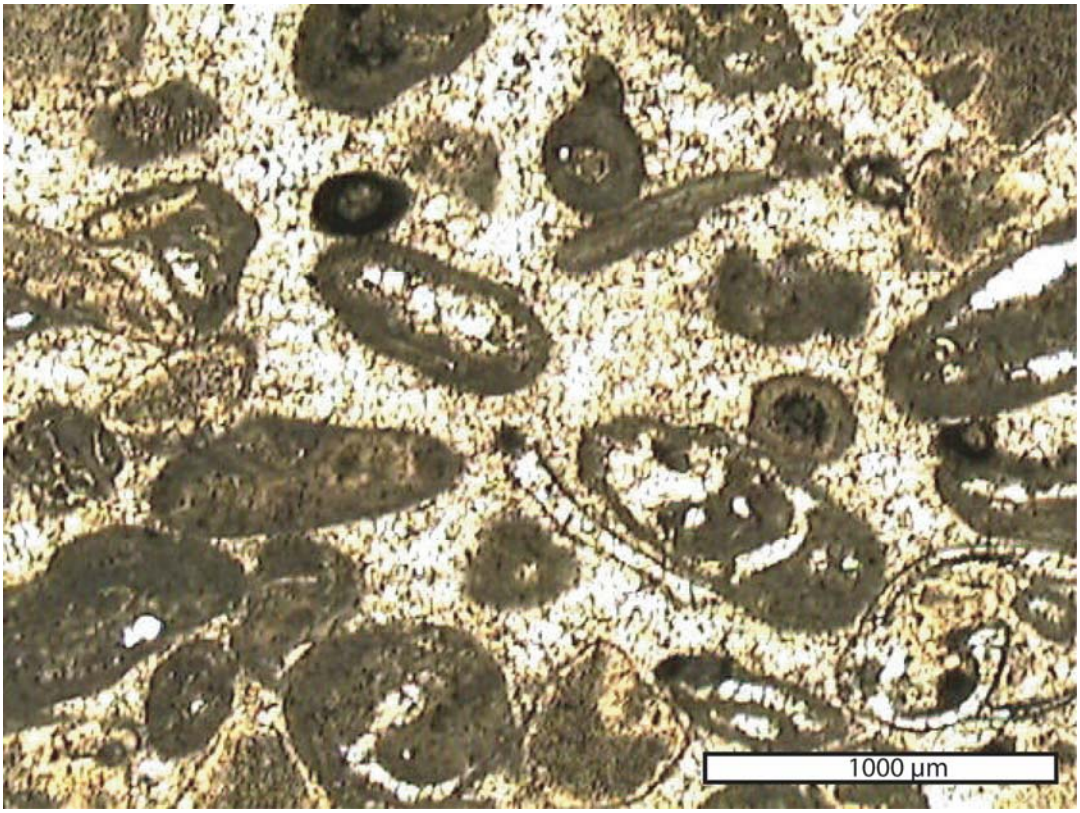

Figure 2.20: Photomicrograph of Subfacies C in the Fossil Fragment Grainstone-Packstone Facies
(Note the better sorting relative to the two previous subfacies and lack of micritic matrix supporting the interpretation of a relatively high energy environment.)

2.4.9 Shaley, Oncoid, Fusulinid Packstone

This facies is distinguished from the Fossil Fragment Grainstone-Packstone facies by the presence of clay and silt as matrix commonly resulting in a fissile, poorly lithified rock. Oncoidal coatings are common consisting of a consortium of encrusting organisms and are often symmetrical (Figure 2.21, 2.22). A majority of the fossil fragments show a moderate degree of abrasion. The abundance of clay and silt in the matrix indicates a location close to a siliciclastic source. The separate zones of oriented and unoriented fusulinids may indicate that this environment was subject to varying energy regimes, for example, within the intertidal zone where tides may have occasionally affect the deposition of this facies. Iron staining is common on the upper surface of this facies. There are no other features indicative of subaerial exposure, so the iron staining could be interpreted as representing a hiatus in deposition and subsequent concentration of iron minerals on bedding planes. This facies was likely deposited in an environment in which water quality may have varied from normal marine, although there are no diagnostic features to indicating exactly how it may have differed from a normal marine environment. This facies was likely deposited in a subtidal environment that experienced intermittent energy necessary to agitate the oncoids, or in a low-energy intertidal environment that was calm enough for the oncoids to grow asymmetrically.

2.4.10 Microbial Mudstone-Wackestone

This facies is characterized by micritic matrix containing centimeter-scale brownish digitate structures composed of pseudospar. Digits are encrusted with crinkly concentric, lamellar micritic, and microsparitic coatings (Figure 2.23). This facies is strongly overprinted with a post-depositional autobreccia texture formed by possible dissolution of microbial structures and subsequent compaction of the sediments. Microscopically much of the matrix and microbial-like structures have undergone recrystallization.

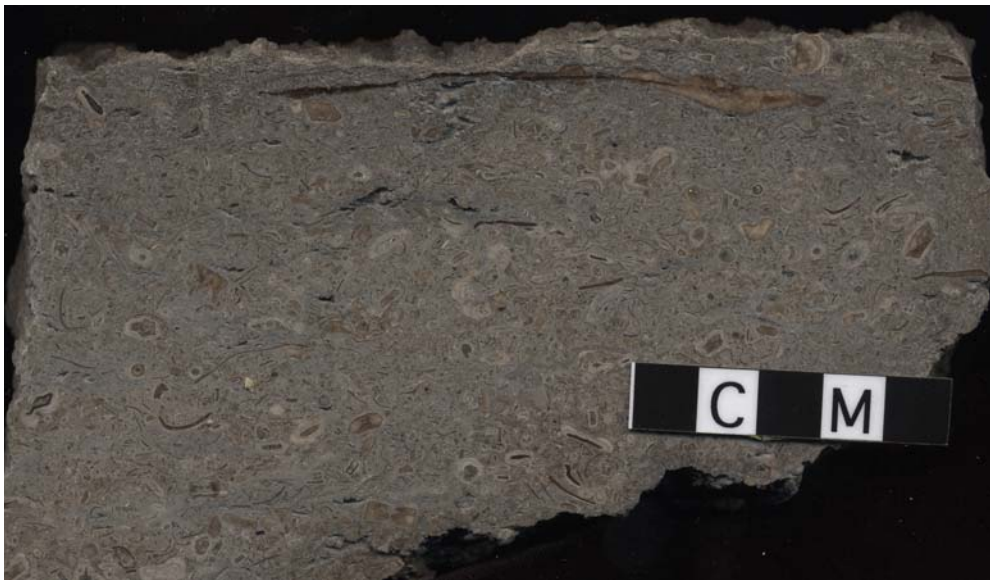

Figure 2.21: Slab Illustrating the Typical Appearance of the Shaley, Oncoid, Fusulinid Packstone

(Oncoidal coatings are ubiquitous in this facies. The matrix is silt and clay-sized quartz and clay minerals.)

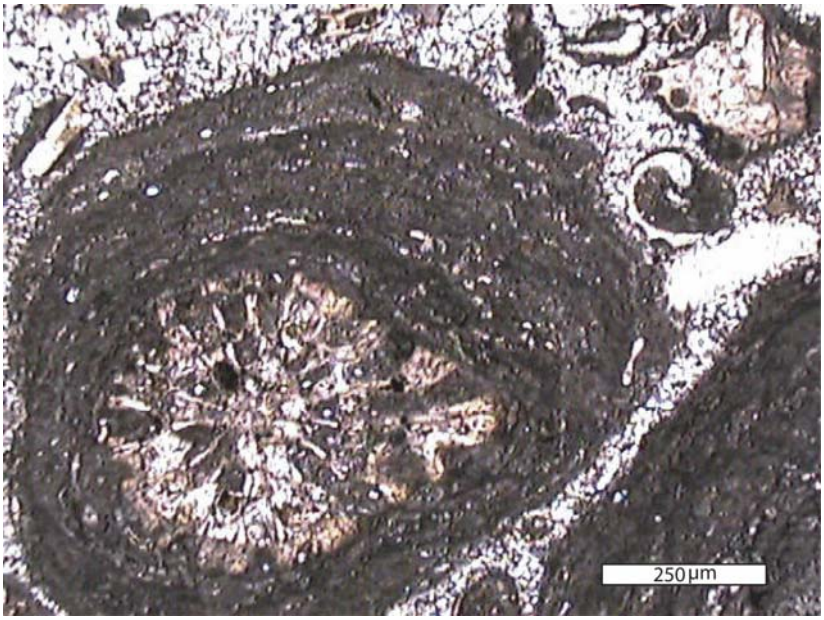

Figure 2.22: Photomicrograph of Consortium of Encrusting Organisms Forming Oncoidal Coatings Commonly Found on Grains in the Shaley, Oncoid, Fusulinid Packstone

The most common microorganism is brachiopods, commonly found in life position.

Other organisms present include trilobites, echinoids, crinoids and fragmented phylloid algal

blades. Similar to the phylloid algal microbial packstone-boundstone facies, according to the presence of stenohaline organisms this facies appears to have been deposited in a subtidal, normal marine environment. Yet, the dominance of microbial structures indicates that the water likely varied from normal marine, although exactly how is not determinable from the data obtained in this study.

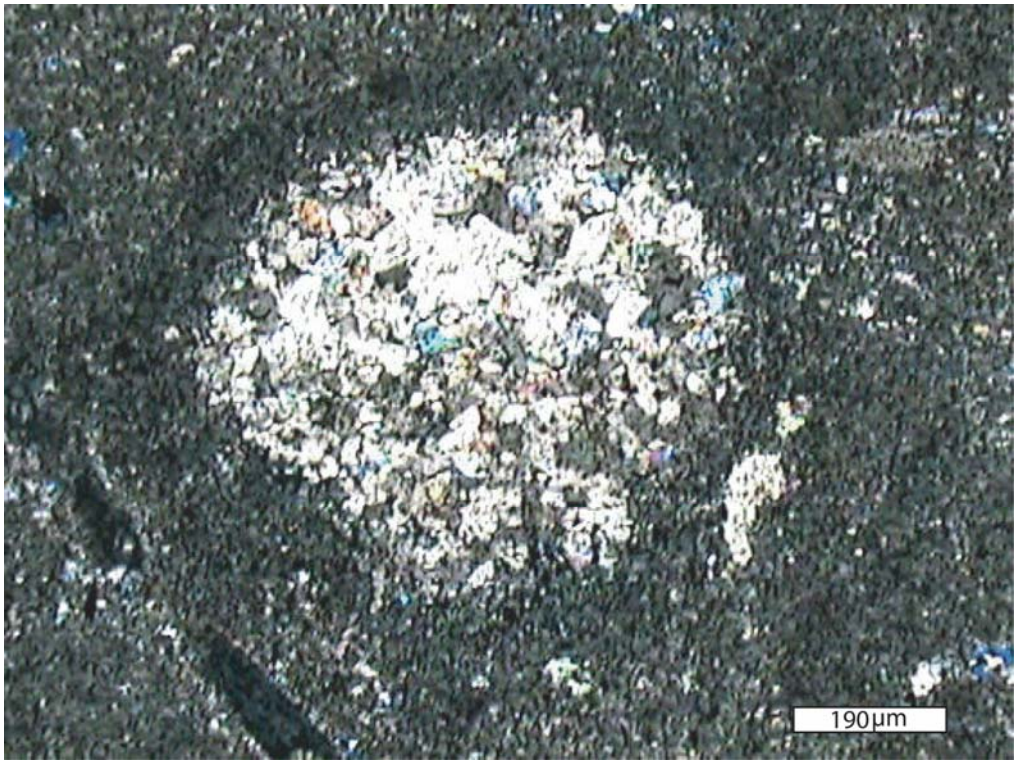

Figure 2.23: Photomicrograph of a Microbial-Like Microspar "Finger" from the Digitate Microbial Facies Illustrating the Micritic Encrustations Commonly Surrounding These Structures (E).

2.5 Stratigraphy and Interpretations

The regional and stratigraphic distribution of lithofacies is presented below. The interpreted depositional environments and detailed sequence stratigraphic observations and interpretations are used to evaluate the controls on the regional distribution of lithofacies. Cross-sections (Figures 2.24-2.26, 2.28) and a fence diagram (Figure 2.27) illustrate correlations, aspects of reconstructed paleotopography and sea-level history for the strata of this study.

Unfortunately, there is no consistent unit within the Liberty Memorial Shale, Frisbie Limestone, Quindaro Shale or Argentine Limestone suitable for use as a stratigraphic datum. The stratigraphic datum used in this study was first used in a study of the upper Farley Limestone by McKirahan et al (2000). The datum consists of the only occurrence of a specific lithology that is consistent in lithologic character, thickness, and stratigraphic position throughout Johnson County. However, the Farley Limestone was either not deposited or has been eroded away in some of the localities in southern Miami County making a different datum necessary for correlation at these sites. In the southernmost areas where the datum used in the north is preserved, the top of the Argentine Limestone appears to be at a consistent stratigraphic distance below the datum. Thus, in areas to the south, the top of the Argentine Limestone is used as the datum for correlation. Use of these data for correlation allow for a reasonable reconstruction of the depositional topography. The reconstructions presented here, however, do not depict exact depositional topography for two major reasons. First, compaction of siltstone and shale following deposition can significantly alter the thickness of stratigraphic successions by as much as 40-50 percent (Tucker, 1991). Secondly, work by Watney et al. (1989) suggested that this area of the Pennsylvanian shelf may have had a low south-southwestward dip. Consequently, the cross sections presented here should be considered a suggestion of paleotopography as opposed to precise reconstructions.

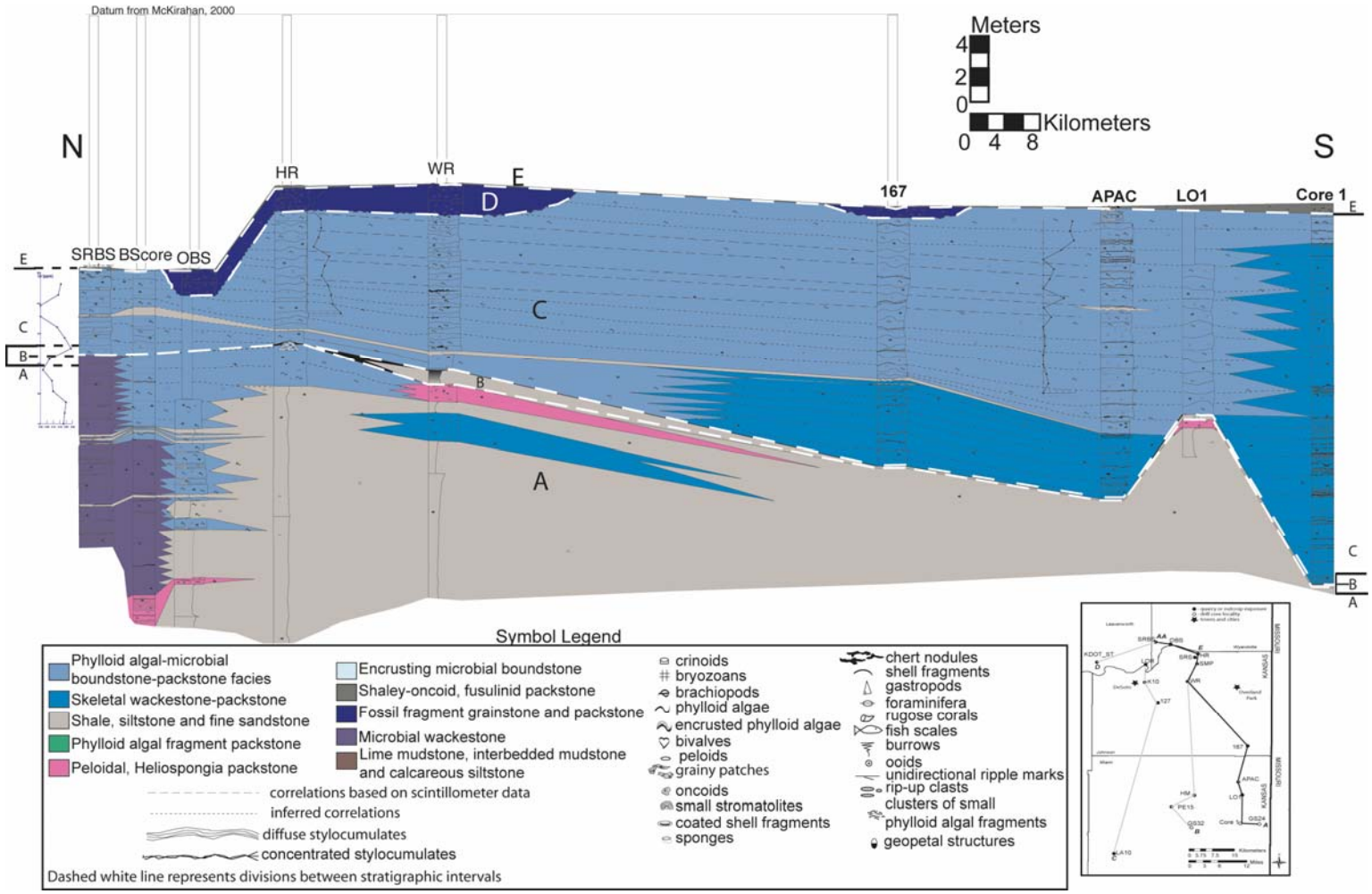

Figure 2.24: Reconstructed Cross-Section along Line AA-A.

(Index map shows location of cross-section in the field area. Scintillometer profiles of the maximum potassium value measured at several of the localities are graphed next to the corresponding measured section and are used correlate between measured sections where applicable.)

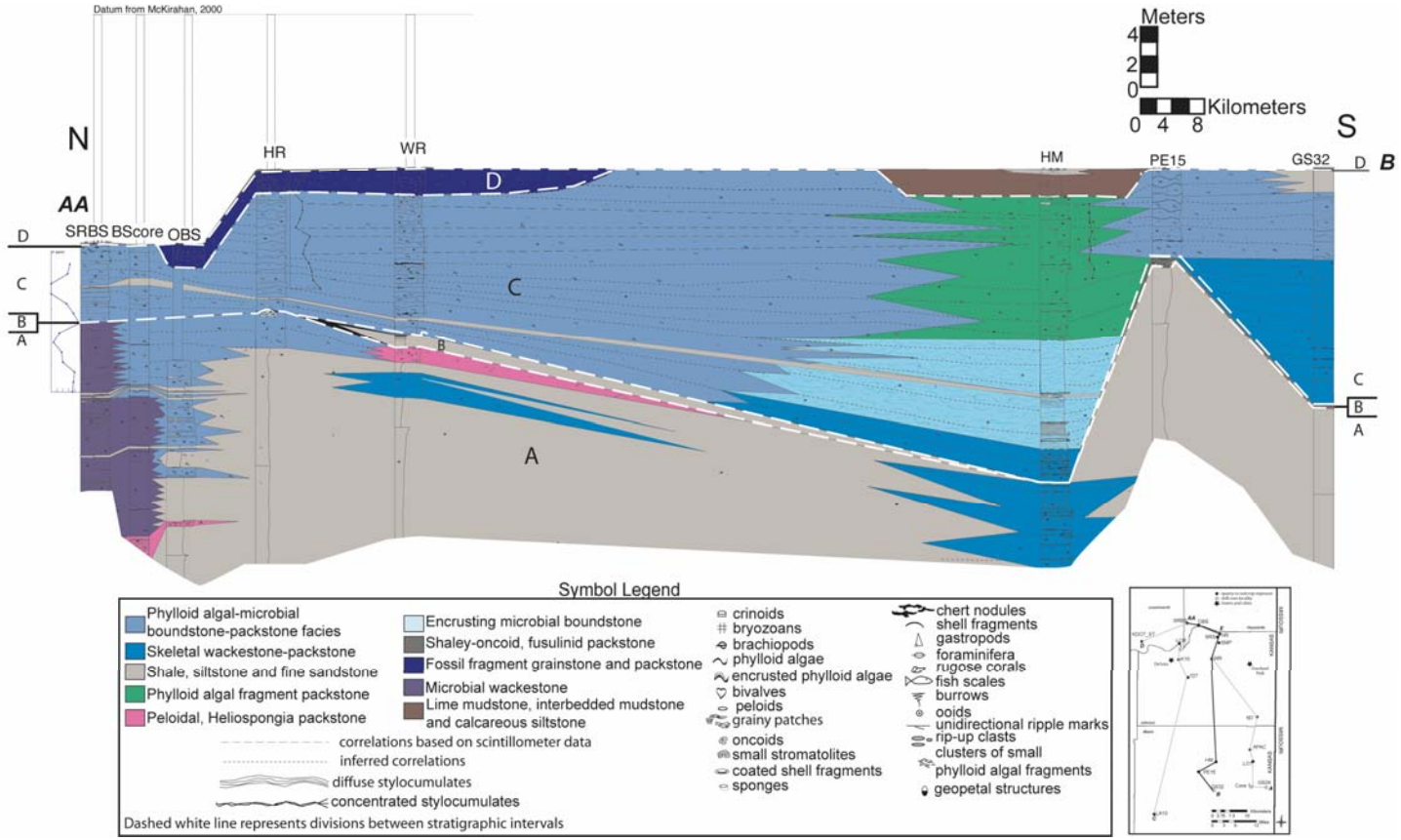

Figure 2.25: Reconstructed Cross-Section along Line AA-B

(Index map shows location of cross-section in the field area. Scintillometer profiles of the maximum potassium value measured at several of the localities are graphed next to the corresponding measured section and are used correlate between measured sections where applicable.)

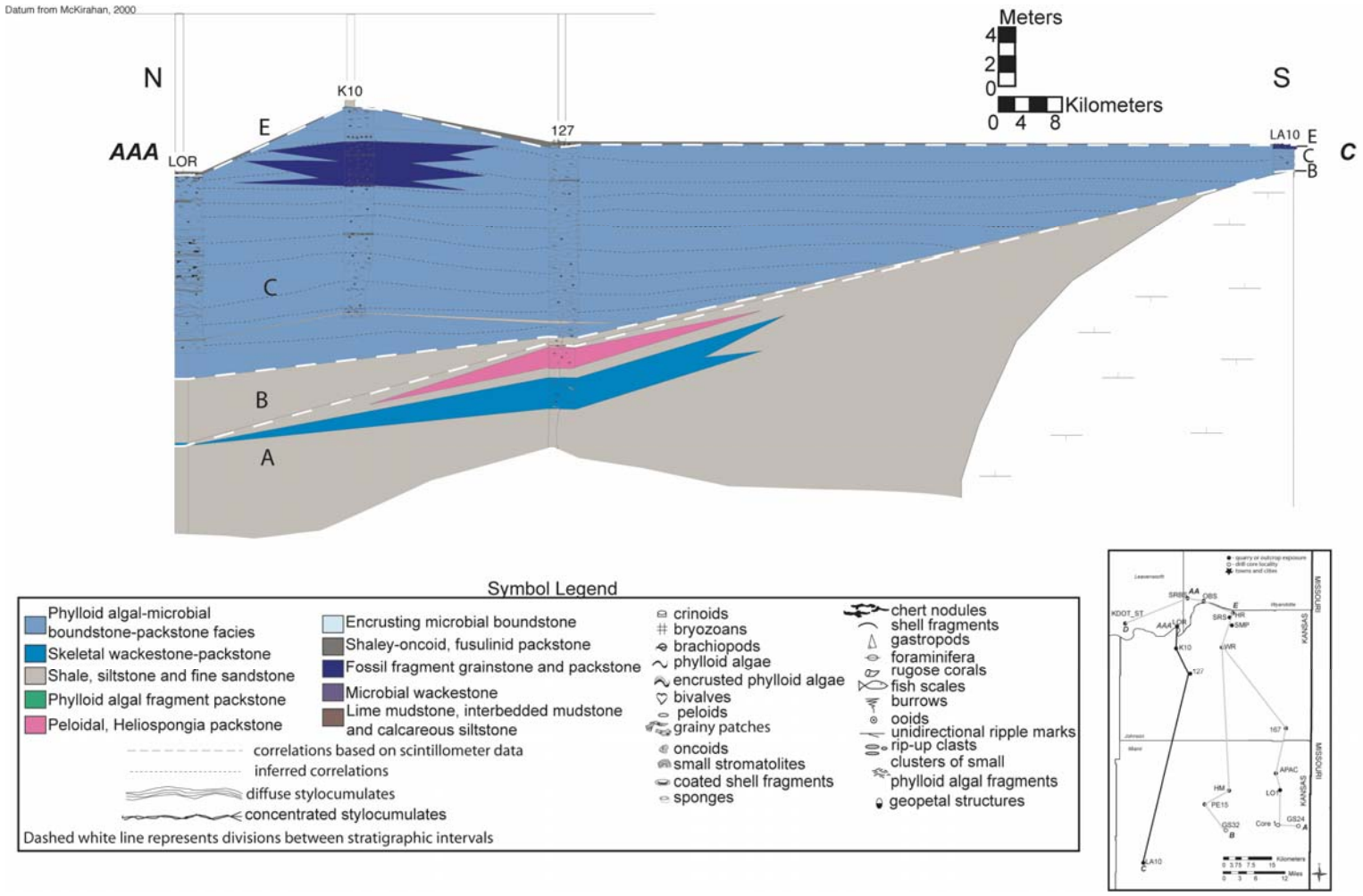

Figure 2.26: Reconstructed Cross-Section Along Line AAA-C
(Index map shows location of cross-section in the field area.)

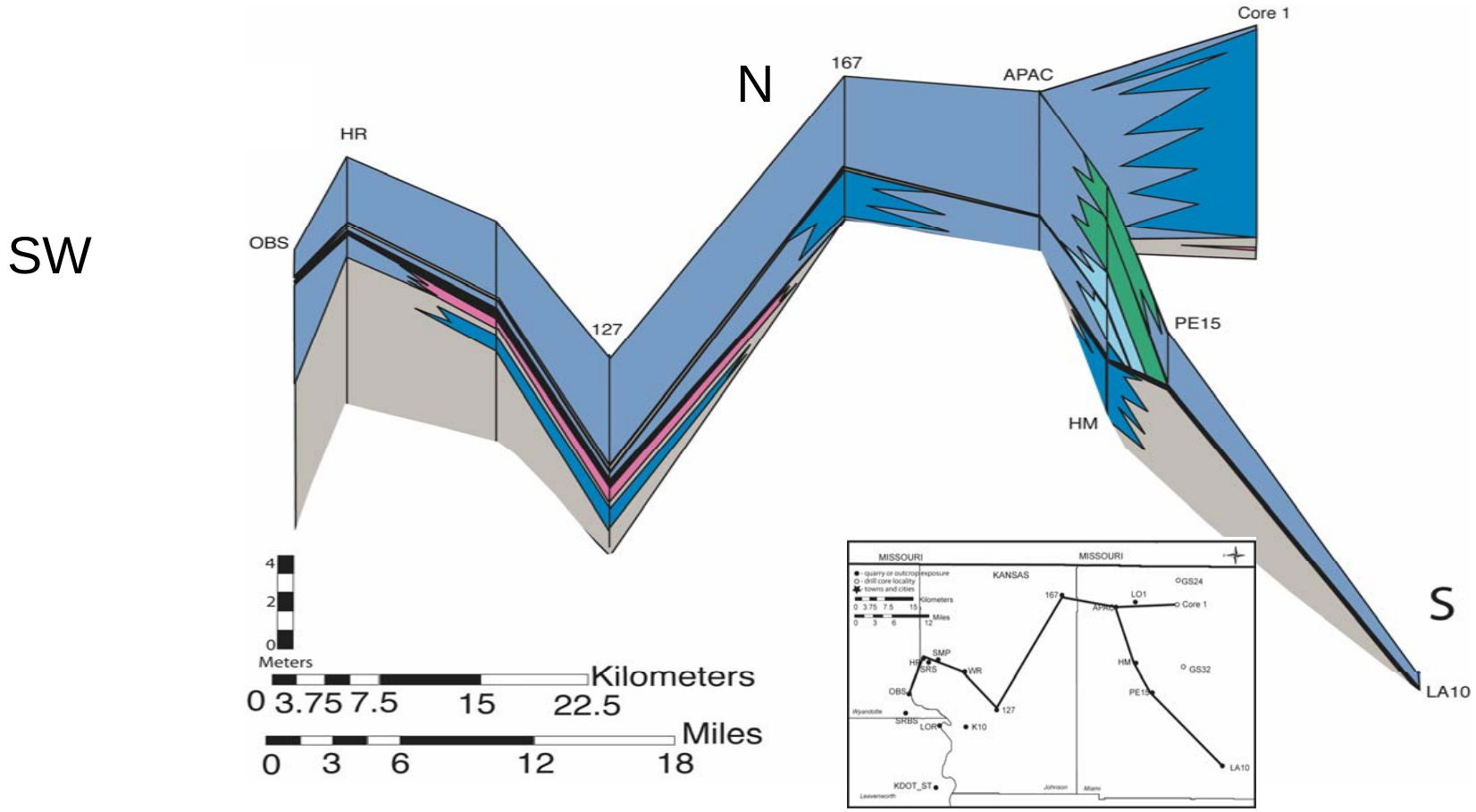

Figure 2.27: Fence Diagram Viewed from the West Showing Stratigraphic Correlations in Three Dimensions
(See Figures 2.24 to 2.26 for facies colors.)

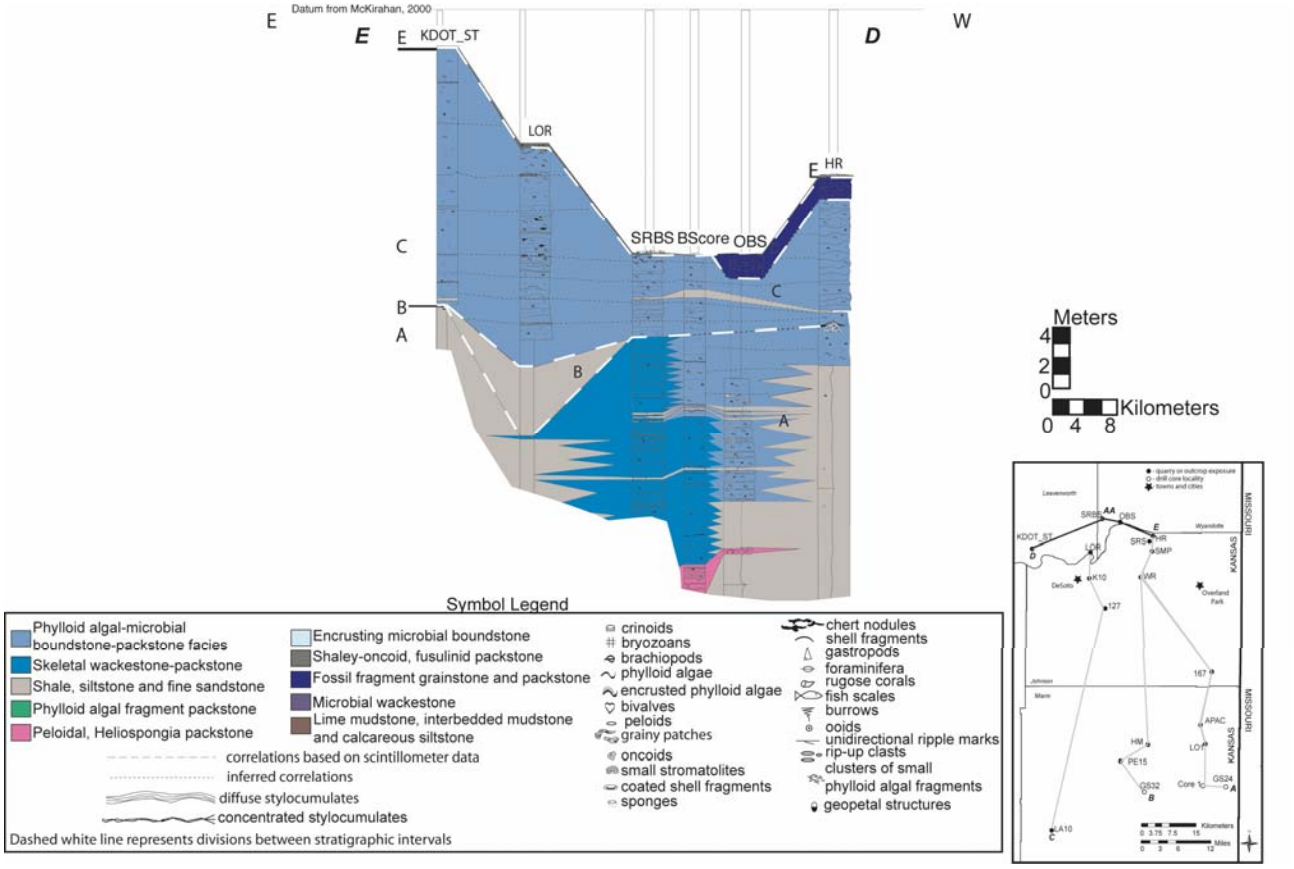

Figure 2.28: Reconstructed East-West Cross-Section from E to D in the Northern Part of Johnson County
(Index map shows location of cross-section in the field area.)

2.5.1 Stratigraphic Interval A – Liberty Memorial Shale-Frisbie-Lower Argentine Interval

The lowermost unit is defined as all of those strata deposited before the Quindaro Shale. It includes the Liberty Memorial Shale, Frisbie Limestone and parts of the lower Argentine Limestone. The Liberty Memorial Shale underlies the Argentine Limestone everywhere in the field area except for the extreme southwest corner of Miami County, where it pinches out against a high in the underlying Raytown Limestone Member of the Iola Formation (Olszewski, 1996). This high in the Raytown Limestone has been interpreted as a phylloid algal mound complex that built significant paleotopography (Olszewski, 1996). The Liberty Memorial Shale consists of the shale, siltstone and fine sandstone facies and was deposited during a time of relatively low sea level, bringing prodeltaic sediments onto the Raytown carbonates (Olszewski, 1996). An isopach map of the Liberty Memorial Shale shows two separate "lobes" of shale, which likely represent deposition from two distinct sources (Figure 2.29). The southern "lobe" of the Liberty Memorial Shale ranges in thickness from 20.0 m (65.7 feet) in extreme eastern Miami County to 0 m (0 feet) in extreme southwestern Miami County and eastern Franklin County. It is elongate in an east-west direction and thins to the west, suggesting a source from the east. The northern "lobe" ranges in thickness from 13.7 m (45 feet) near the Shawnee Rock Bonner Springs quarry and thins south and west to 0 m (0feet) in the extreme southwestern corner of Johnson County. It is elongated in an east-west direction and thins to the west, suggesting another source to the east.

In the northwestern part of the study area (northern Johnson County) carbonates of the Frisbie Limestone and lower Argentine Limestone are interstratified with shale and siltstone identical in lithology to the Liberty Memorial Shale. Locally, at the OBS locality a lateral facies change occurs with a 2-3 m thick wedge of shale/siltstone laterally grading into the carbonate

lithology. Within the shale-siltstone wedge, lenses of carbonate pinch out indicating a true lateral facies change (Figure 2.30). On the outcrop scale, the shale and siltstone facies in the south changes to phylloid algal and possibly microbial facies to the north indicating that the carbonate strata of the Frisbie Limestone and lower Argentine Limestone are time-equivalent to parts of the Liberty Memorial Shale (Figures 2.24 and 2.25).

This relationship indicates that the phylloid algal-microbial boundstone-packstone facies, peloidal *Heliospongia* packstone facies and microbial wackestone facies form at approximately the same water depth as the shale, siltstone and fine sandstone facies, but in areas of clearer water, away from the zone of dispersal of siliciclastic sediments. If anything, decompacting the shale (which would be decompacted more than the limestone) would indicate deposition of the carbonates in slightly deeper water than the shale. The phylloid algal-microbial boundstone-packstone facies may be a facies forming best in areas of high sediment flux, abnormal salinity, and increased nutrients where the environment is not optimal for other more normal marine carbonates to form. Conditions that vary somewhat from normal marine, but that are not extremely restricted are often optimal sites for microbial carbonates to form (Riding, 2000; Dupraz e al, 2004, Arp, 2003). Although localized, meter-scale mounding is known in this facies (Coyle and Evans, 1987; Samankassou and West, 2002); overall, there is no indication of significant buildup or mounding of carbonate facies in Stratigraphic interval A. (Figure 2.24, 2.25 and 2.27). The interpretation of low sea-level for Stratigraphic interval A is consistent with Heckel's (1986) sea-level curve for the units below the Quindaro Shale interval.

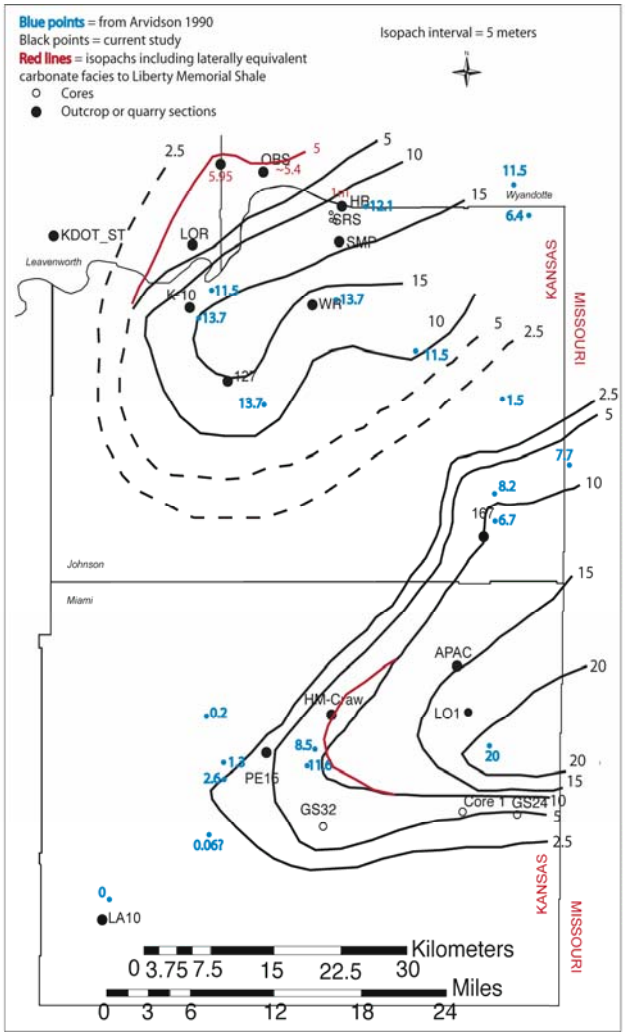

Figure 2.29: Isopach Map of Stratigraphic Interval A

[This figure includes the Liberty Memorial Shale and laterally-equivalent "lower Argentine" carbonates. Black isopachs are only for the Liberty Memorial Shale. Red isopachs are for the Liberty Memorial Shale and time-equivalent carbonates drawn on the basis of data from this project and data referenced in Arvidson (1990).]

Figure 2.30: Outcrop Photo Showing a Lens Shaped Bed in the Frisbie at OBS that is Pinching Out within Siltstone Lithology Identical to the Liberty Memorial Shale at this Locality

(Note the siltstone beds interbedded with more continuous beds of limestone as well.)

2.5.2 Stratigraphic Interval B – Quindaro Shale

The Quindaro Shale is a core shale (Heckel and Basemann, 1975), but not a typical one. The Quindaro Shale-equivalent interval in northeastern Kansas has been somewhat ill-defined in the past (Crowley, 1969) but is critical to understanding the stratigraphy in this area. Previous studies (Crowley, 1969; Arvidson, 1990) assumed that the Quindaro Shale underlies the Argentine Limestone, but more detailed work for this study calls this into question in several areas. At the Holliday Road locality (locality HR) the Quindaro Shale is a black, fissile, unfossiliferous shale that thins as traced over a small phylloid algal mound in the Frisbie Limestone. It grades laterally from black shale to grey, platy shale and back to black shale as it is

traced over the approximately 50 centimeters of positive relief above the small phylloid algal mound of the Frisbie Limestone. The Quindaro Shale is not as enriched in uranium as are most core shales (Watney et al, 1989). It is, however, enriched in uranium relative to surrounding units and is identifiable as a uranium peak in spectral gamma radiation measurements (Emry, 2005; Figure 2.24, 2.25).

Spectral gamma radiation measurements prove useful in locating the Quindaro Shale interval in northwestern Johnson County, where the dark shale is not present. At the Bonner Springs quarry, a significant gamma ray peak locates the Quindaro Shale interval 2.4 meters (7.8 feet) below the upper surface of the Argentine Limestone (Figure 2.24). Even though there is little lithologic evidence for the location of the Quindaro Shale inside this quarry, at an outcrop just outside of the quarry an irregular surface is present approximately 2.5 meters below the top of the Argentine Limestone, which coincides with the position of the uranium spike seen inside the quarry (Figure 2.31).

Figure 2.31: Photograph Showing Location of Quindaro-Equivalent Surface at the OBS Locality Marked by the White Arrow
(1.78 meter biologist for scale.)

This irregular surface (one-cm relief) is covered by a thin veneer of fossil fragments containing abraded fusulinids, brachiopods, bryozoans, crinoids, echinoids, and trilobites. Some of the larger fossil fragments exhibit mm-scale pores that resemble borings. The several millimeters below the surface commonly exhibit a reddish orange stain. The features associated with the surface are often characteristic of condensed sections or hardgrounds (Wilson, 1975; Olszewski and Patzkowsky, 2003).

In Miami County there is a paucity of lithologic data to help identify the stratigraphic position of the Quindaro Shale. Instead, the location of the Quindaro Shale is established from previous studies by Arvidson (1990), Von Bitter and Heckel (1978), Heckel and Baseman (1975) and Mitchell (1981), which showed that the Quindaro Shale is characterized by a recognizable specific conodont assemblage. A diverse conodont assemblage containing certain deep-water species is characteristic of core shales in Heckel's cyclothem model (Heckel and Baseman, 1975,

Bisnett and Heckel, 1996). The Quindaro Shale interval in Miami County contains one of the conodont species characteristic of deeper water and has a relatively diverse conodont assemblage. However, Heckel and Baseman (1975) note that the Quindaro Shale is missing the deepest water species and is somewhat lower in diversity than other core shales. Heckel refers to the Quindaro Shale-equivalent interval as a "phantom black shale". Along with the conodont data, at location PE15 the Quindaro Shale interval is identified by a 3cm-thick fossiliferous packstone consisting of fragmented and abraded foraminifera, crinoids, echinoids, bryozoans, and serpulid worm tubes in a silty shale matrix.

On the basis of the features described, the Quindaro Shale and equivalent interval formed in water deeper than in underlying strata of Interval A. Thus, the Quindaro Shale interval is interpreted to result from a relative sea-level rise, which is supported by Heckel (1986) and Boardman and Heckel (1989) who interpreted an eustatic sea-level rise during this time. This study also suggests that the Quindaro Shale interval may not have been formed in water as deep as that interpreted for other cyclothem units that contain more typical black core shales.

2.5.3 Stratigraphic interval C—"Middle"Argentine Limestone Interval

The Middle Argentine Limestone interval consists of all strata above the Quindaro Shale interval and below an erosional surface that occurs near the top of the Argentine Limestone. Where the erosion surface cannot be recognized the top of the interval locally can be recognized as the contact between the various facies of the Argentine Limestone below and a thin bed of shaley, oncoid, fusulinid packstone above (localities APAC, LO1 and Core1 in Figure 2.24 and locality PE15 in Figure 2.25, localities LOR, K10, and 127 in Figure 2.26) The base of Stratigraphic interval C marks the establishment of carbonate deposition throughout the field area.

In eastern and northern Johnson County the lowermost deposits of this interval consist of phylloid algal-microbial boundstone-packstone. These were deposited on the flanks and top of the northern lobe of the Liberty Memorial Shale (localities SRBS, BSCore, OBS and HR in Figures 2.24 and 2.25; localities KDOT_ST, LOR, SRBS, BSCore, OBS and HR in Figure 2.28). This facies indicates that normal marine conditions within the photic zone were established throughout the northern part of the field area.

In southeastern Johnson County (between localities WR and 167 (Figure 2.24) the lowermost strata of Stratigraphic interval C thicken and undergo a facies change to skeletal wackestone-packstone. This facies change likely resulted from a transition to deeper water due to the original depositional slope. Farther south, this interval thins between localities 167 and APAC, likely onlapping preexisting relief on the southern lobe of the Liberty Memorial Shale (centered at locality LO1; Figure 2.24). Similar, likely time-equivalent skeletal wackestone-packstone was deposited on the south side of this lobe and also appears to onlap it.

For strata immediately above the lowermost parts of Stratigraphic interval C, a north-to-south facies change can be identified. To the north, phylloid algal-microbial boundstone-packstone is most common (localities SRBS, BScore, OBS, HR, WR; Figures 2.24, 2.25 and 2.27). To the south it changes facies to skeletal wackestone-packstone, encrusting microbial boundstone, and phylloid algal fragment packstone (localities 167, APAC, and HM; Figures 2.24, 2.25 and 2.27). The north-to-south transition in facies is consistent with southward deepening, but farther south, the facies appear to onlap a high on the southern lobe of the Liberty Memorial Shale (localities LO1 and PE15; Figures 2.24, 2.25 and 2.27).

Local topography around this lobe affected facies distributions. The HM locality contains encrusting microbial boundstone facies. As this locality is west of the thickest part of

the lobe, it was likely in deeper water than the APAC locality to the east, where the lobe is almost at its thickest. The sparse macroorganisms present in this facies indicate a marine environment, but the dominance of microbial textures suggests that there may have been an imbalance of nutrients, restriction, or change in alkalinity away from normal marine conditions. This modification of water quality was likely induced by the many paleotopographic high areas around HM, with lobes of the Liberty Memorial Shale to the north and south (Figures 2.25 and 2.27) and a paleotopographic high on the Raytown Limestone to the west (Figures 2.26, 2.27).

Towards the top of Stratigraphic interval C, phylloid algal-microbial boundstone-packstone facies was deposited in all localities but HM and K10 (Figures 2.25, 2.26). The upward transition to this facies is consistent with shoaling during deposition of Interval C. In some areas, the phylloid algal-microbial boundstone-packstone facies appears to onlap or thin on paleotopographic highs (localities LA10, PE15, HR, WR, LO1; Figures 2.24, 2.25 and 2.27). For the most part, however, facies are laterally consistent and thicknesses do not change much indicating that most of the paleotopographic relief had been filled. Clearly, this facies is not generating mounds, nor is it forming preferentially on highs, as has been previously inferred (Heckel and Cocke, 1969; Crowley, 1969; Arvidson, 1990; Cunningham and Franseen, 1992, and McKirahan, 2003)

Evidence indicates that the reason this facies in not forming mounds, and is instead filling paleotopographic lows rather than building on paleotopographic highs, is that there is an accommodation limitation. The K10 locality, which was located on the crest of the northern Liberty Memorial Shale lobe, likely represented a remnant high where shallow water, higher energy grainy sediments accumulated (Figure 2.26). At the Loring (LOR) and Bonner Springs (BS, BSCore and OBS) sites located on the flanks of the lobe the uppermost beds of the phylloid

algal-microbial boundstone-packstone facies contain evidence of deposition under a higher energy regime (Figure 2.28). Fragmented phylloid algal remains and discontinuous patches of grainy sediments similar to the sediments deposited at K10 are found at these two localities. It is likely that these grainy sediments were swept off the paleohigh into the deposits flanking the now significantly subdued Liberty Memorial Shale paleohigh. This indicates that the highest areas were indeed subjected to currents, and offers support for accommodation limitation for the entire interval. Previous studies have documented that phylloid algae can preferentially form on paleotopographic highs and produce sediment that is then swept off of the highs and accumulates in lows (Matheny and Longman, 1996). Ball et al. (1977) suggested that phylloid algae did not construct topography but instead were only a source of sediment.

The one locality that is different than the others is locality HM in Miami County, where Stratigraphic interval C passes upward from encrusting microbial boundstone to phylloid algal fragment packstone, lime mudstone, and interbedded mudstone and calcareous siltstone facies (Figure 2.25). As previously mentioned, this locality was in a paleotopographic low area during initial deposition of Stratigraphic interval C. It likely remained restricted by surrounding highs during further sedimentation of the interval. The upward facies transitions are consistent with continuation of the paleotopographically low position and restriction, with phylloid algae being swept off of surrounding highs and into the lows.

The interpretation of stratigraphic interval C forming during a relative fall in sea level is consistent with Heckel's sea-level curve for the units directly above the Quindaro Shale interval (Stratigraphic interval B) (1986).

2.5.4 Stratigraphic Interval D—"Top of the Argentine" Interval

This interval consists of facies deposited at and just below the top of the Argentine Limestone. In the northern part of the study area, it consists of fossil fragment grainstone-

packstone facies overlain by shaley oncoidal packstone (localities OBS, HR, WR, 167 in Figure 2.24). In locality HM, it consists of lime mudstone, interbedded mudstone and calcareous siltstone facies. Where Stratigraphic interval D is present, it is underlain by an erosional surface in all areas with the exception of HM. In Stratigraphic interval D, fossil fragment grainstone-packstone consist of interstratified subfacies that record changes in the energy regime.

The erosion surface at the base of the interval has approximately as much as 1.5 meters of erosional relief. In locality SRS (Figure 2.32), the erosion surface has a symmetrical cross section similar to that which would be expected for a channel. The three-dimensional morphology that would confirm a channel origin, however, cannot be discriminated because of the lack of appropriate outcrop. The surface is overlain by an apparent lag deposit consisting of clasts of the underlying phylloid algal lithology as well as clasts of the lime mudstone and skeletal wackestone-packstone facies, clearly indicating local erosion as well as distant transport of clasts. The deposition of phylloid algal facies at the top of Stratigraphic interval C, would not have produced enough shoaling to increase the energy regime enough to induce erosion as this facies appears to have been deposited in slightly deeper, low energy waters. Therefore the increase in energy necessary to erode, transport and deposit the clasts in the lag deposit indicates a relative fall in sea level after Stratigraphic interval C.

In areas to the north, the lowermost subfacies of the fossil fragment grainstone/packstone facies is characterized by the abundance of "*osagia*-type" coated oncoidal grains, clasts of the underlying phylloid algal lithology, and a high percentage (15-20%) of siliciclastic sand and silt (localities HR, Top1, Top2, Brach and SMP in Figure 2.30). The next subfacies records an upward transition with coarse-grained, poorly sorted, coated, fossil-fragment grainstone at the base, and finer-grained, dominantly peloidal packstone-grainstone with significant amounts of

micritic matrix, phylloid algal fragments or a *Composita* brachiopod packstone at the top. This transition records a decrease in energy during deposition necessary to prevent the micritic matrix from being winnowed away. The uppermost subfacies is underlain by an erosion surface that has 1.5 m of relief locally (Figure 2.32). The three-dimensional morphology of the erosional surface is unclear. This unit contains ooids and has westward-oriented cross beds internally and similarly oriented asymmetric megaripples on its upper surface.

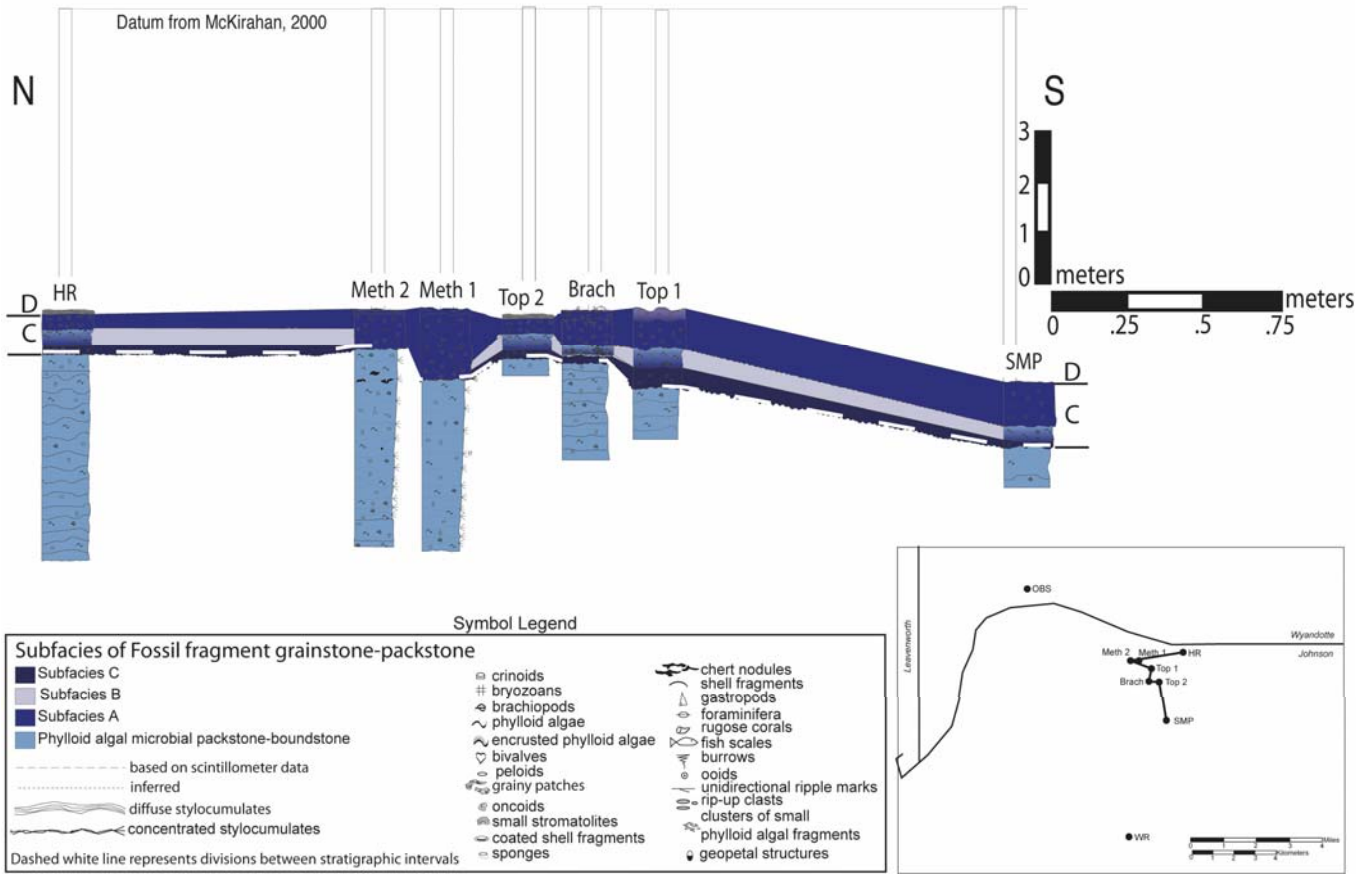

Figure 2.32: Reconstructed Stratigraphic Section of the Top of Stratigraphic Interval C and Stratigraphic Interval D from the SRS Locality within the Johnson County Landfill

The WR locality contains the most ooid-rich and mud-poor example of this subfacies. In this locality, grains are well-sorted and most ooids have not been micritized. The uppermost bed is 1-10 cm of shaley, oncoidal, fusulinid packstone and represents the increased dominance of siliciclastic sedimentation.

The association of carbonate grains and detrital siliciclastics indicates that the fossil fragment packstone-grainstone facies as a whole was deposited relatively close to a terrigenous source. Clasts of local and exotic lithology indicate significant transport. These three subfacies are similar to mixed carbonate-siliciclastic facies in the overlying Farley Limestone (McKirahan, 2003; Harris, 1984). The fossil fragment packstone-grainstone facies as a whole indicates possible channelization, westward-oriented currents, a siliciclastic source, and fluctuating energy regimes that vary laterally and vertically. Facies could be distributed in a complex facies mosaic. In tidal delta systems, it is common to have a mosaic of grain shoals and bars associated with localized protected environments of lower energy (Jindrich, 1969). The subfacies of the fossil fragment packstone-grainstone facies resemble deposits formed on the crests of modern tidal bars in Schooner Cay in the Bahamas. The bars themselves consist of cross-bedded, relatively well-sorted, oolitic sands similar to the third subfacies (Ball, 1976). The first and second subfacies are similar to the lower energy, commonly burrowed, generally less well-sorted, skeletal, peloidal deposits found off of the bar crests (Ball, 1976). A complex mosaic of tidal bars and lower energy areas is the most likely explanation. Previous studies have determined that land was located to the east and possibly southeast (Watney et al. 1989) resulting in tidal currents that likely flowed from the west (offshore) to the east (onshore). Tidal currents that are ebb dominated are indicated by westward oriented current structures.

The overlying shaley, oncoid fusulinid packstone facies could indicate progradation of a siliciclastic tidal delta system into the carbonate-dominant tidal bar belt, resulting in a change in water quality due to the influx of siliciclastics and possibly nutrients derived from the hinterland. This change in water quality could have allowed more siliciclastic and nutrient tolerant microbes to flourish resulting in the preponderance of microbially coated grains found in this facies.

At locality HM, the interbedded mudstone and calcareous siltstone facies, is interpreted to have resulted from deposition in a very restricted environment where all but the most opportunistic organisms, such as sponges, could survive. This extreme restriction was likely caused by the same relative fall in sea level that caused higher energy conditions to the north. Facies characteristics resulted from the paleotopography present in this locality, with the subdued, but still present, paleotopographic low at this locality inducing restriction.

Overlying Stratigraphic interval D are deltaic, prodeltaic and paleosol-altered siliciclastics of the Lane-Island Creek Shales, which represent continued progradation of siliciclastics into the system and sea-level fall. Heckel interpreted a fall in sea-level with the beginning of deposition of the overlying Lane-Island Creek Shales (1986), but my study indicates that the fall likely began somewhat earlier as indicated by the erosion illustrated at the base of Stratigraphic interval D.

2.6 Discussion

The data show that there are two lobate accumulations in the Liberty Memorial Shale, one to the North and one to the South, with both thinning to the west.-southwest. It is interesting that there are also two lobate forms in the overlying Lane-Island Creek Shales, one to the north and one to the south (McKirahan, 2000). Although the distribution of the lobes in the two units is not

identical, the repeated occurrence of northern and southern delta lobes suggests that sediment distribution may have been controlled by long-lived drainage systems in the hinterland.

The phylloid algal microbial packstone-boundstone and digitate microbial facies in Stratigraphic interval A appear to have formed synchronously with deposition of the Liberty Memorial Shale, on the north-northwest side of the northern lobe. At these localities, the facies containing phylloid and other calcareous algae presumably formed in the photic zone. The presence of stenohaline organisms points to a normal marine environment, but the dominance of microbial textures indicates that the water must have varied from normal marine perhaps by an increase of nutrients coming off of land. This is consistent with the stratigraphic setting indicating that these facies are time-equivalent to deltaic deposition and just off of the locus of siliclastic deposition.

To the south, just north of the southern Liberty Memorial lobe, carbonate facies representing deeper water are found (peloidal *Heliospongia* packstone; skeletal wackestone-packstone), providing evidence for some southward deepening. This area of carbonate deposition, between two delta lobes is best characterized as an interdistibutary bay. Interdistributary bays are restricted environments, characterized by the lack of river or tidal currents and are also largely protected from wave energy (Reineck and Singh, 1980). Apparently, this restriction, combined with a slightly deeper setting led to deposition of *Heliospongia* and oncoids. The skeletal wackestone-packstones formed during times of more normal marine conditions in the embayment.

Interval B is present as shales, packstones, or possible omission surfaces that formed after a rise in sea level that, although large, was not high enough to have produced the black shale lithology and the deepest water conodont assemblages seen in other cyclothem core shales

(Heckel, 1986; Heckel and Baseman, 1975, Bisnett and Heckel, 1996). The Quindaro Shale is generally a sparsely fossiliferous grey shale, but has one enigmatic occurrence of black shale lithology at the HR locality. Heckel (1977) suggested that Pennsylvanian black shales were formed by high primary productivity and oxygen depletion that occurred in restricted lows or deeper water after a rise in sea level. This explanation works well for other geographically widespread lithologically monotonous Pennsylvanian black shales, but the Quindaro Shale is problematic because the black shale lithology occurs preferentially on top of the northern lobe of the Liberty Memorial Shale and transitions to gray shale to the north and to the south into deeper water (Figures 2.24, 2.25). On the northern lobe, there is a locality with a local mound in the Frisbie Limestone. In that locality the shale transitions to a gray color only on the top of the mound. It appears that the black shale formed in one of the shallower water areas after a relative sea-level rise instead of preferentially in the deeper areas. In their review of depositional mechanisms and environments of black shales, Arthur and Sageman (1994) showed that black shales can form at the mouths of estuarine systems where excessive nutrients and terrestrially-derived organic carbon are delivered and where water is deep enough to maintain anoxic bottom conditions. Such a setting might be the best explanation for the characteristics of the Quindaro Shale. After a rise in sea level, the drainage system in the hinterland would still deliver nutrients to the location of the northern lobe of the Liberty Memorial Shale. The shallower the water in this area of nutrient delivery, the greater the likelihood of bottom oxygenation. These factors taken together are sufficient to explain the characteristics observed in the Quindaro Shale. Quindaro Shale characteristics are inconsistent with black shale forming only in the deepest water, in a simple oxygen stratified system, or from upwelling.

In Interval C carbonate deposition was established after a relative fall in sea level. In the south skeletal wackestone-packstone deposits indicate that a normal marine environment was established. Phylloid algal deposits to the north indicate shallower water that to the south, where the environment was clearly in the photic zone, and nutrient levels may have remained high as suggested by the microbial component of carbonates found on or flanking topographic highs (localities HR, WR, LO1 Figure 2.24, 2.25) and those found in the lows (localities 167, APAC Figure 2.24, 2.25).

Phylloid algae are common constituents of Pennsylvanian and Permian rocks and after over seventy years of intensive study, there is still debate about what exactly Pennsylvanian and Permian phylloid algae are (Moore, 1935, Johnson, 1946, Wray, 1968, Baars and Torres; Maybury and Evans, 1994). Phylloid algal deposits have been associated most frequently with the construction of mounds or bioherms, commonly rooted on paleotopographic highs. (Heckel and Cocke, 1969; Crowley, 1969; Toomey, 1977; Wray, 1962; Pray and Wray, 1977; Cys, 1985; Doherty et al, 2002). Phylloid algal mounds or mound complexes have been described from a variety of Pennsylvanian-Early Permian localities such as the Paradox basin (Weber et al, 1995), and the Sierra de Cuera and Cantabrian mountains in Spain (Della Porta et al, 2002; DellaPorta, 2004). My study demonstrates phylloid algal deposits can also fill topographically low areas on the sea floor. This is not an entirely new idea, as previous studies have documented that phylloid algae can preferentially grow on paleotopographic highs and be swept off of those highs to accumulate in lows (Matheny and Longman, 1996). Ball et al. (1977) even suggested that phylloid algae did not construct topography at all but instead were only a source of sediment. In their study of the Farley Limestone and associated strata in the same general field area as mine, McKirahan el al. (2000) also demonstrated that phylloid algae collect in paleotopographic lows.

The Argentine Limestone is an example of phylloid algal facies occurring in paleotopographic lows. Some of the phylloid algae show evidence of transport having been broken up and sorted. Others appear to construct small, meter-scale, localized phylloid algal mounds that seem to have formed in the lows; these are interstratified with phylloid algal fragments presumably transported in from surrounding highs. Although these small phylloid algal mounds built small-scale relief on the order of a couple of meters, the relief became subdued with further preferred deposition in surrounding low areas. Thus, although it is apparent that the sediment in the Argentine Limestone is capable of building mounds, the Argentine Limestone is dominated by the filling of topography as opposed to building it. This study suggests that the most important control on whether phylloid algal facies build or fill relief is not the organisms themselves, but rather it is the available accommodation. In cases where base level is rising, one might expect mounds to form, some of which may form preferentially on the highs. In cases in which sea level is low and stable, or falling, as is the case for the Argentine Limestone phylloid algal facies fill available accommodation. In these scenarios of low or falling sea-level, high areas are above base level and phylloid algal sediment is swept off and resedimented into lows. Low areas may continue to be sites of in situ phylloid algal deposition, but depostion and permanent accumulation cannot continue above base level.

The HM locality represents a unique restricted microenvironment. It was an area that remained a low throughout the deposition of Stratigraphic interval C and accumulated facies that were very different from nearby localities. The encrusting microbial boundstone represents the extreme of restriction, likely formed by non-photosynthetic microbes that may have induced the precipitation of calcite in and on the extracellular polymeric substance that coats the bacteria and sediment surfaces (Riding, 2000, Dupraz et al., 2004). This process yielded the micropeloidal

and microspar structures found in the encrusting microbial boundstone facies. This facies persisted in filling the low until phylloid algae became established on the southern lobe of the Liberty Memorial Shale providing sediment that could be washed off into the low.

Before deposition of Stratigraphic Interval D, much of the paleotopography had been subdued by filling in the lows, leading to a relatively low-relief surface, likely filled to the base level for the phylloid algal deposits. A relative fall in sea level is necessary to induce the erosion at the base of Interval D to the north and to induce restriction in the preserved low area at locality HM to the south. At this point in the depositional history, a complex facies mosaic of environments was established. The environments were affected by ebb dominated tidal currents (for reasons discussed earlier). No relative change in sea level is necessary for the increase in siliciclastics. Simple progradation may be all that is called for, culminating in deposition of the Lane-Island Creek Shales (See McKirahan et al., 2003 for controls on the Lane-Island Creek Shales and Farley Limestone that continue the story of building and filling stratigraphically just above the interval of my study).

2.7 Conclusions

Pennsylvanian strata in the US Mid-continent were deposited in association with high-amplitude glacio-eustatic sea-level fluctuations. Many such sequences are thin and maintain similar thickness throughout wide geographic areas. The facies both build and fill relief. Many of those that fill relief are commonly, but incorrectly ascribed to carbonate mounding. Missourian strata were studied in a 3,670 km^2 area of eastern Kansas to evaluate the controls on build-and-fill architecture.

Nine lithofacies were described in association with the Argentine Limestone, Frisbie Limestone, Quindaro Shale and Liberty Memorial Shale: (1)Phylloid Algal-Microbial

Boundstone-Packstone (2) Skeletal Wackestone-Packstone, (3) Shale, Siltstone and Fine Sandstone (4) Lime Mudstone, Interbedded Mudstone and Calcareous Siltstone (5) Peloidal, *Heliospongia* Packstone (6) Encrusting Microbial Boundstone (7) Fossil Fragment Grainstone-Packstone (8) Shaley, Oncoid, Fusulinid Packstone (9) Microbial Mudstone-Wackestone. Lithofacies distributions and correlations were used to evaluate the controls on lithofacies distributions. Relative changes in sea level controlled the large-scale depositional architecture. Local factors such as accommodation and underlying paleotopography were the most important factors controlling which facies either built or filled depositional topography.

Lowermost strata are those of the Liberty Memorial Shale, which created lobate positive topography. Shale facies change laterally to phylloid algal and possible microbial carbonates, but no mound-like topography was built. A subsequent relative rise in sea level resulted in a condensed section. Phylloid algal and other carbonate facies were deposited after a minor relative fall in sea level. Strata were deposited preferentially in low areas, onlapping preexisting topography. Although these lithologies are typically ascribed to carbonate buildups, their distribution and stratal geometries in relation to paleotopography clearly indicate that they filled in low areas and subdued most of the original paleotopography. After a minor relative sea level fall subsequent erosion created variable topography on the upper surface of the Argentine Limestone, the highs of which were previously misidentified as constructional mounds in previous studies.

Results from this study show that the creation of relief in high-frequency glacioeustatic sequences can occur after falls in sea level, with deposition of lobate siliciclastics and erosion of preexisting strata. Intermediate sea-level positions after falls result in carbonate deposits which fill relief and even out topography. Understanding this mechanism of building and filling of

relief is paramount not only to understanding the nature of analogous petroleum reservoirs in the subsurface, but also to understanding these and similar deposits that are utilized as carbonate aggregate sources. Identifying lithologies that produce good aggregate and understanding how and where they form can help with quality control and aggregate resource exploration.

Chapter 3

Part II: A First-Cut Method for Evaluating Limestone Aggregate Durability Using Spectral Scintillometry

3.1 Introduction

Industrial demand for durable carbonate aggregate for state, county, and municipal projects is increasing in the United States. In Kansas, carbonate aggregate is an abundant resource that plays a significant role in the state's economy. KDOT has established a series of physical tests to determine aggregate durability, but a major drawback is that the tests take a minimum of six months to perform. There have also been concerns expressed about the practicability of applying these tests within a timeframe useful for preventing the incorporation of low durability aggregates in Portland cement highway pavements. Concerns about the use of limestone aggregate have led some Kansas municipalities to go so far as to legislate the use of hard rock aggregate from other states. These actions are taking money away from the local aggregate industry and the Kansas economy and increasing costs for municipal infrastructure projects. For example, in Kansas, the often quoted cost for repaving sections of highway made with substandard aggregate is approximately $1 million/mile (Robert Henthorne, personal comm., 2004). The quality control issues, the high demand for aggregate, and the costs associated with using poor quality aggregate are all factors illustrating a growing need for effective first-cut techniques to predict aggregate durability.

A previous K-TRAN research project K-TRAN: KU-97-1 focused on evaluating the factors that affect the quality of limestone aggregate. Factors such as rock type, fossil type, nature of the bedding, spar content, insoluble residue percent, and the presence of shale beds

were studied to delineate which factors had the greatest impact on aggregate quality. Detailed stratigraphic sections were measured at a cm scale emphasizing clay content and clay distribution in order to see if a relationship existed between clay content and KDOT test results for class 1 aggregate. Two important findings from this initial project provided the basis for the current project. The authors noted that a particular rock type, limestones with micritic matrices, tended to produce durable aggregate, and the clay content of the limestones was an important factor in aggregate durability. Matrix for this study is defined as tiny calcite crystals that are not visible with a 10x hand lens and are found between depositional grains and is synonymous with "micrite", a shortened version of Dunham's (1962) microcrystalline calcite.

The meticulous measurement of stratigraphic sections, however, is very time consuming and would require a significant amount of training for quarry operators to be able to implement. The authors determined that a faster first-cut method would be needed to evaluate aggregate durability. A spectral gamma ray logging tool was suggested as a possible first-cut tool to evaluate clay content in limestones. A spectral gamma ray scintillometer measures the amount of the three major sources of gamma radiation in rocks (potassium, uranium and thorium) along with the total gamma radiation. The justification behind using this tool is based on three observations:

1. Clay minerals have significantly higher potassium content than carbonates.
2. Clay minerals are often associated with organic material that fixes uranium.
3. Some clay minerals can absorb thorium (Doveton, 1994).

The authors hypothesized that using a spectral gamma ray scintillometer might be a reliable method to determine clay content and could, therefore, provide a first-cut tool that aids in aggregate quality control. The purpose of this project was to evaluate the validity of using a

spectral gamma ray scintillometer as a first-cut tool to evaluate limestone aggregate durability. The second part of this project was contingent on the first and involved developing a predictive model to evaluate limestone aggregate quality.

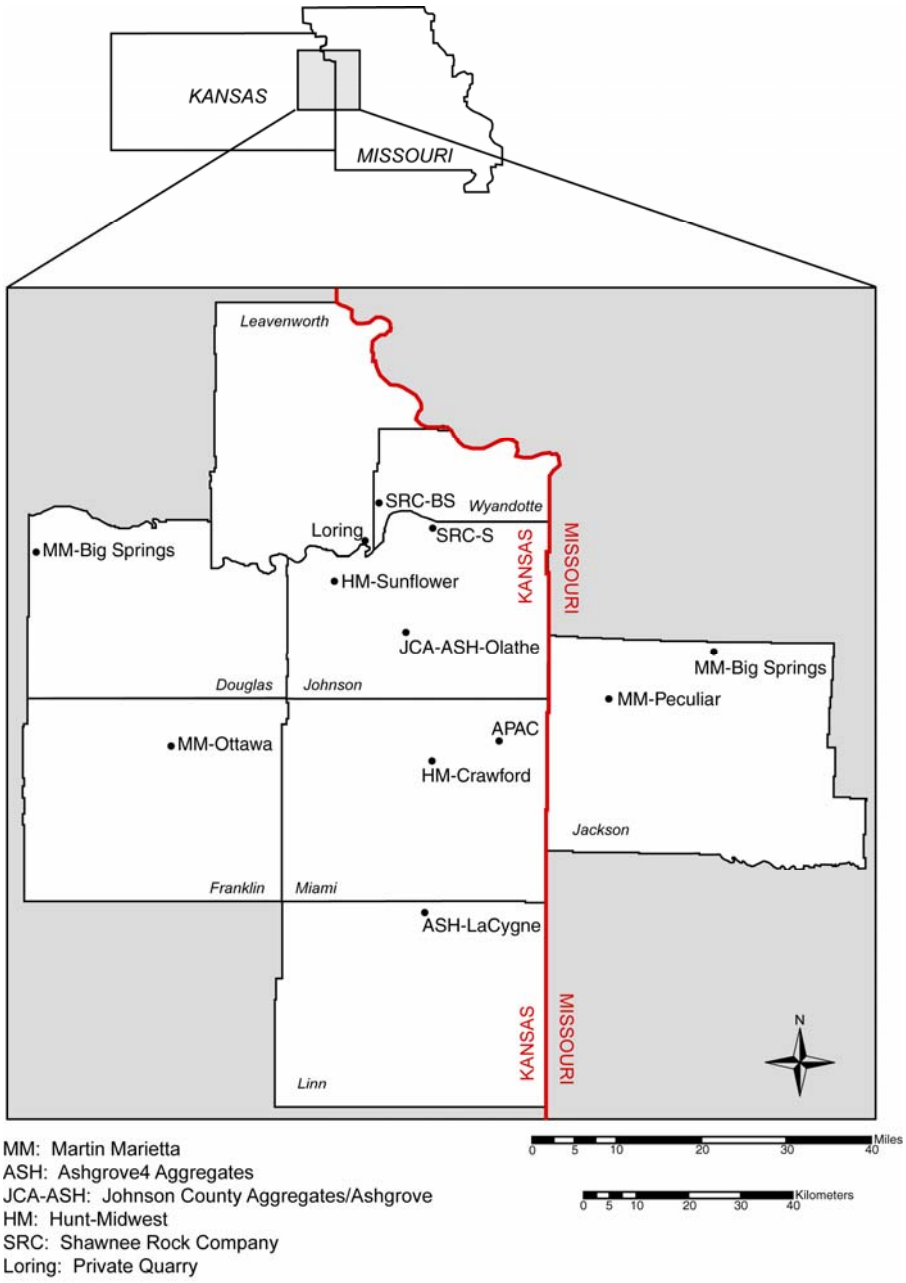

Figure 3.1: Index Map Showing Quarry Locations in Kansas and Missouri
(Multiple ledges were sampled at most of the locations)

3.2 Materials and Methods

The selection of sites for this study was based on three major criteria: location, accessibility, and whether the three major KDOT tests for establishing class 1 or 2 aggregate (Modified Freeze-thaw, Expansion, and Durability Factor) had been performed on the ledges. Quarries producing Pennsylvanian limestone aggregate in eastern Kansas and western Missouri were included in this study. This included quarries run by APAC Quarries, Shawnee Rock Company, Martin Marietta, Ashgrove Aggregates (Johnson County Aggregates), Hamm Quarries, Hunt-Midwest Quarries and one private, family-run quarry (Figure 3.1). Stratigraphic intervals (ledges) from ten different stratigraphic units were sampled including: the Argentine Limestone, Bethany Falls Limestone, Captain Creek Limestone, Ervine Creek Limestone, upper and lower Farley Limestone, Spring Hill Limestone, Stoner Limestone, South Bend Limestone, and Winterset Limestone. Multiple stratigraphic units were sampled in order to include as much lithologic variability as possible.

Quarries commonly remove and stockpile the shales that are interbedded with the limestones in order to access the limestone units for quarrying. During this process, very fine grained shale particles become airborne and often collect on the limestone ledges. Many of the shale units, particularly the black shales, are high in gamma radiation (Watney et. al, 1989), which could bias the readings of the gamma-ray scintillometer. Most of the quarries also actively crush limestone into aggregate-sized pieces creating a large amount of limestone dust that collects on the ledges and could bias the gamma-ray scintillometer readings for each individual ledge. Therefore, each ledge to be tested was cleaned with a powerwasher in order to remove the dust. A 2700 psi gasoline-powered powerwasher was used, supplied with water from a 50 gallon pressurized cement-mixer tank. The ledges were powerwashed for a maximum of

five minutes until most of the water running down the ledge was clear. After drying, each ledge was then marked with spray paint every 11.8 inches (30cm) from the base to top, or as far up as was safely accessible by ladder or lift-bucket (Figure 3.2). The 11.8 inch (30 cm) interval was chosen because the GF Instruments GRM 260 scintillometer has a sampling radius of 11.8 inches (Vit Gregor, personal comm., 2003), which would result in a relatively continuous measurement of the natural gamma radiation of the rock up the face of the ledge.

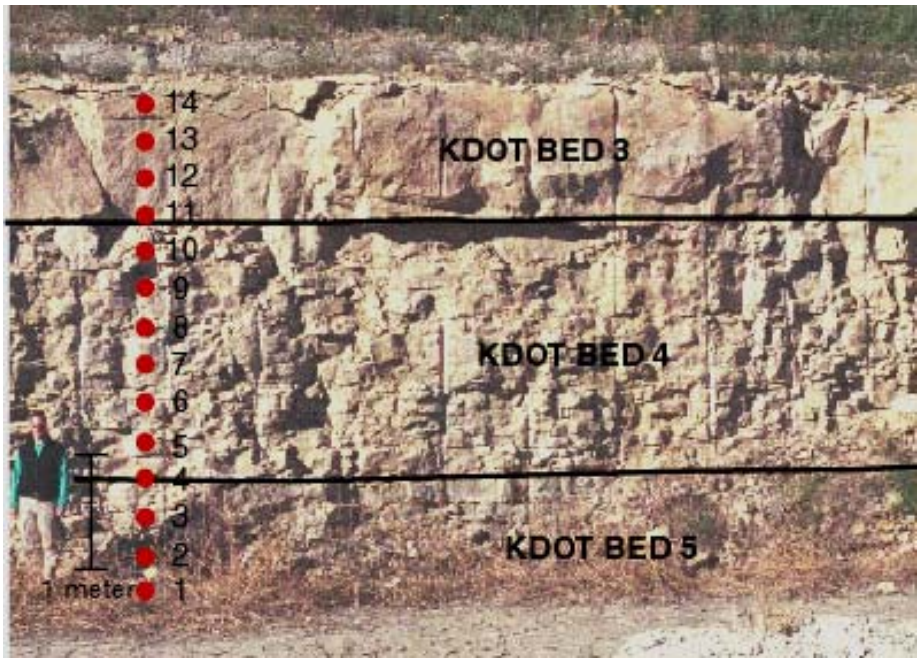

Figure 3.2: Photograph of Ledge at Shawnee Rock Company's Shawnee Quarry Showing Scintillometer Measuring Points at 0.3 cm (1 ft) Intervals
(KDOT beds are based upon the KDOT classifications of rock units by lithological similarities or volumes of rock that are convenient to excavate.)

The scintillometer was placed as flat as was possible against the ledge so that the detector area was aligned with each marked location. The scintillometer was held for a sampling period of three minutes. Three minutes was chosen because this time was the minimum necessary to get accurate readings for rocks that are relatively low in gamma radiation (Vit Gregor, personal comm., 2003).

Gamma radiation data were transferred to Excel spreadsheets. The lowermost reading for each stratigraphic section at or near ground level was significantly higher in radiation than the other readings due to input from soil and weathered material that could not be cleaned off with the powerwasher. In order to avoid contamination due to artificially elevated readings the first measurement at the base of each outcrop and any readings of weathered material at the top of the ledges were removed from the analyses.

Gamma radiation measurements were evaluated for each KDOT bed and compared to the physical test and other data KDOT generated for each bed. KDOT data included values for Modified Freeze-Thaw, Expansion, Durability, percent acid insoluble residue, and percent absorption. KDOT physical tests are run on splits of bulk samples of entire KDOT beds. Thus, summary statistics of the gamma radiation data from each KDOT bed were used for statistical comparison to the KDOT physical test results. Linear regression analysis was also used to test for a relationship between the radiation content and the various KDOT test measurements. Logistic analysis was used to test for a relationship between whether a KDOT bed passed or failed the KDOT physical tests. All of the statistical analyses were performed using Minitab™ and Statistix™ statistical software.

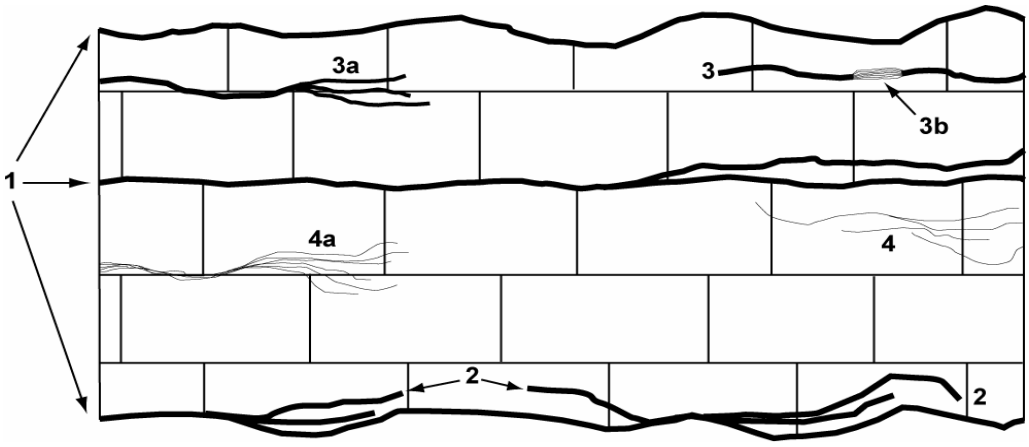

Figure 3.3: Hypothetical Illustration of Two Limestone Beds with Various Forms of Clay Distributed within Them

[(1) Concentrated stylocumulates or thin shale beds are typically located along bedding planes and may branch into surrounding limestones; (2) Concentrated stylocumulates also occur within limestones; (3) These often branch into slightly more diffuse stylocumulates near their ends (3a) or have zones of diffuse stylocumulates within them (3b); and (4) Diffuse stylocumulates also occur as thin wisps or stringers of clay-rich material within limestones and may have a "horsetail" appearance (4a). (after McKirahan, 2000)]

Detailed stratigraphic sections were measured and described. Six facies were differentiated on the basis clay content, distribution of clay, and whether the material between depositional grains was matrix (Dunham, 1962) or sparry calcite. Matrix consists of tiny crystals of calcite that are not visible with a 10x hand lens. It appears as opaque, solid-looking material surrounding the other grains in a limestone. Sparry calcite consists of more translucent, coarsely crystalline calcite visible with a 10x hand lens. Clays were found distributed in the limestones in three ways: disseminated clay, diffuse stylocumulates and concentrated stylocumulates or shale beds.

Stylocumulates are clay-rich zones that occur within limestone beds commonly along bedding planes from pressure dissolution processes. Figure 3.3 indicates the different types of

stylocumulates. Rock samples were also taken for both XRD analysis of clay content and petrographic thin-section analysis.

For determining the mineralogy of clays, the bulk hand samples were rinsed with water to remove quarry dust and crushed using a Bico Chipmunk crusher housed at the Kansas Geological Survey. They were then sieved to KDOT aggregate specifications and crushed again to the smallest size possible to shorten dissolution times. Samples were then ground to a powder in a mortar and pestle and 3 grams of each sample was dissolved with 750ml of 0.3 M acetic acid (Moore and Reynolds, 1997). Stokes law was used to separate the 2μm clay particles from the larger sizes of insoluble residue by allowing the acetic acid/insoluble residue mixture to settle for 37 minutes and 30 seconds in beakers containing 5 cm (approx column height) of the liquid.

The liquid, plus suspended 2μm clay fraction, was then decanted off and run through a Millipore® vacuum apparatus using 1.2μm cellulose filters. The mixture was constantly stirred as it was filtered to ensure that settling velocities were overcome so the clays retained on the filter represented a homogenous representative sample of all grain sizes present. Ten milliliters of distilled water was added at the end of the filtering to remove any acetic acid traces and then clays were transferred to a glass slide using standard methods (Moore and Reynolds, 1997; United States Geological Survey, 2001).

In order to obtain the data needed to identify the major clay minerals and estimate the proportions present within a KDOT bed, each sample was scanned three times using a Brookard D8 X-ray diffractometer with Cu Kα radiation. The first scan between 3˚ 2θ and 15˚ 2θ was performed on samples that were air dried. The second scan was performed on samples that had been exposed to ethylene glycol for five days at room temperature. The samples were scanned

from 3˚ 2θ to 55˚ 2θ. The third scan between 3˚ 2θ to 20˚ 2θ was performed on samples that had been placed in an oven and heated to 250˚ C. The raw scans are included in the appendix.

3.2.1 KDOT Tests

KDOT has several standardized tests they use to evaluate limestone aggregate quality (ASTM, 1995). KDOT divides quarry ledges into "KDOT beds" which range from approximately 2-10 feet in thickness. The KDOT bed divisions are based on lithological characteristics, a thickness that is convenient for quarry operators to quarry out, or a combination of these factors. KDOT personnel then take two 250 pound bulk samples from each KDOT bed and perform a suite of standardized tests to determine aggregate quality. They designate aggregate that passes specific criteria as class 1 (or 2) which is suitable for making Portland cement. Aggregate that does not meet these criteria is not suitable for use in Portland cement and is designated class 0.

The modified freeze-thaw or "soundness" test is KDOT's preliminary test. It is performed on raw aggregate that has been size graded and accurately weighed. The aggregate sample is then subjected to 25 cycles of freezing and thawing and is size graded and reweighed to determine how much mass the sample has lost. Currently, KDOT requires a minimum modified freeze-thaw value of 0.85 to continue with further tests.

The expansion test (C666-92 Procedure B) is conducted on three cylinders made out of the aggregate to be tested. Expansion percent is calculated by noting the average difference in expansion between the three beams before and after the testing procedure. KDOT currently uses an average of 0.02 for the three beams as the maximum expansion limit allowed for class 1 aggregate.

The durability factor is a measure of the ratio of stress to strain that characterizes the stiffness of an object. It is a combination measurement of the relative dynamic modulus of

elasticity, the number of freeze/thaw cycles run before a specified minimum value is reached and/or the test is terminated. KDOT requires a durability factor of at least 95 to qualify an aggregate as class 1.

3.3 Results

The measured sections were originally described using the Dunham (1962) classification system which focuses on depositional textures of carbonate rocks. The measured sections were reclassified into six facies in order to emphasize the type of matrix and presence and distribution of clay to better focus on the factors important for predicting durability in this study. A list of the six facies and examples of each are presented below.

1. Matrix, disseminated clays and diffuse stylocumulates
2. Matrix, disseminated clays
3. Matrix
4. Matrix, diffuse stylocumulates
5. Sparry calcite (disseminated clay-poor, diffuse stylocumulate-poor)
6. Shale/siltstone

Figure 3.4: Polished Slab of the Matrix, Disseminated Clays and Diffuse Stylocumulates Facies
(Note dark brown color of matrix, which is correlated to high clay content. Also note the greater than 2 cm thick zone of diffuse stylocumulates at the top of the slab.)

Figure 3.5: Polished Slab of the Matrix, Disseminated Clays Facies
(Note dark brown/grey color of matrix which is correlated to high clay content. Note absence of stylocumulates.)

Figure 3.6: Polished Slab of the Matrix Facies
(The light color of the matrix indicates little disseminated clay. Note the lack of stylocumulates. The darker gray objects are fossil fragments that have been recrystallized or dissolved and filled with sparry calcite cement.)

Figure 3.7: Polished Slab of the Matrix and Diffuse Stylocumulates Facies
(Note the light color of material between the grains which is common for clay-poor carbonate matrix. This sample also contains several zones of diffuse stylocumulates.)

Figure 3.8: Cut Slab of the Shale Facies
(This facies is dominantly composed of silt and clay sized quartz and clay minerals. It can contain enough carbonate to react mildly in 10% hydrochloric acid. This facies is found interbedded with the carbonate facies in eastern Kansas and western Missouri quarries. It is commonly this material that becomes airborne while being removed as overburden and must be rinsed off the carbonate ledges before testing with the spectral gamma ray scintillometer.)

Figure 3.9: Polished Slab of the Sparry Matrix Facies
(This photo has been enlarged to 2.5 times the scale of the previous figures in order to better see the clear, glassy looking material between the individual grains in the sample. This is another commonly found facies in quarries in eastern Kansas and western Missouri. Previous work has shown that factors other than clay content are important in determining the durability of this facies as limestone aggregate. This indicates that the gamma ray scintillometry method proposed in this paper is not applicable to the sparry matrix facies.)

Data generated by the spectral gamma ray scintillometer, included total radiation, potassium, uranium and thorium in both counts-per-second and concentration (nGyn/Hz, ppm or %) for each sample point in 22 stratigraphic sections. All spectral scintillometry data are presented in the following tables and are organized by quarry location and KDOT bed numbers.

Also included are the KDOT physical test pass/fail status, the three main KDOT test results (freeze/thaw, durability factor and expansion percent), and the summary statistics for each KDOT bed. At locations where it was possible to measure centimeter scale stratigraphic sections, the percent clay-rich rock is also included in the tables. Missing values for the KDOT tests are indicated by "NA" in the tables.

Table 3.1: KDOT Quarry Code 4-061-08, Miami County, APAC "Reno" Quarry

Argentine Limestone													
Sample number	Total (cps)	K (cps)	Ur (cps)	Th (cps)	Total (nGy/Hz)	K (%)	Ur (ppm)	Th (ppm)	Pass/Fail	KDOT Bed	Freeze/Thaw	Durability Factor	Expansion Percent
18 *	497.37	0.56	0.41	0.04	0.00	0.00	3.11	0.31	PASS	3	0.91	99	0.005
19	500.02	0.66	0.37	0.03	8.60	0.11	2.84	0.01	PASS	3	0.91	99	0.005
20	503.41	0.54	0.28	0.04	6.05	0.07	1.90	0.24	PASS	3	0.91	99	0.005
21**	504.04	0.50	0.38	0.04	7.06	0.00	2.77	0.34	PASS	3	0.91	99	0.005
22	506.41	0.48	0.34	0.03	10.87	0.00	2.64	0.00	PASS	3	0.91	99	0.005
23**	506.08	0.63	0.41	0.05	10.34	0.04	3.02	0.49	PASS	3	0.91	99	0.005
24	485.69	0.57	0.35	0.06	0.00	0.03	2.22	0.87	PASS	3	0.91	99	0.005
25**	489.47	0.53	0.42	0.30	0.00	0.00	3.49	0.00	PASS	3	0.91	99	0.005
26	496.96	0.58	0.27	0.09	0.00	0.17	0.83	1.96	FAIL	3	0.91	99	0.005
27	485.79	0.57	0.36	0.04	0.00	0.01	2.69	0.18	FAIL	2	0.94	68	0.081
28**	494.65	1.00	0.40	0.06	0.00	0.45	3.53	0.78	FAIL	2	0.94	68	0.081
29	501.42	0.40	0.40	0.07	2.85	0.00	2.63	1.00	FAIL	2	0.94	68	0.081
30	496.68	0.63	0.33	0.06	0.00	0.14	2.08	0.72	FAIL	2	0.94	68	0.081
31	498.26	0.76	0.41	0.09	0.00	0.23	2.30	1.85	FAIL	2	0.94	68	0.081
32	501.23	0.53	0.42	0.08	2.55	0.00	2.53	1.50	FAIL	2	0.94	68	0.081
33	496.70	0.81	0.29	0.04	0.00	0.39	2.02	0.24	FAIL	2	0.94	68	0.081
34	511.07	1.09	0.41	0.09	18.35	0.66	2.32	1.86	FAIL	1	0.91	71	0.057
35	504.94	1.09	0.50	0.12	8.50	0.58	2.77	2.65	FAIL	1	0.91	71	0.057
36 **	510.32	1.06	0.43	0.12	17.14	0.63	2.04	2.70	FAIL	1	0.91	71	0.057

Table 3.1 (cont'd)													
Summary Statistics													
	Total (cps)	**K (cps)**	**Ur (cps)**	**Th (cps)**	**Total (nGy/Hz)**	**K (%)**	**Ur (ppm)**	**Th (ppm)**					
Bed 3													
std dev.	8.349	0.066	0.047	0.098	4.515	0.042	0.520	0.323					
median	503.41	0.54	0.37	0.04	7.06	0.03	2.77	0.24					
mean	499.30	0.56	0.36	0.08	6.13	0.04	2.70	0.28					
maximum	506.41	0.66	0.42	0.30	10.87	0.11	3.49	0.87					
Bed 2													
std dev.	5.288	0.200	0.048	0.019	1.320	0.189	0.508	0.616					
median	496.70	0.63	0.40	0.06	0.00	0.14	2.53	0.78					
mean	496.39	0.67	0.37	0.06	0.77	0.17	2.54	0.90					
maximum	501.42	1.00	0.42	0.09	2.85	0.45	3.53	1.85					
Bed 1													
std dev.	3.344	0.017	0.047	0.017	5.372	0.040	0.368	0.471					
median	510.32	1.09	0.43	0.12	17.14	0.63	2.32	2.65					
mean	508.78	1.08	0.45	0.11	14.66	0.62	2.38	2.40					
maximum	511.07	1.09	0.50	0.12	18.35	0.66	2.77	2.70					
Bed 1 – w/o shale													
std dev.	4.335	0.000	0.064	0.021	6.965	0.057	0.318	0.559					
median	508.01	1.09	0.46	0.11	13.43	0.62	2.55	2.26					
mean	508.01	1.09	0.46	0.11	13.43	0.62	2.55	2.26					
maximum	511.07	1.09	0.50	0.12	18.35	0.66	2.77	2.65					

Table 3.1 (cont'd)													
	Total (cps)	**K (cps)**	**Ur (cps)**	**Th (cps)**	**Total (nGy/Hz)**	**K (%)**	**Ur (ppm)**	**Th (ppm)**					
Bed 3 – w/o shale													
std dev.	7.991469	0.07	0.04	0.03	4.96148	0.07	0.79	0.83					
median	500.02	0.57	0.34	0.04	6.05	0.07	2.22	0.24					
mean	498.50	0.57	0.32	0.05	5.10	0.08	2.09	0.62					
maximum	506.41	0.66	0.37	0.09	10.87	0.17	2.84	1.96					
Bed 2 – w/o shale													
standard dev.	5.73	0.15	0.05	0.02	1.40	0.16	0.29	0.67					
median	497.48	0.60	0.38	0.07	0.00	0.08	2.42	0.86					
mean	496.68	0.62	0.37	0.06	0.90	0.13	2.38	0.92					
maximum	501.42	0.81	0.42	0.09	2.85	0.39	2.69	1.85					
Total percent of clay rich rock													
KDOT BED													
3	0.8%												
2	2.8%												
1	7.8%												

Table 3.2: KDOT Quarry Code 4-054-11, Leavenworth County, Ashgrove Aggregates Lacygne Quarry

Winterset Limestone													
Sample number	Total (cps)	K (cps)	Ur (cps)	Th (cps)	Total (nGy/Hz)	K (%)	Ur (ppm)	Th (ppm)	Pass/Fail	KDOT Bed	Freeze/Thaw	Durability Factor	Expansion Percent
18 *	497.37	0.56	0.41	0.04	0.00	0.00	3.11	0.31	PASS	3	0.91	99	0.005
19	500.02	0.66	0.37	0.03	8.60	0.11	2.84	0.01	PASS	3	0.91	99	0.005
20	503.41	0.54	0.28	0.04	6.05	0.07	1.90	0.24	PASS	3	0.91	99	0.005
21	504.04	0.50	0.38	0.04	7.06	0.00	2.77	0.34	PASS	3	0.91	99	0.005
22	506.41	0.48	0.34	0.03	10.87	0.00	2.64	0.00	PASS	3	0.91	99	0.005
23	506.08	0.63	0.41	0.05	10.34	0.04	3.02	0.49	PASS	3	0.91	99	0.005
24	485.69	0.57	0.35	0.06	0.00	0.03	2.22	0.87	PASS	3	0.91	99	0.005
25	489.47	0.53	0.42	0.30	0.00	0.00	3.49	0.00	PASS	3	0.91	99	0.005
26	496.96	0.58	0.27	0.09	0.00	0.17	0.83	1.96	FAIL	3	0.91	99	0.005
27	485.79	0.57	0.36	0.04	0.00	0.01	2.69	0.18	FAIL	2	0.94	68	0.081
28	494.65	1.00	0.40	0.06	0.00	0.45	3.53	0.78	FAIL	2	0.94	68	0.081
29	501.42	0.40	0.40	0.07	2.85	0.00	2.63	1.00	FAIL	2	0.94	68	0.081
30	496.68	0.63	0.33	0.06	0.00	0.14	2.08	0.72	FAIL	2	0.94	68	0.081
31	498.26	0.76	0.41	0.09	0.00	0.23	2.30	1.85	FAIL	2	0.94	68	0.081
32	501.23	0.53	0.42	0.08	2.55	0.00	2.53	1.50	FAIL	2	0.94	68	0.081
33	496.70	0.81	0.29	0.04	0.00	0.39	2.02	0.24	FAIL	2	0.94	68	0.081
34	511.07	1.09	0.41	0.09	18.35	0.66	2.32	1.86	FAIL	1	0.91	71	0.057
35	504.94	1.09	0.50	0.12	8.50	0.58	2.77	2.65	FAIL	1	0.91	71	0.057
36 **	510.32	1.06	0.43	0.12	17.14	0.63	2.04	2.70	FAIL	1	0.91	71	0.057

Table 3.2 (cont'd)													
Summary Statistics													
	Total (cps)	**K (cps)**	**Ur (cps)**	**Th (cps)**	**Total (nGy/Hz)**	**K (%)**	**Ur (ppm)**	**Th (ppm)**					
Bed 3													
std dev.	8.349	0.066	0.047	0.098	4.515	0.042	0.520	0.323					
median	503.41	0.54	0.37	0.04	7.06	0.03	2.77	0.24					
mean	499.30	0.56	0.36	0.08	6.13	0.04	2.70	0.28					
maximum	506.41	0.66	0.42	0.30	10.87	0.11	3.49	0.87					
Bed 2													
std dev.	5.288	0.200	0.048	0.019	1.320	0.189	0.508	0.616					
median	496.70	0.63	0.40	0.06	0.00	0.14	2.53	0.78					
mean	496.39	0.67	0.37	0.06	0.77	0.17	2.54	0.90					
maximum	501.42	1.00	0.42	0.09	2.85	0.45	3.53	1.85					
Bed 1													
std dev.	3.344	0.017	0.047	0.017	5.372	0.040	0.368	0.471					
median	510.32	1.09	0.43	0.12	17.14	0.63	2.32	2.65					
mean	508.78	1.08	0.45	0.11	14.66	0.62	2.38	2.40					
maximum	511.07	1.09	0.50	0.12	18.35	0.66	2.77	2.70					
Bed 1 – w/o shale													
std dev.	4.335	0.000	0.064	0.021	6.965	0.057	0.318	0.559					
median	508.01	1.09	0.46	0.11	13.43	0.62	2.55	2.26					
mean	508.01	1.09	0.46	0.11	13.43	0.62	2.55	2.26					
maximum	511.07	1.09	0.50	0.12	18.35	0.66	2.77	2.65					

Table 3.2 (cont'd)													
Total percent of clay rich rock													
KDOT BED													
3	0.8%												
2	2.8%												
1	7.8%												

Table 3.3: KDOT Quarry Code 4-054-11, Leavenworth County, Ashgrove Aggregates Lacygne Quarry

Bethany Falls Limestone													
Sample number	**Total (cps)**	**K (cps)**	**Ur (cps)**	**Th (cps)**	**Total (nGy/Hz)**	**K (%)**	**Ur (ppm)**	**Th (ppm)**	**Pass/Fail**	**KDOT Bed**	**Freeze/Thaw**	**Durability Factor**	**Expansion Percent**
1 *	484.97	0.88	0.59	0.09	0	0.12	4.49	1.18	PASS	3	98	0.004	1 *
2	492.83	0.83	0.46	0.14	10.9	0.26	2.26	2.92	PASS	3	98	0.004	2
3	477.11	0.94	0.53	0.06	0	0.25	4.36	0.16	PASS	3	98	0.004	3
4	478.82	0.93	0.51	0.02	0	0.23	4.77	0	PASS	3	98	0.004	4
5	482.4	0.89	0.59	0.08	0	0.13	4.7	0.64	PASS	3	98	0.004	5
6	470.67	1.08	0.69	0.1	0	0.26	5.4	1.28	PASS	3	98	0.004	6
7	493.98	1.11	0.69	0.09	13.13	0.29	5.49	1.1	PASS	3	98	0.004	7
8	473.56	1.09	0.69	0.05	0	0.24	6.22	0	PASS	2	97	0.018	8
9	467.73	1.04	0.6	0.11	0	0.33	4.36	1.54	PASS	2	97	0.018	9
10	467.64	1.02	0.54	0.13	0	0.38	3.37	2.31	PASS	2	97	0.018	10
11**	474.48	0.78	0.56	0.08	0	0.03	4.28	0.85	PASS	2	97	0.018	11
12	466.74	0.86	0.44	0.12	0	0.29	2.51	2.21	PASS	1	98	0.007	12
13 **	472.93	0.87	0.46	0.07	0	0.24	3.5	0.57	PASS	1	98	0.007	13 **
14	464.38	0.63	0.52	0.09	0	0	3.85	1.05	PASS	1	98	0.007	14

Table 3.3 (cont'd)													
Summary Statistics													
	Total (cps)	**K (cps)**	**Ur (cps)**	**Th (cps)**	**Total (nGy/Hz)**	**K (%)**	**Ur (ppm)**	**Th (ppm)**					
Bed 3													
std dev.	9.175	0.109	0.096	0.040	6.244	0.056	1.178	1.059					
median	480.61	0.94	0.56	0.09	0.00	0.26	4.74	0.87					
mean	482.64	0.96	0.58	0.08	4.01	0.24	4.50	1.02					
maximum	493.98	1.11	0.69	0.14	13.13	0.29	5.49	2.92					
Bed 2													
std dev.	3.677	0.138	0.067	0.035	0.000	0.155	1.196	0.984					
median	470.65	1.03	0.58	0.10	0.00	0.29	4.32	1.20					
mean	470.85	0.98	0.60	0.09	0.00	0.25	4.56	1.18					
maximum	474.48	1.09	0.69	0.13	0.00	0.38	6.22	2.31					
Bed 1													
std dev.	4.416	0.136	0.042	0.025	0.000	0.155	0.695	0.843					
median	466.74	0.86	0.46	0.09	0.00	0.24	3.50	1.05					
mean	468.02	0.79	0.47	0.09	0.00	0.18	3.29	1.28					
maximum	472.93	0.87	0.52	0.12	0.00	0.29	3.85	2.21					
Bed 1 – w/o shale													
std dev.	1.669	0.163	0.057	0.021	0.000	0.205	0.948	0.820					
median	465.56	0.75	0.48	0.11	0.00	0.15	3.18	1.63					
mean	465.56	0.75	0.48	0.11	0.00	0.15	3.18	1.63					
maximum	466.74	0.86	0.52	0.12	0.00	0.29	3.85	2.21					

Table 3.3 (cont'd)													
	Total (cps)	**K (cps)**	**Ur (cps)**	**Th (cps)**	**Total (nGy/Hz)**	**K (%)**	**Ur (ppm)**	**Th (ppm)**					
Bed 2 – w/o shale													
std dev.	3.39	0.04	0.08	0.04	0.00	0.07	1.45	1.18					
median	467.73	1.04	0.60	0.11	0.00	0.33	4.36	1.54					
mean	469.64	1.05	0.61	0.10	0.00	0.32	4.65	1.28					
maximum	473.56	1.09	0.69	0.13	0.00	0.38	6.22	2.31					
Total percent of clay rich rock													
KDOT BED													
3	0.9												
2	0.7												

Table 3.4: KDOT Quarry Code 1-044-01, Jefferson County, Hamm "North Lawrence" Quarry

Plattsmouth Limestone													
Sample number	**Total (cps)**	**K (cps)**	**Ur (cps)**	**Th (cps)**	**Total (nGy/Hz)**	**K (%)**	**Ur (ppm)**	**Th (ppm)**	**Pass/Fail**	**KDOT Bed**	**Freeze/Thaw**	**Durability Factor**	**Expansion Percent**
1 *	497.28	1.17	0.67	0.08	19.55	0.38	5.45	0.76	FAIL	3	0.9	57	0.08
2	465.65	1.03	0.61	0.07	0	0.28	5.02	0.45	FAIL	3	0.9	57	0.08
3	470.13	1.07	0.57	0.13	0	0.41	3.62	2.47	FAIL	3	0.9	57	0.08
4	469.12	0.99	0.55	0.1	0	0.31	3.94	1.4	FAIL	3	0.9	57	0.08
5	460.78	0.83	0.56	0.1	0	0.1	4	1.39	FAIL	3	0.9	57	0.08
6 **	477.39	1.38	0.91	0.11	0	0.41	7.35	1.47	FAIL	3	0.9	57	0.08
7**	486.35	0.84	0.41	0.1	0	0.29	2.54	1.52	FAIL	3	0.9	57	0.08
8**	462.6	0.74	0.37	0.09	0	0.21	2.19	1.37	FAIL	3	0.9	57	0.08
9	467.09	0.7	0.54	0.07	0	0	4.38	0.32	FAIL	3	0.9	57	0.08

Table 3.4 (cont'd)													
Sample number	**Total (cps)**	**K (cps)**	**Ur (cps)**	**Th (cps)**	**Total (nGy/Hz)**	**K (%)**	**Ur (ppm)**	**Th (ppm)**	**Pass/Fail**				
10	470.08	0.92	0.6	0.1	0	0.16	4.45	1.36	FAIL	3	0.9	57	0.08
11	465.08	0.86	0.52	0.12	0	0.19	3.39	1.96	FAIL	2	0.85	NA	0.127
12	457.83	0.84	0.44	0.08	0	0.24	3.19	0.77	FAIL	2	0.85	NA	0.127
Summary Statistics													
	Total (cps)	**K (cps)**	**Ur (cps)**	**Th (cps)**	**Total (nGy/Hz)**	**K (%)**	**Ur (ppm)**	**Th (ppm)**					
Bed 3													
std dev.	7.825	0.206	0.152	0.019	0.000	0.138	1.497	0.628					
median	469.12	0.92	0.56	0.10	0.00	0.28	4.00	1.39					
mean	469.91	0.94	0.57	0.10	0.00	0.24	4.17	1.31					
maximum	486.35	1.38	0.91	0.13	0.00	0.41	7.35	2.47					
Bed 3 w/o shale													
standard dev.	3.583	0.139	0.028	0.023	0.000	0.151	0.491	0.780					
median	468.11	0.96	0.57	0.10	0.00	0.22	4.19	1.38					
mean	467.14	0.92	0.57	0.10	0.00	0.21	4.24	1.23					
maximum	470.13	1.07	0.61	0.13	0.00	0.41	5.02	2.47					
Bed 2													
std dev.	5.127	0.014	0.057	0.028	0.000	0.035	0.141	0.841					
median	461.46	0.85	0.48	0.10	0.00	0.22	3.29	1.37					
mean	461.46	0.85	0.48	0.10	0.00	0.22	3.29	1.37					
maximum	465.08	0.86	0.52	0.12	0.00	0.24	3.39	1.96					
Total percent of clay rich rock													
KDOT BED													
2	1.1%												
3	6.1%												

Table 3.5: KDOT Quarry Code 4-061-05, Miami County, Hunt-Midwest "Crawford" Quarry

Argentine Limestone													
Sample number	**Total (cps)**	**K (cps)**	**Ur (cps)**	**Th (cps)**	**Total (nGy/Hz)**	**K (%)**	**Ur (ppm)**	**Th (ppm)**	**Pass/Fail**	**KDOT Bed**	**Freeze/Thaw**	**Durability Factor**	**Expansion Percent**
12 *	470.26	0.76	0.49	0.08	0	0.07	3.75	0.72	PASS	5	98	0.009	12 *
13**	494.93	0.78	0.48	0	14.98	0.11	3.64	0.73	PASS	5	98	0.009	13
14	474.63	0.76	0.54	0.04	0	0	4.84	0	PASS	5	98	0.009	14
15	470.02	0.84	0.6	0.06	0	0.04	5.18	0	PASS	5	98	0.009	15
16	490.91	0.72	0.57	0.07	7.18	0	4.57	0.47	PASS	5	98	0.009	16
17	467.11	0.76	0.51	0.07	0	0.06	3.59	0.53	PASS	5	98	0.009	17
18	460.9	0.73	0.52	0.09	0	0.01	3.85	1.05	PASS	5	98	0.009	18
19	462.69	0.72	0.5	0.06	0	0	4.17	0	PASS	5	98	0.009	19
20	469.81	0.74	0.53	0.03	0	0	4.91	0	PASS	5	98	0.009	20
Summary Statistics													
	Total (cps)	**K (cps)**	**Ur (cps)**	**Th (cps)**	**Total (nGy/Hz)**	**K (%)**	**Ur (ppm)**	**Th (ppm)**					
Bed 5													
std dev.	11.813	0.037	0.039	0.028	5.261	0.040	0.609	0.402					
median	470.02	0.76	0.52	0.06	0	0.01	4.17	0.47					
Table 3.5 (cont'd)													
	Total (cps)	**K (cps)**	**Ur (cps)**	**Th (cps)**	**Total (nGy/Hz)**	**K (%)**	**Ur (ppm)**	**Th (ppm)**					
Bed 5													
mean	473.47	0.76	0.53	0.06	2.46	0.03	4.28	0.39					
maximum	494.93	0.84	0.6	0.09	14.98	0.11	5.18	1.05					
Total percent of clay rich rock													
KDOT BED													
5	2.7%												

Table 3.6: KDOT Quarry Code 1-046-11, Johnson County, Hunt-Midwest "Sunflower" Quarry

Lower Farley Limestone													
Sample number	**Total (cps)**	**K (cps)**	**Ur (cps)**	**Th (cps)**	**Total (nGy/Hz)**	**K (%)**	**Ur (ppm)**	**Th (ppm)**	**Pass/Fail**	**KDOT Bed**	**Freeze/Thaw**	**Durability Factor**	**Expansion Percent**
50 *	497.19	1.54	0.64	0.21	19.37	0.98	3.1	4.78	FAIL	9	NA	NA	50 *
51	480.65	0.95	0.44	0.09	0	0.38	3	1.14	FAIL	9	NA	NA	51
52	492.07	0.86	0.63	0.1	9.42	0.06	4.73	1.33	FAIL	9	NA	NA	52
53	462.58	0.69	0.42	0.1	0	0.09	2.66	1.5	FAIL	9	NA	NA	53
54	482.29	1.07	0.47	0.15	0	0.54	2.34	3.1	FAIL	9	NA	NA	54
Summary Statistics													
	Total (cps)	**K (cps)**	**Ur (cps)**	**Th (cps)**	**Total (nGy/Hz)**	**K (%)**	**Ur (ppm)**	**Th (ppm)**					
Bed 9													
std dev.	12.293	0.160	0.096	0.027	4.710	0.232	1.066	0.900					
median	481.47	0.91	0.46	0.10	0.00	0.24	2.83	1.42					
mean	479.40	0.89	0.49	0.11	2.36	0.27	3.18	1.77					
Bed 9													
maximum	492.07	1.07	0.63	0.15	9.42	0.54	4.73	3.10					
Bed 9 w/o shale													
std dev.	8.08	0.06	0.13	0.01	6.66	0.23	1.22	0.13					
median	486.36	0.91	0.54	0.10	4.71	0.22	3.87	1.24					
mean	486.36	0.91	0.54	0.10	4.71	0.22	3.87	1.24					
maximum	492.07	0.95	0.63	0.10	9.42	0.38	4.73	1.33					

Table 3.7: KDOT Quarry Code 1-046-11, Johnson County, Hunt-Midwest "Sunflower" Quarry

Upper Farley Limestone													
Sample number	**Total (cps)**	**K (cps)**	**Ur (cps)**	**Th (cps)**	**Total (nGy/Hz)**	**K (%)**	**Ur (ppm)**	**Th (ppm)**	**Pass/Fail**	**KDOT Bed**	**Freeze/Thaw**	**Durability Factor**	**Expansion Percent**
39 *	500.7	2.2	0.88	0.24	26.19	1.56	4.29	5.86	PASS	7	98	0.014	39 *
40 **	468.87	1.51	0.61	0.2	0	0.98	2.86	4.62	PASS	7	98	0.014	40 **
41	459.88	0.86	0.36	0.09	0	0.36	2.16	1.2	PASS	6	94	0.014	41
42	456.63	0.69	0.26	0.05	0	0.23	1.79	0.02	PASS	6	94	0.014	42
43	462.8	0.76	0.31	0.12	0	0.31	1.17	2.32	PASS	6	94	0.014	43
44	456.18	0.68	0.31	0.11	0	0.21	1.35	1.96	PASS	6	94	0.014	44
Summary Statistics													
	Total (cps)	**K (cps)**	**Ur (cps)**	**Th (cps)**	**Total (nGy/Hz)**	**K (%)**	**Ur (ppm)**	**Th (ppm)**					
Bed 6													
std dev.	5.21	0.35	0.14	0.06	0.00	0.32	0.68	1.70					
median	459.88	0.76	0.31	0.11	0.00	0.31	1.79	1.96					
mean	460.87	0.90	0.37	0.11	0.00	0.42	1.87	2.02					
maximum	468.87	1.51	0.61	0.20	0.00	0.98	2.86	4.62					
Bed 6 w/o shales													
std dev.	4.36	0.05	0.04	0.05	0.00	0.06	0.44	1.63					
median	459.72	0.73	0.29	0.09	0.00	0.27	1.48	1.17					
mean	459.72	0.73	0.29	0.09	0.00	0.27	1.48	1.17					
maximum	462.80	0.76	0.31	0.12	0.00	0.31	1.79	2.32					

Table 3.8: KDOT Quarry Code 1-046-11, Johnson County, Hunt-Midwest "Sunflower" Quarry

Argentine Limestone													
Sample number	**Total (cps)**	**K (cps)**	**Ur (cps)**	**Th (cps)**	**Total (nGy/Hz)**	**K (%)**	**Ur (ppm)**	**Th (ppm)**	**Pass/Fail**	**KDOT Bed**	**Freeze/Thaw**	**Durability Factor**	**Expansion Percent**
20 *	489.92	0.79	0.52	0.08	5.25	0.08	4.03	0.7	FAIL	10	NA	NA	20 *
21	456.91	0.76	0.39	0.08	0	0.18	2.74	0.81	FAIL	12	NA	NA	21
22	470.67	0.98	0.63	0.12	0	0.22	4.46	1.87	FAIL	12	NA	NA	22
23	460.09	0.81	0.47	0.06	0	0.15	3.89	0.02	FAIL	12	NA	NA	23
24	460.94	0.65	0.47	0.05	0	0	3.98	0	FAIL	12	NA	NA	24
25	460.09	0.71	0.42	0.07	0	0.09	3.06	0.6	FAIL	12	NA	NA	25
26	461.03	0.84	0.48	0.07	0	0.18	3.82	0.37	FAIL	12	NA	NA	26
27	455.67	0.64	0.42	0.07	0	0.01	3.11	0.6	FAIL	12	NA	NA	27
28	459.68	0.76	0.42	0.07	0	0.15	3.2	0.42	FAIL	12	NA	NA	28
29	455.69	0.72	0.44	0.07	0	0.07	3.34	0.58	FAIL	12	NA	NA	29
30	457.69	0.67	0.39	0.08	0	0.08	2.68	0.81	FAIL	12	NA	NA	30
31	482.68	0.66	0.46	0.09	0	0	3.23	1.1	FAIL	12	NA	NA	31
32	462.17	0.81	0.48	0.05	0	0.12	2.09	0	FAIL	12	NA	NA	32
33	484.53	0.78	0.39	0.09	0	0.23	2.47	1.35	FAIL	12	NA	NA	33
Summary Statistics	**Total (cps)**	**K (cps)**	**Ur (cps)**	**Th (cps)**	**Total (nGy/Hz)**	**K (%)**	**Ur (ppm)**	**Th (ppm)**					
Bed 10													
std dev.	9.630	0.095	0.064	0.019	0.000	0.080	0.667	0.549					
median	460.090	0.760	0.440	0.070	0.000	0.120	3.200	0.600					
mean	463.680	0.753	0.451	0.075	0.000	0.114	3.236	0.656					
maximum	484.530	0.980	0.630	0.120	0.000	0.230	4.460	1.870					
Bed 10--w/o shale													
standard dev.	8.10	0.09	0.07	0.02	0.00	0.08	0.70	0.56					
median	460.09	0.76	0.43	0.07	0.00	0.14	3.16	0.59					
mean	462.10	0.76	0.45	0.07	0.00	0.12	3.24	0.62					
maximum	484.53	0.98	0.63	0.12	0.00	0.23	4.46	1.87					

Table 3.9: KDOT Quarry Code 1-046-07, Johnson County, Johnson County Aggregate/Ashgrove Aggregate "Olathe" Quarry

Stoner Limestone													
Sample number	**Total (cps)**	**K (cps)**	**Ur (cps)**	**Th (cps)**	**Total (nGy/Hz)**	**K (%)**	**Ur (ppm)**	**Th (ppm)**	**Pass/Fail**	**KDOT Bed**	**Freeze/Thaw**	**Durability Factor**	**Expansion Percent**
1 *	500.39	1.19	0.68	0.14	25.6	0.44	4.56	2.74	FAIL	4	78	0.068	1 *
2	501.73	0.92	0.55	0.1	28.2	0.22	3.94	1.4	FAIL	4	78	0.068	2
3**	472.21	0.98	0.63	0.13	0	0.23	4.24	2.41	FAIL	4	78	0.068	3
4**	470.07	0.9	0.6	0.11	0	0.15	4.36	1.53	FAIL	4	78	0.068	4
5	491.69	1.12	0.63	0.07	8.69	0.35	5.33	0.26	FAIL	4	78	0.068	5
6	504.46	1.27	0.76	0.12	33.5	0.45	5.65	1.96	FAIL	3	93	0.021	6
7**	505.59	1.74	1.44	0.21	35.69	0.32	11.24	4.08	FAIL	3	93	0.021	7
8**	468.1	1.06	0.73	0.09	0	0.18	5.92	0.89	FAIL	3	93	0.021	8
9	481.21	0.79	0.52	0.06	0	0.07	4.3	0.16	FAIL	3	93	0.021	9
10	484.03	0.84	0.46	0.07	0	0.22	3.45	0.58	FAIL	3	93	0.021	10
11	469.79	0.93	0.49	0.15	0	0.34	2.56	3.07	FAIL	3	93	0.021	11
Summary Statistics													
	Total (cps)	**K (cps)**	**Ur (cps)**	**Th (cps)**	**Total (nGy/Hz)**	**K (%)**	**Ur (ppm)**	**Th (ppm)**					
Bed 3													
std dev.	15.346	0.099	0.038	0.025	13.298	0.083	0.602	0.883					
median	481.95	0.95	0.62	0.11	4.35	0.23	4.30	1.47					
mean	483.93	0.98	0.60	0.10	9.22	0.24	4.47	1.40					
maximum	501.73	1.12	0.63	0.13	28.20	0.35	5.33	2.41					
Bed 4													
std dev.	16.329	0.356	0.369	0.056	17.878	0.134	3.080	1.539					
median	482.62	1.00	0.63	0.11	0.00	0.27	4.98	1.43					
mean	485.53	1.11	0.73	0.12	11.53	0.26	5.52	1.79					
maximum	505.59	1.74	1.44	0.21	35.69	0.45	11.24	4.08					

Bed 3—w/o shales													
std dev.	14.44	0.22	0.14	0.04	16.75	0.16	1.32	1.33					
median	482.62	0.89	0.51	0.10	0.00	0.28	3.88	1.27					
mean	484.87	0.96	0.56	0.10	8.38	0.27	3.99	1.44					
maximum	504.46	1.27	0.76	0.15	33.50	0.45	5.65	3.07					
Bed 4—w/o shales													
std dev.	7.10	0.14	0.06	0.02	13.80	0.09	0.98	0.81					
median	496.71	1.02	0.59	0.09	18.45	0.29	4.64	0.83					
mean	496.71	1.02	0.59	0.09	18.45	0.29	4.64	0.83					
maximum	501.73	1.12	0.63	0.10	28.20	0.35	5.33	1.40					
Total percent of clay rich rock													
KDOT BED													
3	1.9%												
4	4.6%												

Table 3.10: KDOT Quarry Code 1-046-07, Johnson County, Johnson County Aggregate/Ashgrove Aggregate "Olathe" Quarry

Spring Hill Limestone													
Sample number	**Total (cps)**	**K (cps)**	**Ur (cps)**	**Th (cps)**	**Total (nGy/Hz)**	**K (%)**	**Ur (ppm)**	**Th (ppm)**	**Pass/Fail**	**KDOT Bed**	**Freeze/Thaw**	**Durability Factor**	**Expansion Percent**
30 *	497.48	1.28	0.62	0.15	19.94	0.63	3.58	2.98	PASS	10	97	0.011	30 *
31	467.98	0.99	0.55	0.09	0	0.31	4.03	1.22	PASS	10	97	0.011	31
32**	478.07	0.76	0.58	0.11	0	0	4.04	1.73	PASS	10	97	0.011	32
33	501.26	0.88	0.61	0.05	27.28	0.07	5.38	0	PASS	10	97	0.011	33
34 **	494.09	0.96	0.59	0.13	13.35	0.24	3.85	2.44	PASS	10	97	0.011	34 **
35**	473.15	1.26	0.81	0.09	0	0.35	6.61	1.01	FAIL	9	75	0.079	35
36	498.73	1.32	0.82	0.11	22.36	0.42	6.54	1.37	FAIL	9	75	0.079	36

Table 3.10 Cont													
Sample number	**Total (cps)**	**K (cps)**	**Ur (cps)**	**Th (cps)**	**Total (nGy/Hz)**	**K (%)**	**Ur (ppm)**	**Th (ppm)**	**Pass/Fail**	**KDOT Bed**	**Freeze/Thaw**	**Durability Factor**	**Expansion Percent**
37	473.86	1.27	0.78	0.15	0	0.43	5.48	2.83	FAIL	9	75	0.079	37
38 **	479.65	0.93	0.72	0.12	0	0.06	5.26	1.97	FAIL	9	75	0.079	38 **
39	488.79	1.28	0.59	0.11	3.06	0.64	4.24	1.56	FAIL	8	T	0.1	39
40	488.97	0.99	0.47	0.14	3.41	0.44	2.37	2.92	FAIL	8	T	0.1	40
Summary Statistics													
	Total (cps)	**K (cps)**	**Ur (cps)**	**Th (cps)**	**Total (nGy/Hz)**	**K (%)**	**Ur (ppm)**	**Th (ppm)**					
Bed 8													
std dev.	1.579	0.177	0.067	0.017	1.876	0.148	0.943	0.722					
median	488.79	0.99	0.48	0.11	3.06	0.44	3.09	1.82					
mean	487.97	1.08	0.51	0.12	2.16	0.48	3.23	2.10					
maximum	488.97	1.28	0.59	0.14	3.41	0.64	4.24	2.92					
Bed 9													
std dev.	11.948	0.179	0.045	0.025	11.180	0.174	0.702	0.796					
median	476.76	1.27	0.80	0.12	0.00	0.39	6.01	1.67					
mean	481.35	1.20	0.78	0.12	5.59	0.32	5.97	1.80					
maximum	498.73	1.32	0.82	0.15	22.36	0.43	6.61	2.83					
Bed 9 - w/o shale													
std dev.	17.59	0.04	0.03	0.03	15.81	0.01	0.75	1.03					
median	486.30	1.30	0.80	0.13	11.18	0.43	6.01	2.10					
mean	486.30	1.30	0.80	0.13	11.18	0.43	6.01	2.10					
maximum	498.73	1.32	0.82	0.15	22.36	0.43	6.54	2.83					
Bed 10													
std dev.	15.102	0.103	0.025	0.034	13.035	0.144	0.709	1.028					
median	486.08	0.92	0.59	0.10	6.68	0.16	4.04	1.48					
mean	485.35	0.90	0.58	0.10	10.16	0.16	4.33	1.35					
maximum	501.26	0.99	0.61	0.13	27.28	0.31	5.38	2.44					

Bed 10 – w/o shale													
std dev.	23.53	0.08	0.04	0.03	19.29	0.17	0.95	0.86					
median	484.62	0.94	0.58	0.07	13.64	0.19	4.71	0.61					
mean	484.62	0.94	0.58	0.07	13.64	0.19	4.71	0.61					
maximum	501.26	0.99	0.61	0.09	27.28	0.31	5.38	1.22					
Total percent of clay rich rock													
KDOT BED													
10	4.5%												

Table 3.11: KDOT Quarry Code 1-046-07, Johnson County, Johnson County Aggregate/Ashgrove Aggregate "Olathe" Quarry

Captian Creek Limestone													
Sample number	**Total (cps)**	**K (cps)**	**Ur (cps)**	**Th (cps)**	**Total (nGy/Hz)**	**K (%)**	**Ur (ppm)**	**Th (ppm)**	**Pass/Fail**	**KDOT Bed**	**Freeze/Thaw**	**Durability Factor**	**Expansion Percent**
20 *	469.13	1.77	0.64	0.17	0	1.23	3.79	3.52	FAIL	7	91	0.024	20 *
21	469.78	1.24	0.57	0.2	0	0.69	2.47	4.64	FAIL	7	91	0.024	21
22	505.18	1.12	0.63	0.15	34.9	0.43	3.91	2.96	FAIL	7	91	0.024	22
23	495.68	1.23	0.71	0.09	16.45	0.43	5.6	1.1	FAIL	7	91	0.024	23
24	476.4	1	0.63	0.13	0	0.25	4.24	2.41	PASS	6	97	0.015	24
25	460.81	0.78	0.46	0.09	0	0.15	3.08	1.29	PASS	6	97	0.015	25
26	482.15	0.78	0.48	0.08	0	0.11	3.64	0.73	PASS	5	99	0.017	26
27	494.87	1.02	0.53	0.17	14.87	0.42	2.62	3.58	PASS	5	99	0.017	27
Summary Statistics													
	Total (cps)	**K (cps)**	**Ur (cps)**	**Th (cps)**	**Total (nGy/Hz)**	**K (%)**	**Ur (ppm)**	**Th (ppm)**					
Bed 7													
std dev.	18.322	0.067	0.070	0.055	17.460	0.150	1.567	1.771					
median	495.68	1.23	0.63	0.15	16.45	0.43	3.91	2.96					
mean	490.21	1.20	0.64	0.15	17.12	0.52	3.99	2.90					
maximum	505.18	1.24	0.71	0.20	34.90	0.69	5.60	4.64					

Table 3.11 (cont'd)													
	Total (cps)	K (cps)	Ur (cps)	Th (cps)	Total (nGy/Hz)	K (%)	Ur (ppm)	Th (ppm)					
Bed 6													
std dev.	11.02	0.16	0.12	0.03	0.00	0.07	0.82	0.79					
median	468.61	0.89	0.55	0.11	0.00	0.20	3.66	1.85					
mean	468.61	0.89	0.55	0.11	0.00	0.20	3.66	1.85					
maximum	476.40	1.00	0.63	0.13	0.00	0.25	4.24	2.41					
Bed 5													
std dev.	8.99	0.17	0.04	0.06	10.51	0.22	0.72	2.02					
median	488.51	0.90	0.51	0.13	7.44	0.27	3.13	2.16					
mean	488.51	0.90	0.51	0.13	7.44	0.27	3.13	2.16					
maximum	494.87	1.02	0.53	0.17	14.87	0.42	3.64	3.58					
Bed 7—w/o shales													
std dev.	NA	NA	NA	NA	NA	NA	NA	NA					
median	469.78	1.24	0.57	0.2	0	0.69	2.47	4.64					
mean	469.78	1.24	0.57	0.2	0	0.69	2.47	4.64					
maximum	469.78	1.24	0.57	0.2	0	0.69	2.47	4.64					

Table 3.12: KDOT Quarry Code 1-052-01, Leavenworth County, (Privately-Owned) Loring Quarry

Argentine Limestone													
Sample number	Total (cps)	K (cps)	Ur (cps)	Th (cps)	Total (nGy/Hz)	K (%)	Ur (ppm)	Th (ppm)	Pass/Fail	KDOT Bed	Freeze/Thaw	Durability Factor	Expansion Percent
1 *	492.84	0.83	0.37	0.07	10.92	0.29	2.7	0.47	FAIL	14	91	0.028	1 *
2	491.17	0.66	0.51	0.03	7.67	0	4.68	0	FAIL	14	91	0.028	2
3	489.22	0.66	0.37	0.05	3.88	0.06	2.97	0	FAIL	14	91	0.028	3
4	456.69	0.81	0.53	0.07	0	0.09	4.18	0.51	FAIL	14	91	0.028	4
5 **	492.53	0.82	0.44	0.07	10.33	0.19	3.43	0.41	FAIL	14	91	0.028	5

Table 3.12 (cont'd)													
Sample number	**Total (cps)**	**K (cps)**	**Ur (cps)**	**Th (cps)**	**Total (nGy/Hz)**	**K (%)**	**Ur (ppm)**	**Th (ppm)**	**Pass/Fail**	**KDOT Bed**	**Freeze/Thaw**	**Durability Factor**	**Expansion Percent**
6 **	493.67	0.75	0.43	0.07	12.53	0.13	3.17	0.6	FAIL	13	78	0.042	6
7	491.27	0.61	0.47	0.06	7.87	0	3.89	0.01	FAIL	13	78	0.042	7
8	489.18	0.6	0.57	0.04	3.82	0	5.03	0	FAIL	13	78	0.042	8
9 **	465.69	0.54	0.4	0.08	0	0	2.8	0.79	PASS	13	78	0.042	9
10 *	457.04	719.25	0.34	0.04	0	3897.5	421.04	6295.22	PASS	13	78	0.042	10 *
11	482.24	0.54	0.33	0.04	0	0	2.62	0	PASS	13	78	0.042	11
12	487.18	0.42	0.19	0.04	0	0	1.27	0	PASS	12	98	0.007	12
13	462.34	0.46	0.33	0.03	0	0	2.95	0	PASS	12	98	0.007	13
14	469.46	0.71	0.41	0.05	0	0.08	3.36	0	PASS	12	98	0.007	14
15 **	469.13	0.76	0.36	0.04	0	0.19	3.04	0	PASS	12	98	0.007	15
16	474.35	0.78	0.42	0.08	0	0.37	1.96	1.39	PASS	11	63	0.183	16
17	474.03	0.85	0.34	0.09	0	0.37	1.96	1.39	FAIL	11	63	0.183	17
18 **	471.22	1.09	0.44	0.18	0	0.62	1.6	4.02	FAIL	11	63	0.183	18 **
1 *	492.84	0.83	0.37	0.07	10.92	0.29	2.7	0.47	FAIL	14	91	0.028	1 *
Summary Statistics													
	Total (cps)	**K (cps)**	**Ur (cps)**	**Th (cps)**	**Total (nGy/Hz)**	**K (%)**	**Ur (ppm)**	**Th (ppm)**					
Bed 11													
std dev.	1.72	0.16	0.05	0.06	0.00	0.14	0.21	1.52					
median	474.03	0.85	0.42	0.09	0.00	0.37	1.96	1.39					
mean	473.20	0.91	0.40	0.12	0.00	0.45	1.84	2.27					
maximum	474.35	1.09	0.44	0.18	0.00	0.62	1.96	4.02					

Table 3.12 (cont'd)													
	Total (cps)	**K (cps)**	**Ur (cps)**	**Th (cps)**	**Total (nGy/Hz)**	**K (%)**	**Ur (ppm)**	**Th (ppm)**					
Bed 11 - w/o shale													
std dev.	0.23	0.05	0.06	0.01	0.00	0.00	0.00	0.00					
median	474.19	0.82	0.38	0.09	0.00	0.37	1.96	1.39					
mean	474.19	0.82	0.38	0.09	0.00	0.37	1.96	1.39					
maximum	474.35	0.85	0.42	0.09	0.00	0.37	1.96	1.39					
Bed 12													
std dev.	10.62	0.17	0.09	0.01	0.00	0.09	0.94	0.00					
median	469.30	0.59	0.35	0.04	0.00	0.04	3.00	0.00					
mean	472.03	0.59	0.32	0.04	0.00	0.07	2.66	0.00					
maximum	487.18	0.76	0.41	0.05	0.00	0.19	3.36	0.00					
Bed 13													
std dev.	11.30	0.09	0.09	0.02	5.39	0.06	0.98						
median	489.18	0.60	0.43	0.06	3.82	0.00	3.17						
mean	484.41	0.61	0.44	0.06	4.84	0.03	3.50						
maximum	493.67	0.75	0.57	0.08	12.53	0.13	5.03						
Bed 14													
std dev.	17.20	0.09	0.07	0.02	4.51	0.08	0.76						
median	490.20	0.74	0.48	0.06	5.78	0.08	3.81						
mean	482.40	0.74	0.46	0.06	5.47	0.09	3.82						
maximum	17.20	0.09	0.07	0.02	4.51	0.08	0.76						

Table 3.12 (cont'd)													
	Total (cps)	K (cps)	Ur (cps)	Th (cps)	Total (nGy/Hz)	K (%)	Ur (ppm)						
Bed 13 w/o clay													
std dev.	4.73	0.04	0.12	0.01	3.94	0.00	1.21						
median	489.18	0.60	0.47	0.04	3.82	0.00	3.89						
mean	487.56	0.58	0.46	0.05	3.90	0.00	3.85						
maximum	491.27	0.61	0.57	0.06	7.87	0.00	5.03						
Bed 14 w/o clay													
std dev.	1.00	19.37	0.09	0.09	0.02	3.84	0.05						
median	489.22	0.66	0.51	0.05	3.88	0.06	4.18						
mean	479.03	0.71	0.47	0.05	3.85	0.05	3.94						
Total percent of clay rich rock													
KDOT BED													
14	2.9%												
13	3.8%												
12	3.5%												

Table 3.13: KDOT Quarry Code MO-021, Cass County, Martin Marietta Peculiar Quarry

Bethany Falls Limestone													
Sample number	Total (cps)	K (cps)	Ur (cps)	Th (cps)	Total (nGy/Hz)	K (%)	Ur (ppm)	Th (ppm)	Pass/Fail	KDOT Bed	Freeze/Thaw	Durability Factor	Expansion Percent
1 *	498	1.12	0.72	0.1	20.95	0.29	5.63	1.26	PASS	11	96	0.009	1 *
2	466.21	0.79	0.63	0.07	0	0	5.34	0.24	PASS	11	96	0.009	2
3	482.49	1.02	0.76	0.09	0	0.1	6.39	0.51	PASS	11	96	0.009	3

Table 3.13 (cont'd)													
Sample number	**Total (cps)**	**K (cps)**	**Ur (cps)**	**Th (cps)**	**Total (nGy/Hz)**	**K (%)**	**Ur (ppm)**	**Th (ppm)**	**Pass/Fail**	**KDOT Bed**	**Freeze/Thaw**	**Durability Factor**	**Expansion Percent**
4	486.83	1.18	0.83	0.08	0	0.21	7.08	0.63	PASS	11	96	0.009	4
5	467.58	0.88	0.68	0.09	0	0.01	5.47	0.92	PASS	11	96	0.009	5
6	477.38	1.09	0.83	0.08	0	0.11	7.17	0.44	PASS	11	96	0.009	6
7	471.69	1.09	0.82	0.08	0	0.11	6.97	0.63	PASS	11	96	0.009	7
8	472.15	1.16	0.77	0.07	0	0.25	6.64	0.32	PASS	11	96	0.009	8
9	470.24	0.87	0.68	0.08	0	0	5.51	0.74	PASS	11	96	0.009	9
10	462.99	0.84	0.64	0.09	0	0.01	5.03	0.96	PASS	11	96	0.009	10
11	470	0.92	0.61	0.11	0	0.17	4.32	1.71	PASS	11	96	0.009	11
12 **	469.81	0.85	0.49	0.08	0	0.18	3.75	0.72	PASS	11	96	0.009	12 **
13 **	483.28	1.37	0.67	0.1	0	0.66	5.12	1.32	PASS	11	96	0.009	13 **
Summary Statistics													
	Total (cps)	**K (cps)**	**Ur (cps)**	**Th (cps)**	**Total (nGy/Hz)**	**K (%)**	**Ur (ppm)**	**Th (ppm)**					
Bed 11													
std dev.	7.414	0.141	0.087	0.012	0.000	0.092	0.986	0.422					
median	470.97	0.97	0.72	0.08	0.00	0.11	5.95	0.63					
mean	472.76	0.98	0.73	0.08	0.00	0.10	5.99	0.71					
maximum	486.83	1.18	0.83	0.11	0.00	0.25	7.17	1.71					
Total percent of clay rich rock													
KDOT BED													
11	0.98%												

Table 3.14: KDOT Quarry Code 1-089-05, Cass County, Martin Marietta Big Springs Quarry

Ervine Creek Limestone													
Sample number	**Total (cps)**	**K (cps)**	**Ur (cps)**	**Th (cps)**	**Total (nGy/Hz)**	**K (%)**	**Ur (ppm)**	**Th (ppm)**	**Pass/Fail**	**KDOT Bed**	**Freeze/Thaw**	**Durability Factor**	**Expansion Percent**
1 *	503.88	2.79	1.63	0.37	32.37	1.53	10.49	9.2	FAIL	2	82	0.142	1 *
2	476.12	1.55	1.04	0.16	0	0.5	7.96	2.81	FAIL	2	82	0.142	2
3	508.29	1.37	1.04	0.09	40.94	0.22	9.03	0.81	FAIL	2	82	0.142	3
4	508.82	1.43	0.96	0.12	41.96	0.42	7.73	1.79	FAIL	2	82	0.142	4
5**	477.54	1.37	0.88	0.11	0	0.42	7.16	1.32	FAIL	1	NA	NA	5
6	477.27	1.61	1.01	0.08	0	0.54	0.96	0.31	FAIL	1	NA	NA	6
7**	494.96	1.36	1.08	0.19	15.04	0.25	7.72	4.02	FAIL	1	NA	NA	7
8 **	467.2	1.18	0.92	0.12	0	0.14	7.34	1.81	FAIL	1	NA	NA	8 **
9	502.19	1.4	0.99	0.12	29.1	0.34	0.01	1.76	FAIL	1	NA	NA	9
Summary Statistics													
	Total (cps)	**K (cps)**	**Ur (cps)**	**Th (cps)**	**Total (nGy/Hz)**	**K (%)**	**Ur (ppm)**	**Th (ppm)**					
Bed 1													
std dev.	14.32	0.15	0.08	0.04	13.07	0.15	3.81	1.36					
median	477.54	1.37	0.99	0.12	0.00	0.34	7.16	1.76					
mean	483.83	1.38	0.98	0.12	8.83	0.34	4.64	1.84					
maximum	502.19	1.61	1.08	0.19	29.10	0.54	7.72	4.02					
Bed 1 - w/0 shale													
std dev.	17.62	0.15	0.01	0.03	20.58	0.14	0.67	1.03					
median	489.73	1.51	1.00	0.10	14.55	0.44	0.49	1.04					
mean	489.73	1.51	1.00	0.10	14.55	0.44	0.49	1.04					

Table 3.14 (cont'd)													
	Total (cps)	**K (cps)**	**Ur (cps)**	**Th (cps)**	**Total (nGy/Hz)**	**K (%)**	**Ur (ppm)**	**Th (ppm)**					
Bed 1													
maximum	502.19	1.61	1.01	0.12	29.10	0.54	0.96	1.76					
Bed 2													
std dev.	18.73	0.09	0.05	0.04	23.94	0.14	0.69	1.00					
median	508.29	1.43	1.04	0.12	40.94	0.42	7.96	1.79					
mean	497.74	1.45	1.01	0.12	27.63	0.38	8.24	1.80					
maximum	508.82	1.55	1.04	0.16	41.96	0.50	9.03	2.81					
Total percent of clay rich rock													
KDOT BED													
2	4%												
1	6.7%												

Table 3.15: KDOT Quarry Code 4-054-11, Leavenworth County, Martin Marietta Greenwood Quarry

Winterset Limestone													
Sample number	**Total (cps)**	**K (cps)**	**Ur (cps)**	**Th (cps)**	**Total (nGy/Hz)**	**K (%)**	**Ur (ppm)**	**Th (ppm)**	**Pass/Fail**	**KDOT Bed**	**Freeze/Thaw**	**Durability Factor**	**Expansion Percent**
1 *	498	1.33	0.62	0.11	20.96	0.66	4.49	1.72	FAIL	3	NA	0.144	1 *
2	489.34	0.82	0.45	0.11	4.12	0.22	2.75	1.84	FAIL	3	NA	0.144	2
3	490.82	0.98	0.62	0.09	7	0.2	4.8	0.98	FAIL	3	NA	0.144	3
4	489.25	0.92	0.48	0.07	3.96	0.28	3.76	0.38	FAIL	3	NA	0.144	4
5	493.11	0.93	0.61	0.09	11.45	0.17	4.6	1.17	FAIL	3	NA	0.144	5

Table 3.15 (cont'd)													
Sample number	**Total (cps)**	**K (cps)**	**Ur (cps)**	**Th (cps)**	**Total (nGy/Hz)**	**K (%)**	**Ur (ppm)**	**Th (ppm)**	**Pass/Fail**	**KDOT Bed**	**Freeze/Thaw**	**Sample number**	**Total (cps)**
6	487.28	1.17	0.62	0.12	0.13	0.47	4.31	2.07	FAIL	3	NA	0.144	6
7	494.58	1.05	0.74	0.09	14.31	0.16	6.09	0.88	FAIL	3	NA	0.144	7
8**	493.78	1.14	0.58	0.08	12.76	0.46	4.5	0.85	FAIL	3	NA	0.144	8
9	475.04	1.21	0.84	0.08	0	0.24	7.19	0.62	FAIL	3	NA	0.144	9
10**	462.98	0.91	0.49	0.11	0	0.28	3.24	1.63	FAIL	3	NA	0.144	10
Summary Statistics													
	Total (cps)	**K (cps)**	**Ur (cps)**	**Th (cps)**	**Total (nGy/Hz)**	**K (%)**	**Ur (ppm)**	**Th (ppm)**					
Bed 3													
std dev.	10.493	0.135	0.126	0.017	5.697	0.115	1.371	0.572					
median	489.34	0.98	0.61	0.09	4.12	0.24	4.50	0.98					
mean	486.24	1.01	0.60	0.09	5.97	0.28	4.58	1.16					
maximum	494.58	1.21	0.84	0.12	14.31	0.47	7.19	2.07					
Bed 3 w/o shale													
standard dev.	6.42	0.14	0.14	0.02	5.44	0.11							
median	489.34	0.98	0.62	0.09	4.12	0.22							
mean	488.49	1.01	0.62	0.09	5.85	0.25							
maximum	494.58	1.21	0.84	0.12	14.31	0.47							
Total percent of clay rich rock													
KDOT BED													
3	4.4%												

Table 3.16: KDOT Quarry Code 4-054-11, Cass County, Martin Marietta Greenwood Quarry

Bethany Falls Limestone													
Sample number	**Total (cps)**	**K (cps)**	**Ur (cps)**	**Th (cps)**	**Total (nGy/Hz)**	**K (%)**	**Ur (ppm)**	**Th (ppm)**	**Pass/Fail**	**KDOT Bed**	**Freeze/Thaw**	**Durability Factor**	**Expansion Percent**
30 *	490.52	0.91	0.51	0.08	6.41	0.24	3.86	0.72	FAIL	7	85	0.035	30 *
31	465.24	0.71	0.49	0.07	0	0	3.84	0.54	FAIL	7	85	0.035	31
32	465.24	0.71	0.49	0.07	0	0	3.84	0.54	FAIL	7	85	0.035	32
33	463.94	0.85	0.44	0.04	0	0.21	3.88	0	FAIL	7	85	0.035	33
34	474.15	0.86	0.46	0.12	0	0.27	2.63	2.2	FAIL	7	85	0.035	34
35	487.56	0.83	0.47	0.09	0.67	0.19	3.34	1.1	FAIL	6	58	0.117	35
36	490.08	0.71	0.56	0.06	5.57	0	4.64	0.12	FAIL	6	58	0.117	36
37	463.18	0.99	0.49	0.07	0	0.36	3.93	0.37	FAIL	6	58	0.117	37
38	464.24	0.93	0.52	0.06	0	0.24	4.25	0.17	FAIL	6	58	0.117	38
39	486.22	0.86	0.47	0.06	0	0.22	3.74	0.21	FAIL	6	58	0.117	39
40	487.52	0.92	0.61	0.09	0.58	0.15	4.65	1.17	PASS	5	96	0.015	40
41	478.78	0.89	0.48	0.07	0	0.26	3.67	0.56	PASS	5	96	0.015	41
42	491.53	0.73	0.41	0.06	8.37	0.12	3.22	0.07	PASS	5	96	0.015	42
Summary Statistics													
	Total (cps)	**K (cps)**	**Ur (cps)**	**Th (cps)**	**Total (nGy/Hz)**	**K (%)**	**Ur (ppm)**	**Th (ppm)**					
Bed 5													
std dev.	6.520	0.102	0.101	0.015	4.674	0.074	0.731	0.551					
median	487.52	0.89	0.48	0.07	0.58	0.15	3.67	0.56					
mean	485.94	0.85	0.50	0.07	2.98	0.18	3.85	0.60					
maximum	491.53	0.92	0.61	0.09	8.37	0.26	4.65	1.17					

Table 3.16 (cont'd)													
	Total (cps)	**K (cps)**	**Ur (cps)**	**Th (cps)**	**Total (nGy/Hz)**	**K (%)**	**Ur (ppm)**	**Th (ppm)**					
Bed 6													
std dev.	13.356	0.106	0.038	0.013	2.433	0.130	0.495	0.406					
median	486.22	0.86	0.49	0.06	0.00	0.22	3.93	0.21					
mean	478.26	0.86	0.50	0.07	1.25	0.20	3.98	0.39					
maximum	490.08	0.99	0.56	0.09	5.57	0.36	4.64	1.10					
Bed 7													
std dev.	4.712	0.084	0.024	0.033	0.000	0.141	0.612	0.955					
median	465.24	0.78	0.48	0.07	0.00	0.11	3.84	0.54					
mean	467.14	0.78	0.47	0.08	0.00	0.12	3.55	0.82					
maximum	474.15	0.86	0.49	0.12	0.00	0.27	3.88	2.20					
Total percent of clay rich rock													
KDOT BED													
7	3.8												
6	4.4												

Table 3.17: KDOT Quarry Code 4-030-02 Franklin County, Martin Marietta Ottawa Quarry

Stoner Limestone													
Sample number	**Total (cps)**	**K (cps)**	**Ur (cps)**	**Th (cps)**	**Total (nGy/Hz)**	**K (%)**	**Ur (ppm)**	**Th (ppm)**	**Pass/Fail**	**KDOT Bed**	**Freeze/Thaw**	**Durability Factor**	**Expansion Percent**
1 *	488.98	0.94	0.8	0.12	3.42	0	6.2	1.72					1 *
2	464.09	1.02	0.88	0.08	0	0	7.26	0.4	PASS	5	0.92	98	0.009
3	494.04	0.88	0.69	0.09	13.26	0	5.59	0.91	PASS	5	0.92	98	0.009

Table 3.17 (cont'd)													
Sample number	**Total (cps)**	**K (cps)**	**Ur (cps)**	**Th (cps)**	**Total (nGy/Hz)**	**K (%)**	**Ur (ppm)**	**Th (ppm)**	**Pass/Fail**	**KDOT Bed**	**Freeze/Thaw**	**Durability Factor**	**Expansion Percent**
4	451.97	0.77	0.57	0.03	0	0	5.21	0	PASS	4	0.89	98	0.007
5	471.82	0.61	0.53	0.09	0	0	3.91	1.04	PASS	4	0.89	98	0.007
6	467.7	0.77	0.54	0.08	0	0.04	4.2	0.68	PASS	4	0.89	98	0.007
7	488.03	0.82	0.44	0.12	1.58	0.23	2.55	2.03	PASS	4	0.89	98	0.007
8	482.21	0.83	0.45	0.06	0	0.2	3.57	0.22	PASS	4	0.89	98	0.007
9	481.21	0.79	0.52	0.06	0	0.07	4.3	0.16	PASS	4	0.89	98	0.007
10	484.03	0.84	0.46	0.07	0	0.22	3.45	0.58	PASS	4	0.89	98	0.007
11	469.79	0.93	0.49	0.15	0	0.34	2.56	3.07	PASS	4	0.89	98	0.007
Summary Statistics													
	Total (cps)	**K (cps)**	**Ur (cps)**	**Th (cps)**	**Total (nGy/Hz)**	**K (%)**	**Ur (ppm)**	**Th (ppm)**					
Bed 4													
std dev.	11.720	0.091	0.047	0.038	0.559	0.127	0.897	1.065					
median	476.52	0.81	0.51	0.08	0.00	0.14	3.74	0.63					
mean	474.60	0.80	0.50	0.08	0.20	0.14	3.72	0.97					
maximum	488.03	0.93	0.57	0.15	1.58	0.34	5.21	3.07					
Bed 5													
std dev.	21.178	0.099	0.134	0.007	9.376	0.000	1.181	0.361					
median	479.07	0.95	0.79	0.09	6.63	0.00	6.43	0.66					
mean	479.07	0.95	0.79	0.09	6.63	0.00	6.43	0.66					
maximum	494.04	1.02	0.88	0.09	13.26	0.00	7.26	0.91					
Total percent of clay rich rock													
KDOT BED													
4	4.0%												
5	0.3%												

Table 3.18: KDOT Quarry Code 1-105-02 Wyandotte County, Shawnee Rock Company Bonner Springs Quarry

Argentine Limestone													
Sample number	**Total (cps)**	**K (cps)**	**Ur (cps)**	**Th (cps)**	**Total (nGy/Hz)**	**K (%)**	**Ur (ppm)**	**Th (ppm)**	**Pass/Fail**	**KDOT Bed**	**Freeze/Thaw**	**Durability Factor**	**Expansion Percent**
1 *	493.62	0.78	0.4	0.04	12.43	0.18	3.34	0	PASS				1 *
2	462.18	0.71	0.34	0.09	0	0.19	2	1.21	PASS	9	NA	NA	2
3	467.36	0.72	0.32	0.05	0	0.2	2.41	0	PASS	9	NA	NA	3
4	482.93	0.56	0.22	0.03	0	0.1	1.67	0	PASS	9	NA	NA	4
5	464.73	0.64	0.34	0.06	0	0.09	2.51	0.3	PASS	9	NA	NA	5
6	485.29	0.57	0.33	0.07	0	0.02	2.25	0.49	PASS	9	NA	NA	6
7	481.42	0.64	0.38	0.09	0	0.07	2.39	1.17	PASS	9	NA	NA	7
8	467.92	0.74	0.31	0.04	0	0.24	2.44	0	PASS	9	NA	NA	8
9	456.69	0.75	0.36	0.06	0	0.19	2.77	0.11	PASS	9	NA	NA	9
10	486.8	0.69	0.34	0.04	0	0.13	2.82	0	PASS	10	NA	NA	10
11	462.9	0.62	0.42	0.07	0	0	3.06	0.6	PASS	10	NA	NA	11
12	489.81	0.61	0.41	0.07	5.04	0	2.94	0.61	PASS	10	NA	NA	12
13	471.88	0.73	0.39	0.06	0	0.14	3.05	0.09	PASS	10	NA	NA	13
14	478.02	0.72	0.37	0.08	0	0.16	2.52	0.82	PASS	10	NA	NA	14
Bed 9													
std dev.	10.688	0.075	0.048	0.022	0.000	0.077	0.337	0.511					
median	467.64	0.68	0.34	0.06	0.00	0.15	2.40	0.21					
mean	471.07	0.67	0.33	0.06	0.00	0.14	2.31	0.41					
maximum	485.29	0.75	0.38	0.09	0.00	0.24	2.77	1.21					
Bed 10													
std dev.	10.981	0.056	0.032	0.015	2.254	0.079	0.223	0.358					
median	478.02	0.69	0.39	0.07	0.00	0.13	2.94	0.60					
mean	477.88	0.67	0.39	0.06	1.01	0.09	2.88	0.42					
maximum	489.81	0.73	0.42	0.08	5.04	0.16	3.06	0.82					
Total percent of clay rich rock for KDOT BED													
9	5.5%												
10	3%												

Table 3.19: KDOT Quarry Code 1-105-02 Wyandotte County, Shawnee Rock Company Shawnee (JCL-Meth) Quarry

Argentine Limestone													
Sample number	**Total (cps)**	**K (cps)**	**Ur (cps)**	**Th (cps)**	**Total (nGy/Hz)**	**K (%)**	**Ur (ppm)**	**Th (ppm)**	**Pass/Fail**	**KDOT Bed**	**Freeze/Thaw**	**Durability Factor**	**Expansion Percent**
1 *	514.41	1.5	0.72	0.19	23.72	0.91	3.97	4.53	PASS	5	98	0.01	1 *
2	504.31	1.02	0.5	0.18	7.49	0.53	1.78	4.52	PASS	5	98	0.01	2
3	500.96	0.96	0.38	0.06	2.12	0.5	2.6	0.69	PASS	5	98	0.01	3
4	491.24	0.98	0.49	0.11	0	0.43	2.98	2.14	PASS	5	98	0.01	4
5	485.3	0.87	0.5	0.12	0	0.3	2.85	2.47	PASS	4	98	0.01	5
6	493.39	0.9	0.46	0.09	0	0.36	2.85	1.65	PASS	4	98	0.01	6
7	487.9	0.98	0.46	0.09	0	0.46	2.85	1.65	PASS	4	98	0.01	7
8	493.63	0.85	0.59	0.07	0	0.13	4.57	0.87	PASS	4	98	0.01	8
9	497.54	1	0.7	0.1	0	0.23	5.16	1.81	PASS	4	98	0.01	9
10	491.28	0.92	0.54	0.08	0	0.29	3.85	1.41	PASS	4	98	0.01	10
Summary Statistics													
	Total (cps)	**K (cps)**	**Ur (cps)**	**Th (cps)**	**Total (nGy/Hz)**	**K (%)**	**Ur (ppm)**	**Th (ppm)**					
Bed 5													
std dev.	6.789	0.031	0.067	0.060	3.861	0.051	0.613	1.934					
median	500.96	0.98	0.49	0.11	2.12	0.50	2.60	2.14					
mean	498.84	0.99	0.46	0.12	3.20	0.49	2.45	2.45					
maximum	504.31	1.02	0.50	0.18	7.49	0.53	2.98	4.52					
Bed 4	4.383	0.060	0.092	0.017	0.000	0.112	1.008						
std dev.	492.34	0.91	0.52	0.09	0.00	0.30	3.35						
median	491.51	0.92	0.54	0.09	0.00	0.30	3.69						
mean	497.54	1.00	0.70	0.12	0.00	0.46	5.16						
maximum	4.383	0.060	0.092	0.017	0.000	0.112	1.008						
Total percent of clay rich rock for KDOT BED													
5	1.1%												
4	0.7%												

Table 3.20: KDOT Quarry Code 1-046-13, Johnson County, Shawnee Rock Company "Lone Elm" Quarry

Argentine Limestone													
Sample number	**Total (cps)**	**K (cps)**	**Ur (cps)**	**Th (cps)**	**Total (nGy/Hz)**	**K (%)**	**Ur (ppm)**	**Th (ppm)**	**Pass/Fail**	**KDOT Bed**	**Freeze/Thaw**	**Durability Factor**	**Expansion Percent**
1 *	494.05	0.93	0.63	0.09	13.27	0.15	4.91	0.97	FAIL	13	82	0.079	1 *
2	464.27	1.01	0.53	0.1	0	0.36	3.77	1.42	FAIL	12	NA	NA	2
3	463.88	1.36	0.74	0.2	0	0.63	4.26	4.49	FAIL	12	NA	NA	3
4	465.07	1.16	0.61	0.09	0	0.44	4.74	1	FAIL	12	NA	NA	4
5	471.7	1.06	0.49	0.08	0	0.46	3.69	0.74	FAIL	12	NA	NA	5
6	466.04	1.11	0.46	0.07	0	0.54	3.53	0.41	FAIL	12	NA	NA	6
7	459.74	0.86	0.49	0.11	0	0.23	3.15	1.81	FAIL	12	NA	NA	7
8	461.4	0.87	0.44	0.12	0	0.29	2.51	2.21	FAIL	12	NA	NA	8
9	461.99	0.94	0.57	0.12	0	0.25	3.84	1.93	FAIL	12	NA	NA	9
10	491.55	1.23	0.74	0.08	8.42	0.39	6.12	0.71	FAIL	12	NA	NA	10
11	462.02	0.77	0.55	0.08	0	0.03	4.22	0.85	FAIL	11	92	0.038	11
12	475.99	0.96	0.67	0.08	0	0.11	5.44	0.57	FAIL	11	92	0.038	12
13	458.39	0.94	0.63	0.12	0	0.17	4.51	1.87	FAIL	11	92	0.038	13
14	467.83	1.12	0.49	0.09	0	0.54	3.47	1.28	FAIL	11	92	0.038	14
Summary Statistics													
	Total (cps)	**K (cps)**	**Ur (cps)**	**Th (cps)**	**Total (nGy/Hz)**	**K (%)**	**Ur (ppm)**	**Th (ppm)**					
Bed 11													
std dev.	7.679	0.143	0.081	0.019	0.000	0.226	0.815	0.566					
median	464.93	0.95	0.59	0.09	0.00	0.14	4.37	1.07					
mean	466.06	0.95	0.59	0.09	0.00	0.21	4.41	1.14					
maximum	475.99	1.12	0.67	0.12	0.00	0.54	5.44	1.87					
Bed 12													
std dev.	9.715	0.167	0.113	0.039	2.807	0.134	1.027	1.235					
median	464.27	1.06	0.53	0.10	0.00	0.39	3.77	1.42					
mean	467.29	1.07	0.56	0.11	0.94	0.40	3.96	1.64					
maximum	491.55	1.36	0.74	0.20	8.42	0.63	6.12	4.49					

Table 3.21: KDOT Quarry Code 4-061-08, Miami County, APAC "Reno" Quarry, Upper Farley

Upper Farley Limestone													
Sample number	**Total (cps)**	**K (cps)**	**Ur (cps)**	**Th (cps)**	**Total (nGy/Hz)**	**K (%)**	**Ur (ppm)**	**Th (ppm)**	**Pass/Fail**	**KDOT Bed**	**Freeze/Thaw**	**Durability Factor**	**Expansion Percent**
1 *	505.44	0.84	0.38	0.12	9.31	0.4	1.61	2.56	PASS	1	97	0.007	1 *
2	506.87	0.76	0.37	0.07	11.61	0.26	2.3	1.03	PASS	1	97	0.007	2
3	505.6	0.62	0.49	0.05	9.57	0	3.87	0.42	PASS	1	97	0.007	3
4	494.92	0.57	0.27	0.06	0	0.13	1.46	0.77	PASS	1	97	0.007	4
5	503.55	0.62	0.43	0.06	6.28	0.02	3.01	0.81	PASS	1	97	0.007	5
6	505.68	0.49	0.32	0.07	9.69	0	1.84	1.06	PASS	1	97	0.007	6
7	503.65	0.51	0.31	0.06	6.43	0	1.8	0.9	PASS	1	97	0.007	7
8	497.03	0.51	0.34	0.07	0	0	1.92	1.22	PASS	1	97	0.007	8
9	505.03	0.62	0.24	0.08	8.65	0.23	0.87	1.47	PASS	1	97	0.007	9
10	511.87	0.69	0.37	0.1	19.63	0.19	1.82	2.05	PASS	1	97	0.007	10
Summary Statistics													
	Total (cps)	**K (cps)**	**Ur (cps)**	**Th (cps)**	**Total (nGy/Hz)**	**K (%)**	**Ur (ppm)**	**Th (ppm)**					
Bed 1													
std dev.	5.094	0.090	0.077	0.015	5.994	0.110	0.880	0.468					
median	505.03	0.62	0.34	0.07	8.65	0.02	1.84	1.03					
mean	503.80	0.60	0.35	0.07	7.98	0.09	2.10	1.08					
maximum	511.87	0.76	0.49	0.10	19.63	0.26	3.87	2.05					

The 22 measured sections which correspond to the scintillometer readings are presented below. The individual scintillometer measurement points, KDOT bed number and KDOT physical test pass/fail status are also included on the figures. The figure legend that applies to all of the measured sections is shown as Figure 3.10.

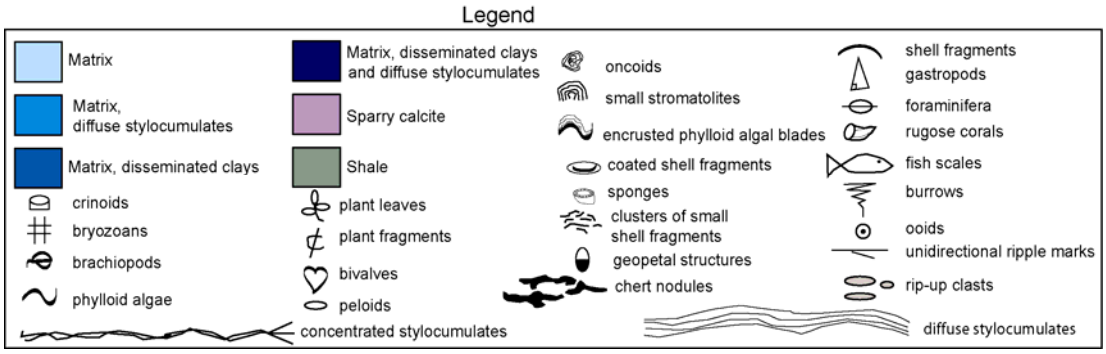

Figure 3.10: Figure Legend for Each of the Measured Sections

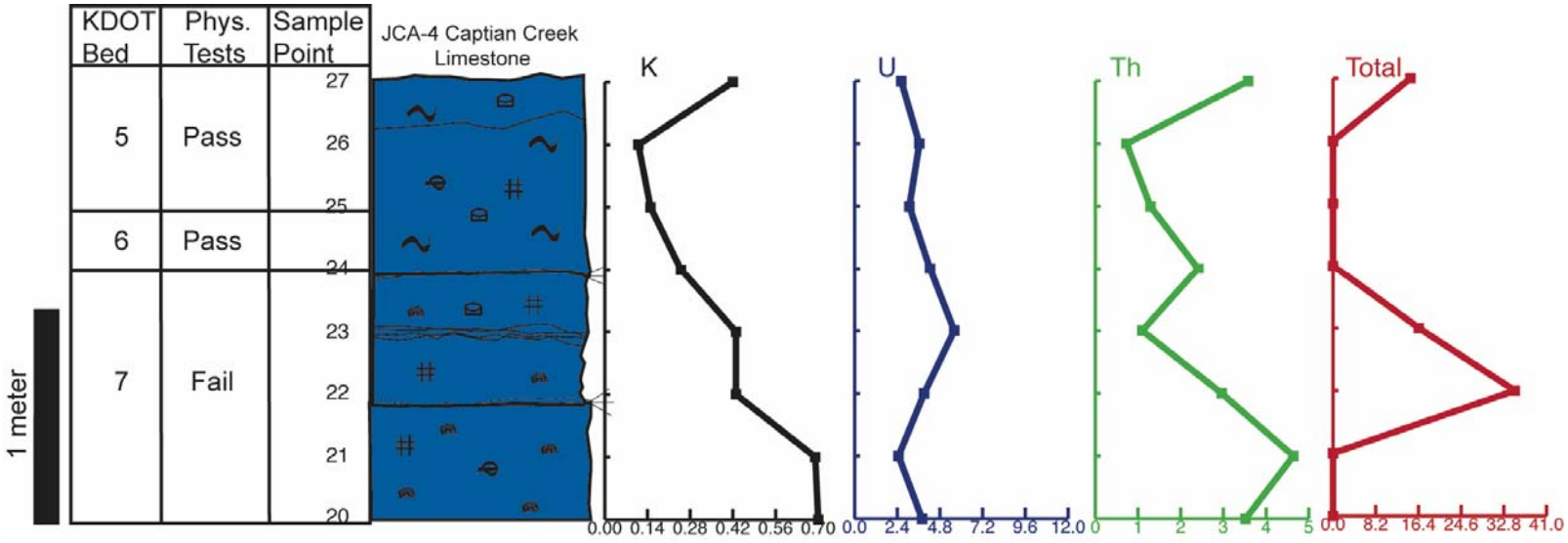

Figure 3.11: Measured Section of the Captain Creek Limestone in Olathe, Kansas

[(Johnson County Aggregate Quarry) Radiation values are plotted similar to well logs. Potassium is given as a percentage, Uranium and Thorium are in ppm and total radiation is in nGyn/Hz. The KDOT Bed number, results of KDOT tests, and the sampling points are shown to the left of the section.]

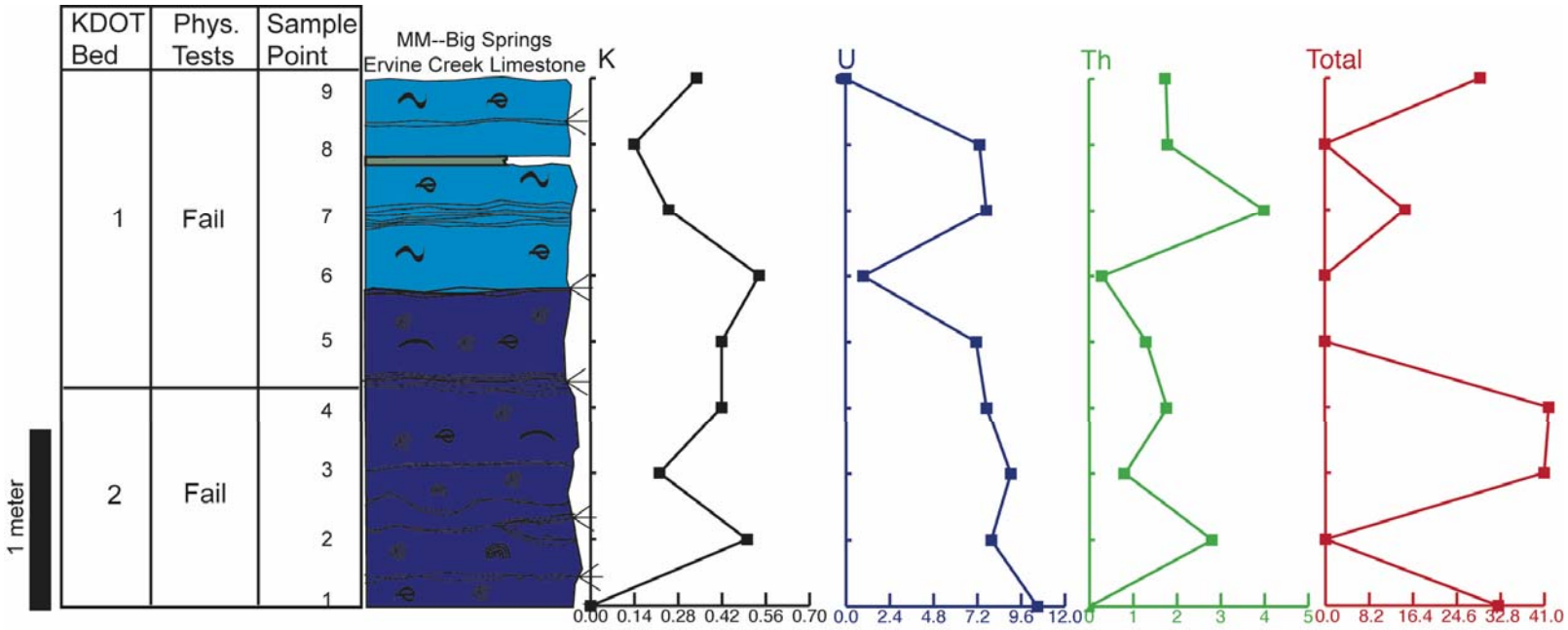

Figure 3.12: Measured Section of the Ervine Creek Limestone in Big Springs, Kansas

[(Martin Marietta Quarry) Radiation values are plotted similar to well logs. Potassium is given as a percentage, Uranium and Thorium are in ppm and total radiation is in nGyn/Hz. The KDOT Bed number, results of KDOT tests, and the sampling points are shown to the left of the section.]

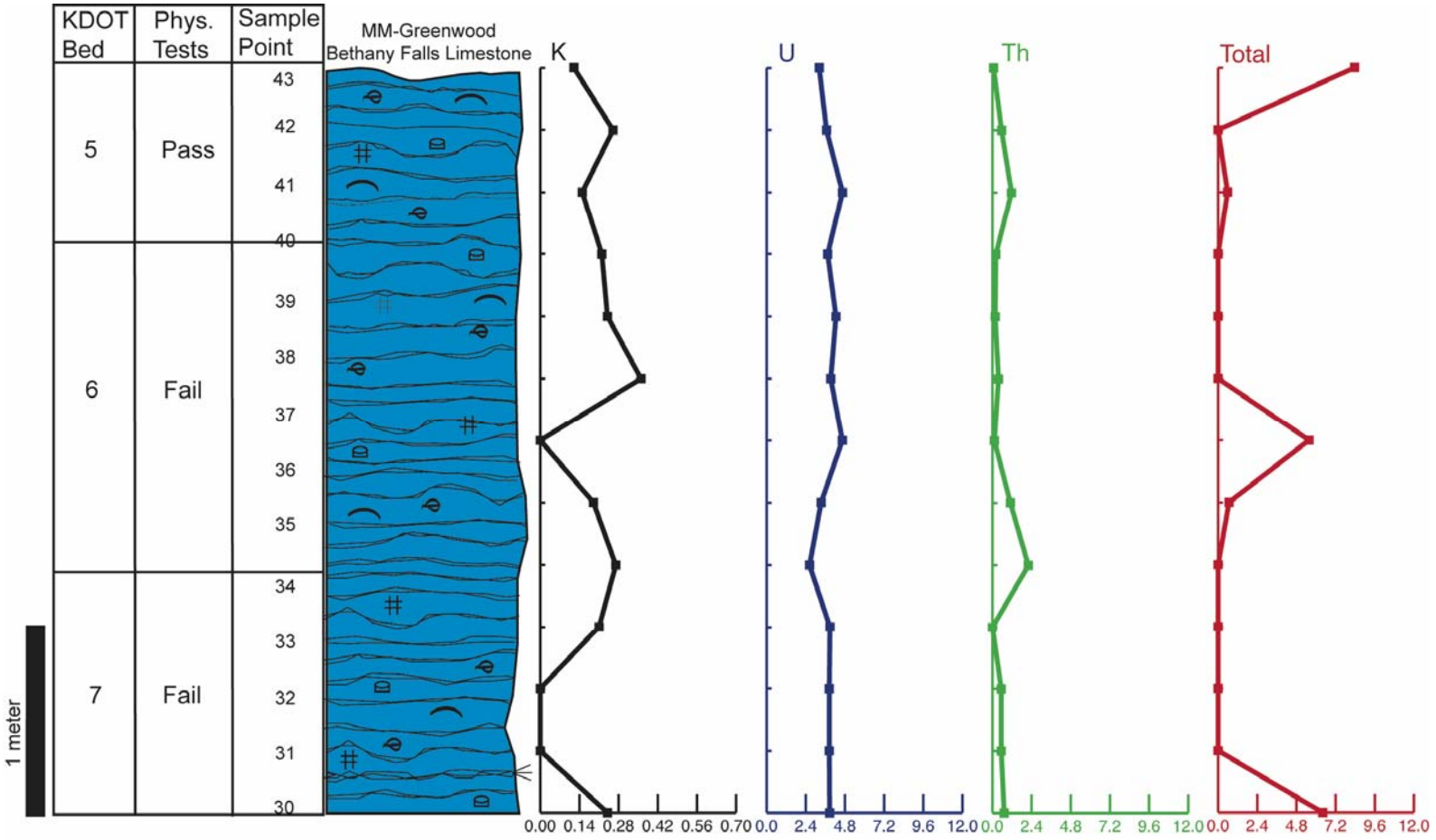

Figure 3.13: Measured Section of the Bethany Falls Limestone in Greenwood, Missouri

[(Martin Marietta Quarry) Radiation values are plotted similar to well logs. Potassium is given as a percentage, Uranium and Thorium are in ppm and total radiation is in nGyn/Hz. The KDOT Bed number, results of KDOT tests, and the sampling points are shown to the left of the section.]

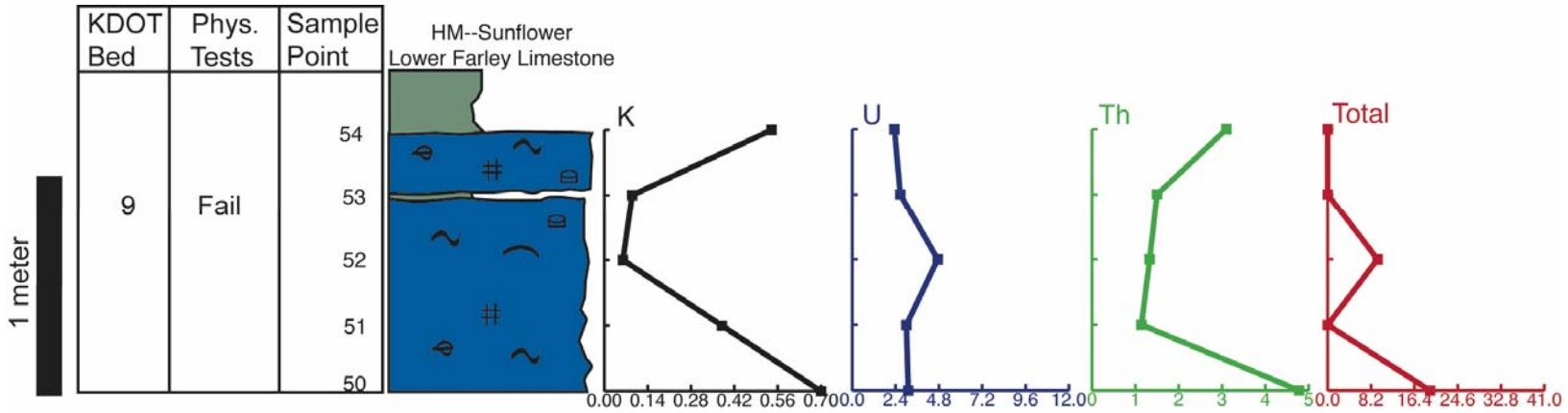

Figure 3.14: Measured Section of the Bethany Falls Limestone in Greenwood, Missouri

[(Martin Marietta Quarry) Radiation values are plotted similar to well logs. Potassium is given as a percentage, Uranium and Thorium are in ppm and total radiation is in nGyn/Hz. The KDOT Bed number, results of KDOT tests, and the sampling points are shown to the left of the section.]

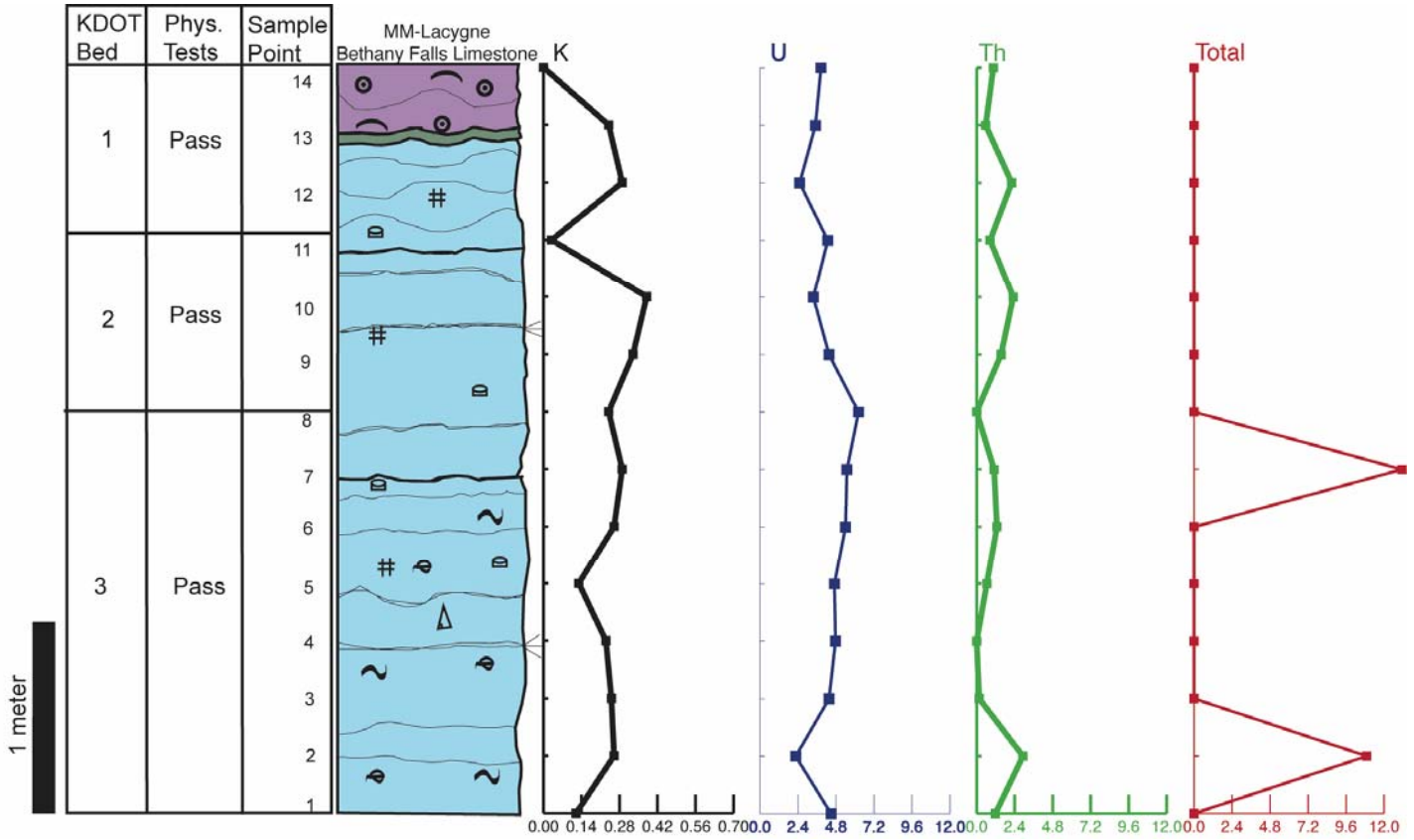

Figure 3.15: Measured Section of the Bethany Falls Limestone in La Cygne, Kansas

[(Martin Marietta Quarry) Radiation values are plotted similar to well logs. Potassium is given as a percentage, Uranium and Thorium are in ppm and total radiation is in nGyn/Hz. The KDOT Bed number, results of KDOT tests, and the sampling points are shown to the left of the section.]

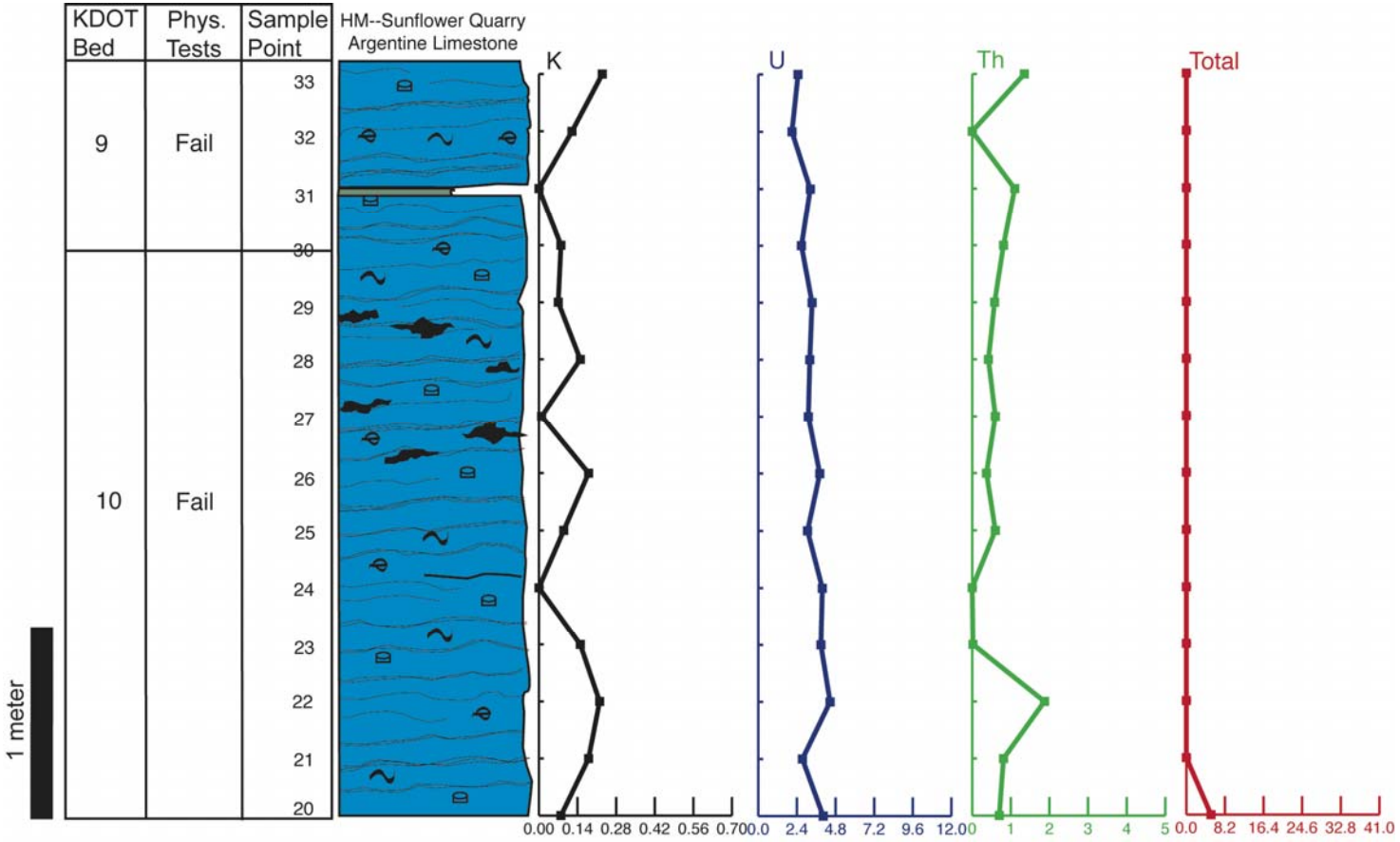

Figure 3.16: Measured Section of the Argentine Limestone in DeSoto, Kansas

[(Hunt Midwest Quarry) Radiation values are plotted similar to well logs. Potassium is given as a percentage, Uranium and Thorium are in ppm and total radiation is in nGyn/Hz. The KDOT Bed number, results of KDOT tests, and the sampling points are shown to the left of the section.]

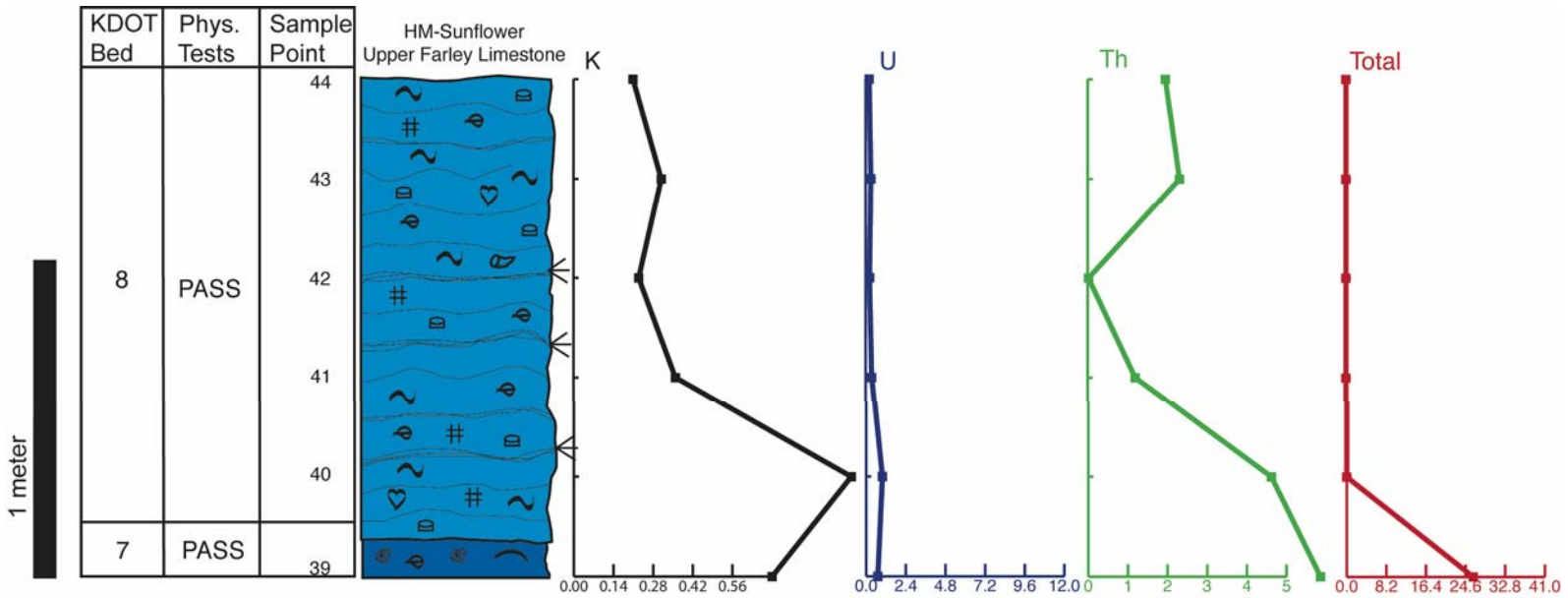

Figure 3.17: Measured Section of the Upper Farley Limestone in DeSoto, Kansas

[(Hunt Midwest Quarry) Radiation values are plotted similar to well logs. Potassium is given as a percentage, Uranium and Thorium are in ppm and total radiation is in nGyn/Hz. The KDOT Bed number, results of KDOT tests, and the sampling points are shown to the left of the section.]

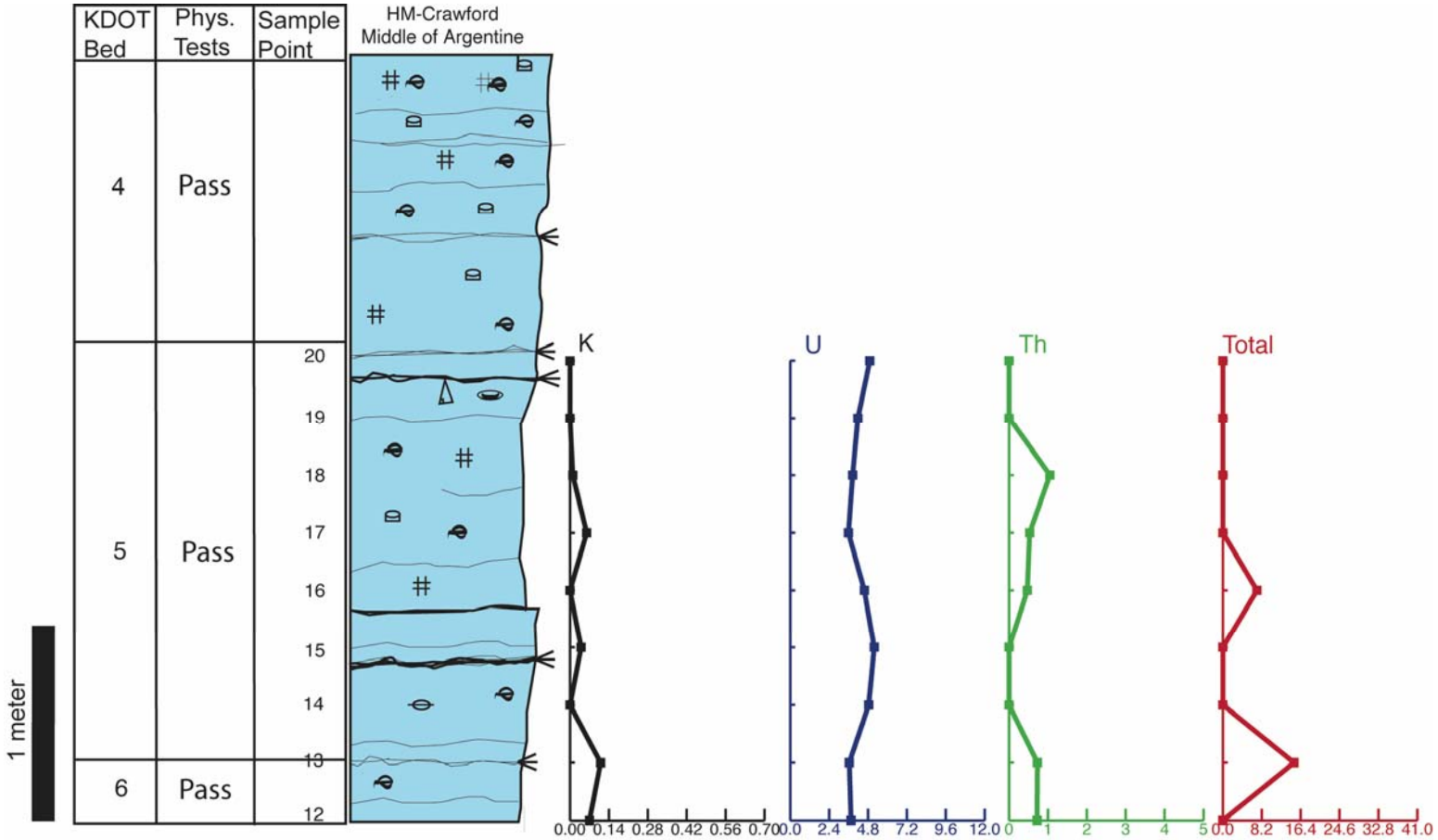

Figure 3.18: Measured Section of the Argentine Limestone in Louisburg, Kansas

[(Martin Marietta "Crawford" Quarry) Radiation values are plotted similar to well logs. Potassium is given as a percentage, Uranium and Thorium are in ppm and total radiation is in nGyn/Hz. The KDOT Bed number, results of KDOT tests, and the sampling points are shown to the left of the section.]

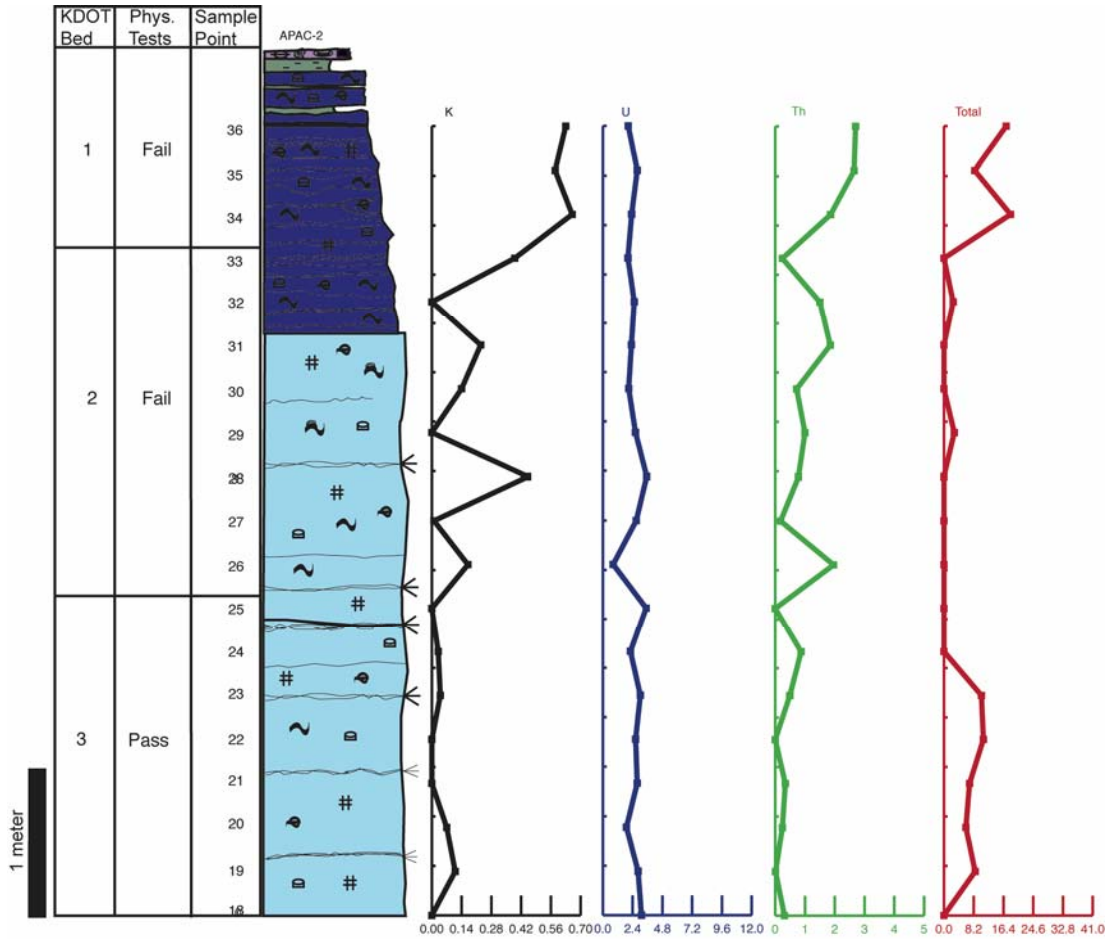

Figure 3.19: Measured Section of the Argentine Limestone in Louisburg, Kansas

[(APAC Quarry) Radiation values are plotted similar to well logs. Potassium is given as a percentage, Uranium and Thorium are in ppm and total radiation is in nGyn/Hz. The KDOT Bed number, results of KDOT tests, and the sampling points are shown to the left of the section.]

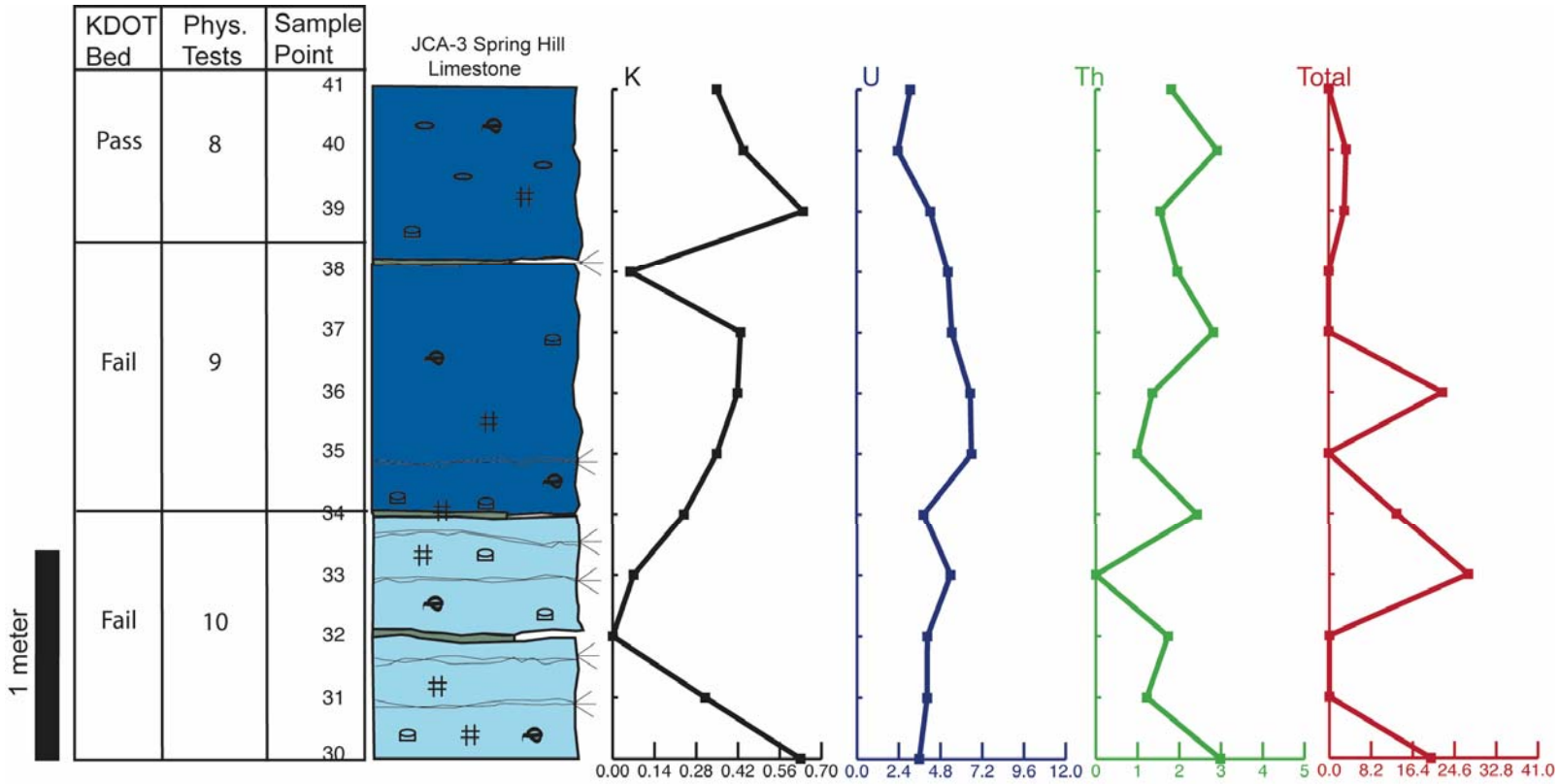

Figure 3.20: Measured Section of the Spring Hill Limestone in Olathe, Kansas

[(Johnson County Aggregate Quarry) Radiation values are plotted similar to well logs. Potassium is given as a percentage, Uranium and Thorium are in ppm and total radiation is in nGyn/Hz. The KDOT Bed number, results of KDOT tests, and the sampling points are shown to the left of the section.]

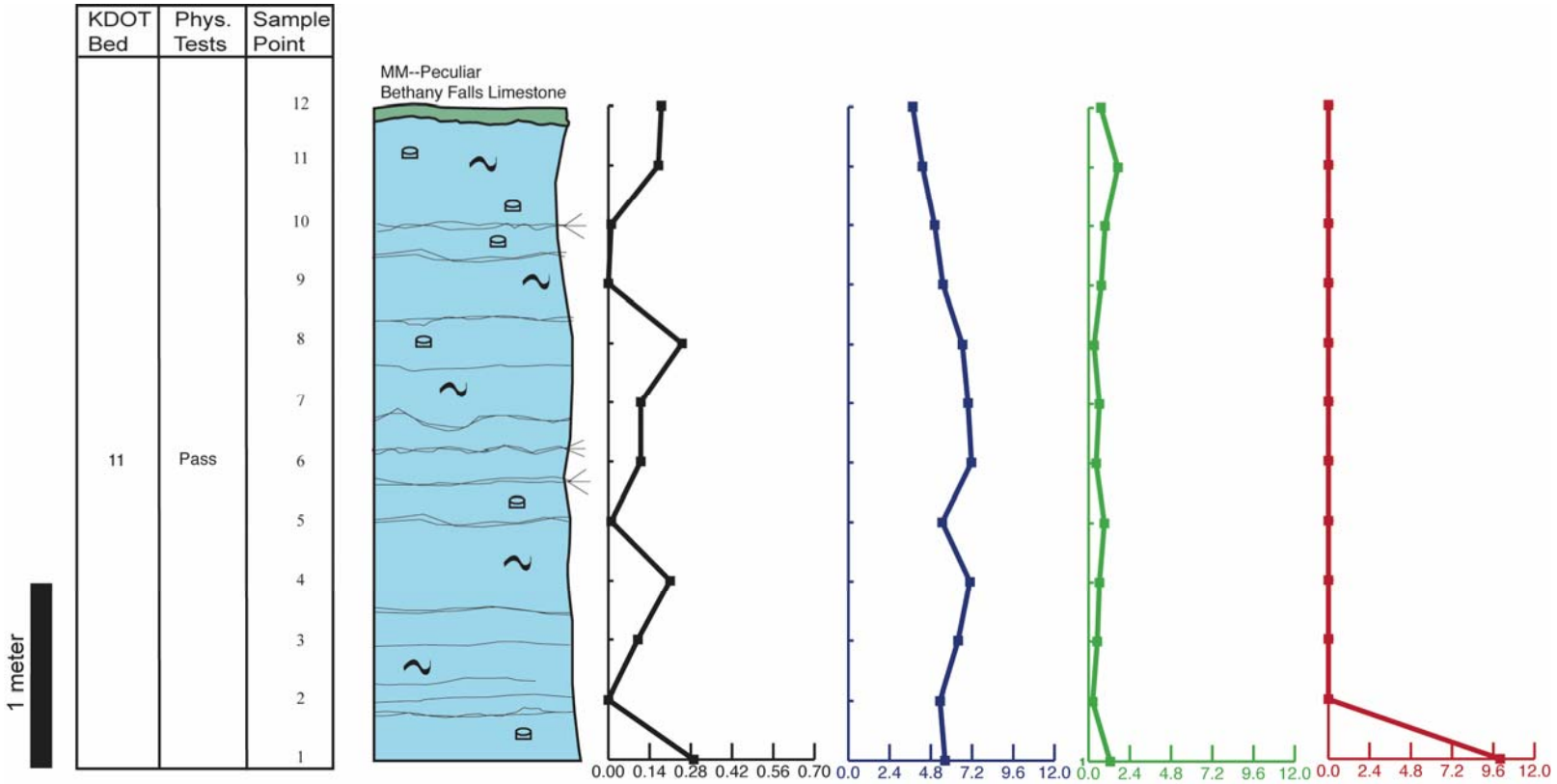

Figure 3.21: Measured Section of the Bethany Falls Limestone in Peculiar, Missouri

[(Martin Marietta Quarry) Radiation values are plotted similar to well logs. Potassium is given as a percentage, Uranium and Thorium are in ppm and total radiation is in nGyn/Hz. The KDOT Bed number, results of KDOT tests, and the sampling points are shown to the left of the section.]

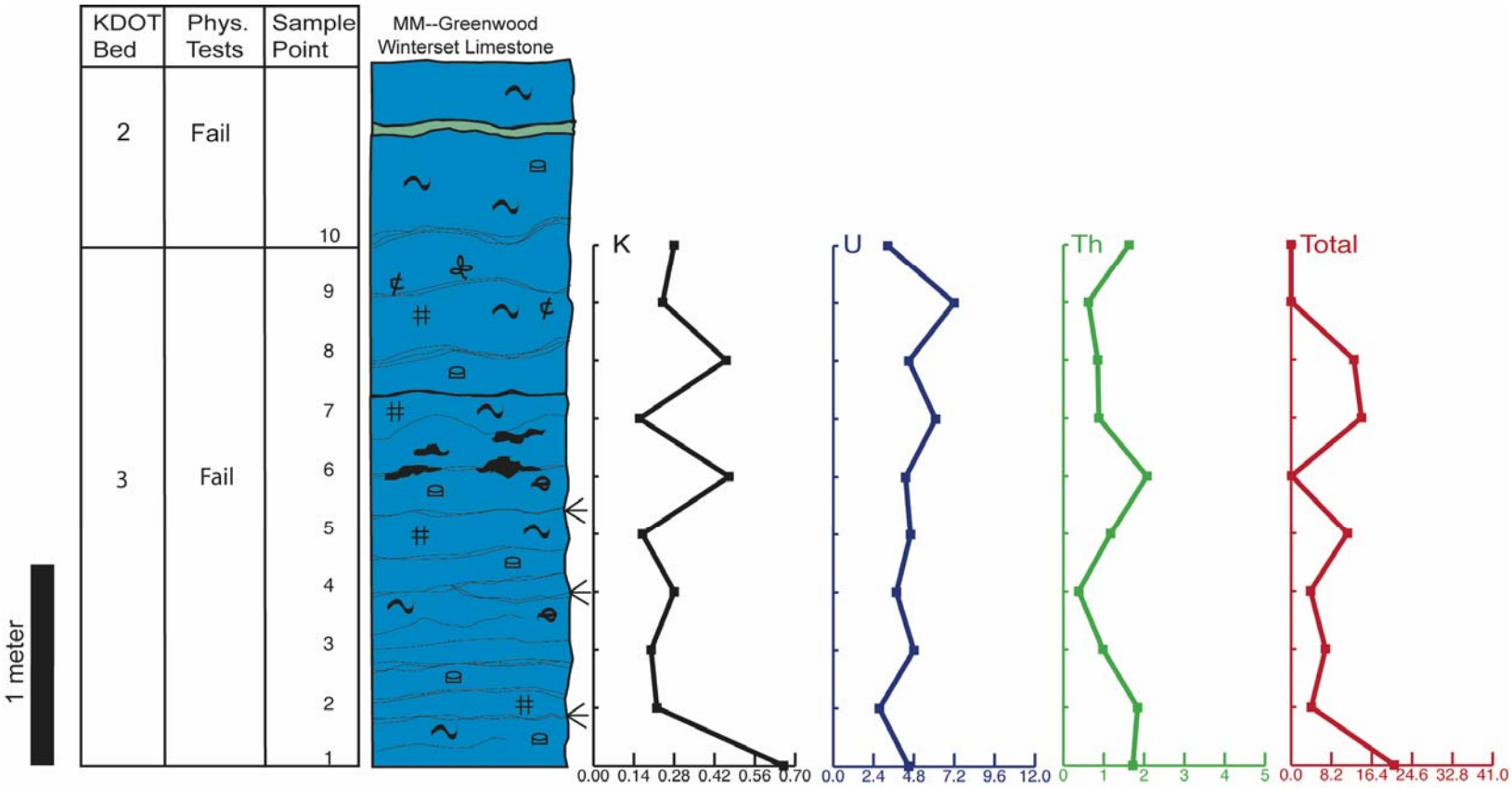

Figure 3.22: Measured Section of the Winterset Limestone in Greenwood, Missouri

[(Martin Marietta Quarry) Radiation values are plotted similar to well logs. Potassium is given as a percentage, Uranium and Thorium are in ppm and total radiation is in nGyn/Hz. The KDOT Bed number, results of KDOT tests, and the sampling points are shown to the left of the section.]

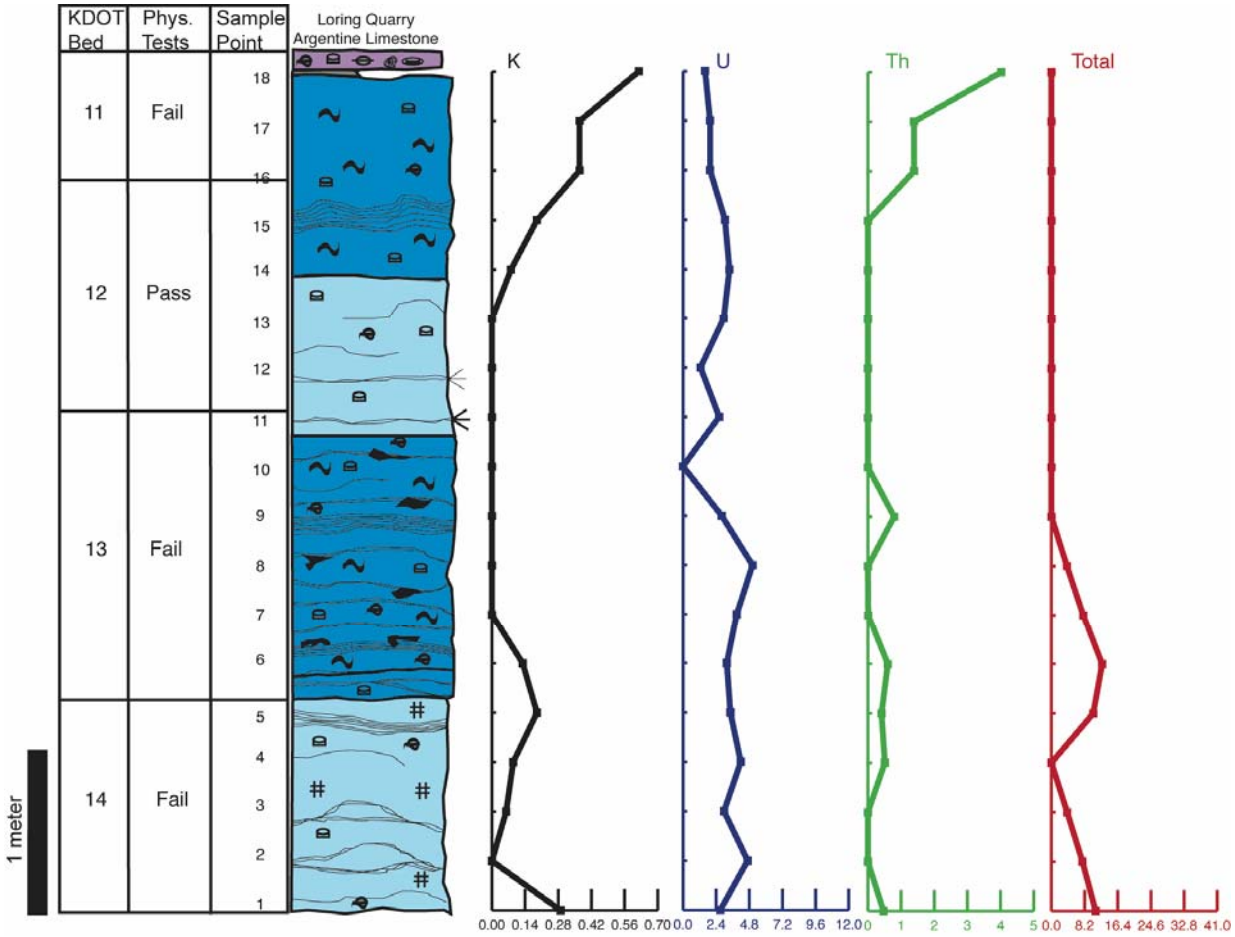

Figure 3.23: Measured Section of the Argentine Limestone in Loring, Kansas

[(Privately Owned Quarry) Radiation values are plotted similar to well logs. Potassium is given as a percentage, Uranium and Thorium are in ppm and total radiation is in nGyn/Hz. The KDOT Bed number, results of KDOT tests, and the sampling points are shown to the left of the section.]

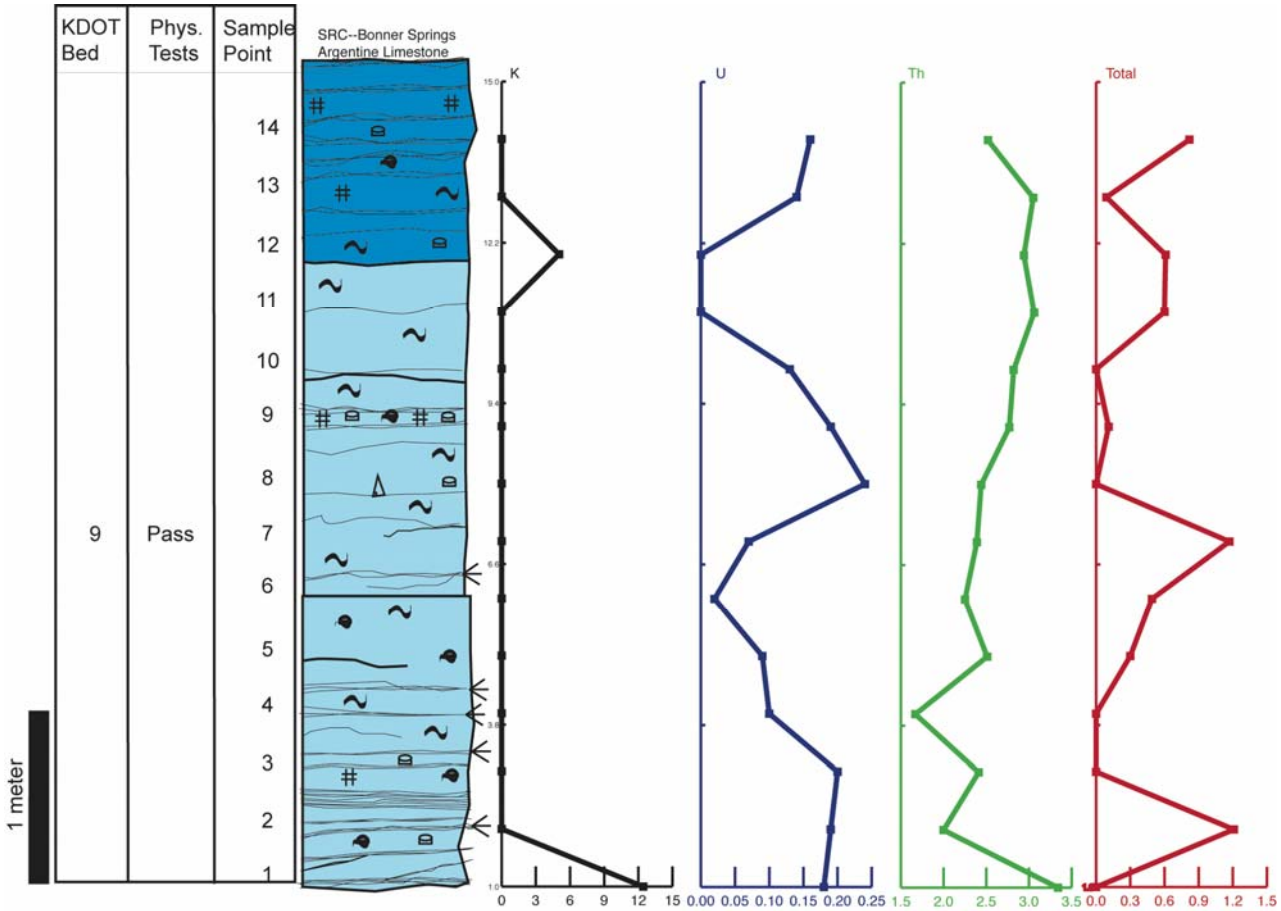

Figure 3.24: Measured Section of the Argentine Limestone in Bonner Springs, Kansas

[(Shawnee Rock Company Quarry) Radiation values are plotted similar to well logs. Potassium is given as a percentage, Uranium and Thorium are in ppm and total radiation is in nGyn/Hz. The KDOT Bed number, results of KDOT tests, and the sampling points are shown to the left of the section.]

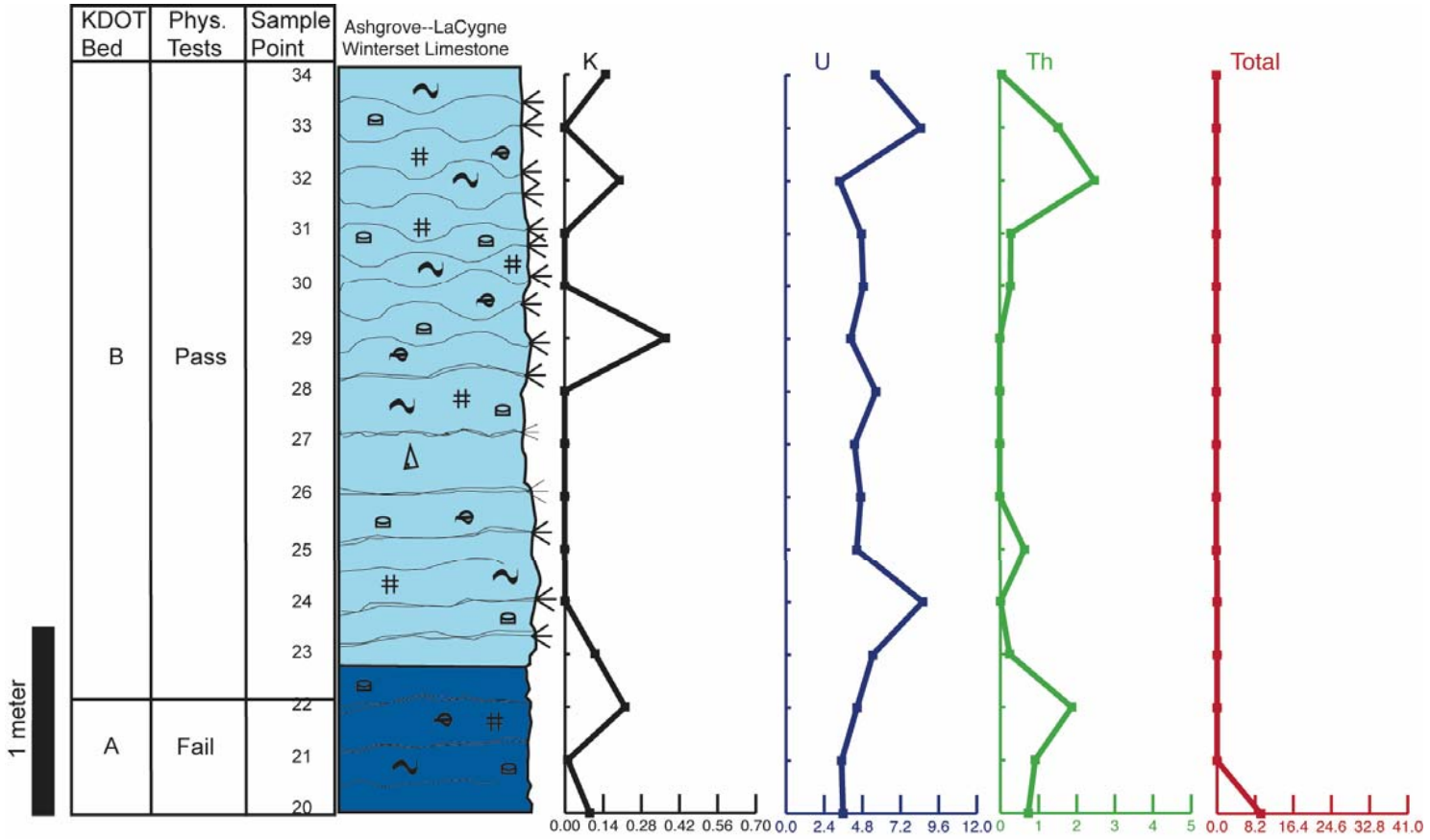

Figure 3.25: Measured Section of the Winterset Limestone in LaCygne, Kansas

[(Ashgrove Aggregates Quarry) Radiation values are plotted similar to well logs. Potassium is given as a percentage, Uranium and Thorium are in ppm and total radiation is in nGyn/Hz. The KDOT Bed number, results of KDOT tests, and the sampling points are shown to the left of the section.]

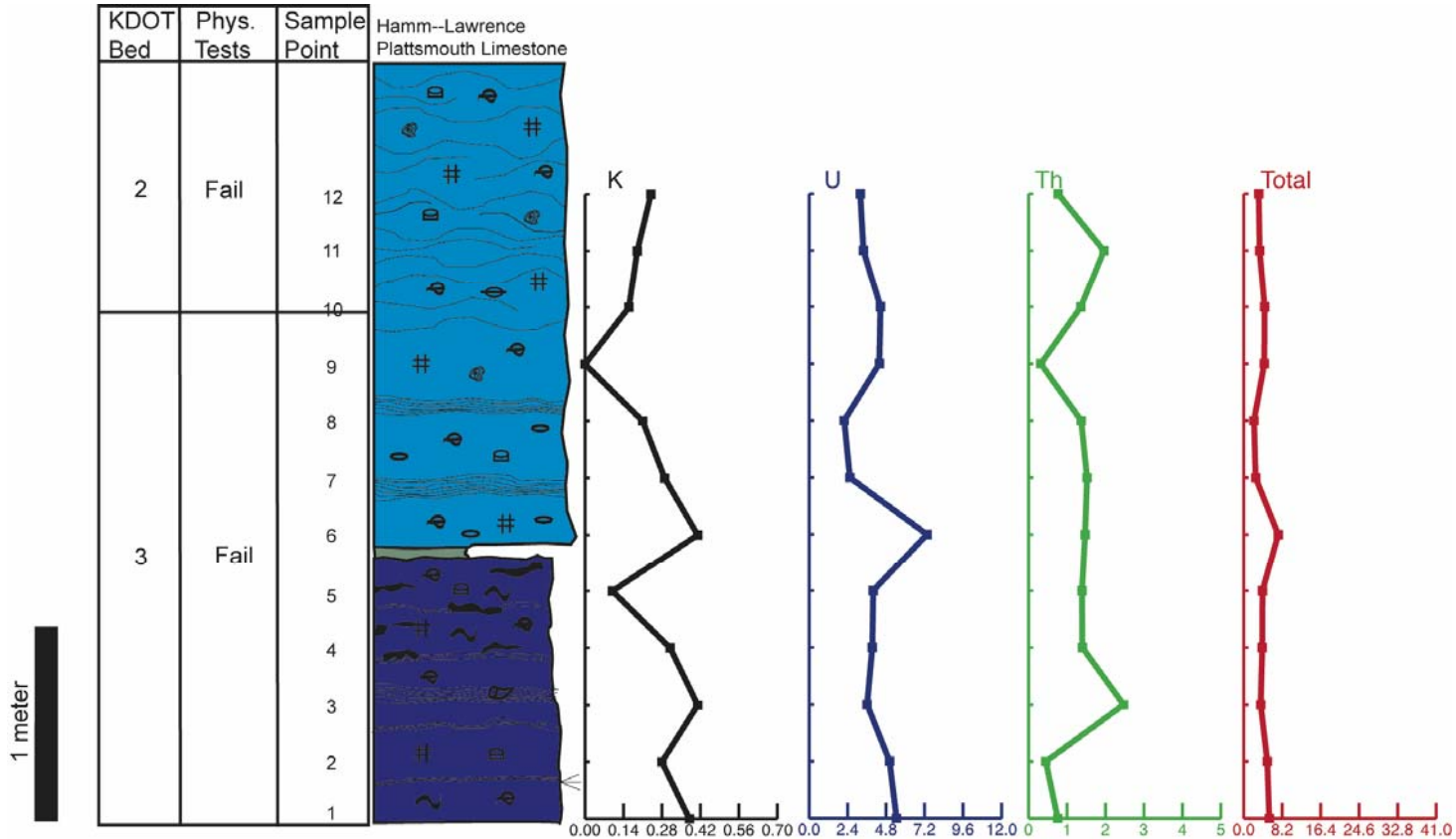

Figure 3.26: Measured Section of the Plattsmouth Limestone in Lawrence, Kansas

[(Hamm Construction Quarry) Radiation values are plotted similar to well logs. Potassium is given as a percentage, Uranium and Thorium are in ppm and total radiation is in nGyn/Hz. The KDOT Bed number, results of KDOT tests, and the sampling points are shown to the left of the section.]

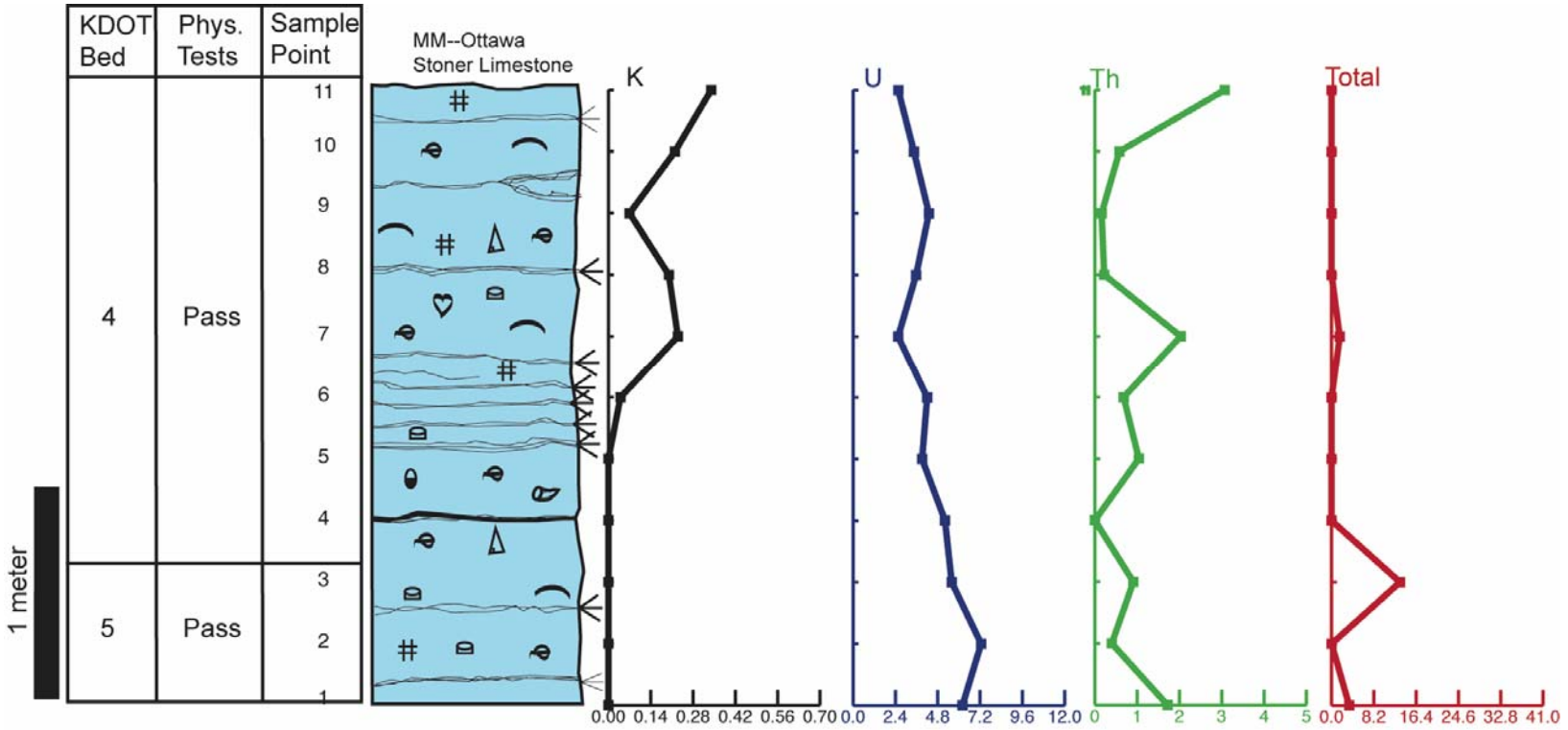

Figure 3.27: Measured Section of the Stoner Limestone in Ottawa, Kansas

[(Martin Marietta Quarry) Radiation values are plotted similar to well logs. Potassium is given as a percentage, Uranium and Thorium are in ppm and total radiation is in nGyn/Hz. The KDOT Bed number, results of KDOT tests, and the sampling points are shown to the left of the section.]

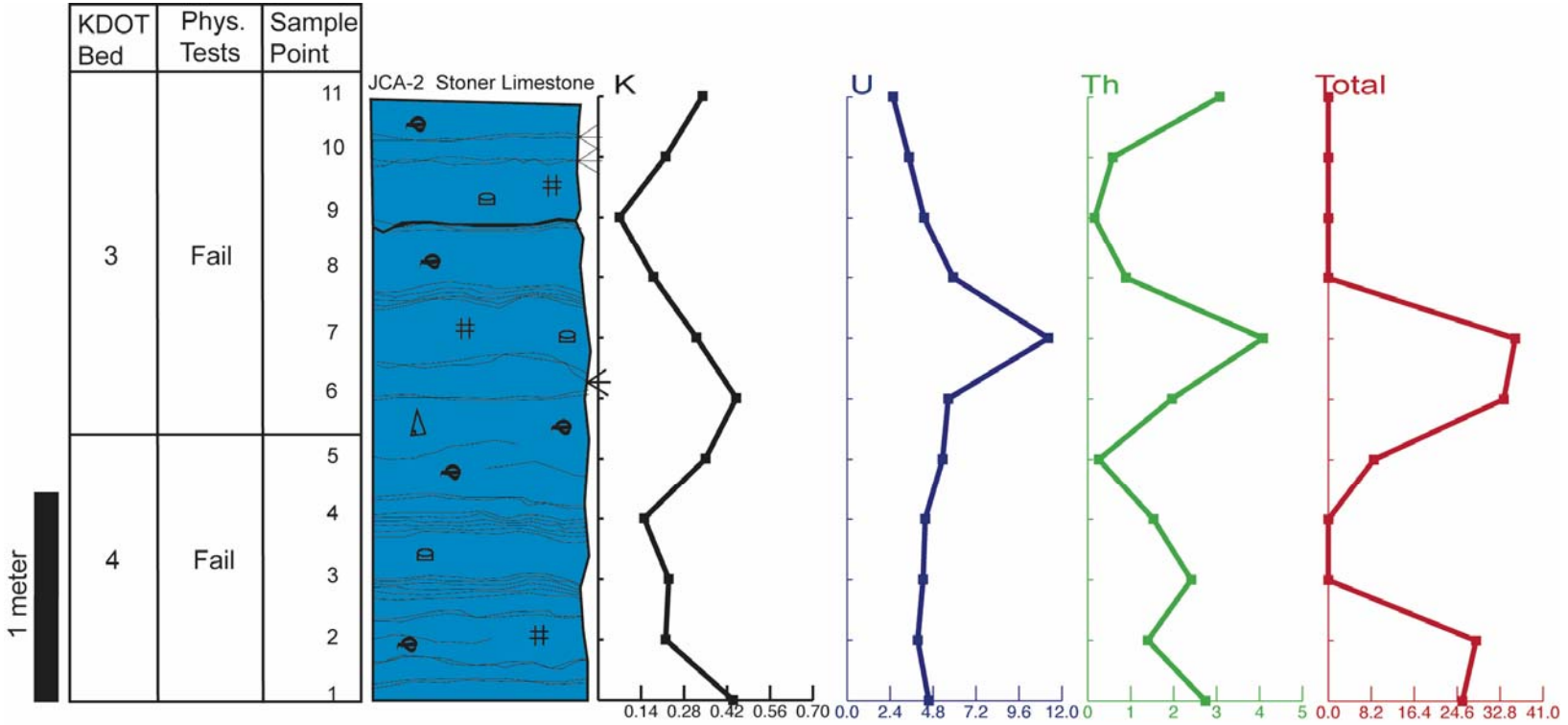

Figure 3.28: Measured Section of the Bethany Falls Limestone in Olathe, Kansas

[(Johnson County Aggregate Quarry) Radiation values are plotted similar to well logs. Potassium is given as a percentage, Uranium and Thorium are in ppm and total radiation is in nGyn/Hz. The KDOT Bed number, results of KDOT tests, and the sampling points are shown to the left of the section.]

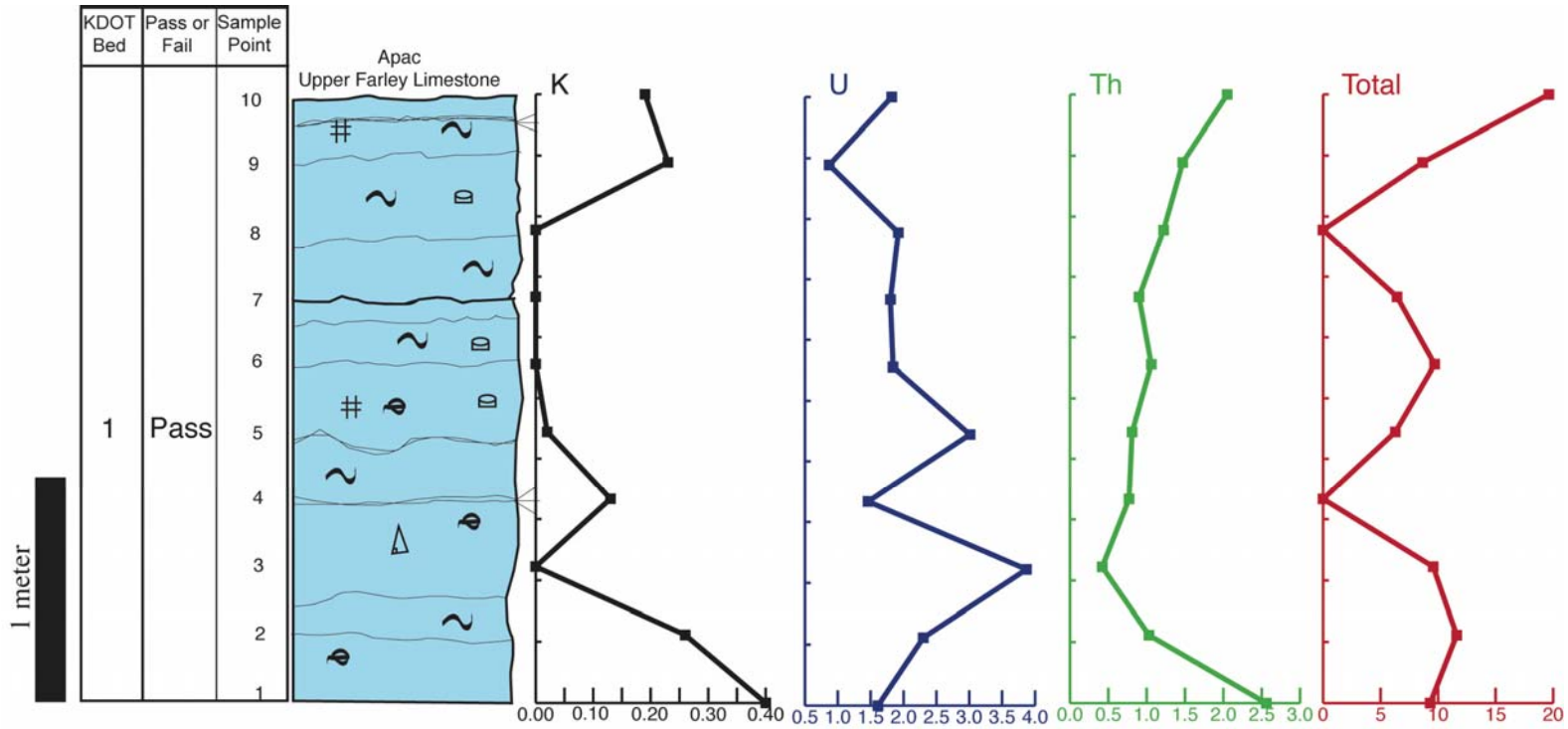

Figure 3.29: Measured Section of the Upper Farley Limestone in Louisburg, Kansas

[(APAC Quarry) Radiation values are plotted similar to well logs. Potassium is given as a percentage, Uranium and Thorium are in ppm and total radiation is in nGyn/Hz. The KDOT Bed number, results of KDOT tests, and the sampling points are shown to the left of the section.]

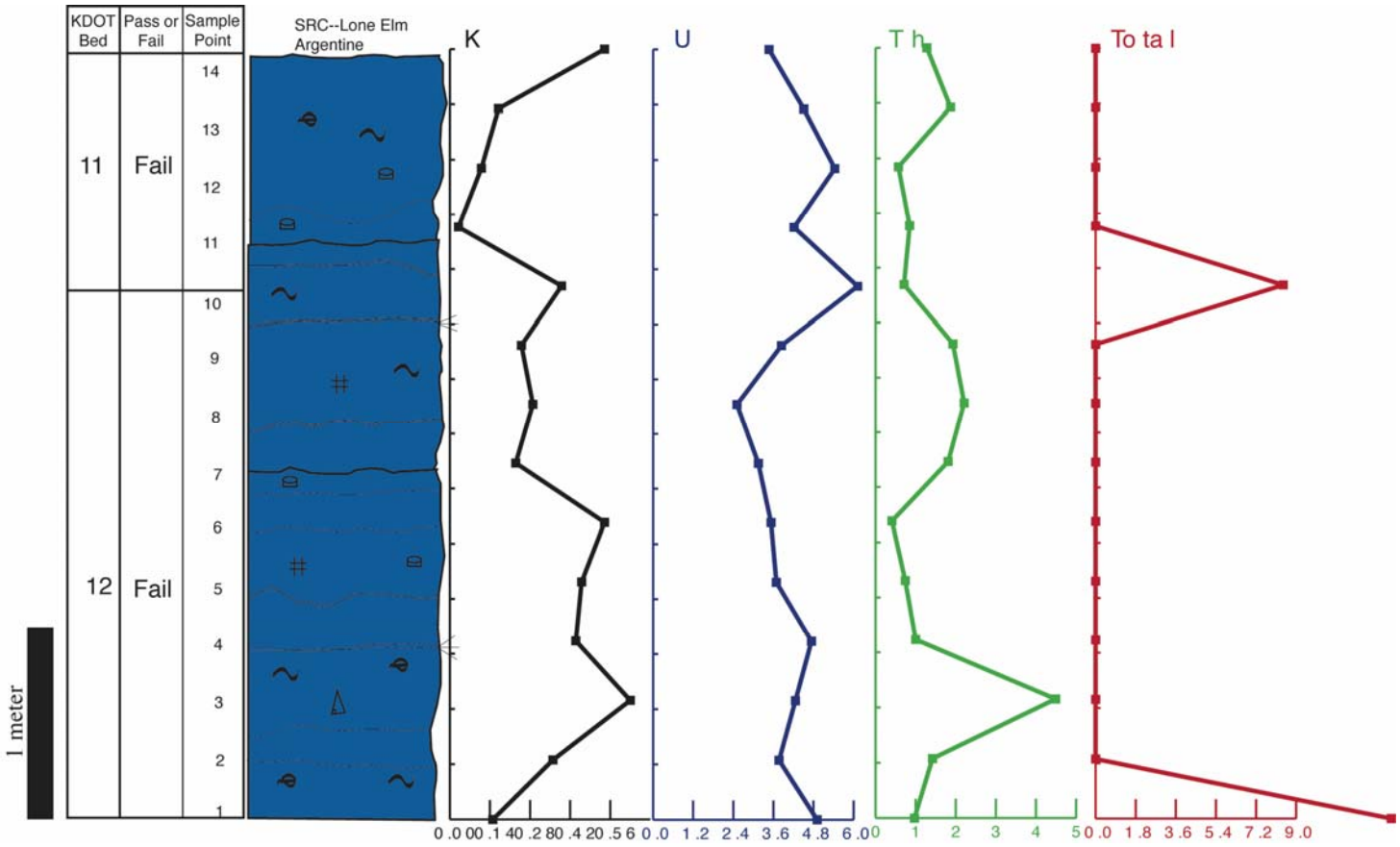

Figure 3.30: Measured Section of the Argentine Limestone in Lone Elm, Kansas

[(Shawnee Rock Company Quarry) Radiation values are plotted similar to well logs. Potassium is given as a percentage, Uranium and Thorium are in ppm and total radiation is in nGyn/Hz. The KDOT Bed number, results of KDOT tests, and the sampling points are shown to the left of the section.

The XRD analyses indicate that all of the samples contain quartz in significantly greater abundance than clay minerals. Almost all of the samples also contain evidence of small amounts of feldspar minerals. All samples contain at least one detectable clay mineral. Illite and chlorite are ubiquitous. Smectite is present in 35% of the samples. Kaolinite was found in 22% of the samples.

Table 3.22: Results of X-Ray Diffraction Clay Mineral Analysis

Site (quarry)	Sample #	KDOT Bed	Major Clay	P_F	chlorite	illite	kaolinite	smectite	#of Clays
Big	2	2	illite	Fail	yes	yes	no	yes	3
Big	3	1	illite	Fail	yes	yes	no	no	2
Craw	2	56	illite	Pass	yes	yes	no	yes	3
Craw	1	4	illite	Pass	yes	yes	no	no	2
Green	1,2	3	ill_chl	Fail	yes	yes	no	no	2
Green	3	4	illite	Fail	yes	yes	yes	no	3
Green	1,2,3,4	7,6	illite	Fail	yes	yes	no	no	2
Hamm	1	3	ill_chl	Fail	yes	yes	yes	yes	4
Hamm	2	2	ill_chl	Fail	yes	yes	no	no	2
JCA	2.1	4	illite	Fail	yes	yes	no	no	2
JCA	2.2	3	illite	Fail	yes	yes	yes	yes	4
JCA	3.1	10	illite	Pass	yes	yes	no	no	2
JCA	3.2	9	illite	Fail	yes	yes	no	no	2
JCA	3.3	8	illite	Fail	yes	yes	yes	yes	4
JCA	4.1	7	illite	Fail	yes	yes	no	yes	3
JCA	4.2	6	illite	Pass	yes	yes	no	yes	3
JCA	4.3	5	illite	Pass	yes	yes	no	yes	3
Lacy	6,7	1	ill_chl	Pass	yes	yes	no	no	2
Lacy	3	3	illite	Pass	yes	yes	no	no	2
Lacy	2	B	illite	Pass	yes	yes	no	no	2
Lacy	4.5	2	ill_chl	Pass	yes	yes	no	no	2
Lacy	1	A	illite	Fail	yes	yes	no	no	2
Lone	1	15	illite	Fail	yes	yes	no	no	2
Lone	2	14	illite	Pass	yes	yes	no	yes	3
Lor	5	11	illite	Fail	yes	yes	no	yes	3
Lor	4	12	chlorite	Pass	yes	yes	no	no	2
Lor	1	14	ill_chl	Fail	yes	yes	no	no	2
Lor	2,3	13	ill_chl	Fail	yes	yes	no	no	2
MM_OQ	1,2	4,5	illite	Pass	yes	yes	no	no	2
Pec	1	11	illite	Pass	yes	yes	no	no	2

Table 3.22 (cont'd)

Site (quarry)	Sample #	KDOT Bed	Major Clay	P_F	chlorite	illite	kaolinite	smectite	#of Clays
SRBS	Far 1	5	illite	Fail	yes	yes	yes	yes	4
SRBS	Arg 1	10	illite	Pass	yes	yes	no	no	2
SRBS	Arg 2	9	illite	Pass	yes	yes	yes	yes	4
SunArg	2	10	ill_chl	Fail	yes	yes	yes	no	3
Sunf(Upper)	Far2	7.8	illite	Pass	yes	yes	yes	yes	4
Sunf	Arg1	9	illite	Fail	yes	yes	no	no	2
Sunf(Lower)	1	5	illite	Fail	yes	yes	no	no	2

3.4 Discussion

3.4.1 Spectral Scintillometry

Results from spectral scintillometry appear useful in evaluating the durability of limestone aggregate. Support for the general hypothesis that rocks that fail the KDOT physical tests produce higher radiation than class 1 rocks is well illustrated in a comparison of Figures 3.21 and 3.28. The potassium values (black) and total radiation values (red) are higher in the Johnson County Aggregate location (Figure 3.28) than in the Martin Marietta Peculiar section (Figure 3.21). The uranium and thorium data are less useful in evaluating durability.

A variety of statistical analyses were performed on several summary statistics (mean, median, minimum, maximum and standard deviation) to determine the degree to which radiation values can be related to KDOT test results. K_{max} was the most useful radiation measurement and will be the focus of the remaining discussion. All additional analyses are included in Appendix X. Data such as percent shale were also tested but showed little predictive value and are included in the appendix. Only 10 out of 48 linear regression analyses were statistically significant. Additionally, the R-squared values, which indicate the percent of variation in the data explained by the linear model, were weak in all analyses performed with a maximum R-squared value of 0.4536 (Appendix). Therefore, the results of the regression analyses were not

strong enough to serve as a basis for using radiation measurements to predict KDOT physical test results.

Further statistical analyses determined if radiation measurements could reliably indicate whether a KDOT bed would simply pass or fail the KDOT physical tests. Since the radiation measurements are continuous variables and pass/fail is a categorical variable, logistic analysis was performed to compare radiation values to whether a KDOT bed passed (1) or failed (0) the physical tests for aggregate durability. Logistic regression analyses were performed on all of the summary statistics for each isotope and several combinations of isotopes.

It is important to point out that there was one anomalously high K_{max} value from the upper Farley Limestone at the Hunt Midwest Sunflower quarry that was removed from the analyses. In statistical analysis one can justify discarding data if the data no longer represent valid observations from the original sample (Gotelli and Ellison, 2004). The area from which this value was generated is a significant distance from where the original samples were taken for the KDOT tests. The upper Farley shows significant lateral variation within this quarry, and according to the quarry operator, the physical appearance of the current ledge is significantly different from the appearance of the rock that was collected in 1998 for the KDOT tests. The anomalous value (0.98 %) is much higher than all of the other K_{max} values, the next highest value is 0.69.

As a tool useful in predicting the likelihood of a ledge passing or failing the KDOT physical test of aggregate durability, potassium maximum value (K_{max}) provided the most statistically significant and highly predictive model with logistic regression analysis. Figure 3.31 shows the pass/fail data graphed along with the logistic curve for Kmax. It is divided into regions A, B, and C to facilitate the discussion below.

This model shows that the probability of passing class 1 designation decreases as the Kmax value increases. The equation for this model is:

$$p = \frac{e^{2.81+(-9.27)K_{max}}}{1+e^{2.81+(-9.27)K_{max}}}$$

Where p is the probability that a KDOT bed with a given Kmax value will pass the KDOT physical tests for class 1 designation.

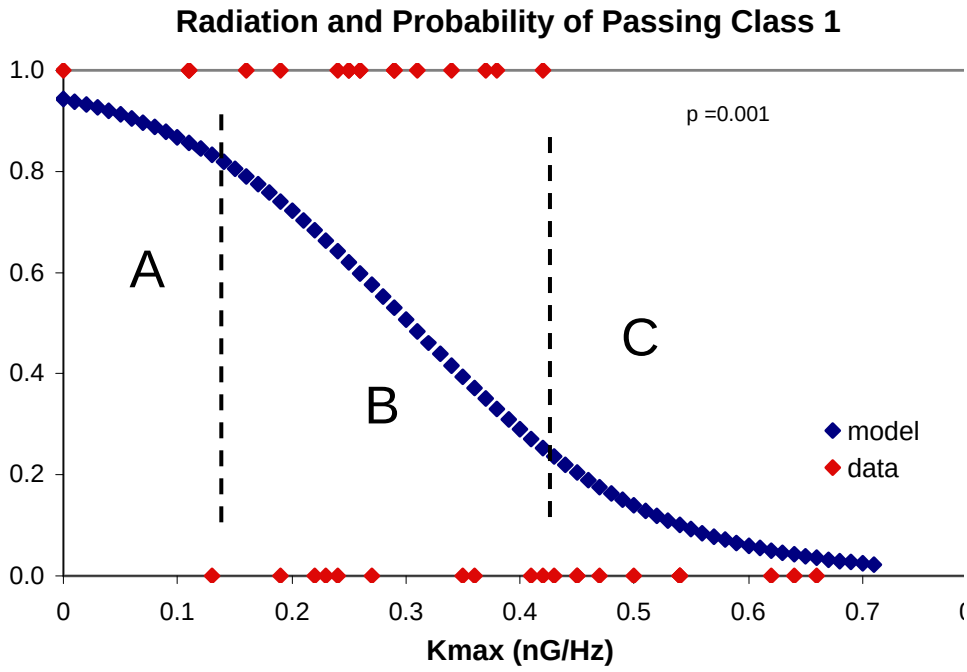

Figure 3.31: Graph of the Logistic Model of the Relationship between the Maximum Value for Potassium (K_{max}) and the Data from which it was Derived
(Data plotted along the 0 line are those samples that failed and those plotted along the 1 line are samples that pass. Region A represents values that have ≥ 80% probability of passing. Region C represents values that have a ≤20% probability of passing, or a ≥ 80% probability of failing. Region B illustrates the portion of the model that is not as useful in confidently predicting the probability of passing or failing.)

It is apparent from Figure 3.31 that there are roughly two ranges of Kmax values (A and C) where the probabilities of passing the KDOT physical tests are either high or low. These two regions (the top and the bottom of the curve) are characterized by relatively flat slopes indicating consistently high or low probabilities of passing. In contrast, the steep slope in region B indicates that a small change in K_{max} would produce large changes in the probability of a ledge passing or failing the KDOT physical tests. Looking at the actual K_{max} data (red points) in region B there and an approximately equal number of samples that pass and fail the KDOT physical tests. Model predictions from K_{max} values in region B would be less reliable than those in regions A and C.

Logistic models allow the user to define upper and lower threshold values that provide the appropriate risk for decision-making purposes. The 80% threshold was chosen as a semi-conservative value that would not limit the detection of class 1 aggregates with marginal K_{max} values. Any ledge with a K_{max} value in region A will have an 80% or greater probability of passing the KDOT physical tests. Any ledge with K_{max} value in region C will have an 80% or greater probability of failing the KDOT physical tests. Choosing a different threshold value will be a decision that ultimately will have to be made by KDOT and quarry operators and will necessarily include cost-benefit factors not addressed in this study. An Excel™ spreadsheet that can be used to calculate probability of passing or failing will be supplied with this report and will be discussed further in the Implementation/Training section of this report.

Many quarry operators and KDOT geology staff believe that the thick, concentrated stylocumulate seams and shale beds “pop out” when the limestone is crushed and are, therefore, not included in the final aggregate product. In order to test this assumption, a second logistic analysis was performed excluding all values within 20 centimeters (11.8 inches) of a shale or

thick stylolite bed. Figure 3.32 shows the logistic regression without the shale/stylolite data. The equation for this model is: Where *p* is the probability that a rock with a given K_{max} value will pass the KDOT physical tests for class 1 designation.

$$p = \frac{e^{1.38+(-4.45)K_{max}}}{1+e^{1.38+(-4.45)K_{max}}}$$

Where *p* is the probability that a rock with a given K_{max} value will pass the KDOT physical tests for class 1 designation.

Removing the shale/stylolite values increased the p-value from 0.001 to 0.028, indicating that this model is less statistically significant. More important than the statistical significance is the resulting shape of the curve in model B. The curve in model B is more linear than the curve in model A. This is an important distinction because the characteristics of a logistic model produce a curve that fits the data best at the highest probability of passing or failing. In an ideal situation the part of the curve delineating the highest probability of passing would be a horizontal line perpendicular to the vertical axis. In the nearly linear curve of model B it is much more difficult to define threshold radiation values where the probability of passing or failing the physical tests rapidly declines.

There are two possible explanations for why model B was less statistically significant. First, it could be an effect of a reduction of sample size. A larger sample size allows detection of finer scale differences within a data set, providing more confidence that the statistical difference represents real-world differences (Sokal and Rohlf, 1995). Second, the decreased significance of model B could be an indication that the shale and concentrated stylocumulates do not "pop out" and are instead incorporated in the final aggregate. This is supported by observations of class 1

stockpiles that contained aggregate pieces composed of zones of concentrated stylocumulates (Figure 3.33).

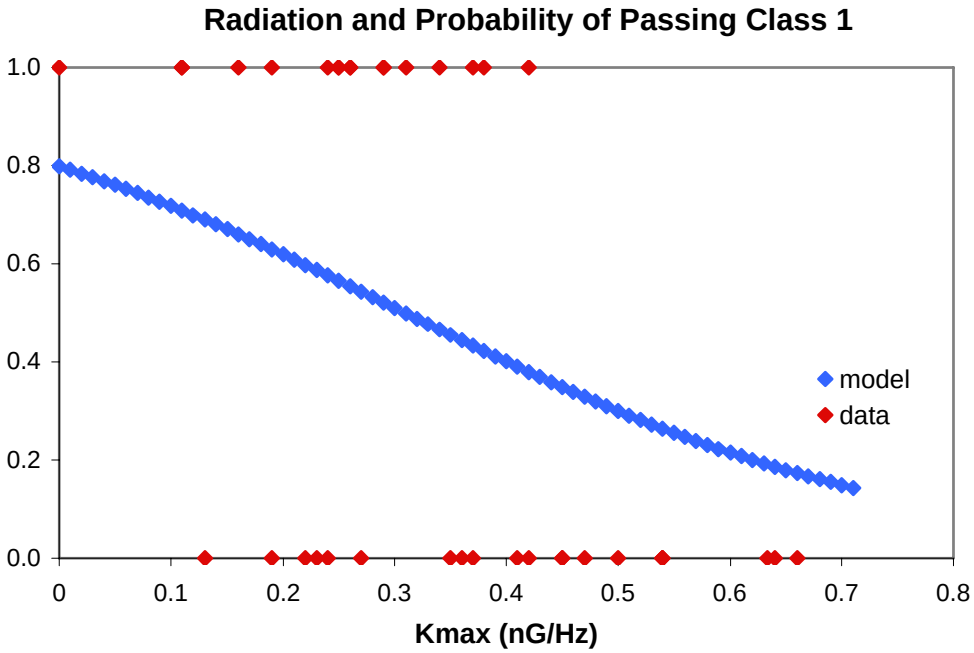

Figure 3.32: Graph of the Logistic Model of the Relationship between the Maximum Value for Potassium (K_{max}) ,After Removing Points within 30 cm of a Shale/Stylolite Beds, and the Data from which it was Derived
(Note that the curve in this graph is more linear in shape than the curve in Figure 3.31.)

Moreover, limestone with disseminated clay would also survive crushing to be included in the aggregate. As these lithologies may be concentrated immediately above and below shale beds and concentrated stylocumulates, some of the highest K_{max} values, may have been removed. Thus, it appears that readings near stylocumulates should be included in any logistic model.

There was an initial concern that each stratigraphic unit might have a range of unique K_{max} values which might necessitate having a separate model for each formation. In order to address this concern the values of the various formations were visually assessed with respect to one another. Figure 3.34 shows the K_{max} values color-coded by formation.

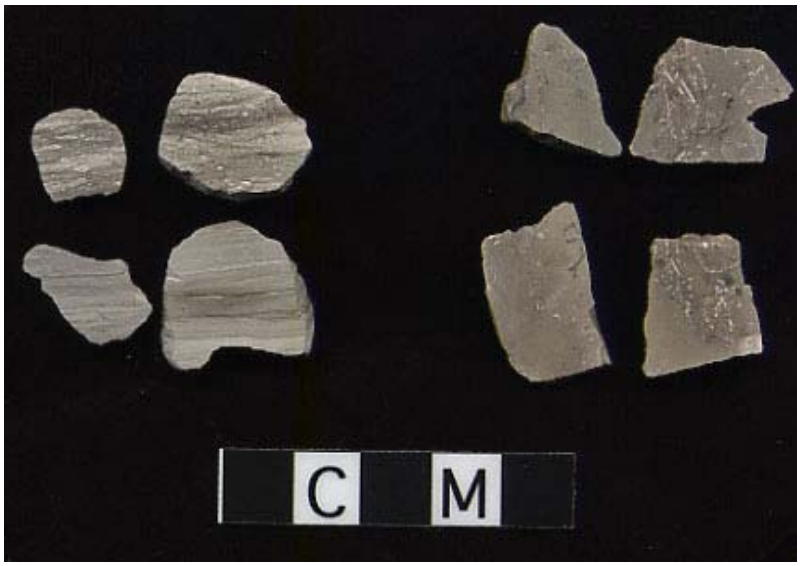

Figure 3.33: Aggregate Pieces Consisting of Diffuse Stylocumulates Recovered from a Class 1 Stockpile Shown on the Left
(This illustrates the type of stylocumulates present in class 1 stockpiles that are incorrectly believed to "pop-out" during crushing. Typical diffuse class 1 aggregate pieces lacking diffuse stylocumulates are shown on the right for comparison.)

It is apparent that each formation includes a broad range of values, and no formation has values that are clumped within a small range. For example, the Argentine Limestone includes one of the lowest values and the highest value for K_{max}. This lack of unique ranges in radiation values for individual stratigraphic units supports the methodology of sampling several formations utilized in this study.

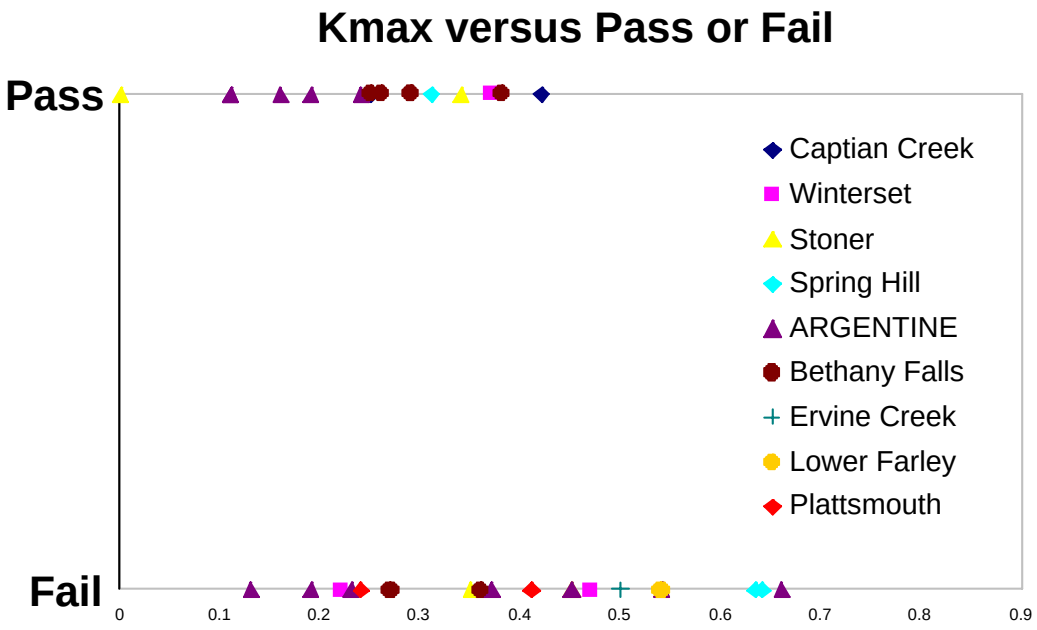

Figure 3.34: Plot of Kmax versus Pass or Fail with Individual Stratigraphic Units Indicated by Different Colored Symbols

3.4.2 Clays

McKirahan et al. (2000) suggested that the presence of certain clay minerals, specifically smectite, may affect the durability of carbonate aggregates. To test this idea, the clay diffractograms were interpreted to determine which clays were present using the methodology outlined in Moore and Reynolds (1990) with help from Dr. Richard Berry at the Clay Analysis Laboratory at San Diego State University. Figure 3.35 is a plot of the number of samples that contain or do not contain smectite and whether they pass or fail the KDOT tests.

It is apparent from the plot that smectite-rich samples both pass and fail the KDOT physical tests. Of those that fail, 48% contain smectite; of those that pass 37 % contain smectite. These data were analyzed using a Chi-square test, which showed that presence of smectite was

independent of whether a KDOT bed passed or failed the KDOT physical tests. Clearly, the presence of smectite is not a reliable indicator of whether a sample will pass of fail the KDOT tests.

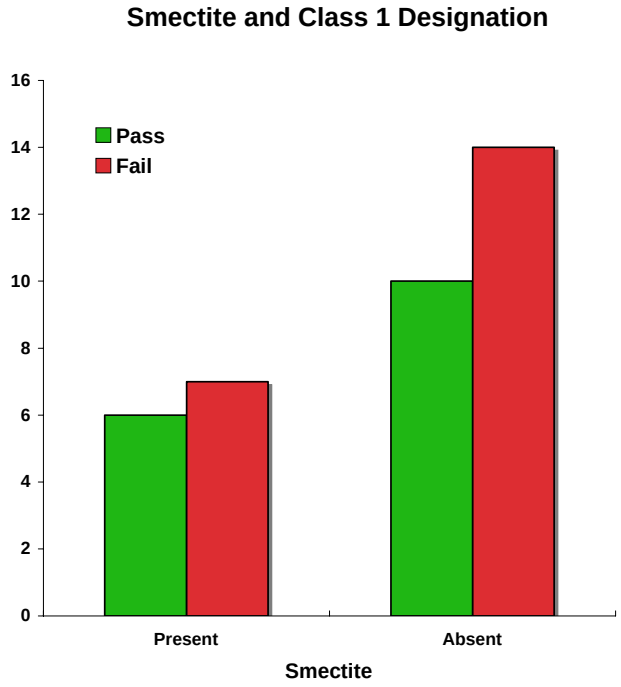

Figure 3.35: Graph Illustrating the Effect of Smectite on Whether a Bed will Pass or Fail the KDOT Physical Tests
(The presence or absence of smectite was detemined by XRD analysis.)

Additional Chi-square analyses were used to test whether the presence of kaolinite was independent of whether an aggregate sample passed or failed the KDOT tests. Kaolinite was not significantly associated with whether a KDOT bed would pass or fail KDOT physical tests. Illite and chlorite were present in all samples and could therefore not be used in an analysis of presence or absence as was performed for smectite and kaolinite. McKirahan et al. (2000) hypothesized that the number of major clay types present in the aggregate may be used to evaluate if an aggregate will pass of fail the KDOT physical tests. To address this question a Chi-square test was performed to determine if the number of clay types present in an aggregate

sample was independent of whether it passed or failed KDOT physical tests. The number of clay types present is independent of whether an aggregate sample passes or fails the KDOT tests. Results of all Chi-square tests can be found in the appendix.

These results suggest that further work on clay mineralogy as a predictor of aggregate durability is not warranted. The fact that K_{max} can reliably predict that a bed will pass or fail the KDOT physical tests indicates that the amount of clays is more important than clay mineralogy and that the scintillometer is a viable tool for first-cut evaluation. Further work should focus on quantitative analysis of the amount of clay minerals in an aggregate sample.

3.5 Application

There are a variety of scenarios in which the spectral gamma ray scintillometer methodology could be very useful. This tool would be ideal for use in a quarry development mode. Spectral scintillometry data could be taken as soon as the ledge was opened to obtain a baseline value for material that could be correlated with the KDOT physical tests. Subsequent readings could be compared to the original values to track quality control of the ledge, Also, when a visual change is seen in a class 1 ledge in an active quarry, spectral scintillometer measurements would be warranted, enabling KDOT and quarry operators to test the probability that the ledge would continue to pass the KDOT the physical tests without having to contact KDOT to retrieve a sample and run the 6-month physical tests. In a more qualitative vein, the spectral gamma ray scintillometer could be used to track quality as a ledge is being quarried. Periodically, spectral gamma ray scintillometer readings could be taken on subsequent faces of an active ledge. The radiation data could be used to track consistencies or discover inconsistencies in K_{max} values within a ledge. This could help identify consistent sources of durable aggregate or at the very least identify nascent problems. Tracking consistency in this manner could ensure that inferior

aggregate is not included in aggregates that are used for highway construction. As previously mentioned, inferior aggregate has been a serious problem which leads to highway repairs and loss of revenue for both quarries and KDOT.

The methodology could also be useful in an exploration mode. When a new quarry is opened or a new ledge in a previously opened quarry, the tool could be used to predict whether the ledge would pass or fail. For example, if the K_{max} value predicted a very low probability of passing, below the accepted threshold value, then it would be a good indication that the ledge would not produce class 1 aggregate allowing time and resources to be directed to more likely candidates.

If this methodology is broadly implemented, an intriguing use, both qualitatively and quantitatively, would be the development of a radiation measurement database for each stratigraphic unit. As quarry operators and KDOT staff generate data consisting of K_{max} values and spectral scintillometer logs of active ledges a database of radiation measurements could be produced. These parameters could be made available for anyone presented with any of the above scenarios and could go a long way in helping to convince government officials that the quality of limestone aggregate resources can be assured and even predicted. Building databases and thus adding more data could help refine the statistical model and improve the accuracy of the tool for predicting whether a bed will pass or fail the KDOT tests.

3.6 Further Work

This project was a preliminary test of whether the spectral gamma ray scintillometer method could be used to predict aggregate durability. It concentrated on vertical stratigraphic sampling. It has been well established that there is significant lateral variation in the limestones that are used to produce aggregate in Kansas. The spectral gamma ray scintillometer may yet prove

useful in evaluating the likelihood of a ledge changing its physical characteristics in either increasing or decreasing its utility as an aggregate resource.

This study established that the type of clay present in an aggregate sample was independent of whether a bed passed or failed the KDOT physical tests. A predictive model based on logistic regression, which illustrated a threshold value for $K_{max,}$ was established and it is reasonable to hypothesize that the K_{max} threshold value relates to a threshold amount of clay. XRD analysis of clay minerals is generally not suited to quantitatively calculate the amount of clay in a sample. As part of a continuing study, more quantitative chemical analyses would better address the question of the amount of clay present in the samples, how it impacts durability, and if it can be related to the threshold value of $K_{max.}$

3.7 Implementation Recommendations

The following summarizes recommendations for implementing the spectral gamma ray scintillometer methodology in the field. It includes an illustrated step-by-step guide to both field and spreadsheet analysis techniques. Also provided is an Excel-based program in which to record radiation readings, to automatically calculate the potassium maximum (K_{max}) value and to predict the probability that a ledge will pass or fail the KDOT physical tests.

3.7.1 Step 1

Determine if the limestone ledge to be tested has the required micritic matrix for the spectral gamma ray scintillometer methodology. Micrite is microcrystalline calcite and it should appear as a dense, opaque substance between the other grains in the rock. It consists of a calcite mineralogy and will react in 10% HCl. The examples below are photographs of unpolished, rinsed, fresh surfaces at a scale consistent with what can be seen with a 20x hand lens.

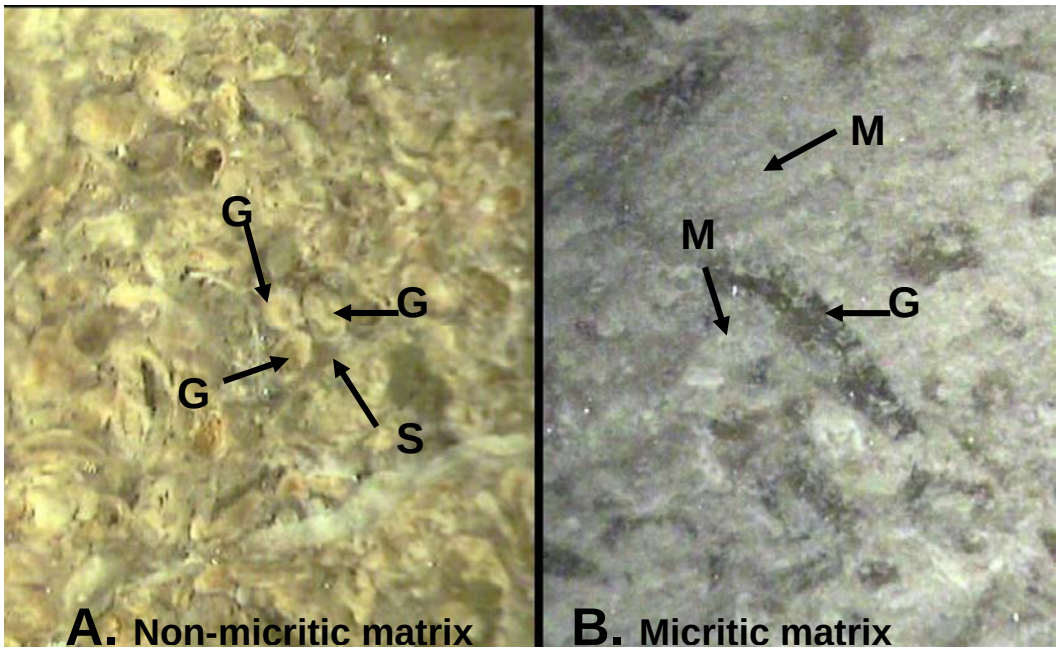

Figure 3.36: Example of Non-Micritic Matrix Facies
[(A) versus micritic matrix facies; (B) Photo scale and detail are consistent with a 20 x hand lens; (M) = micritic matrix, (S) = sparry matrix, (G) = grain.]

Photo A in Figure 3.36 illustrates an example of non-micritic matrix, in this case the matrix is sparry calcite. It appears somewhat transparent, shiny, and can contain crystals that are large enough to be visible with a 20x hand lens. Notice the clear, almost glassy looking matrix (S) between the three labeled grains (G). Photo B is an example of micritic matrix. Note that the whitish material between the darker grey recrystallized fossil fragments is opaque with no obvious crystals visible.

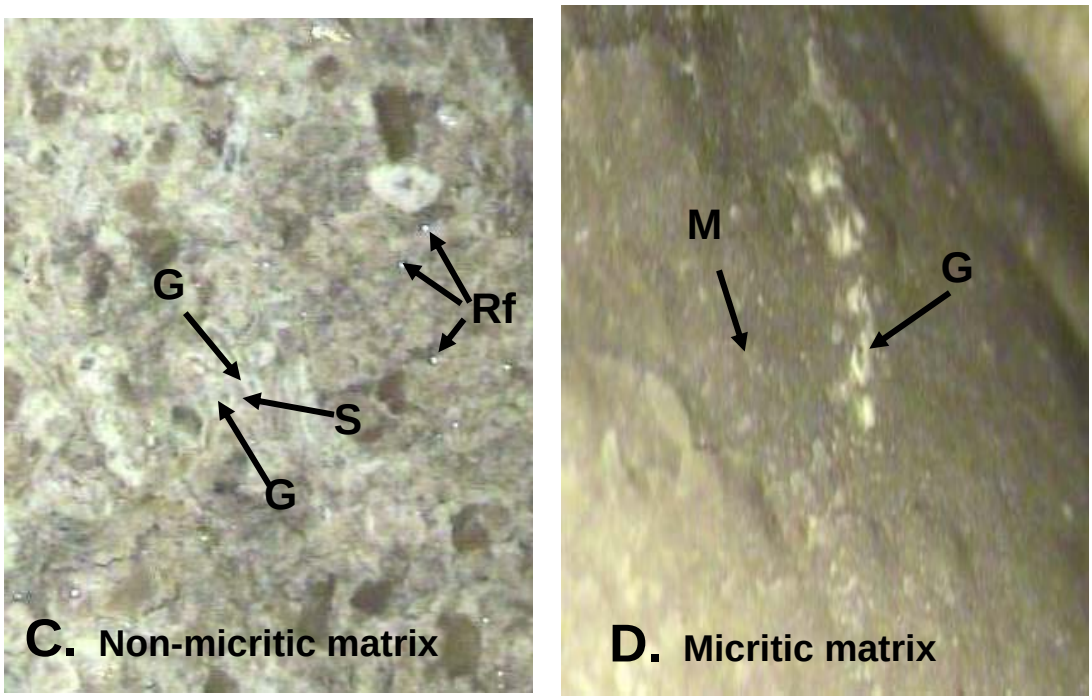

Figure 3.37: Example of Non-Micritic Matrix Facies
[(C) versus micritic matrix facies; (D) Photo scale and detail are consistent with a 20 x hand lens; (M) = micritic matrix, (S) = sparry matrix, (G) = grain, (Rf) = point of reflected light.

Photo C in Figure 3.37 is another example of the sparry matrix facies, which illustrates a common feature of sparry calcite. When viewed in sunlight or other bright lighting the spar will appear to sparkle, or reflect bright points of light, which can be seen in the photograph (labeled Rf). Photo D is an excellent example of micritic matrix that illustrates how micrite may show a rough or concoidal fracture. This sample is dominantly micrite and the only grain (G) is a bryozoan fragment.

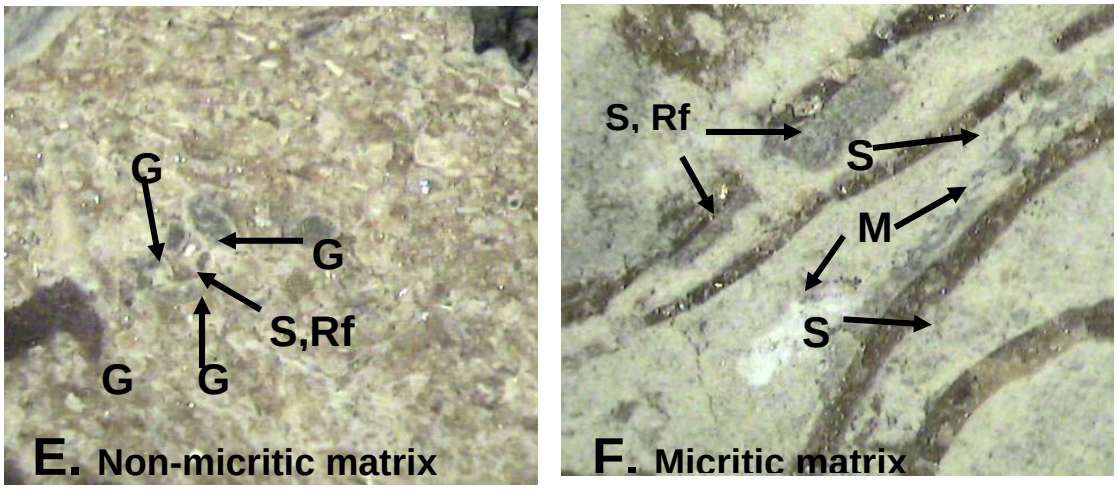

Figure 3.38: Example of Non-Micritic Matrix Facies
[(E) versus micritic matrix facies; (F) Photo scale and detail are consistent with a 20 x hand lens; (M) = micritic matrix, (S) = sparry matrix, (G) = grain, (Rf) = point of reflected light.]

Photo E in Figure 3.38 is an example of the sparry calcite facies where the grains are smaller than in the previous examples. Reflections coming from sparry calcite between the grains are visible. In Photo F, sparry calcite is visible as a replacement feature of the original structure inside the brownish wavy lines, which are phylloid algal fossils. The important feature to notice is that the light colored matrix between the phylloid algal fossils is still opaque, creamy looking micrite.

3.7.2 Step 2

Look carefully at the ledge for any beds or patches of blue-gray or red-brown coloration. This indicates that there are iron-rich carbonates present. The presence of iron-rich minerals may be a factor, other than clay content, causing beds to exclusively fail the KDOT physical tests. Figure 3.39 is an excellent example of the characteristic appearance of this type of rock. Beds or zones that display this distinctive coloration should not be sampled or included in the spectral gamma ray analysis of a ledge.

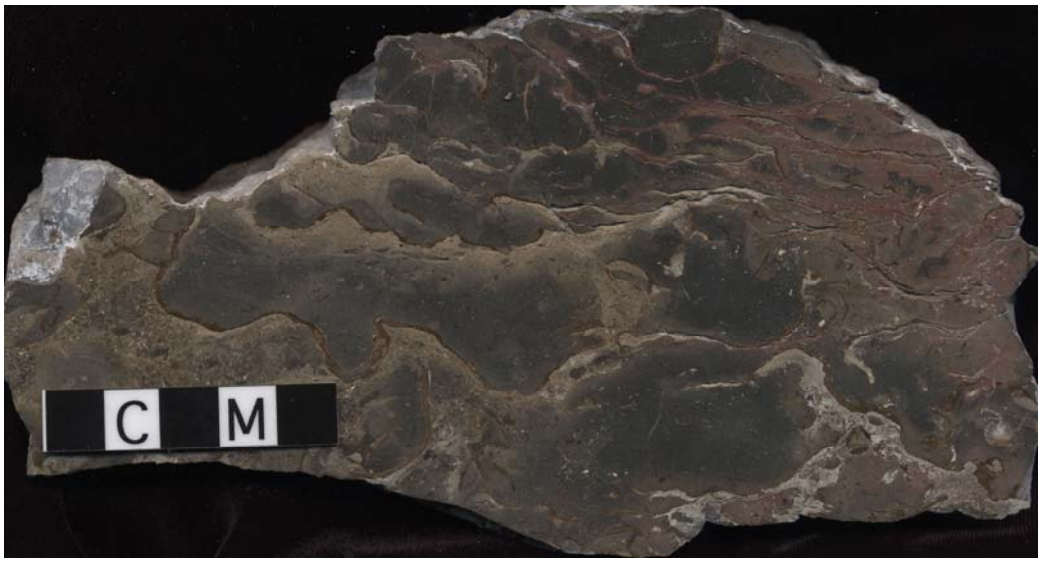

Figure 3.39: Example of the Discoloration of Potential Limestone Aggregate Sources Due to the Presence of Iron Rich Carbonates
(Any zones or beds that look similar should not be included in spectral gamma ray analysis.)

3.7.3 Step 3

Powerwash the outcrop to remove quarry dust for a maximum of five minutes or until most of the water runs clear off the ledge (Figure 3.40). This is necessary to remove quarry dust that could bias the scintillometry values.

Figure 3.40: Quarry Face Being Powerwashed Using 2700 psi Gasoline-Powered Powerwasher Supplied with Water from a 50 gallon Pressurized Cement-Mixer Tank
(Biologist is 1.78 meters in height for scale.)

3.7.4 Step 4

Mark the outcrop at 30 cm (11.8 inch) vertical intervals with spray paint (Figure 3.41). The first sampling point should be 30 cm (11.8 inches) from the base of the outcrop. Beginning 30 cm (11.8 inches) above the base eliminates the problem of bias from soil or weathered material on the ground surface.

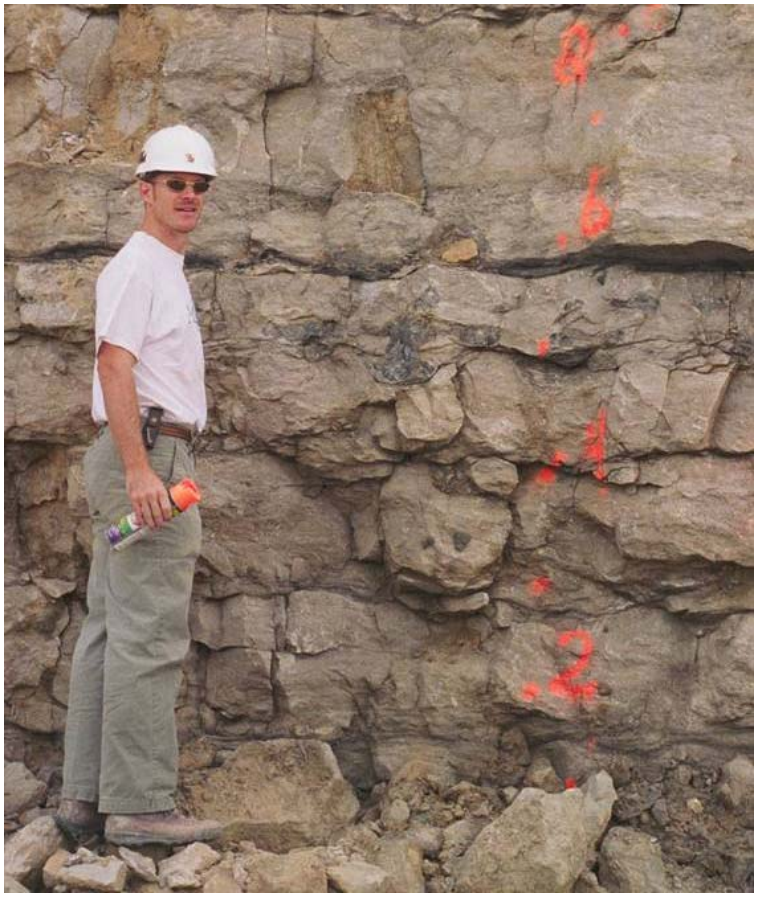

Figure 3.41: Quarry Face Marked with Spray Paint for Successive Spectral Gamma Ray Scintillometer Readings Every 30 centimeters (11.8 inches)
[Biologist is 1.78 meters in height for scale. Try to avoid any areas where the rock looks loose (similar to the area to the left of the marks) in order to have a significant thickness of rock for the instrument to penetrate in order to take a reading. 1.78 meter biologist for scale.]

3.7.5 Step 5

Take spectral gamma ray scintillometer readings and record them in the memory of the instrument corresponding to numbers on the outcrop. Be sure to note where the detector is on the instrument and place that area as flat as possible against the rock surface (Figure 3.42). Hold detector for three minutes at each 11.8 inch interval.

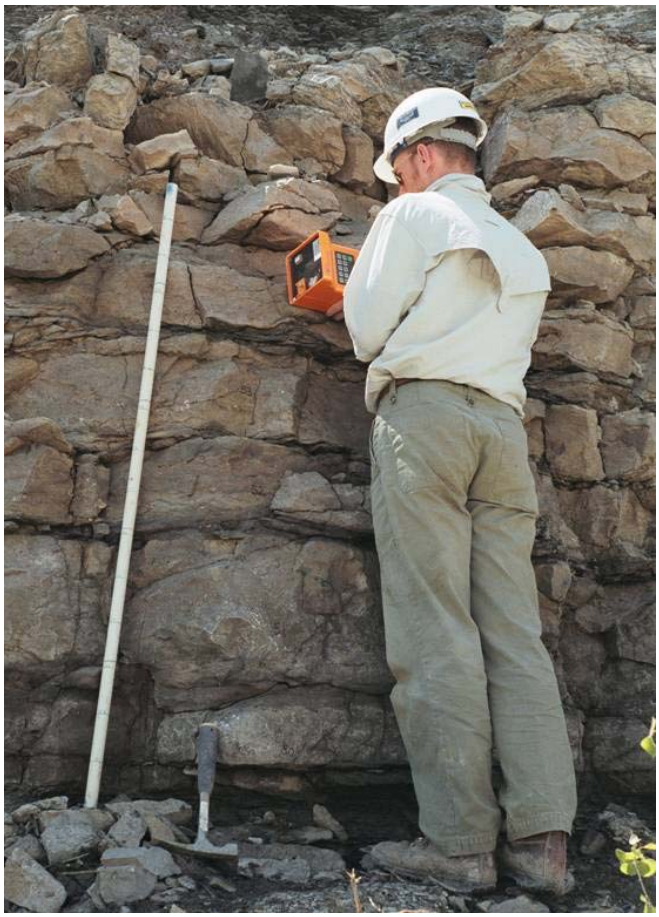

Figure 3.42: Hold Detector as Flush against the Outcrop as Possible
(Try not to bump or jar the scintillometer while readings are being taken. Biologist is 1.78 meters tall for scale.)

3.7.6 Step 6

Open the disk that is provided with this report and make sure you see a file named "FirstCut.xla". To install this Add-In, launch Excel first, and then you can use one of two methods to complete installation:

1. Use Windows Explorer to find the FirstCut.xla file on the disk and double-click.
2. From Excel go to the Tools │ Add-Ins Menu and browse to the FirstCut.xla file. Click "OK" (Figure 3.43).

Using either technique you will now have a “FirstCut” item in the Tools | Add-Ins dialog box, two new buttons on the tool bar, and two new items on the File menu. Once this Add-In is installed it will load automatically each time Excel is started.

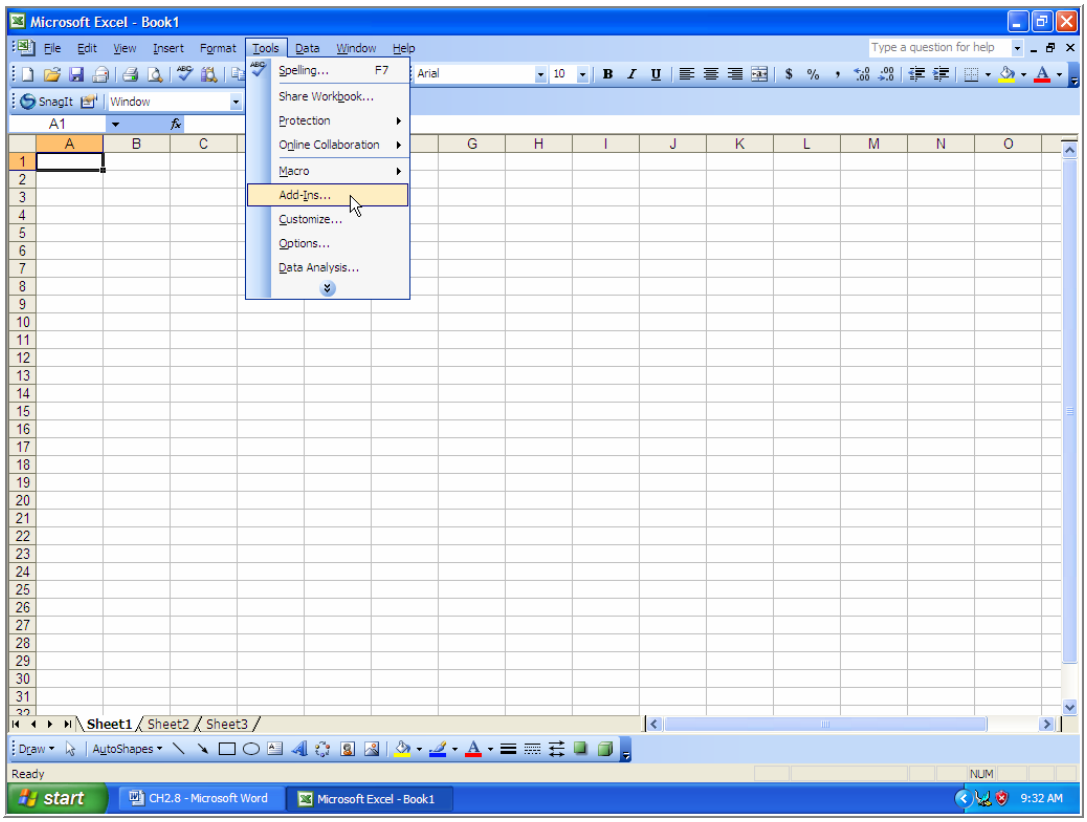

Figure 3.43: Screen Shot of Excel during the First Step of Method 2 for Installing an Add-In

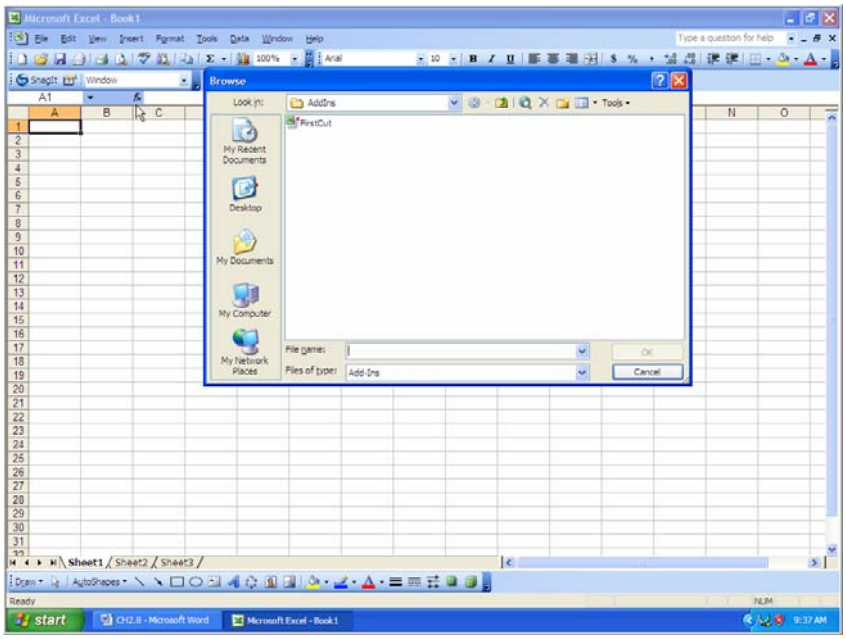

Figure 3.44: Screen Shot of Excel during the Second Step of Method 2 for Installing an Add-In

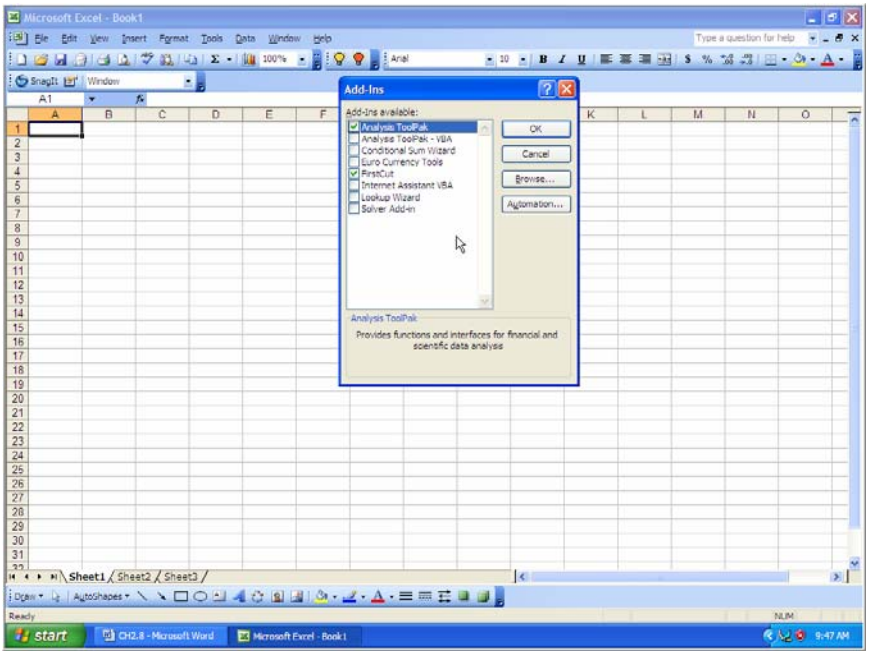

Figure 3.45: Screen Shot of the Tools | Add-Ins Dialog Box after Installation is Complete

3.7.7 Step 7

In order to open a new pre-formatted worksheet in which to enter your spectral gamma ray scintillometer readings click the yellow light bulb icon on the toolbar (Figure 3.46) or go to the File Menu and click on "FirstCut: New Data Workbook" (Figure 3.47).

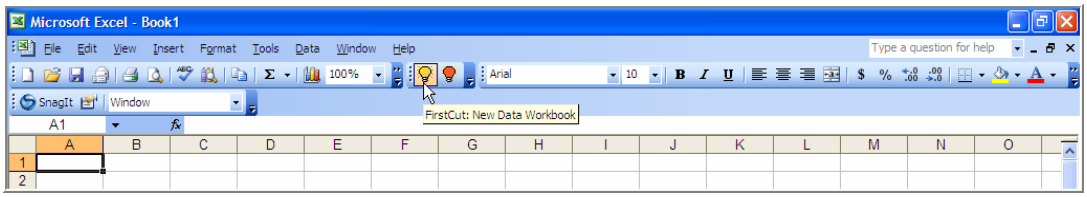

Figure 3.46: Screen Shot of Yellow Lightbulb Icon that Opens a New Workbook

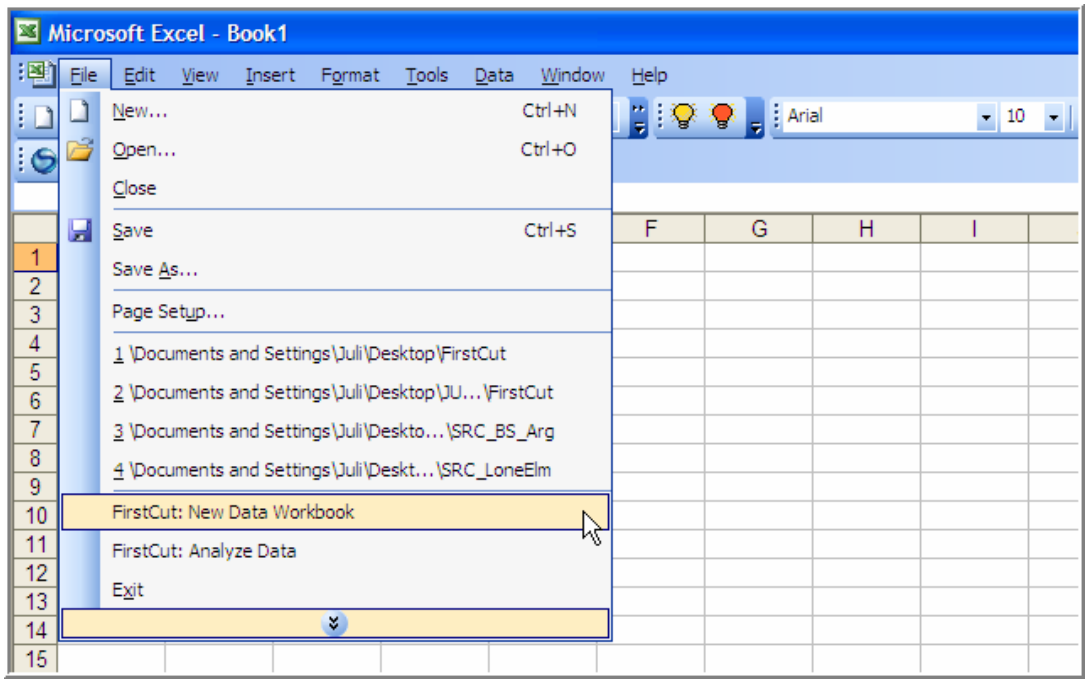

Figure 3.47: Screen Shot of Method for Opening a New Data Workbook using the File Menu Option

3.7.8 Step 8

You should now have a blank formatted workbook that will accept your spectral gamma ray scintillometer data for a ledge. Enter your data as outlined by the directions on the worksheet (Figure 3.48).

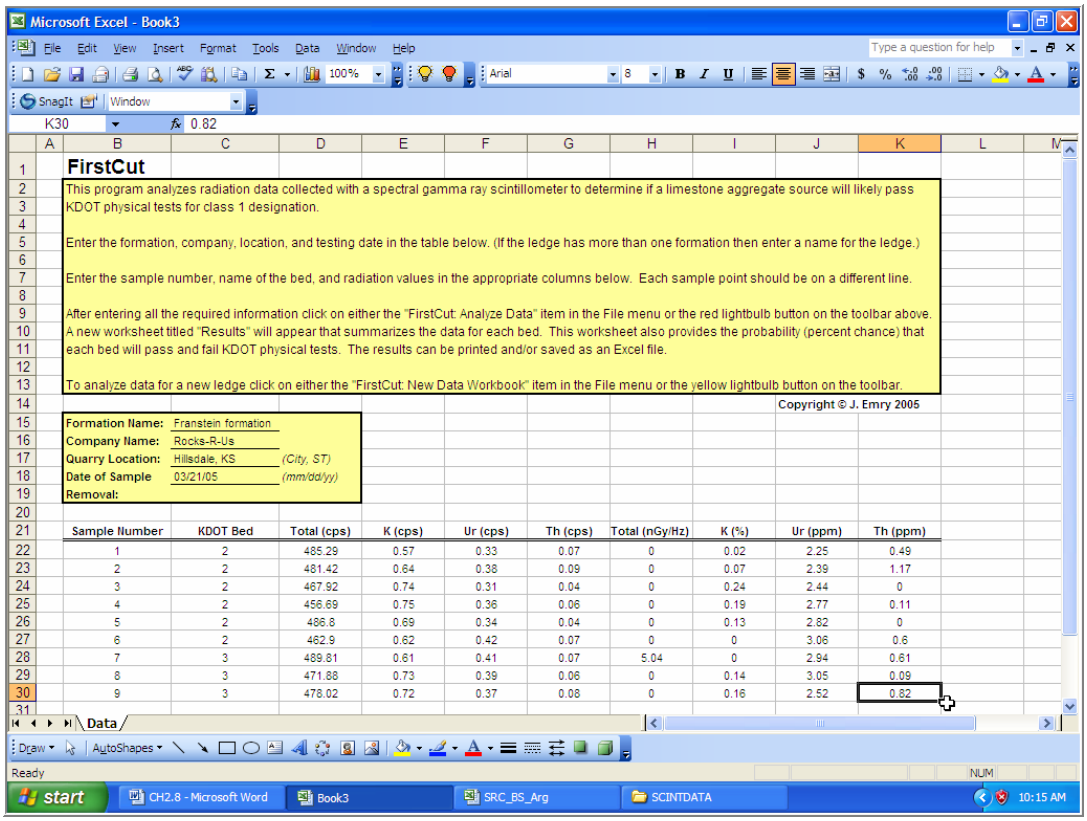

Figure 3.48: Screen Shot of Workbook with an Example of Appropriately Entered Data

3.7.9 Step 9

Once sample data have been entered, click on the red light bulb icon to run the FirstCut program. You can also run the program from the file menu by selecting "FirstCut: Analyze Data." A new worksheet titled "Results" will appear that summarizes the data for each bed. This worksheet also gives the probability (percent chance) that each bed will pass and fail KDOT physical tests (Figure 3.49).

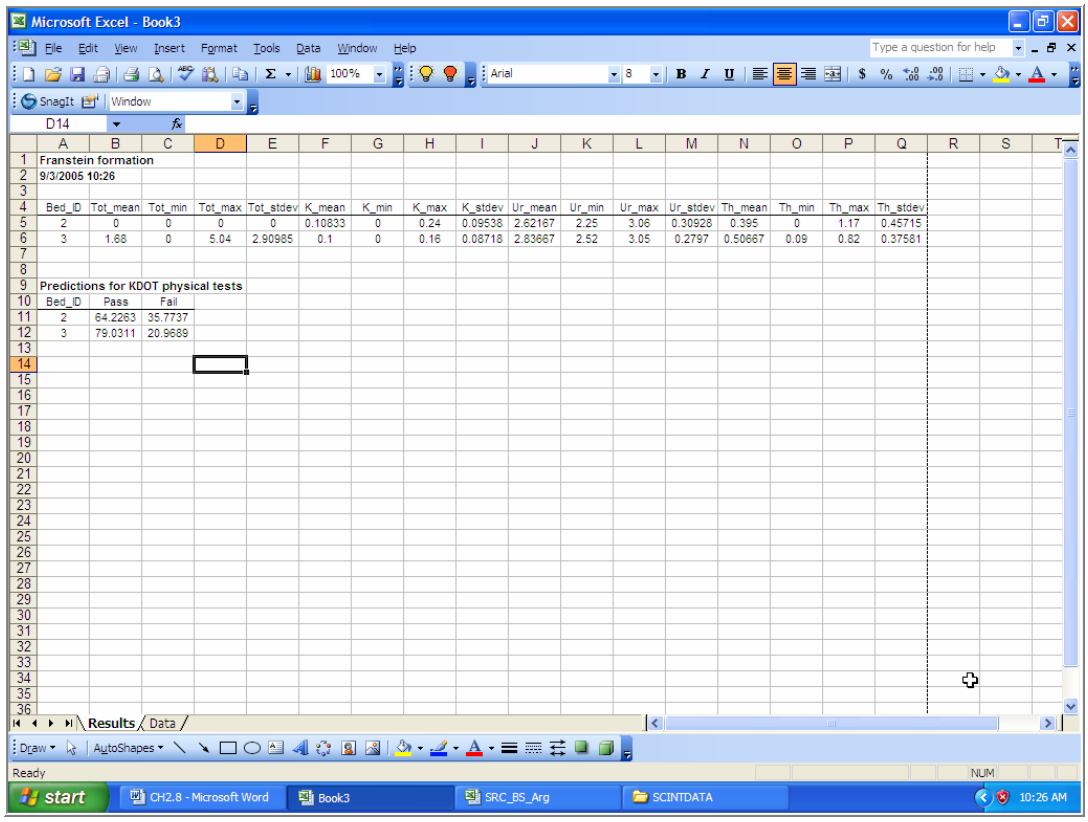

Figure 3.49: Screen Shot of the Results Sheet Produced after the Data have been Analyzed

3.7.10 Step 10

Print the "Results" sheet or save the workbook for your records. If you have data for another ledge go back to step seven and analyze those data in a separate workbook.

Chapter 4

Conclusions

4.1 Controls on Architecture of Argentine Limestone and Associated Strata in Northeastern Kansas

Pennsylvanian strata in the US Midcontinent were deposited in association with high-amplitude glacio-eustatic sea-level fluctuations. Many such sequences are thin and maintain similar thickness throughout wide geographic areas. The facies both build and fill relief. Many of those that fill relief are commonly, but incorrectly ascribed to carbonate mounding. Missourian strata were studied in a 3,670 km^2 area of eastern Kansas to evaluate the controls on build-and-fill architecture.

Nine lithofacies were described in association with the Argentine Limestone, Frisbie Limestone, Quindaro Shale and Liberty Memorial Shale: (1)Phylloid Algal-Microbial Boundstone-Packstone (2) Skeletal Wackestone-Packstone, (3) Shale, Siltstone and Fine Sandstone (4) Lime Mudstone, Interbedded Mudstone and Calcareous Siltstone (5) Peloidal, *Heliospongia* Packstone (6) Encrusting Microbial Boundstone (7) Fossil Fragment Grainstone-Packstone (8) Shaley, Oncoid, Fusulinid Packstone (9) Microbial Mudstone-Wackestone. A sequence stratigraphic framework was established based upon lithofacies distributions and correlations in order to evaluate the controls on lithofacies distributions. Relative changes in sea level controlled the large-scale depositional architecture. Local factors such as accommodation and underlying paleotopography were the most important factors controlling which facies either built or filled depositional topography.

Lowermost strata are those of the Liberty Memorial Shale which created lobate positive topography. Shale facies changed laterally to phylloid algal and possible microbial carbonates,

but no mound-like topography was built. A subsequent relative rise in sea level resulted in a condensed section. Phylloid algal and other carbonate facies were deposited after a minor relative fall in sea level. Strata were deposited preferentially in low areas, onlapping preexisting topography. Although these lithologies are typically ascribed to carbonate buildups, geometries clearly filled topography, subduing most of the original paleotopography and resulting in a relatively flat surface. After a minor relative sea level fall, erosion created topography on the upper surface of the Argentine Limestone, which was previously misidentified as the result of mounding.

Results from this study show that the creation of relief in high-frequency glacioeustatic sequences can occur after falls in sea level, with deposition of lobate siliciclastics and erosion of preexisting strata. High or falling sea levels result in carbonate deposits which fill relief and even out topography. Understanding this mechanism of building and filling of relief is paramount to understanding the nature of deposits that are utilized as carbonate aggregate sources. Identifying lithologies that produce good aggregate and understanding how and where they form can help with quality control and aggregate resource exploration.

4.2 A First-Cut Method for Evaluating Limestone Aggregate Durability Using Spectral Scintillometry

There continues to be an increase in demand for durable carbonate aggregate resources for state and regional highway construction projects**.** KDOT has specific protocols for evaluating aggregate durability, but these tests take a minimum of six months to perform necessitating the development of faster, on-the-outcrop first-cut techniques to evaluate the potential durability of an aggregate resource.

This chapter evaluated the use of a spectral gamma ray scintillometer as a first-cut tool for evaluating limestone aggregate durability. Twenty ledges were sampled in nine stratigraphic units with a spectral gamma-ray scintillometer. Five facies were described based only upon matrix lithology and clay distribution: (1) Matrix, disseminated clays and diffuse stylocumulates, (2) Matrix, disseminated clays (3) Matrix (4) Matrix, diffuse stylocumulates (5) Sparry calcite (disseminated clay-poor, diffuse stylocumulate-poor) (6) Shale/siltstone.

A previous K-TRAN study determined that the clay content and clay distribution in limestones, as disseminated clay and clay-rich seams, as well as clay minerology, appear to be important factors in the durability of limestone aggregate. Logistic models for determining the probability that an aggregate would pass or fail KDOT physical tests were developed for limestones with micritic matrices. These models were based on the relationship between the maximum measurement of the potassium contribution to the natural gamma radiation (K_{max}) and the pass/fail status of a particular KDOT bed. The first model included all of the measurements for a particular KDOT bed. A second logistic model was developed because it is generally believed that shale beds and concentrated stylocumulate zones are removed from the final aggregate product by the crushing process. Therefore, the second model omitted measurements within 30 cm of shale beds and concentrated stylocumulate zones. The first model more accurately predicted the pass/fail status of the aggregate tested suggesting that such clay-rich zone is not removed during crushing.

The type of clays were determined by X-ray diffraction of the clay-sized fraction of acid insoluble residue to test for a correlation between clay mineralogy and whether an aggregate sample would pass or fail the KDOT physical tests. Results showed that the mineralogy of the clays present, and even the number of clays present did not directly correlate with whether an

aggregate sample would pass or fail the KDOT physical tests. Instead, it was determined that the amount of clay present, independent of its mineralogy, may be a more important factor. A handbook of instructions for implementation of the first cut test of aggregate durability is provided along with an Excel add-in that will automatically calculate the probability of an aggregate passing or failing the KDOT physical tests.

References

ASTM, 1995, Annual Book of ASTM Standards, Section 4, Construction: vol. 04.02, Concrete and Aggregates, Publication Code Number 01-040295-07.

Arp, G., Reimer, Reitner, J., 2003, Microbialite formation in seawater of increased alkalinity, Satonda Crater Lake, Indonesia: Journal of Sedimentary Research, v. 73, no. 1, p. 105-127.

Arthur, M.A., and Sageman, B.B., 1994, Marine black shales: depositional mechanisms and environments of ancient deposits: Annual Review of Earth and Planetary Sciences, v. 22, p. 499-551.

Arvidson, R.S., 1990, Stratigraphy, carbonate petrology, diagenesis and trace element cement geochemistry of the Wyandotte limestone (Upper Pennslyvanian), Miami County, Kansas: Unpublished, Master's Thesis, University of Iowa, 213 p.

Baars, D.L., and Torres, A.M., 1991, Late Paleozoic Phylloid Algae—A Pragmatic Review: Palaios, v. 6, p. 513-515.

Ball, M.M., 1967, Carbonate sand bodies of Florida and the Bahamas: Journal of Sedimentary Petrology, v. 37, p. 556-591

Ball, S.M., Pollard, W.D., and Roberts, J.W., 1977, Importance of phylloid algae in development of depositional topography—reality or myth?, *in* Reef and Related Carbonates, Ecology and Sedimentology: American Association of Petroleum Geologists, Studies in Geology, No. 4, p. 239-256.

Bisnett, A.J., and Heckel P.H., 1996, Sequence stratigraphy helps to distinguish offshore black shales in the Midcontinent Pennsylvanian succession *in* Witze B.J., Ludvigson, G.A., and Day, J., eds., Paleozoic Sequence Stratigraphy: Views from the North American Craton: Boulder, CO, Geological Society of America Special Paper 306, p. 341-350

Boardman, D.R., and Heckel, P.H., 1989, Glacial-eustatic sea-level curve for early Late Pennsylvanian sequence in north-central Texas and biostratigraphic correlation with curve for Mid-Continent North America: Geology (Boulder), v. 17, no. 9, p. 802-805.

Crowley, D.J., 1969, Algal-Bank Complex in Wyandotte Limestone (Late Pennslyvanian) in Eastern Kansas: Kansas Geological Survey, Bulletin 198, 52 p.

Coyle, W.G. III, and Evans, K.R., 1987, Phylloid algal mounds in the Frisbie Limestone (Pennsylvanian), northeastern Kansas. *in* Abstracts - SEPM Midyear Meeting: v. 4, p. 16.

Cunningham, K.J., and Franseen, E.K., 1992, Field, Petrographic and Paleomagnetic Investigations of an Enigmatic Surface at the Top of the Argentine Limestone, Johnson County Kansas, part I: Kansas Geologic Survey, Open File Report No. 92-46, 34 p.

Cys, J.M., 1985, Lower Permian phylloid algal mounds, southern Tatum Basin, Southeastern New Mexico, U.S.A.: *in* Paleoalgology; contemporary research and applications Toomey, D.F., and Nitecki, M.H. eds., p. 179-187.

Della Porta, G., Kentner-Jeroen, A.M., Immenhauser, A., and Bahamonde, J.R., 2002, Lithofacies character and architecture across a Pennsylvanian inner-platform transect (Sierra de Cuera, Asturias, Spain): Journal of Sedimentary Research, v. 72, no. 6, p. 898-916.

Della Porta, G., Kentner-Jeroen, A.M., and Bahamonde, J.R., 2004, Depositional facies and stratal geometry of an Upper Carboniferous prograding and aggrading high-relief carbonate platform (Cantabrian Mountains, N. Spain): Sedimentology, v. 51, no. 2, p. 267-295.

Doherty, P.D., Soreghan, G.S., and Castagna, J.P., 2002, Outcrop-based reservoir characterization: A composite phylloid algal mound, western Orogrande basin (New Mexico): American Association of petroleum Geologists Bulletin, v. 86, no. 5, p. 779-795.

Doveton, 1994, Doveton's Geologic Log interpretation SEPM short course No 29, 1994, 1698 p.

Dupraz, C., Visscher, P.T., Baumgartner, L.K., and Reid, R.P., 2004, Microbe-mineral interactions: early carbonate precipitation in a hypersaline lake (Eleuthera Island, Bahamas): Sedimentology: v. 51, p. 745-765.

Dunham, R.J., 1962, Classification of carbonate rocks according to depositional texture *in* Classification of Carbonate Rocks—A Symposium: American Association of Petroleum Geologists, Memoir no. 1, p. 108-121.

Finks, R.M., 2003, Evolution and ecological history of sponges during Paleozoic times: *in* Treatise on Invertebrate Paleontology, Part E, Porifera Revised, Volume 2: Introduction to the Porifera Kaesler, R., ed., p. 260-274.

Franseen, E.K., Goldstein, R.H., 2004, Build and fill: a stratigraphic pattern induced in cyclic sequences by sea level and paleotopography: Geological Society of American Annual Meeting Abstracts, v. 36, no. 5, p. 377.

Gotelli, N.J. and Ellison, A.M., 2004, A Primer of Ecological Statistics: Massachusetts, Sinauer Associates Inc., 510 p.

Harris P.M., 1984, Cores from a modern Carbonate Sand Body: The Joulters ooid Shoal, Great Bahama bank i*n* Harris, P.M., ed., Carbonate Sands—A Core Workshop: Society of Economic Paleontologists and Minerologists Core Workshop, No. 5, p. 429-464.

Heckel, P.H., 1972, Recognition of ancient shallow marine environments *in* Rigby, J.K., and Hamblin, W.K., eds., Recognition of Ancient Sedimentary Environments: Society of Economic Paleontologists and Mineralogists, Special Publication No. 16, p. 226-286.

Heckel, P.H., and Baseman, J.F, 1975, Environmental Interpretation of Conodont Distribution in Upper Pennsylvanian (Missourian) Megacyclothems in Eastern Kansas: American Association of Petroleum Geologists Bulletin 59, p. 486-508.

Heckel, P.H., and Cocke, J.M., 1969, Phylloid algal-mound complexes in outcropping Upper Pennsylvanian rocks of Mid-Continent: American Association of Petroleum Geologists, Bulletin 53, p. 1058-1074.

Heckel, P.H., 1977, Origin of phosphatic black shale facies in Pennsylvanian cyclothems of mid-continent North America: AAPG Bulletin, v. 61, no. 7, Pages 1045-1068.

Heckel, P.H., 1986, Sea-level curve for Pennsylvanian eustatic marine transgressive-regressive depositional cycles along Midcontinent outcrop belt, North America: Geology (Boulder), v. 14, no. 4, p. 330-334.

Jindrich, V., 1969, Recent carbonate sedimentation by tidal channels in the lower Florida Keys: Journal of Sedimentary Petrology, v. 39, p. 531-553.

Johnson, J.H., 1946, Lime-Secreting Algae from the Pennsylvanian and Permian of Kansas: Bulletin of the Geological Society of America, v. 57, p. 1087-1120.

Kirkland B.L., Moore, C.H., and Dickson, J.A.D., 1993, Well-preserved aragonitic phylloid algae (Eugonophyllum, Udoteacea) from the Pennsylvanian Holder Formation, Sacremento Mountains, New Mexico: Palaios, v. 8, no.1, p. 111-120.

Matheny J. P., and Longman, M.W., 1996, Power Desert Creek Reservoirs in the Paradox Basin: examples of phylloid algae filling depositional lows related to salt dissolution *in* Longman, M.W., & Sonnenfield, M.D., eds., Paleozoic Systems of the Rocky Mountain Regions: Rocky Mountain Section, Society of Economic Paleontologists and Minerologists Bulletin, v. 41 p. 2723-2751.

McKirahan J.R., Goldstein, R.H., and Franseen, E.K, 2000, Sequence Stratigraphy of the Lane-Island Creek Shales and the Farley Limestone in northeastern Kansas and geologic factors affecting the quality of limestone aggregates: Topeka, Kansas Department of Transportation K_TRAN: KU-97-1 Final report. 236 p.

McKirahan, J.R, Goldstein, R.H., and Franseen, E.K, 2003, Build-and-fill sequences: how subtle paleotopography affects 3_D heterogeneity of potential reservoir facies, *in* Ahr, W.M., Harris, P.M., Morgan, W.A., and Somerville, I.D., eds., Special Publication - Society for Sedimentary Geology, v. 78; Pages 97-116.

Maybury, C.A., and Evans, K.R., 1994, Pennsylvanian phylloid algae interpreted as shallow water xenophyophores: Lethaia, v. 27, p. 29-33.

Mitchell, J.C., 1981, Stratigraphy and Depositional History of the Iola Limestone, Upper Pennsylvanian (Missourian), Northern Midcontinent U.S.: Iowa City, University of Iowa Doctoral Dissertation, 364 p.

Moore, D.M., Reynolds, R.C. Jr., 1997, X-ray Diffraction and the Identification and Analysis of Clay Minerals: New York, Oxford University Press, 378 p.

Moore, R.C., 1935, Stratigraphic Classification of the Pennsylvanian Rocks of Kansas: Kansas Geological Survey, Bulletin 21, 203 p.

Moore, R.C., Konrad, E.M., Cooke, G.F., and Newell, N.D., 1936, Guidebook of Annual Field Conference 10: Wichita, Kansas Geological Society, p. 7-73.

Moore, R.C., 1964, Paleoecological Aspects of Kansas Pennsylvanian and Permian Cyclothems, Kansas Geological Survey, http://www.kgs.ku.edu/Publications/Bulletins/169/Moore/index.html, accessed 1 October, 2004.

Olszewski, T., 1996, Sequence Stratigraphy of an Upper Pennsylvanian, Midcontinent Cyclothem from North America (Iola Limestone, Kansas and Missouri, USA): FACIES, v. 35, p. 81-104.

Olszewski, T., and Patzkowsky, M,. 2003, From cyclothems to sequences: the record of eustacy and climate on an icehouse epiric platform (Pennsylvanian-Permian, North American mid-continent): Journal of Sedimentary Research, v. 73, No. 1, p. 15-30.

Pray, L.C., and Wray, J.L., 1963, Porous algal facies (Pennsylvanian), Honaker Trail, San Juan Canyon, Utah: in Shelf Carbonates of the Paradox Basin – A Symposium: Four Conrners Geological Society, Fourth Field Conference, p. 204-234.

Pray, L.C., and Wray, J.L., 1977, Origin of some Pennsylvanian algal bioherms in southwestern United States, *in* Pray, L.C., Wilson, J.L., Toomey, D.F., Butler, J.H., Delgado, D.J., and Van Wagoner, J.C., eds., Geology of the Sacramento Mountains, Otero County, New Mexico: West Texas Geological Society, 164 p.

Purdy, E.G., 1963, Recent calcium carbonate facies of the Great Bahama Bank, 2, Sedimentary Facies: Journal of Geology, v. 71, no. 3, p 334-355.

Ramsbottom, W.H.C., 1978, Carboniferous, *in* McKerrow, W.S., ed., The Ecology of Fossils: Massachusetts, The MIT Press, p. 146-183.

Reineck, H.E., and Singh, I.B., 1973, Depositional Sedimentary Environments: New York, Springer-Verlag, 430 p.

Riding, R., 2000, Microbial carbonates: the geological record of calcified bacterial-algal mats and biofilms: Sedimentology, v. 47, suppl. 1, p. 179-214.

Scholle, P.A., Bebout, D.G., and Moore, C.H., eds, 1983, Carbonate Depositional Environments: American Association of Petroleum Geologists Memoir, no. 33, 708 p.

Shen, J.W., and Webb, G.E., 2005, Metazoan-microbial framework fabrics in a Mississippian (Carboniferous) coral-sponge-microbial reef, Monto, Queensland, Austraila: Sedimentary Geology, v. 178, p. 113-133.

Samankassou, E., and West R.R., 2002, Construction versus accumulation in phylloid algal mounds; an example of a small constructed mound in the Pennsylvanian of Kansas, USA: Palaeogeography, Palaeoclimatology, Palaeoecology, v. 185, no. 3-4, p. 379-389.

Sokal, R.R. and Rohlf, F.J., 1995, Biometry, 3rd Edition. New York, W.H. Freeman and Company, 887 p.

Tedesco, L.P., and Wanless, H.R., 1989, Role of burrow excavation and infilling in creating the preserved depositional fabric of Pennsylvanian phylloid mounds of southeastern Kansas, *in* Watney, W.L., French, J.A., and Franseen, E.K., eds., Sequence Stratigraphic Interpretations and Modeling of Cyclothems in the Upper Pennsylvanian (Missourian), Lansing and Kansas City Groups in Eastern Kansas: Guidebook of the Kansas Geological Society, 41st Annual Fieldtrip, p. 179-182.

Thompson, T.L., 2001, Lexicon of Stratigraphic Nomenclature in Missouri: Missouri Department of Natural Resources, Report of Investigation Number 73, 371 p.

Toomey, D.F., Wilson, J.L., and Rezak, R., 1977, Evolution of Yucca Mound complex, late Pennsylvanian phylloid-algal buildup, Sacramento Mountains, New Mexico: AAPG Bulletin, v. 61, no. 12, p. 2115-2133.

Tucker, M.E., 1991, Sedimentary petrology: An introduction to the Origin of Sedimentary Rocks: Oxford, Blackwell Scientific Publications, 260 p.

USGS, 2001, A laboratory manual for X-ray Powder Diffraction: U.S. Department of the Interior, U.S. Geological Survey, http://pubs.usgs.gov/of/of01-041/htmldocs/xrpd.htm, accessed March 15, 2005.

Von Bitter, P.H., and Heckel, P.H., 1978, Differentiation of black "core" shales in Missourian and Virgilian cyclothems (Pennsylvanian) in Iowa and Kansas, using conodonts: Geological Society of America Abstracts with Programs, v. 10, no. 7, p. 510.

Watney, W.L., and Heckel, P.H., 1994, Revision of the stratigraphic nomenclature of the Marmaton, Pleasanton, and Kansas City groups in Kansas: Kansas Geological Survey, Open File Report 94-34, p. 1-18

Watney, W. L., French, J.A., Franseen, E.K., 1989, Sequence stratigraphic interpretations and modeling of cyclothems in the Upper Pennsylvanian (Missourian), Lansing and Kansas City groups in eastern Kansas: Guidebook of the Kansas Geological Survey, 41st Annual Fieldtrip, 211 p.

Weber, L.J., Wright, J.F., and Wright, F.M., 1995, Sequence stratigraphy and reservoir delineation of the Middle Pennsylvanian (Desmoinesian), Paradox Basin and Aneth Field, Southwestern USA, *in* J.F. Read, Kerans, C., Weber, J.L., Sarg, J.F., and Wright, F.M., eds., Milankovitch Sea Level Changes, Cycles and Reservoirs on Carbonate Platforms in Greenhouse and Ice-House Worlds: SEPM Short Course Notes, 35 p.

Wray, J.L., 1964, Archaeolithophyllum, an abundant calcareous alga in limestone of the Lansing Group (Pennsylvanian), southestern Kansas: Kansas Geological Survey Bulletin 170, pt. 1, 13 p.

Wilson, J.L., 1975, Carbonate Facies in Geologic History: New York, Springer-Verlag, 472 p.

APPENDIX

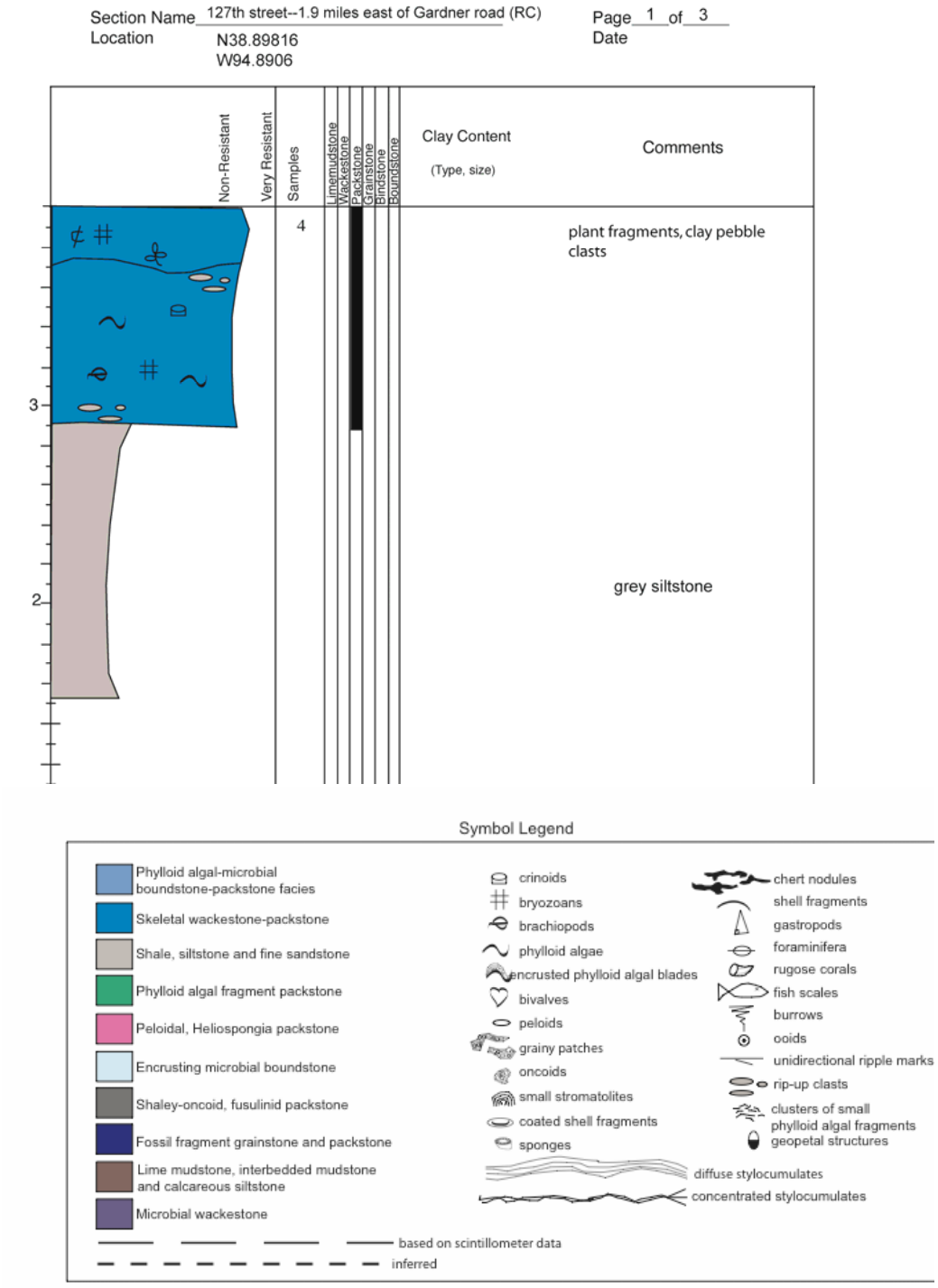

This stratigraphic and fossil key applies to all of the measured sections in the Appendix. Red numbers next to the left axis are scintillometer sampling points

Section Name 127th street--1.9 miles east of Gardner road (RC) Page 1 of 3

Location N38.89816
W94.8906

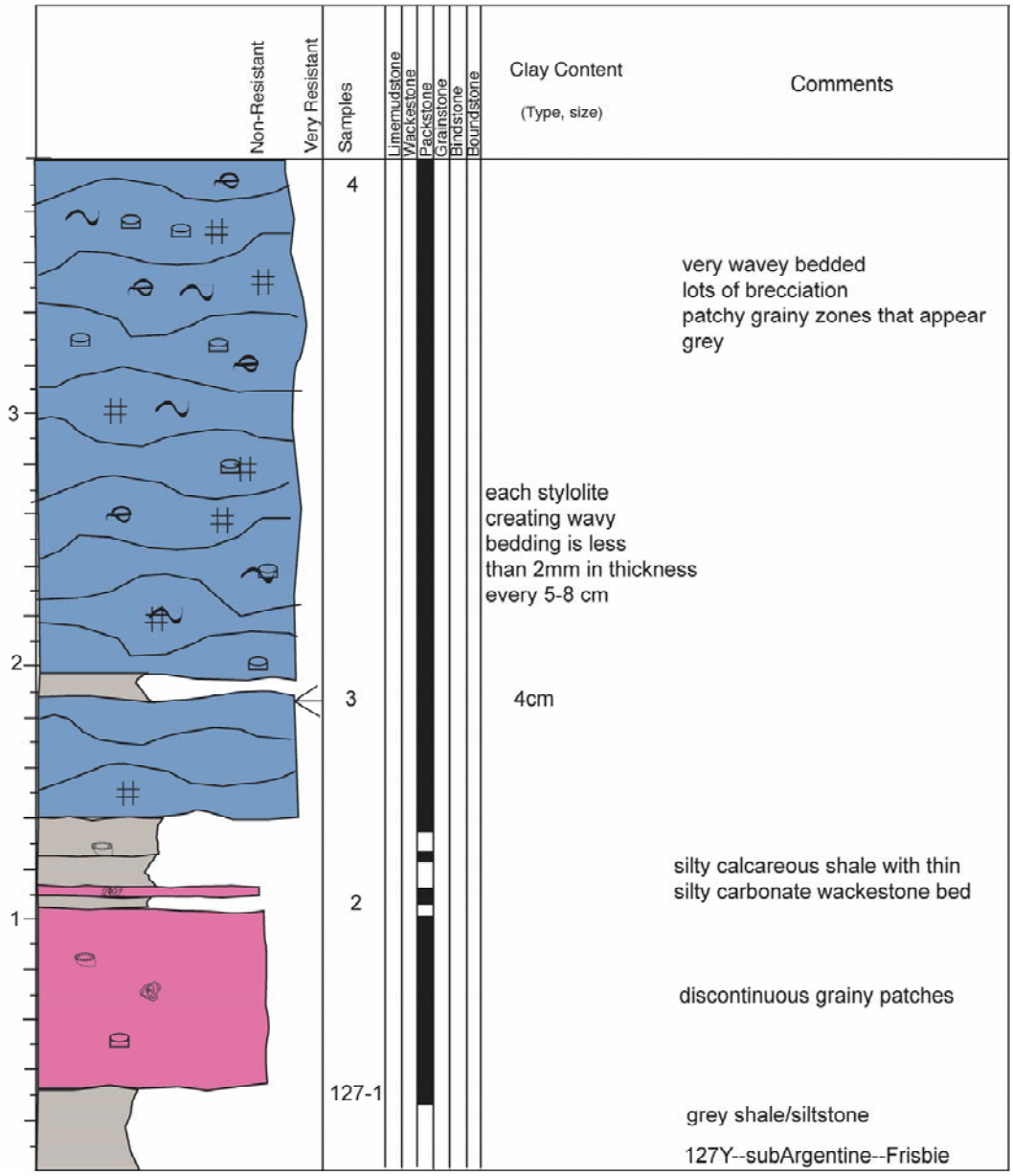

Section Name 127th street--1.9 miles east of Gardner road (RC) Page 3 of 3

Location N38.89816
W94.8906

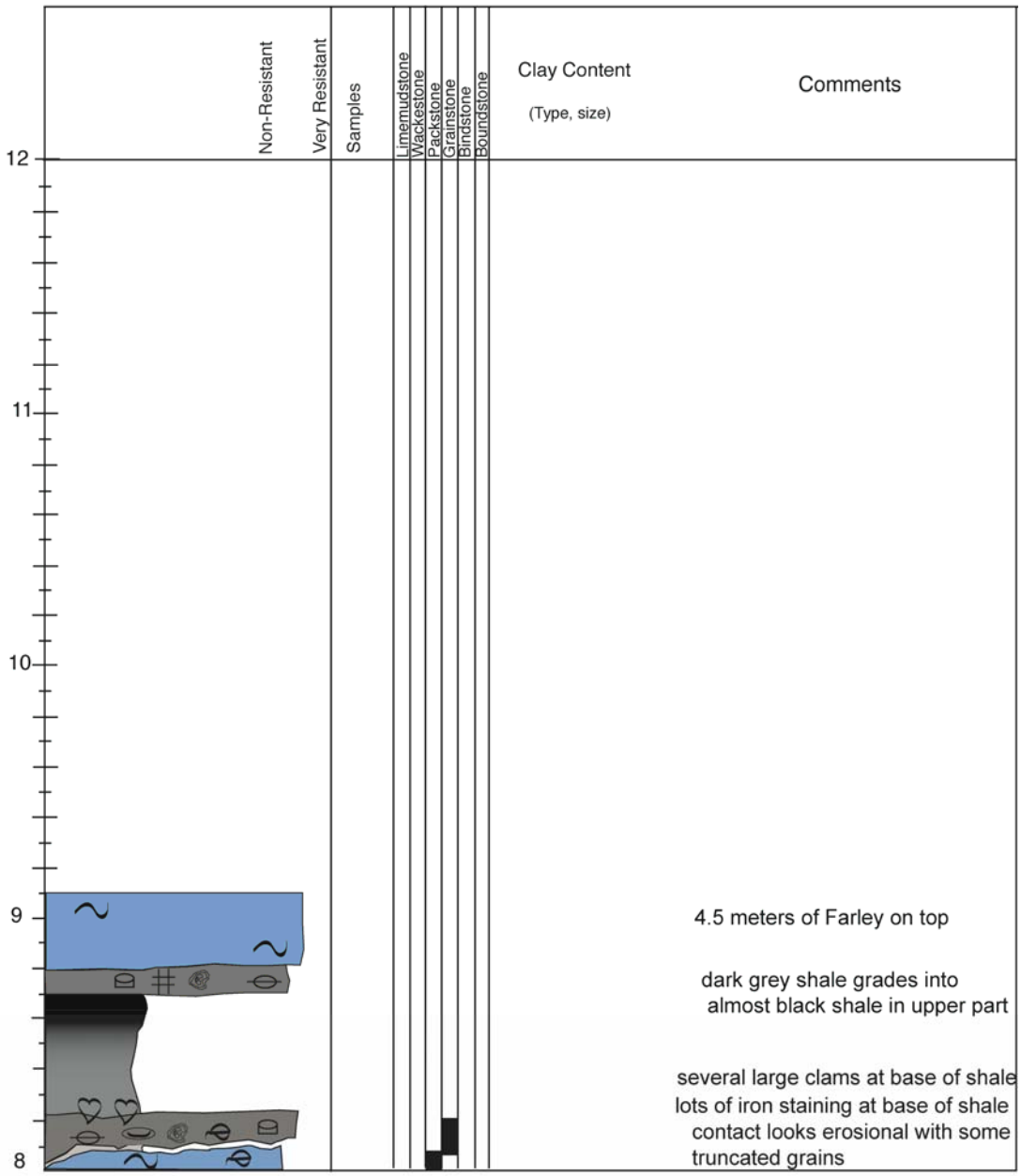

Section Name Arvidson's PE15 south of Paola

Page 1 of 3

Location on major highway just south of Paola
north side of the highway

Date

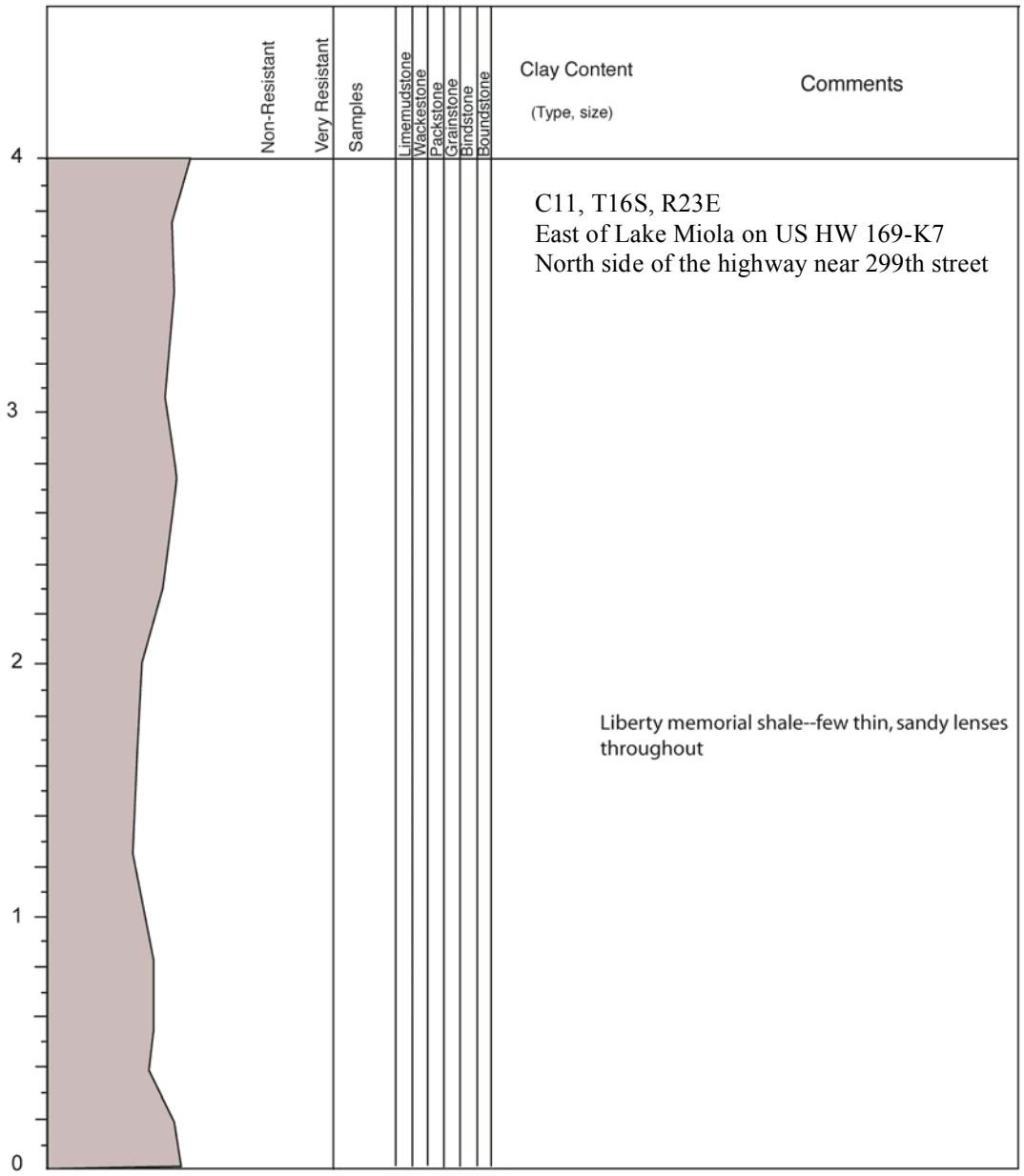

Section Name Arvidson's PE15 south of Paola

Page 2 of 3

Location on major highway just south of Paola
north side of the highway

Date

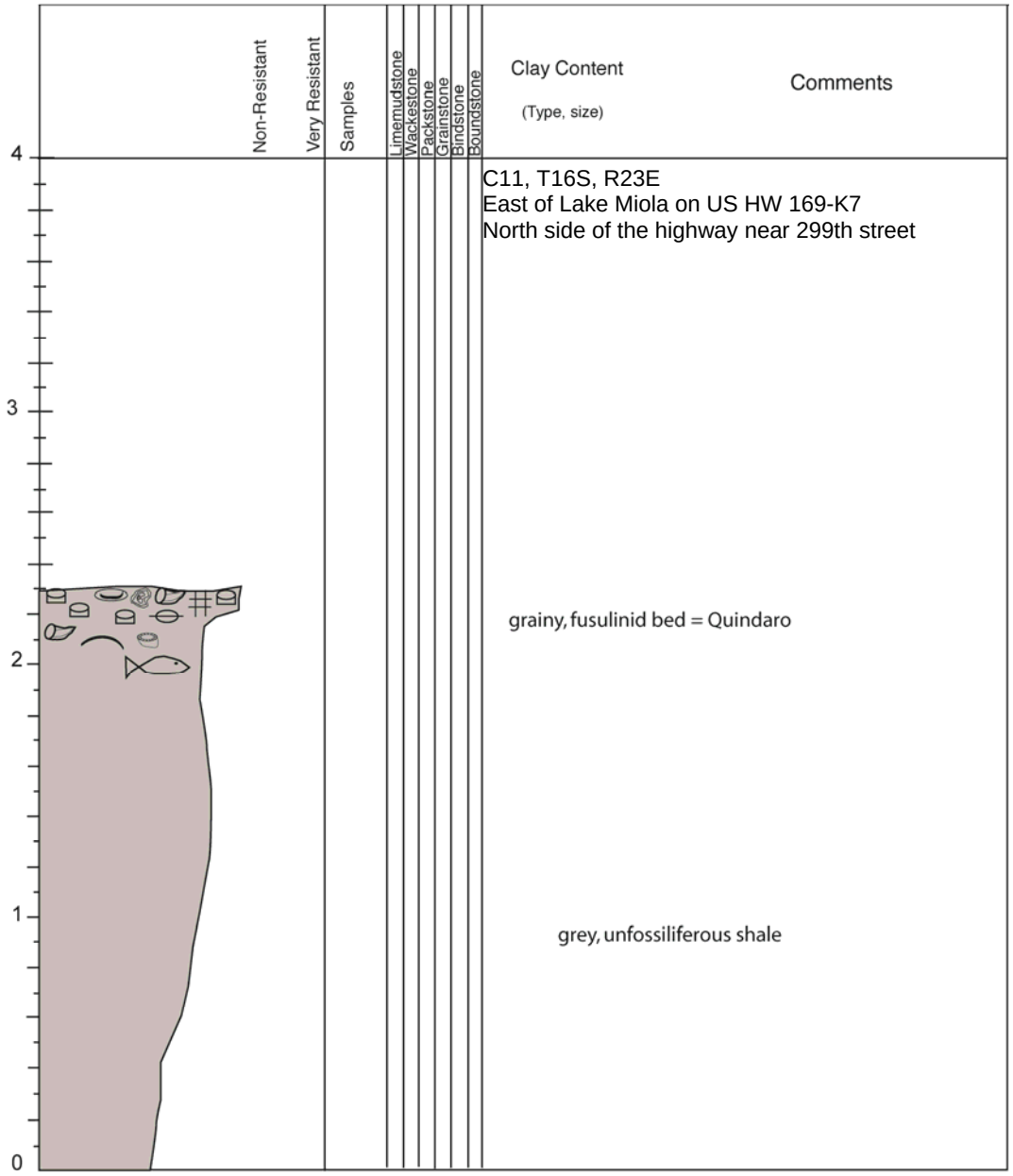

Section Name Arvidson's PE15 south of Paola Page 3 of 3

Location on major highway just south of Paola
north side of the highway

Date

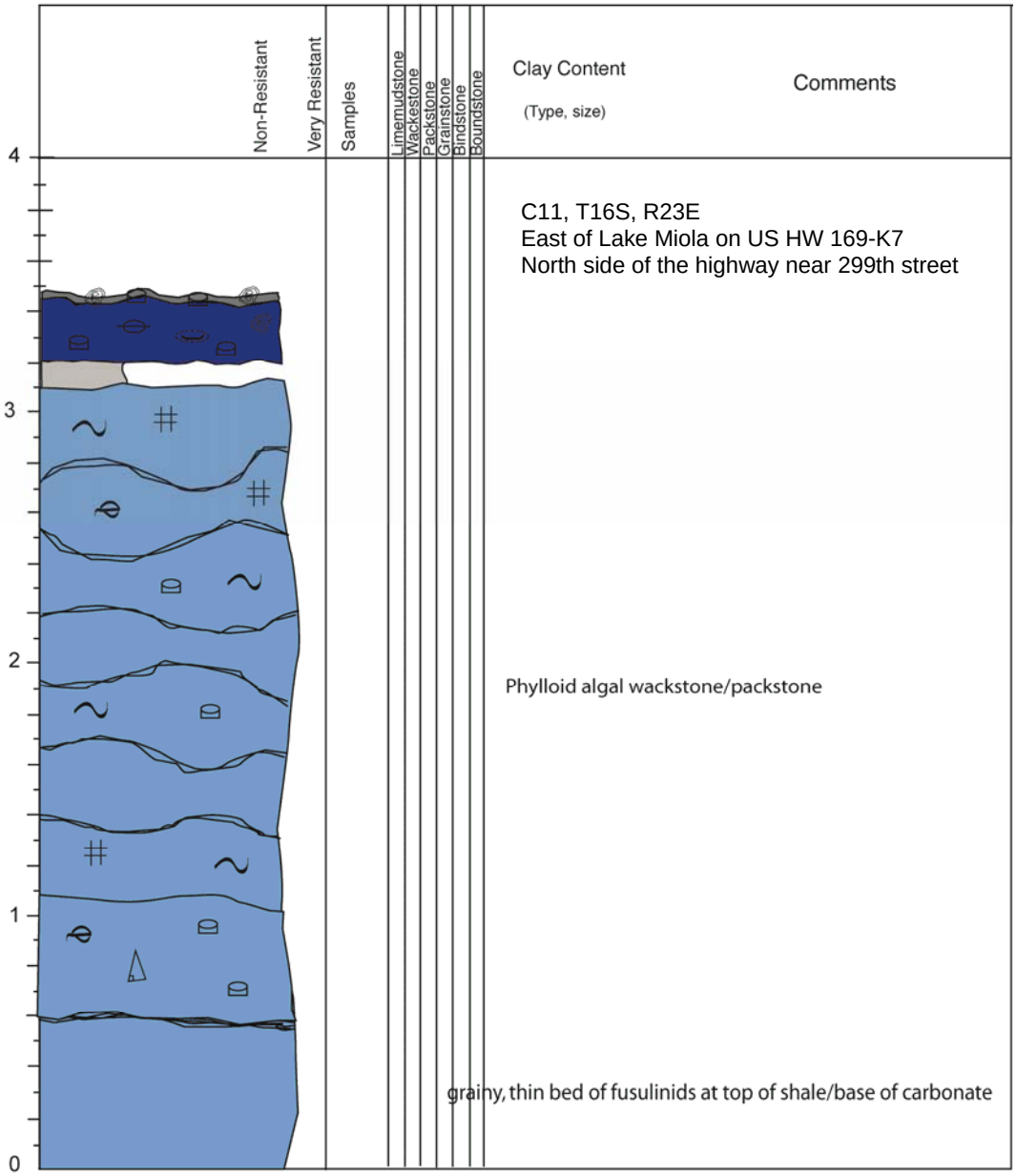

Section Name APAC-2A--The Wall

Page 1 of 2

Location APAC quarry--
Just north of Louisberg on 69

N38.66483
W94.69092

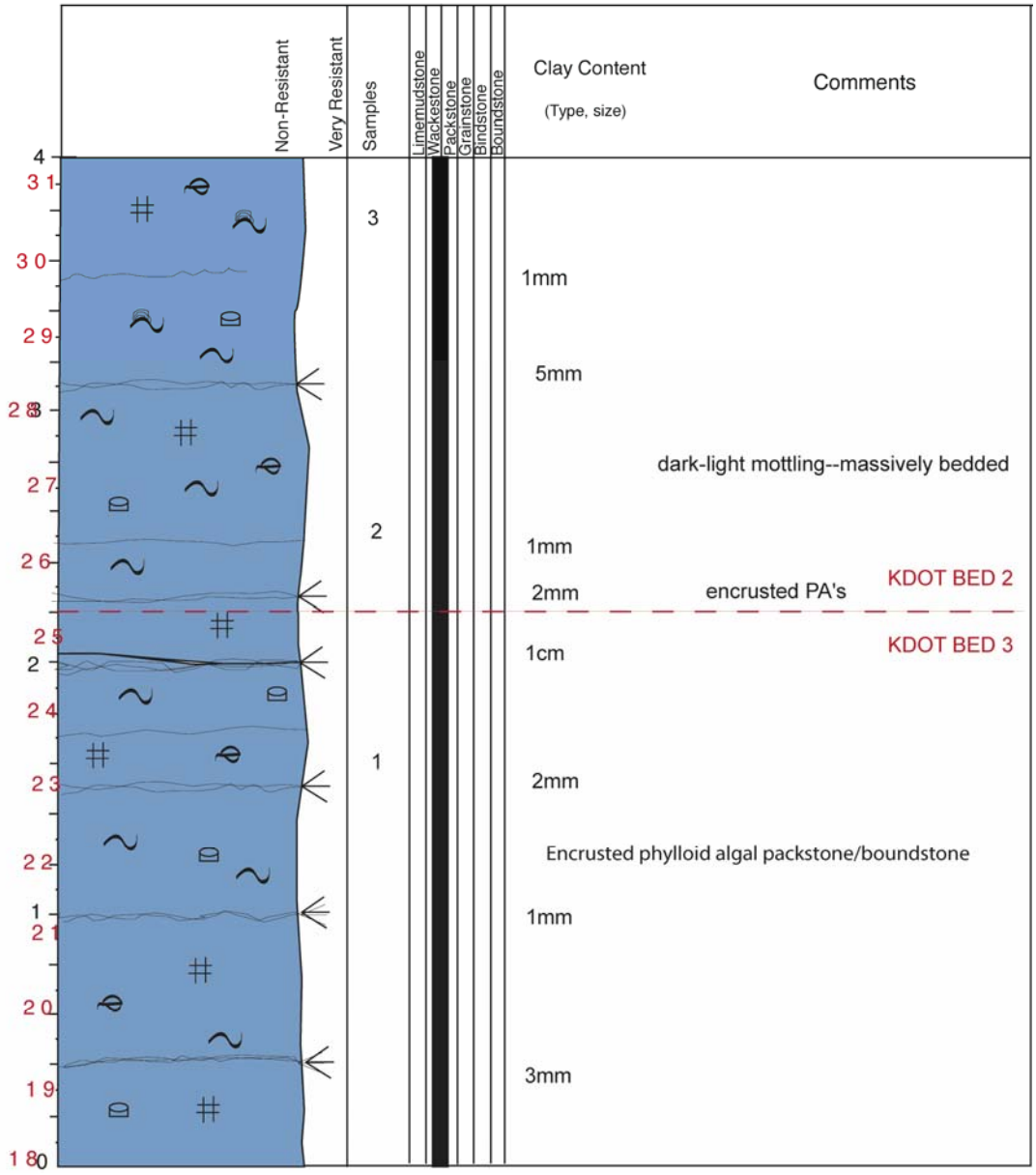

Section Name APAC-2B--the wall

Location APAC quarry--
Just north of Louisberg on 69

N38.66483
W94.69092

Page 2 of 2

Date

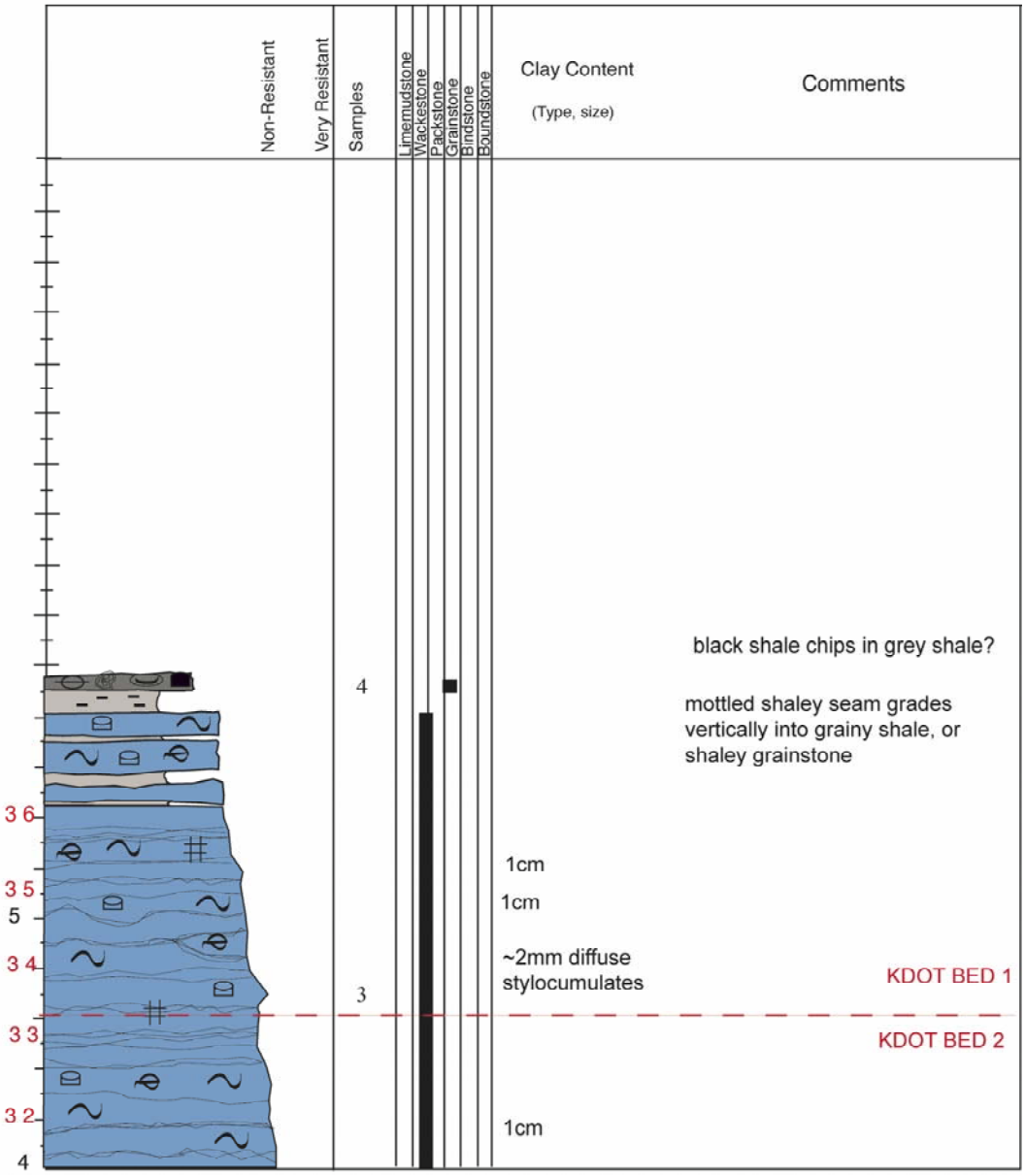

Section Name APAC-3: Lower Argentine--"stuck truck" Page 1 of 3

Location N38.66483 W94.69092 measured on NW wall Date

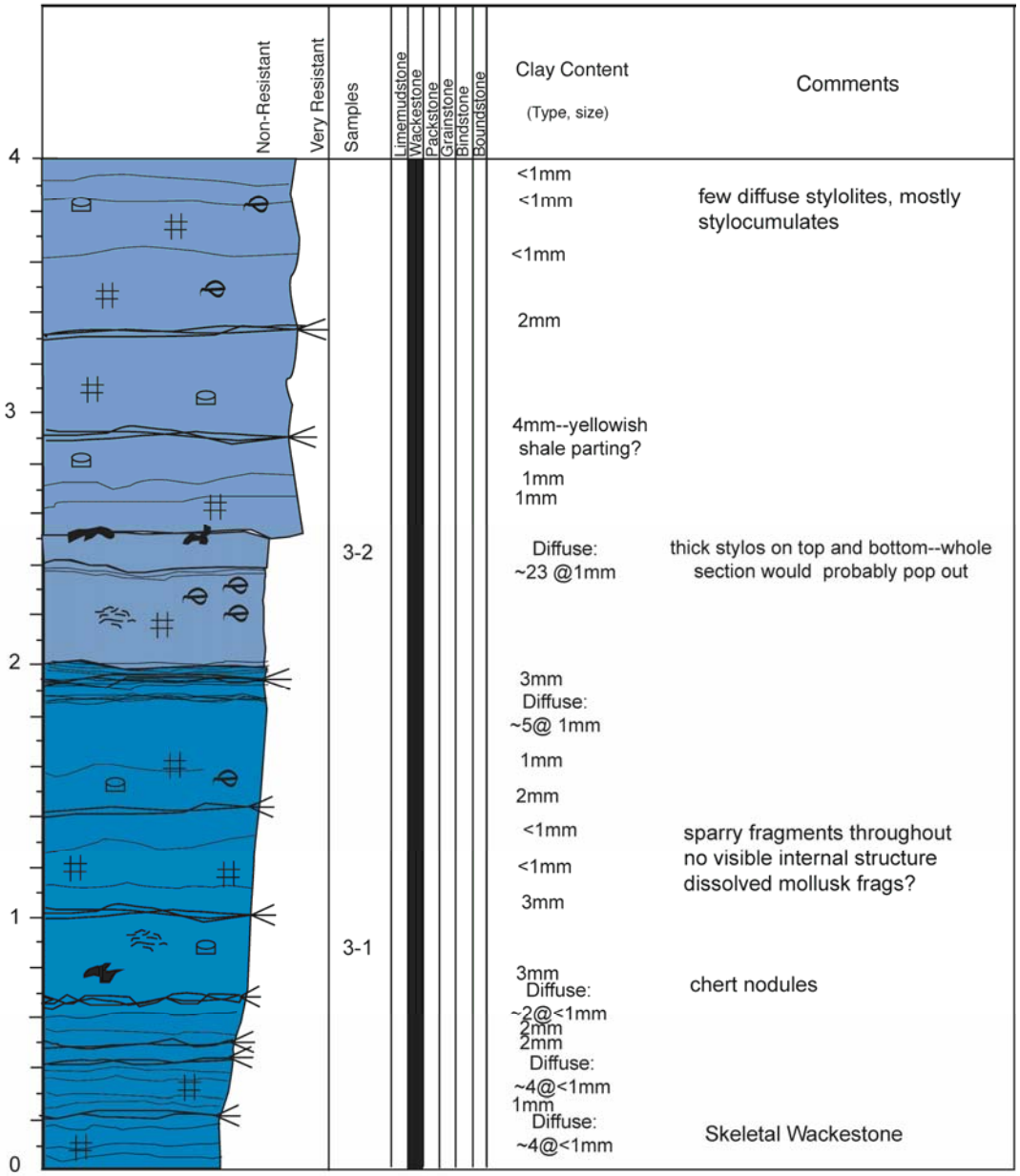

Section Name APAC-3: Lower Argentine--"stuck truck"
Location N38.66483
W94.69092

Page 2 of 3
Date

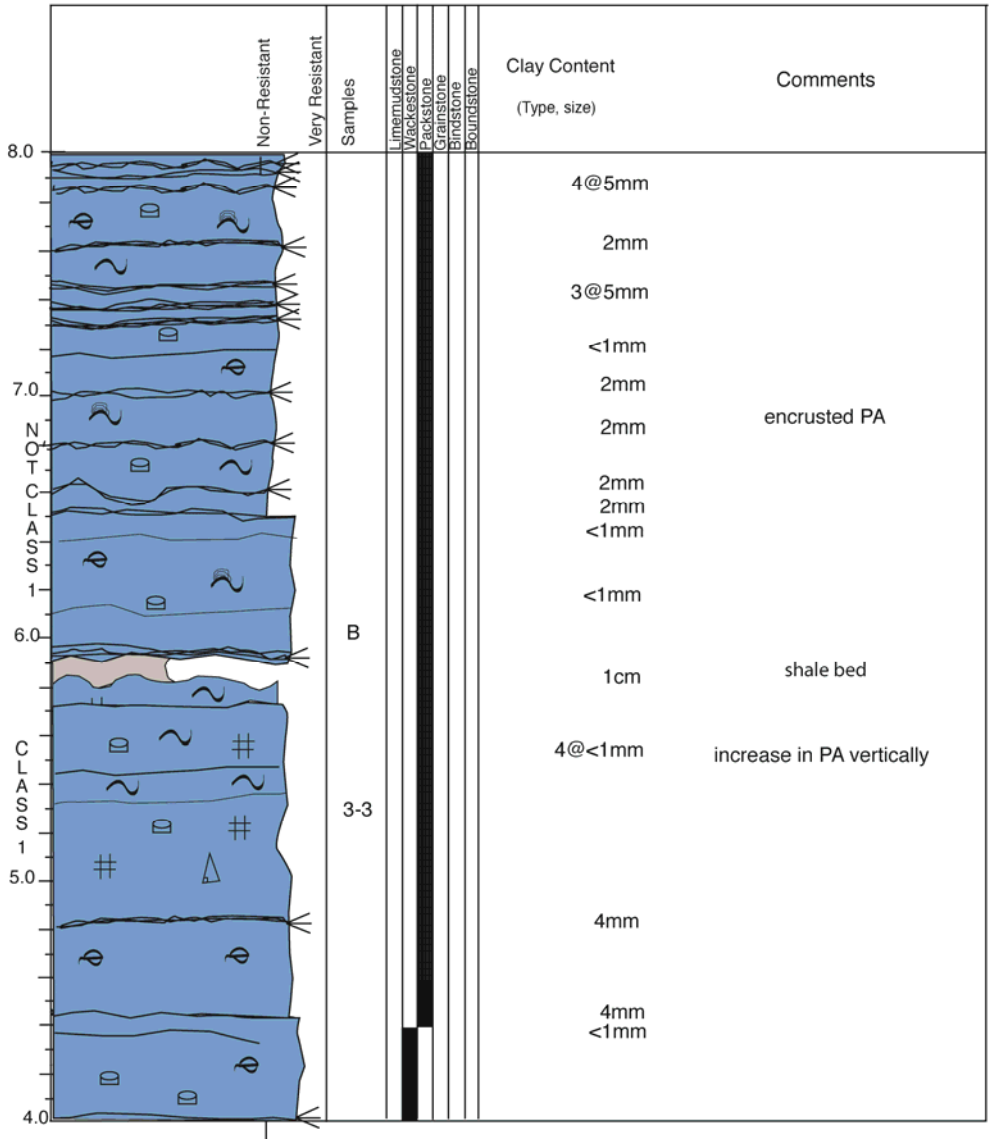

Section Name Apac 3--"Stuck Truck" Page 3 of 3

Location N38.66483
W94.69092

Date

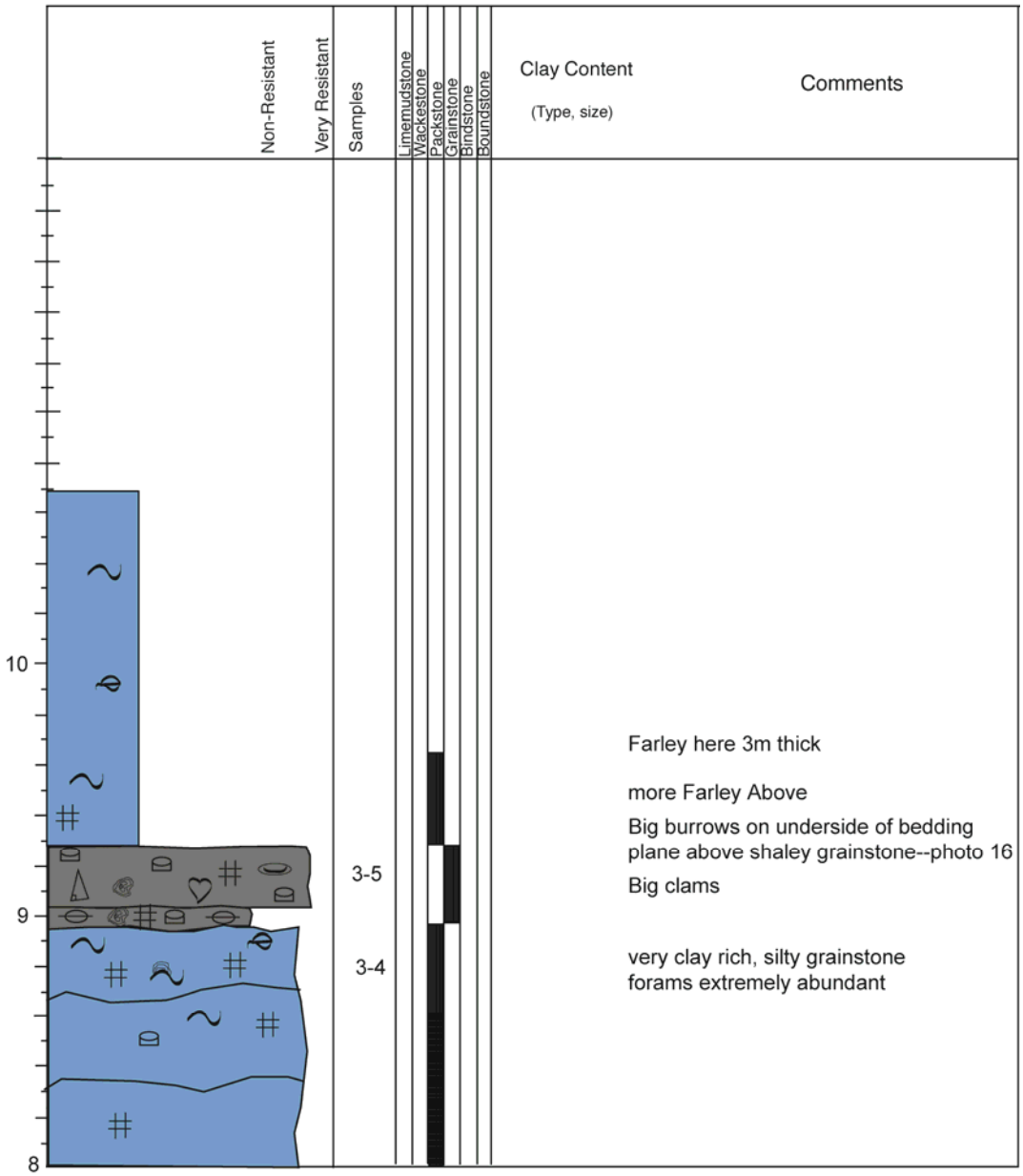

Section Name BS1_A--Shawnee Rock Company quarry
Location N39.07367
W94.89730

Page 1 of 3
Date

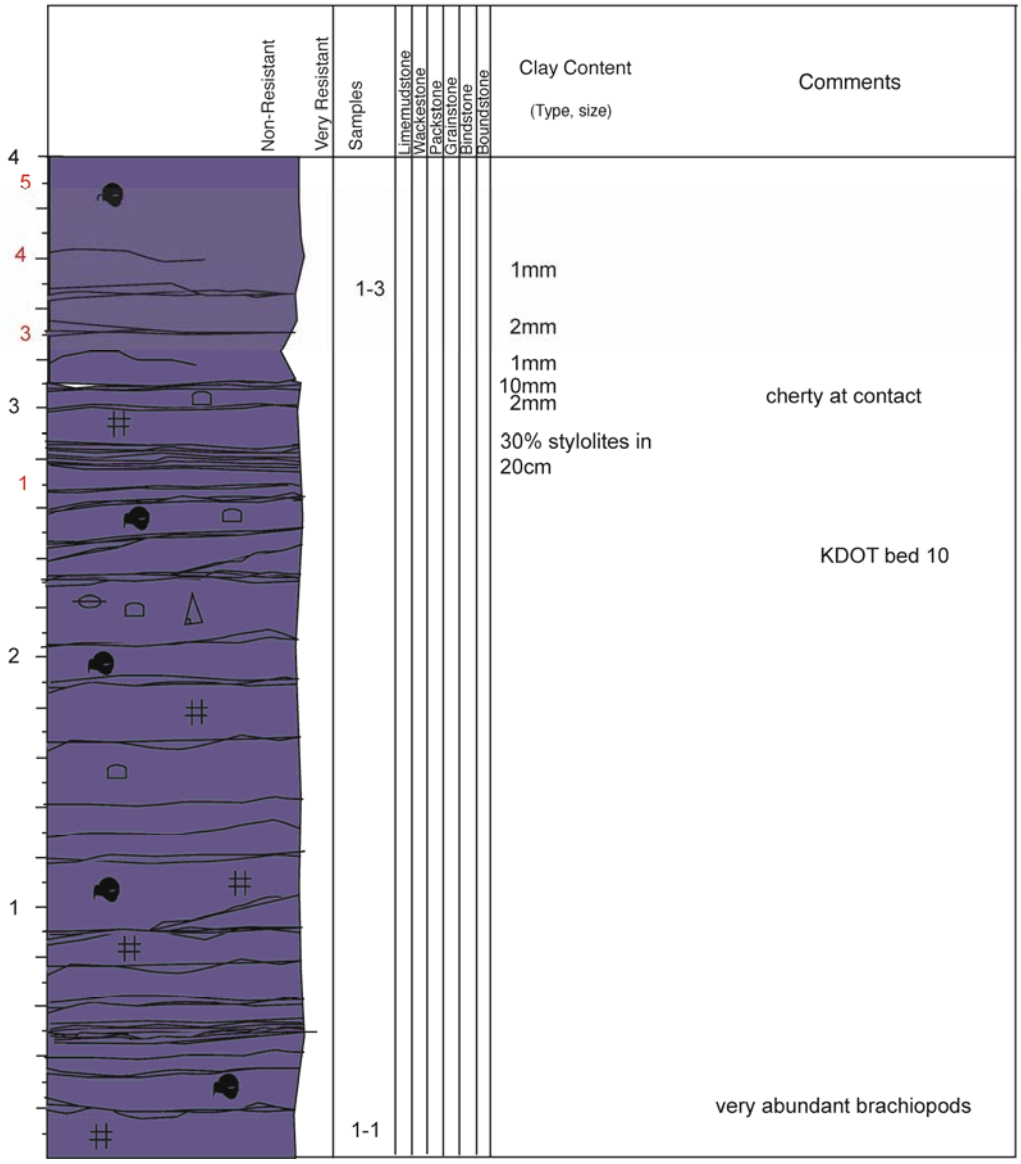

Section Name BS1_A--Shawnee Rock Company quarry Page 2 of 3

Location N39.07367
W94.89730

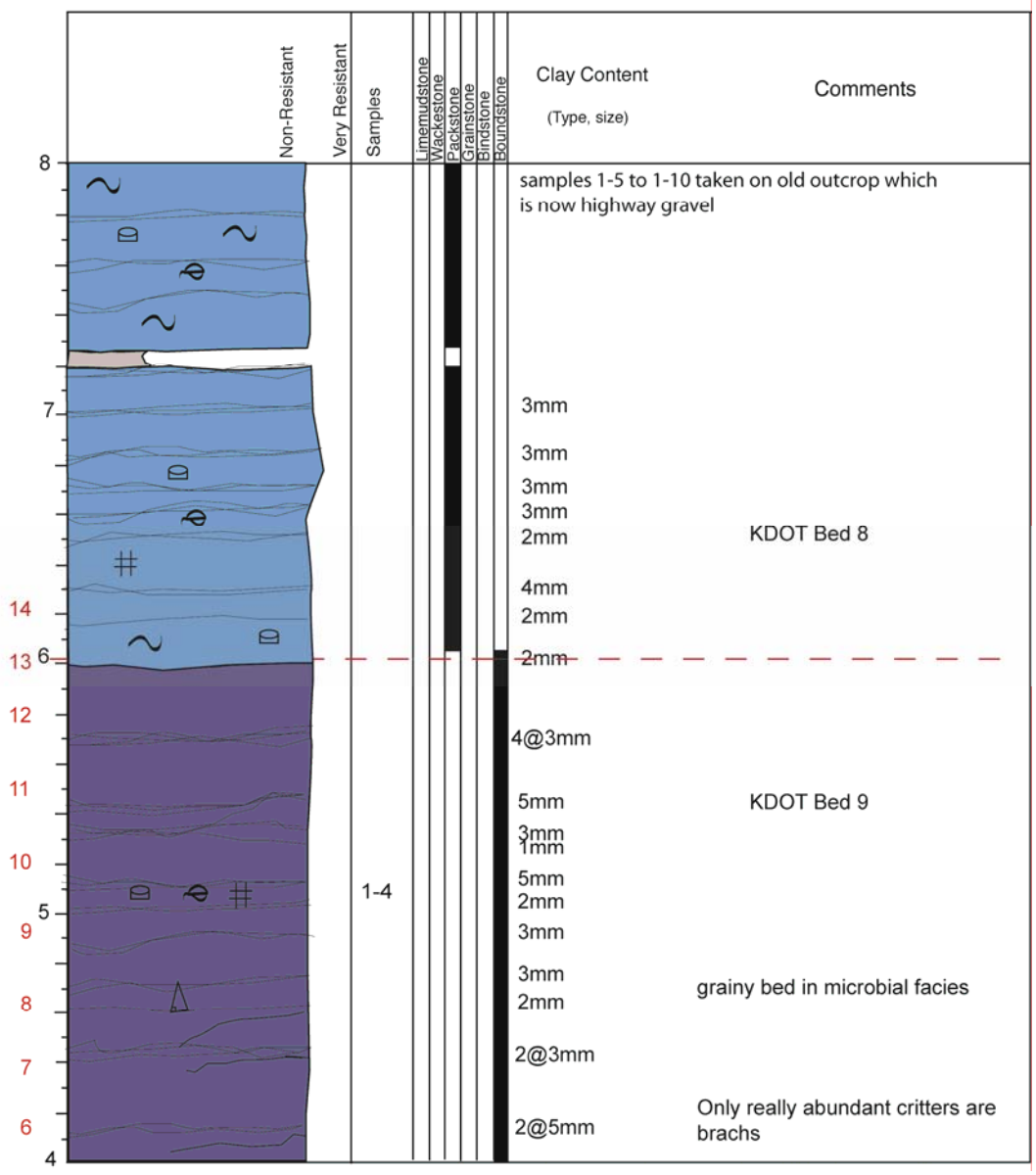

Section Name BS1_A--Shawnee Rock Company quarry
Location N39.07367
W94.89730

Page 3 of 3
Date

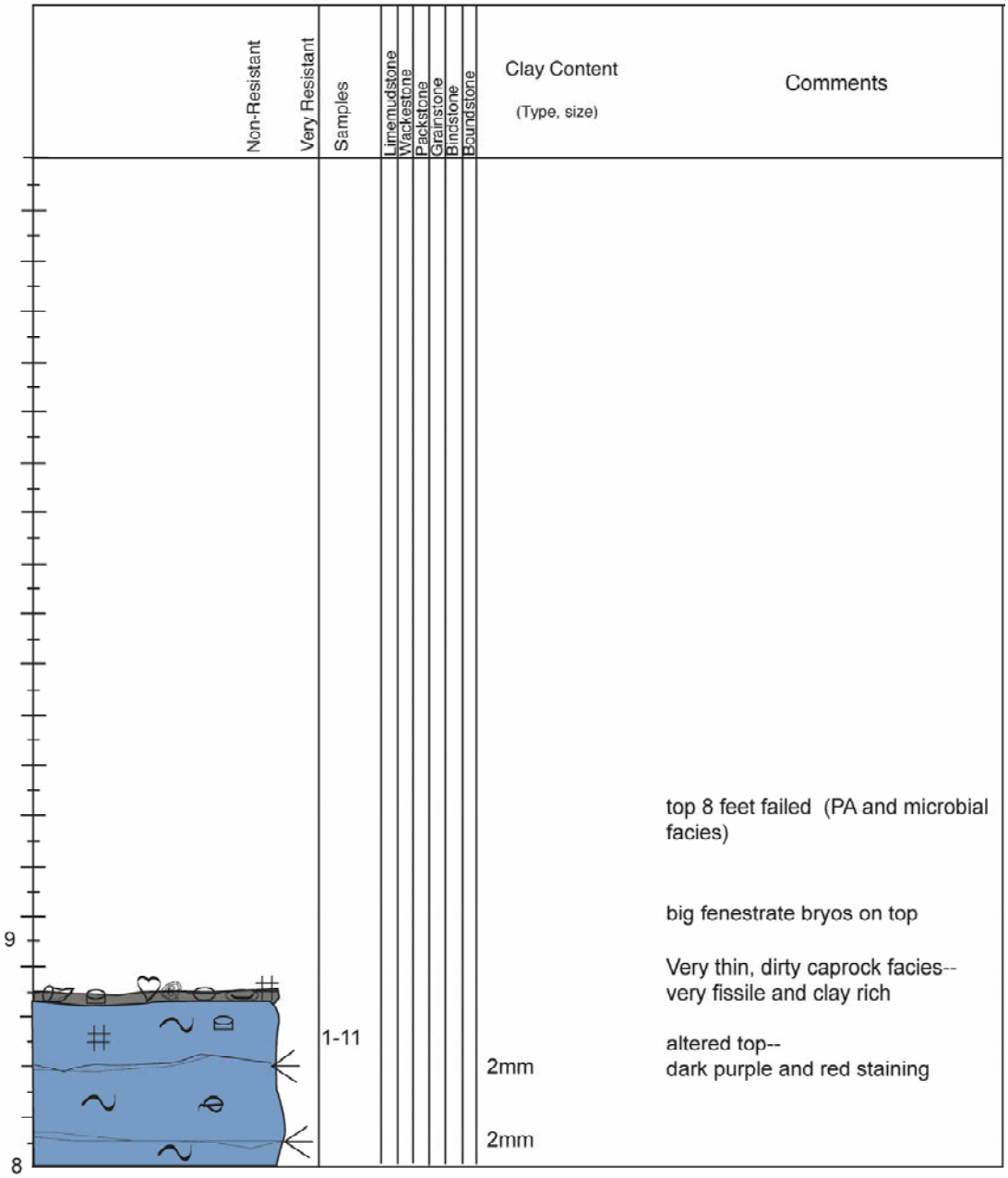

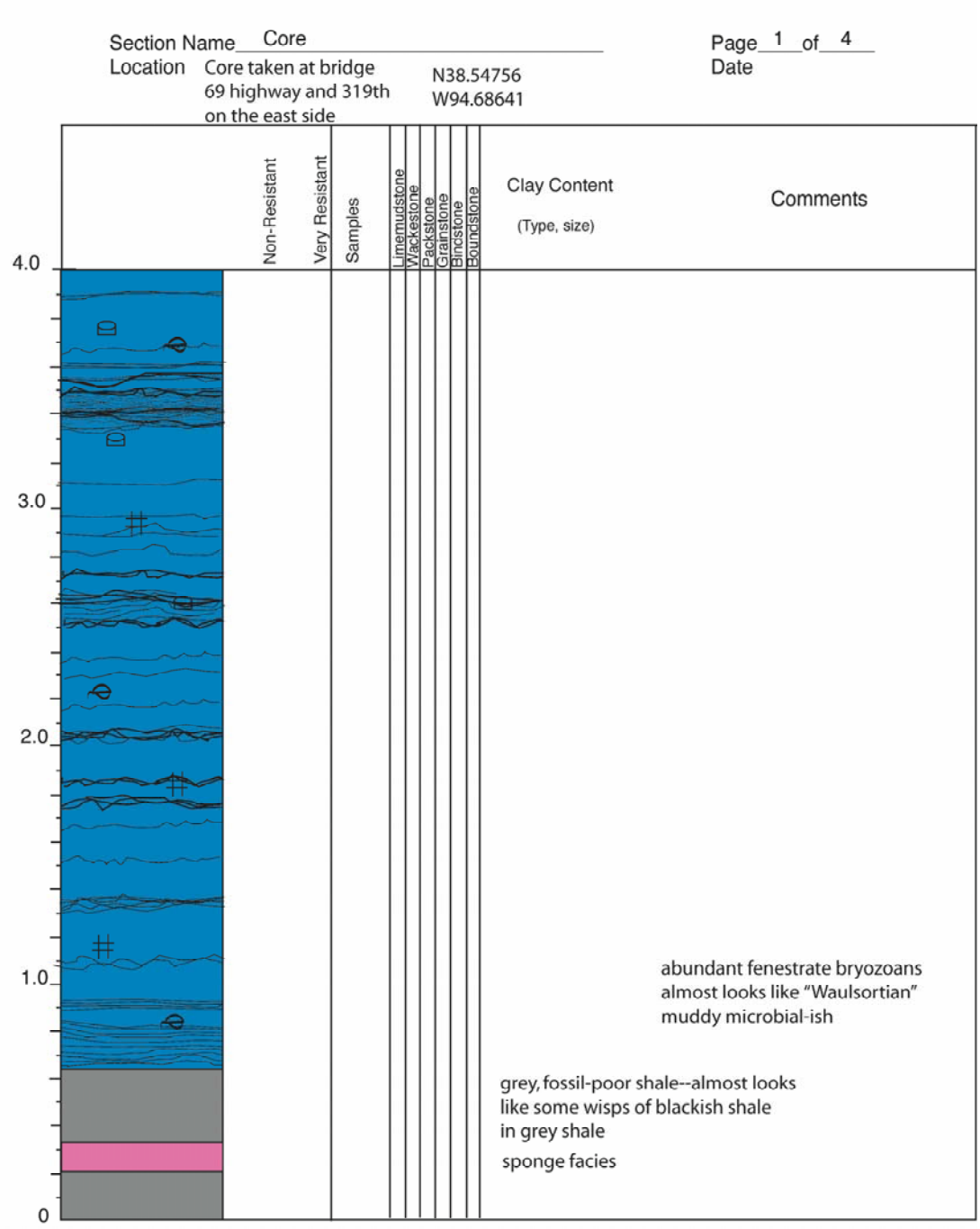
Section Name Core
Page 1 of 4
Location Core taken at bridge 69 highway and 319th on the east side
N38.54756
W94.68641
Date
Non-Resistant
Very Resistant
Samples
Limemudstone
Wackestone
Packstone
Grainstone
Bindstone
Boundstone
Clay Content
(Type, size)
Comments
4.0
3.0
2.0
1.0
0
abundant fenestrate bryozoans
almost looks like "Waulsortian"
muddy microbial-ish
grey, fossil-poor shale--almost looks
like some wisps of blackish shale
in grey shale
sponge facies

Section Name Core

Page 2 of 4

Location Core taken at bridge 69 highway and 319th on the east side N38.54756 W94.68641

Date

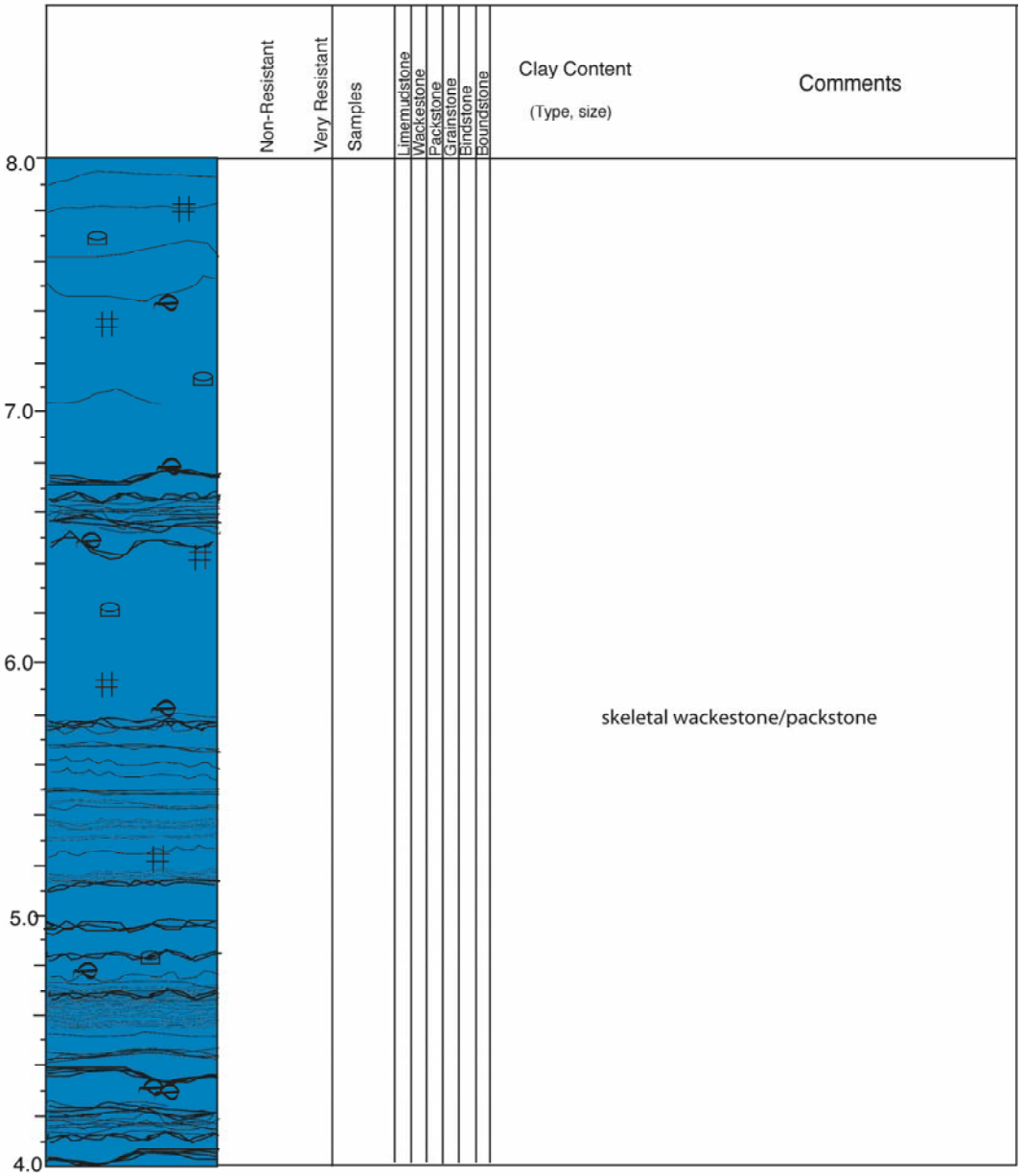

Section Name Core

Page 3 of 4

Location Core taken at bridge 69 highway and 319th on the east side N38.54756 W94.68641

Date

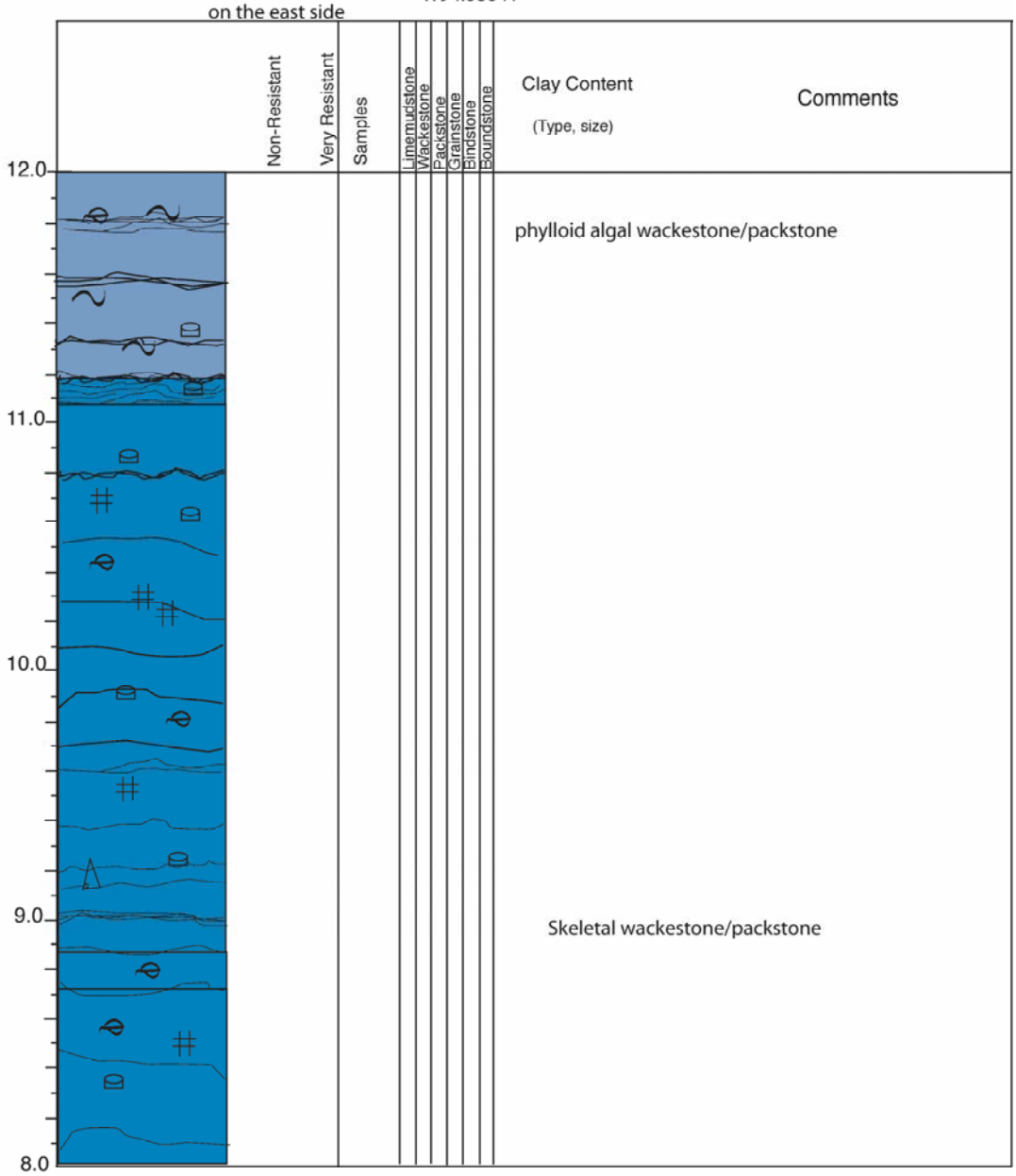

Section Name Core

Page 4 of 4

Location Core taken at bridge 69 highway and 319th on the east side

N38.54756
W94.68641

Date

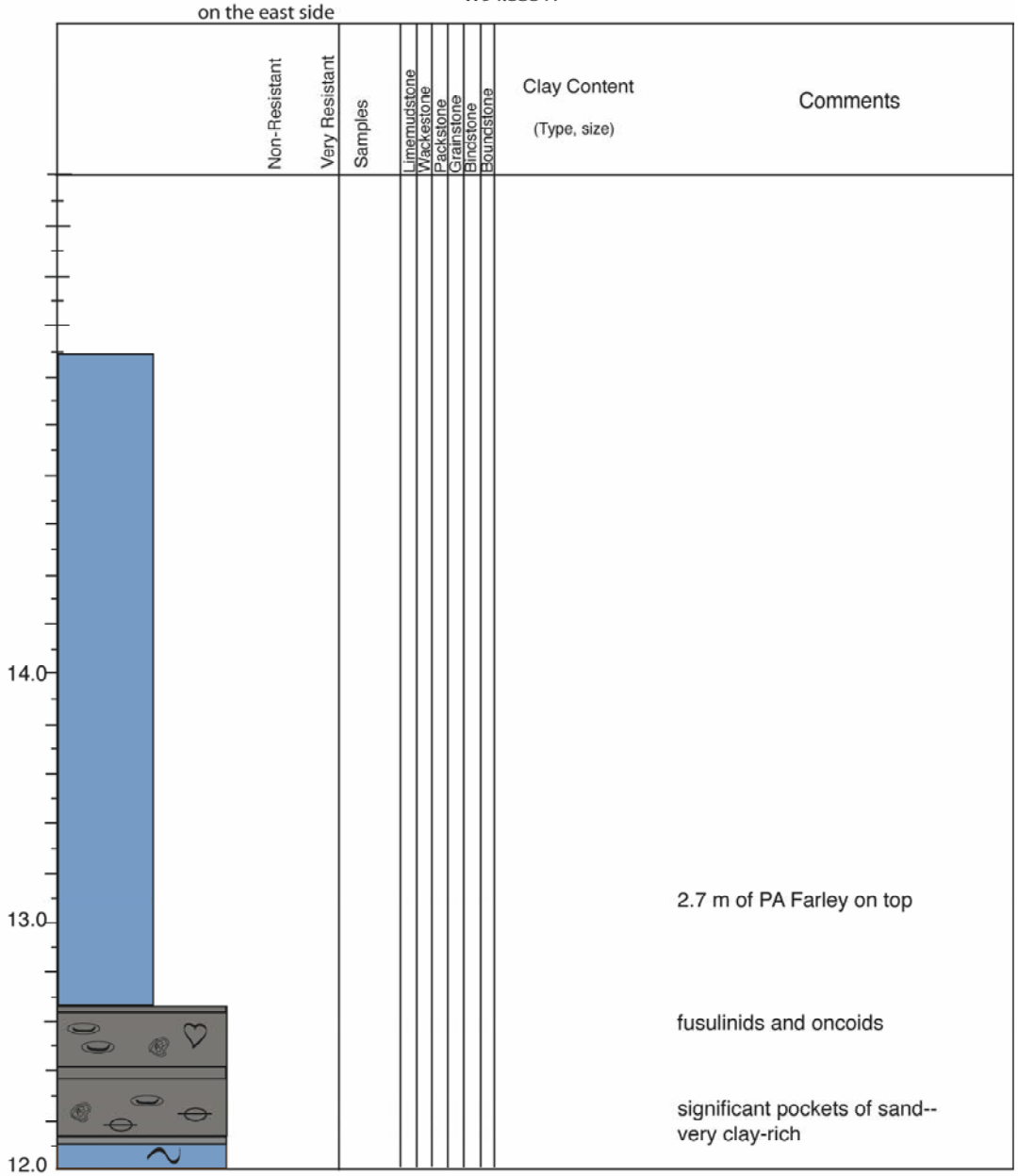

Top part

Section Name Hunt-Midwest "Crawford" Quarry- 1--Lower Argentine Page 1 of 3

Location N38.62572
W094.8007 Date

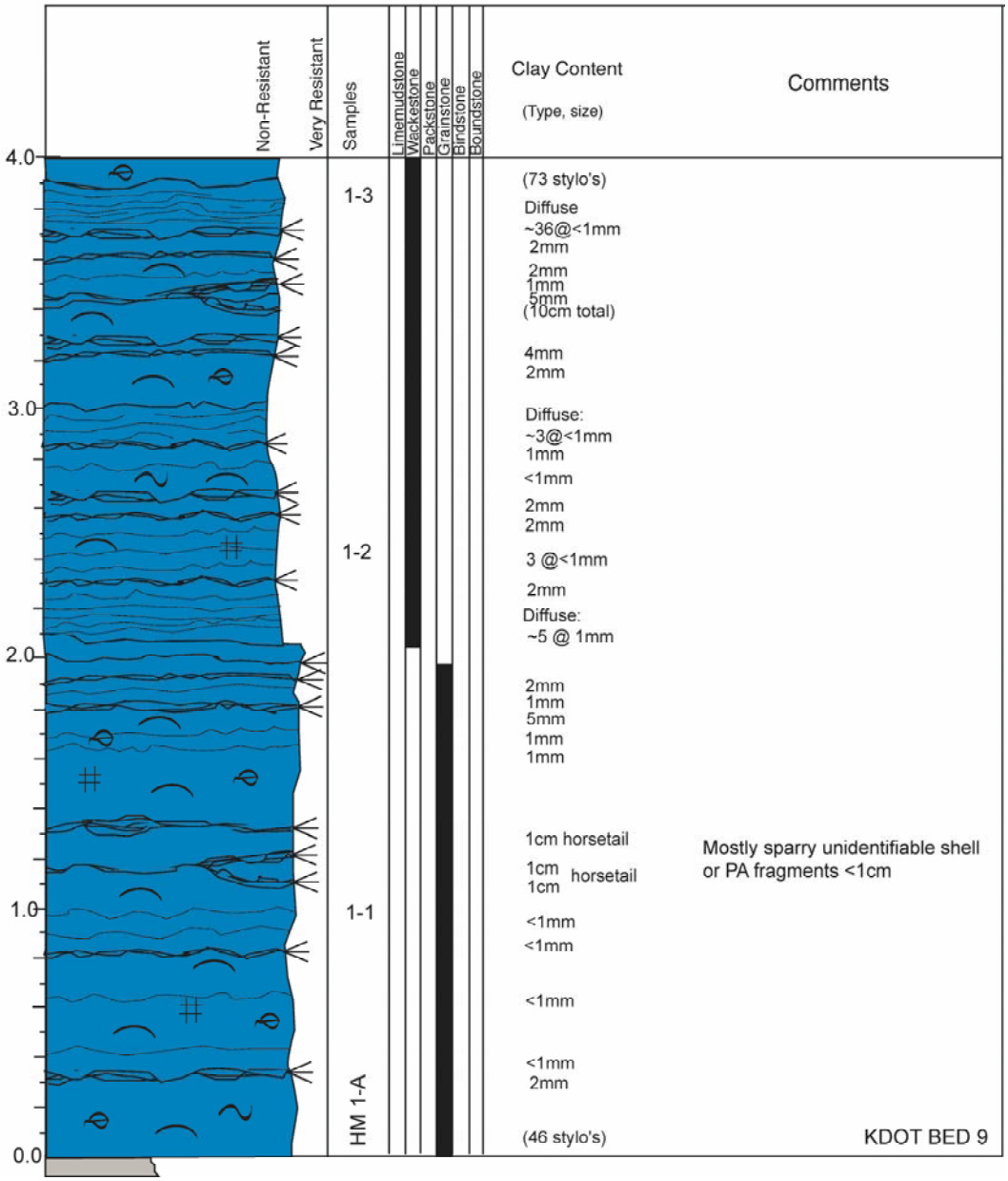

Section Name Hunt-Midwest "Crawford" Lower Argentine--E pit Page 2 of 3

Location N38.62572
W094.8007

Date

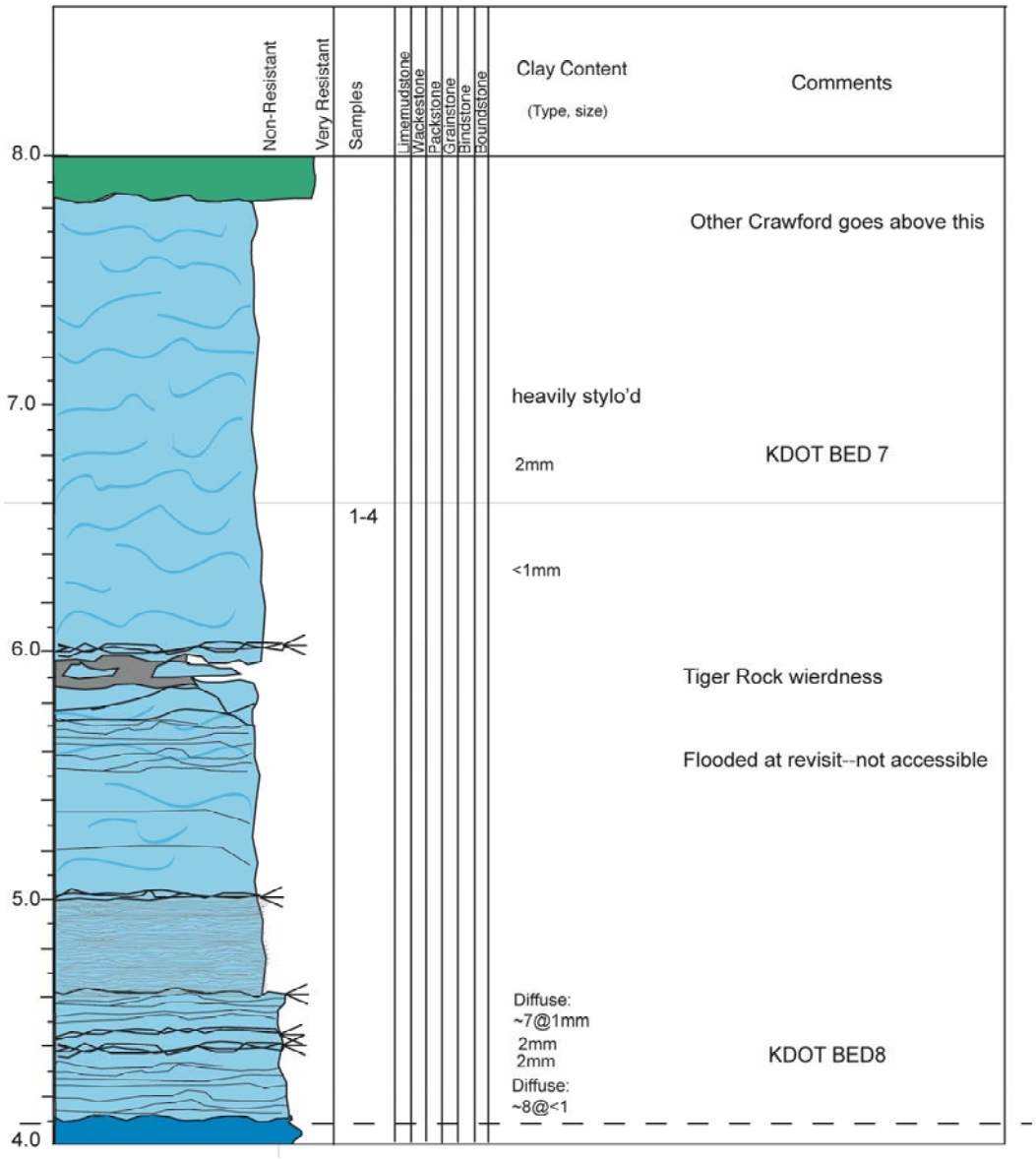

W pit

Section Name Hunt-Midwest"Crawford" Quarry 2--Upper Argentine Page 1 of 2

Location N38.63006
W094.80577

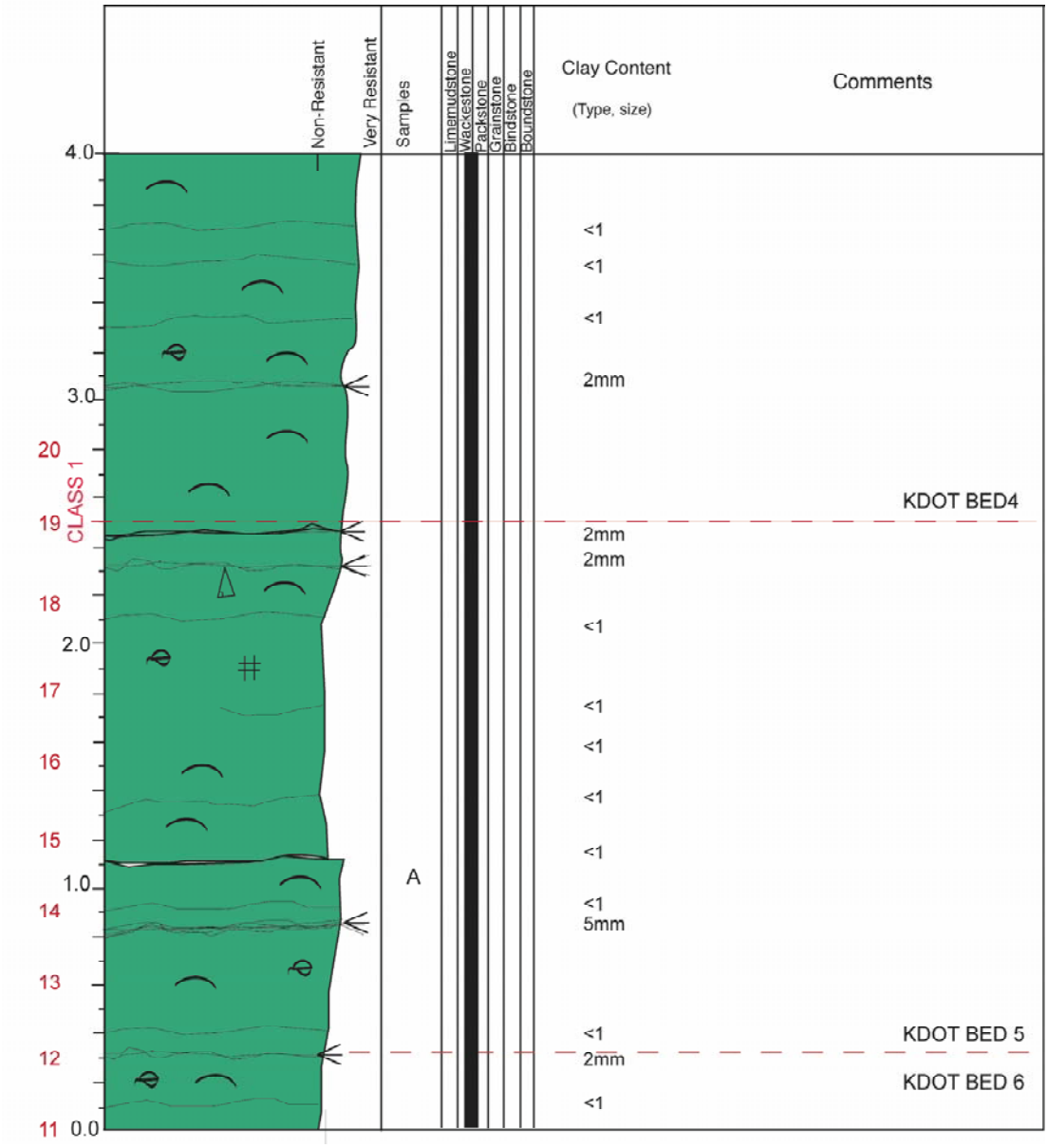

Section Name Hunt-Midwest"Crawford" Quarry 2--Upper Argentine Page 2 of 2
Location N38.63006
W094.80577 Date

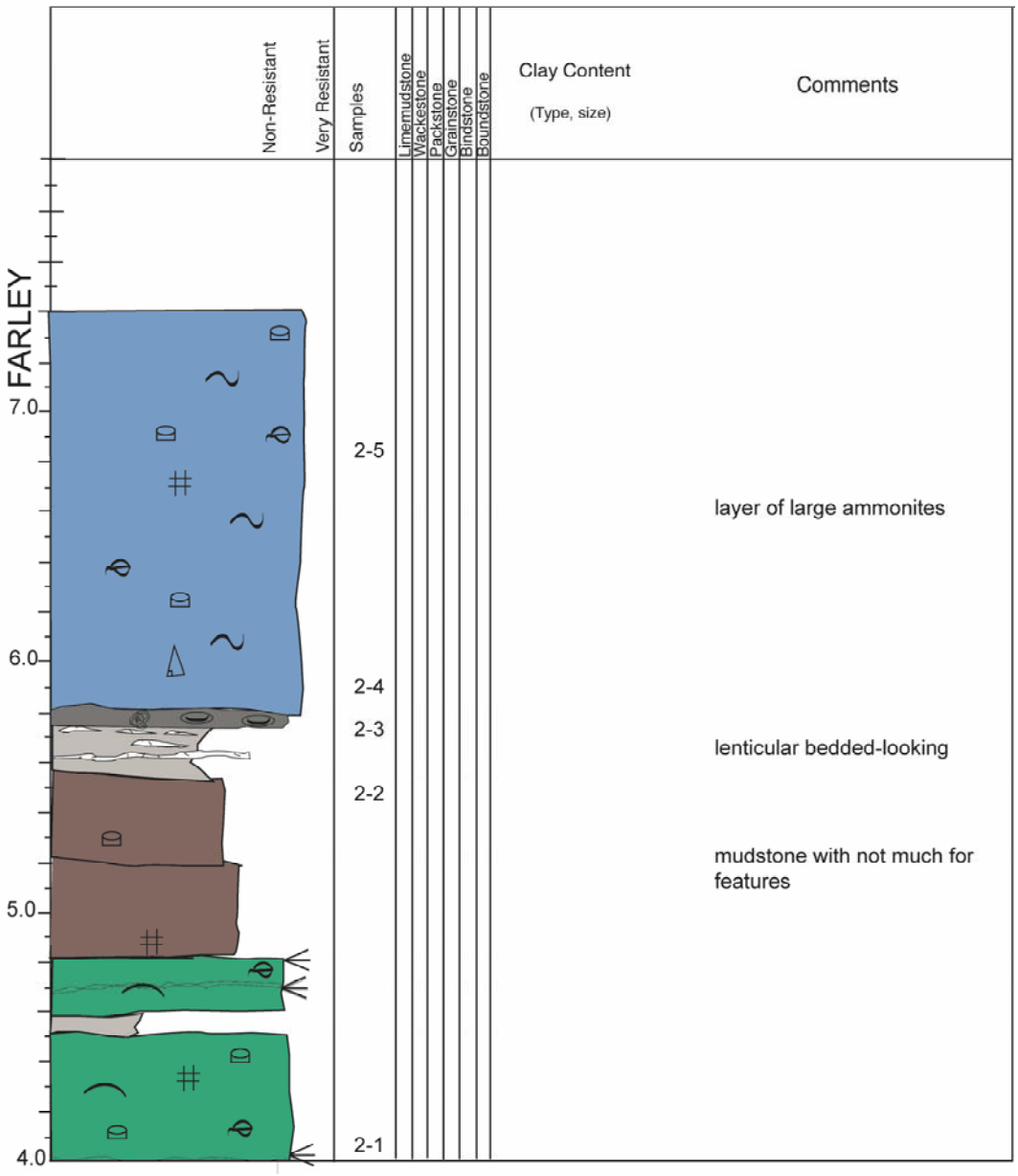

Section Name Holliday Road--outside JCL

Page 1 of 1

Location N39.04067
W94.79168

Date

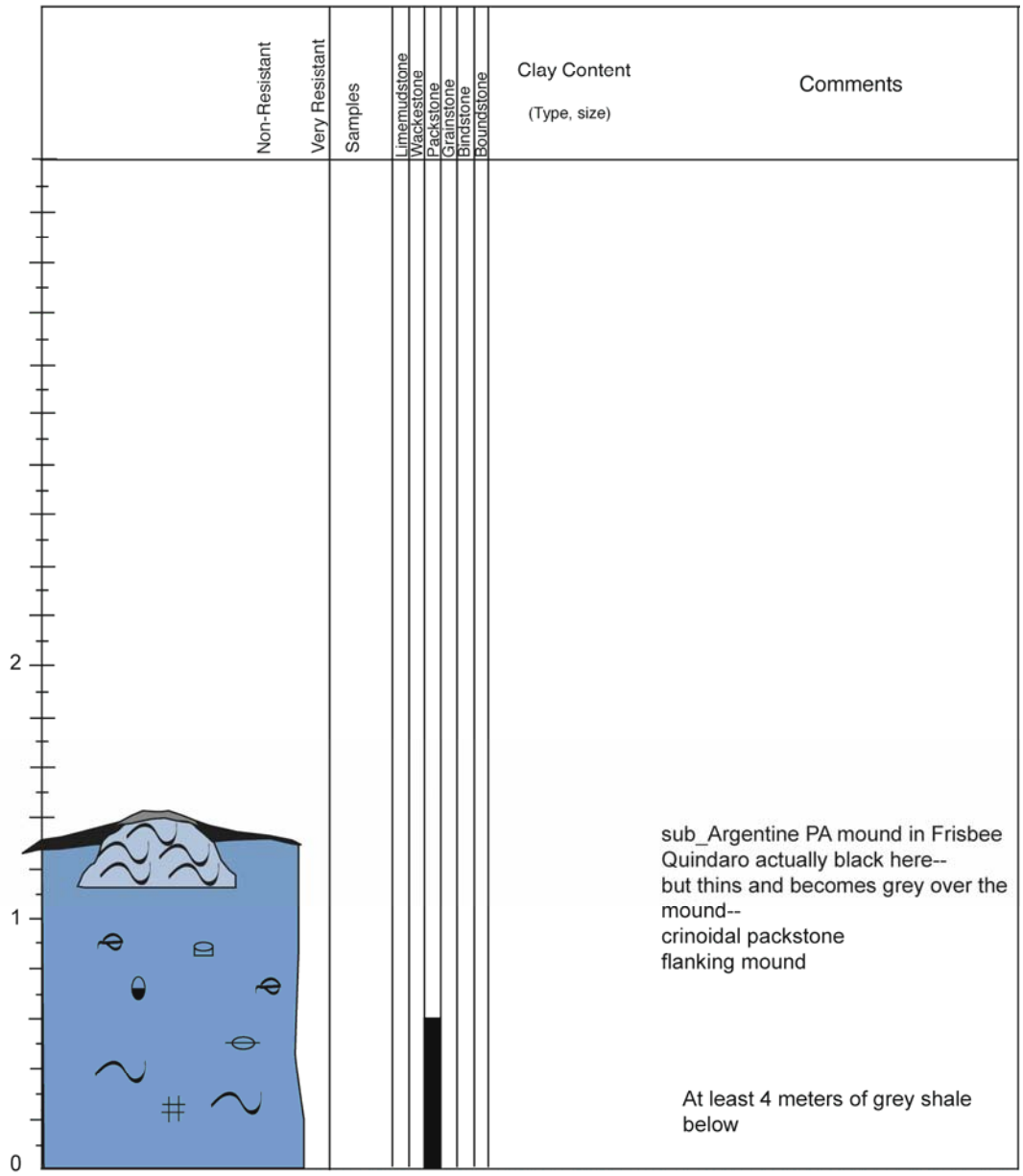

Section Name Holliday Road--outside JCL

Page 1 of 2

Location N39.04067
W94.79168

Date

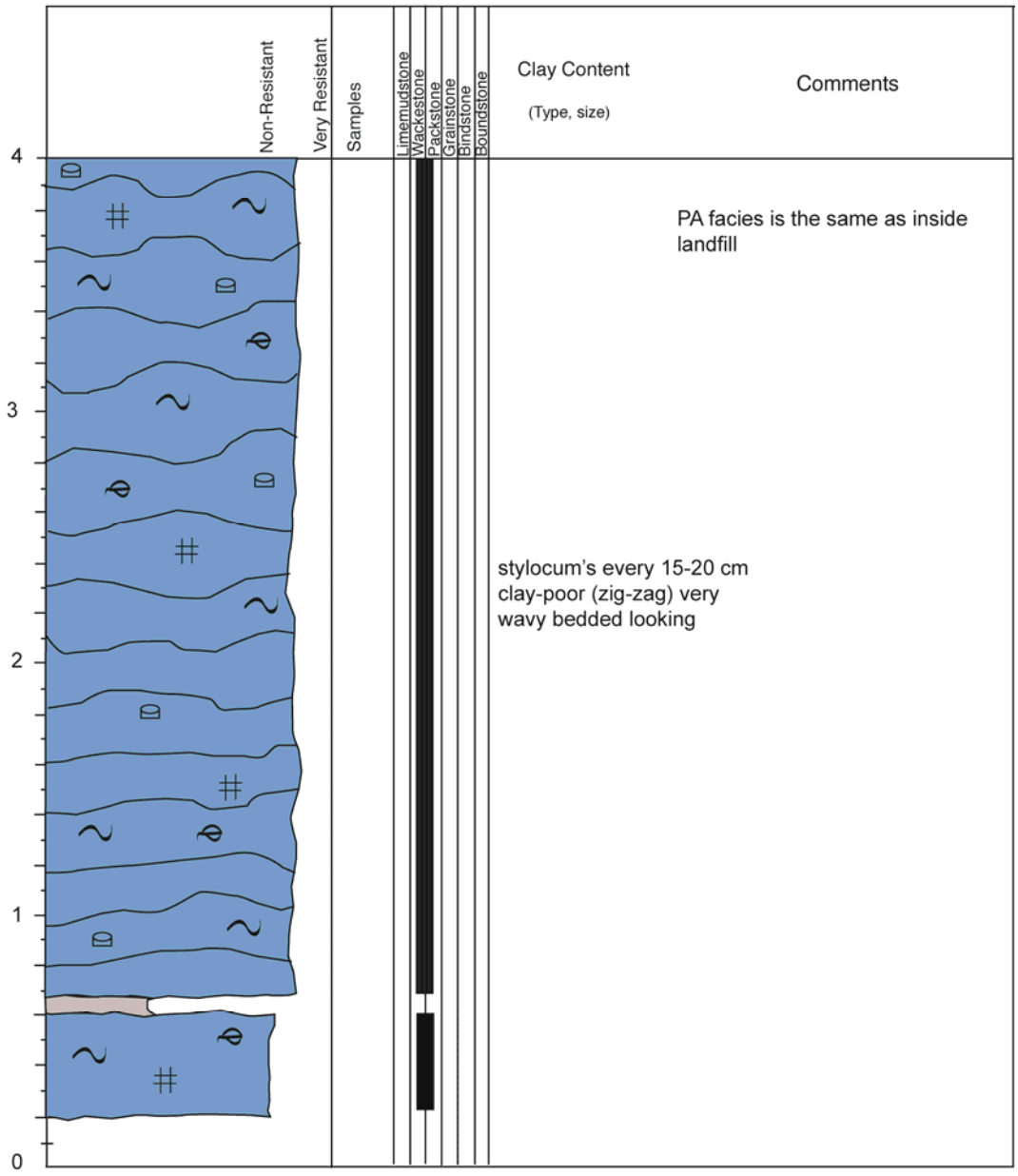

Section Name Holliday Road--outside JCL

Page 2 of 2

Location N39.04067
W94.79168

Date

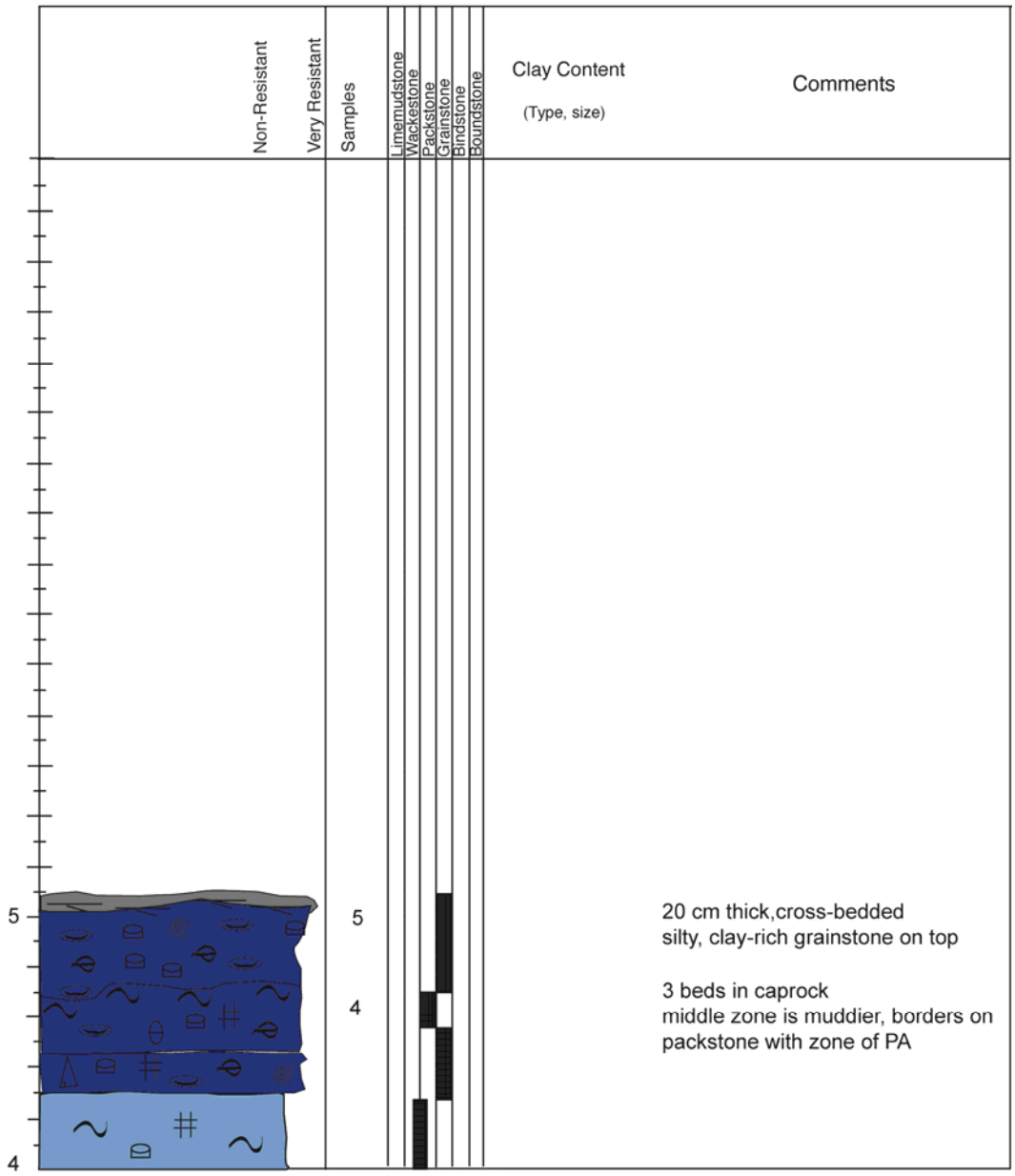

Section Name JCL-1-"Brachiopod layer" Page 1 of 1

Location N39.02698
W94.80316 Date

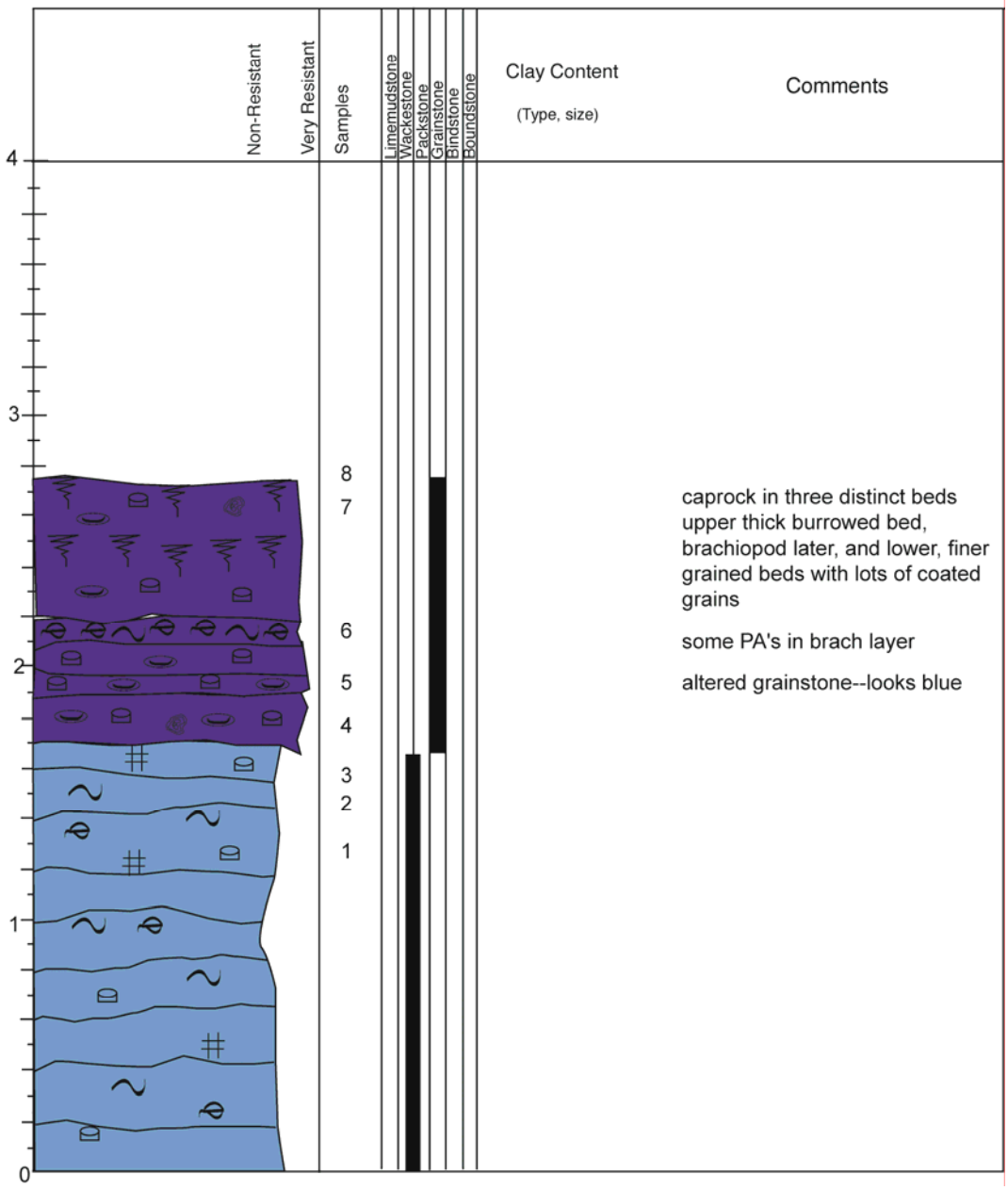

Section Name JCL-2_top--1st part measured

Page 1 of 1

Location 200 meters directly south of Brachiopod locality

Date

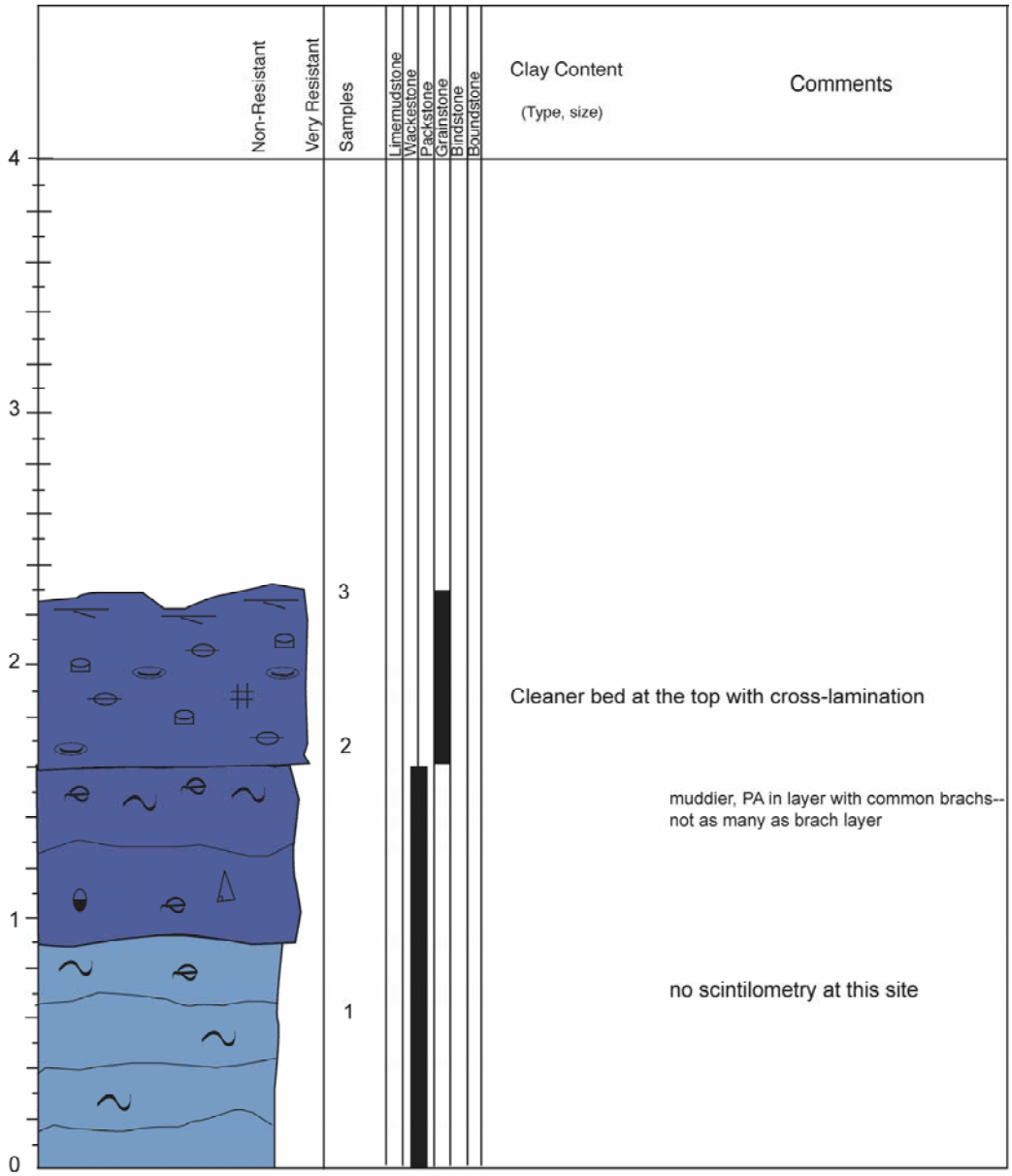

Section Name JCL-"behind" JCl-2--as quarrying went north
Location N39.02698
W94.80316

Page 1 of 1
Date

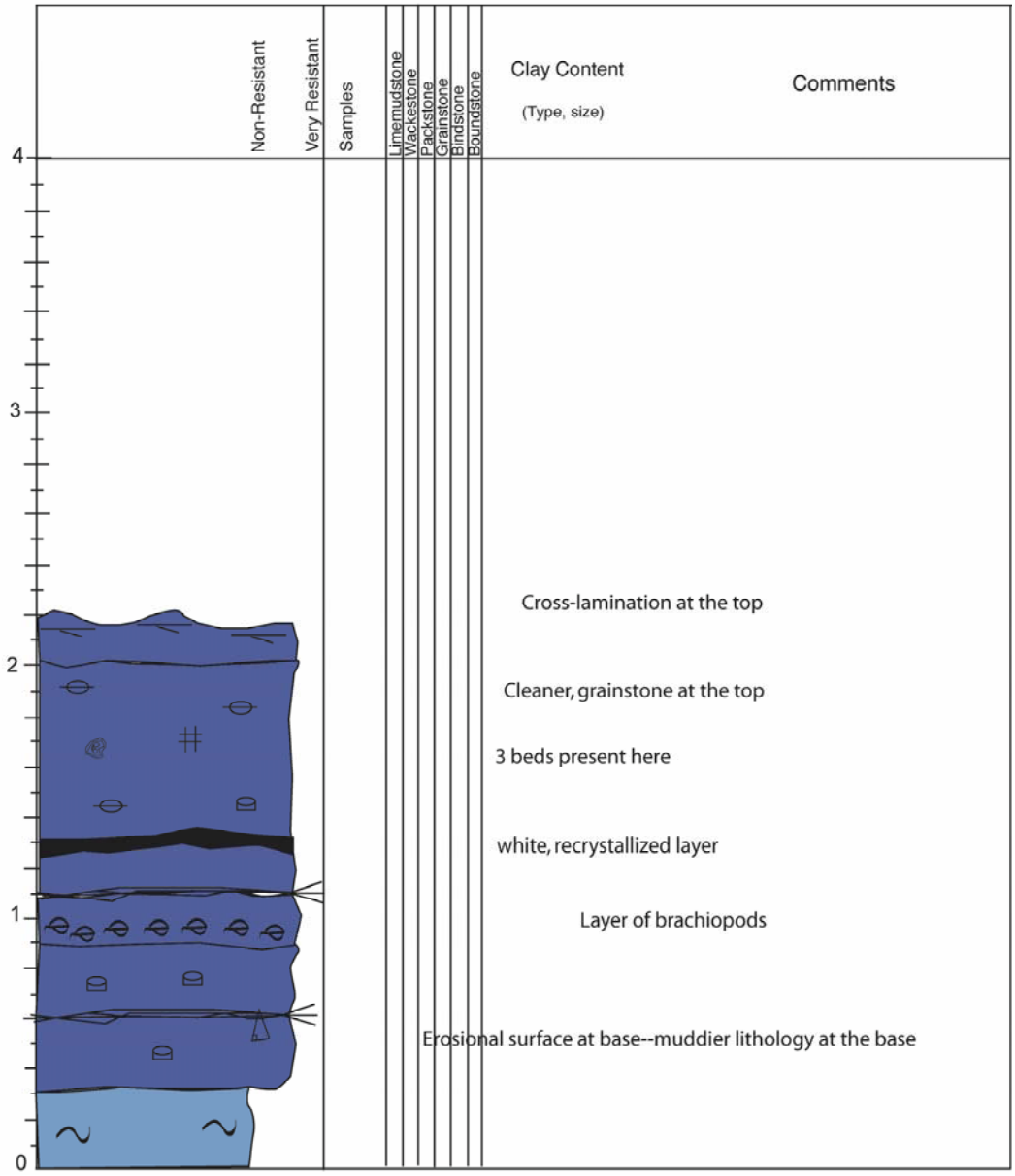

Section Name Johnson County Landfill--Methane Plant 1--N end Page 1 of 2

Location N39.03302
W94.8058

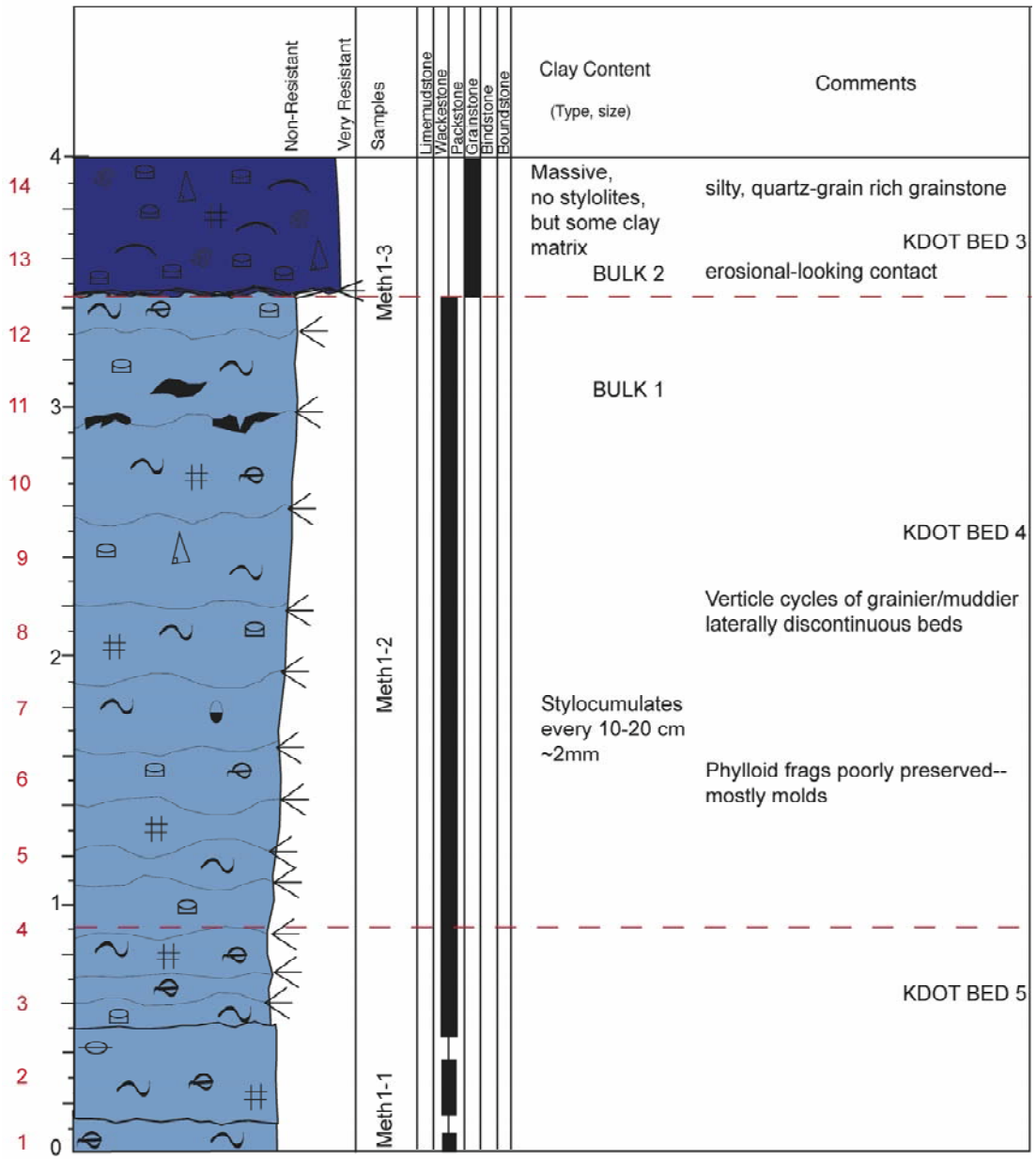

Section Name Johnson County Landfill--Methane Plant 1--N end Page 2 of 2

Location N39.03302
W94.8058

Date

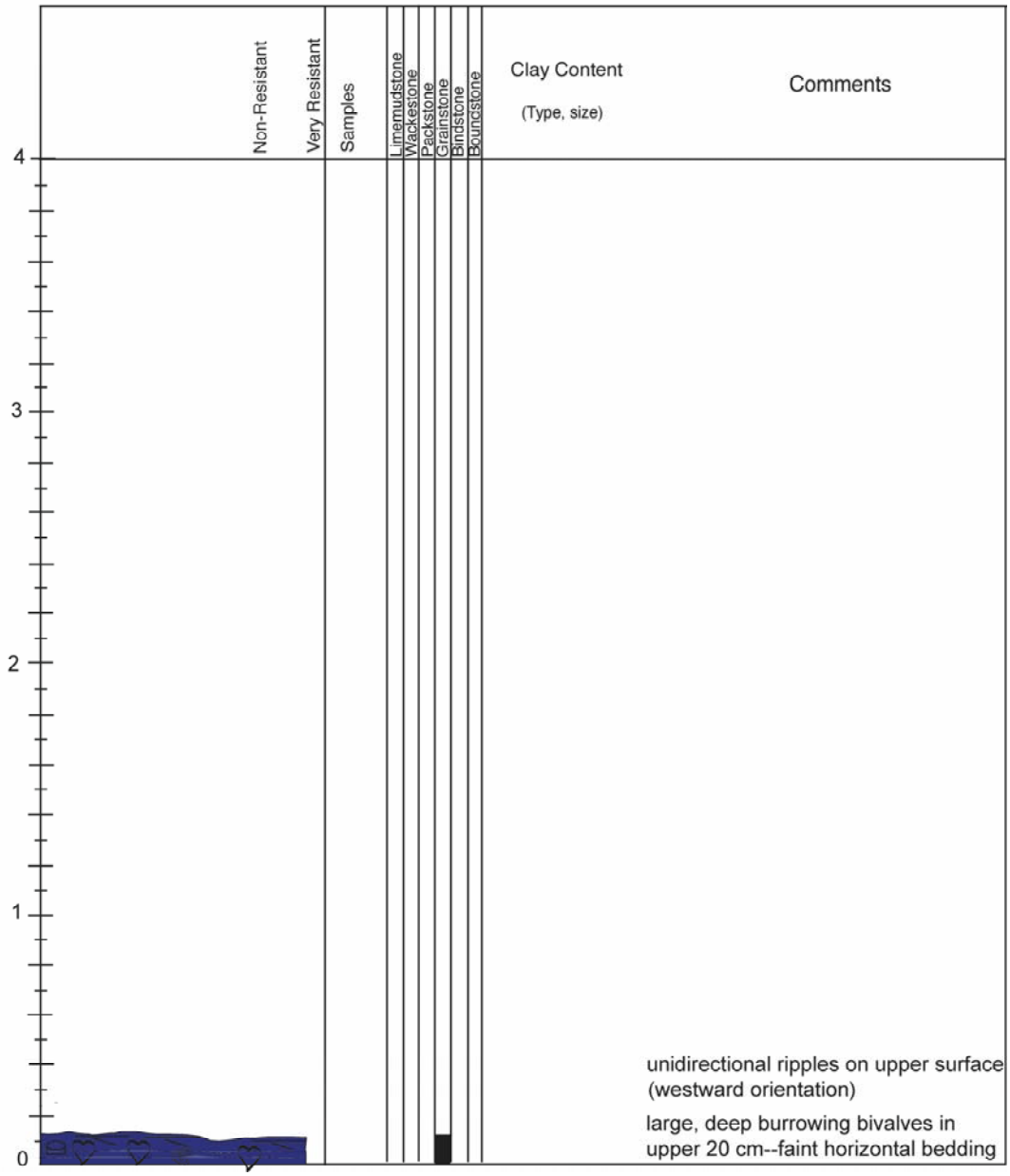

Section Name K-10-1 Page 1 of 2

Location just east of Kill Creek Road exit (1.5miles) Date

A--east end of outcrop: N 38.95829 W94.92512 B--west end of outcrop: N38.95883 W94.92735

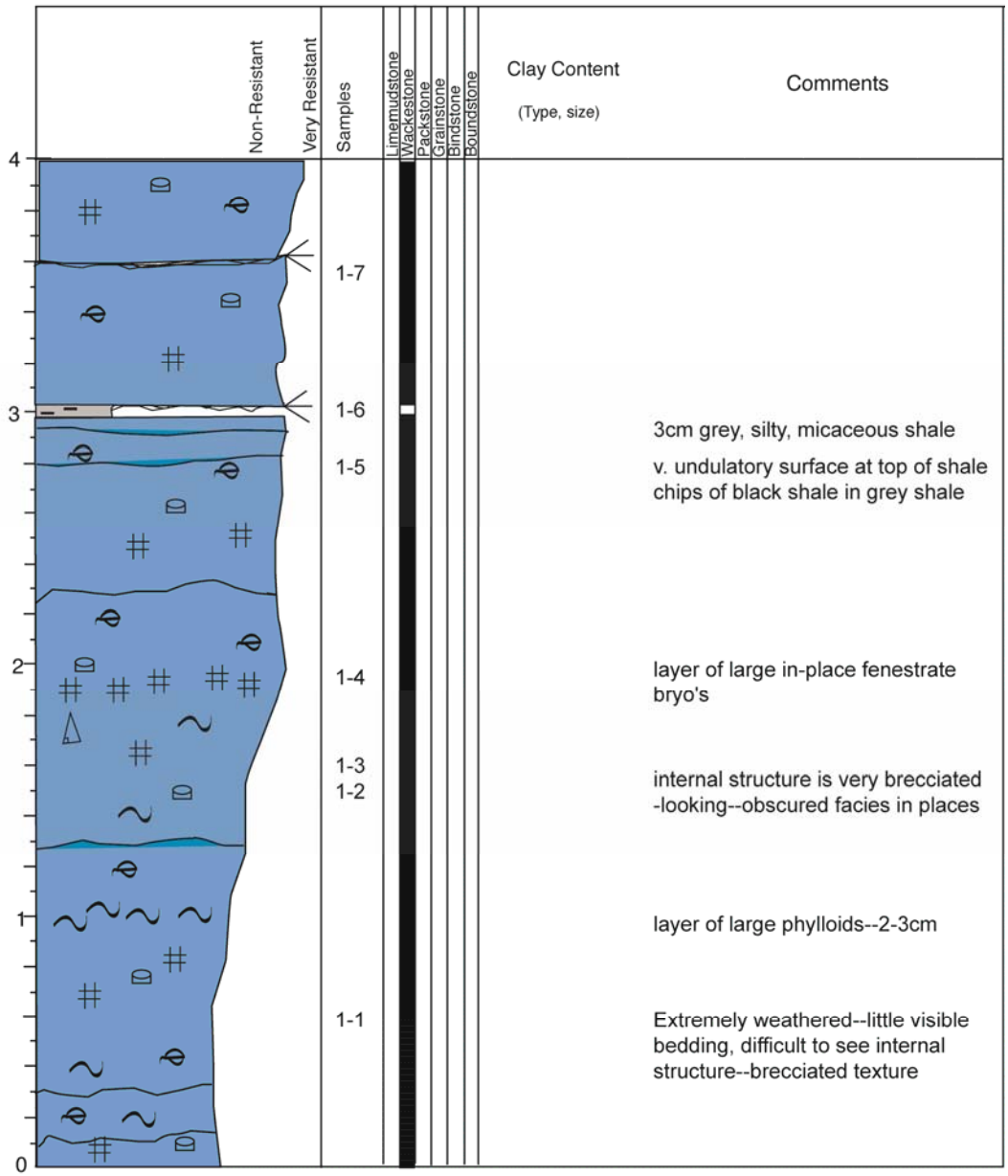

Section Name K-10-1 Page 2 of 2

Location just east of Kill Creek Road exit (1.5miles) Date

A--east end of outcrop: N 38.95829 W94.92512 B--west end of outcrop: N38.95883 W94.92735

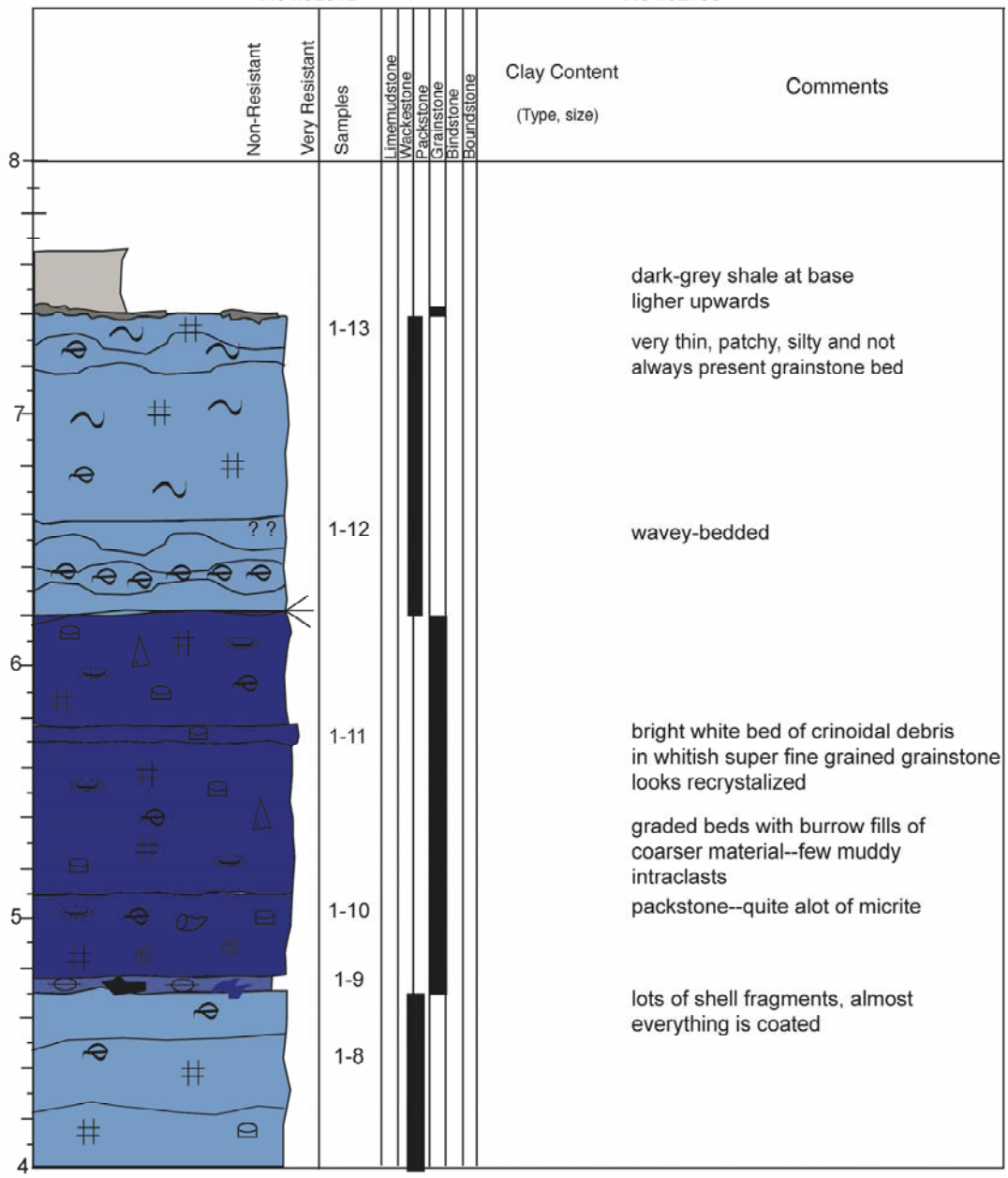

Abandoned quarry on the North side of the road
with a cool old stone building at the front

Section Name Arvidson LA10 Page 1 of 1

Location C, NW, SE, Sec.20, T18S, R22E Date

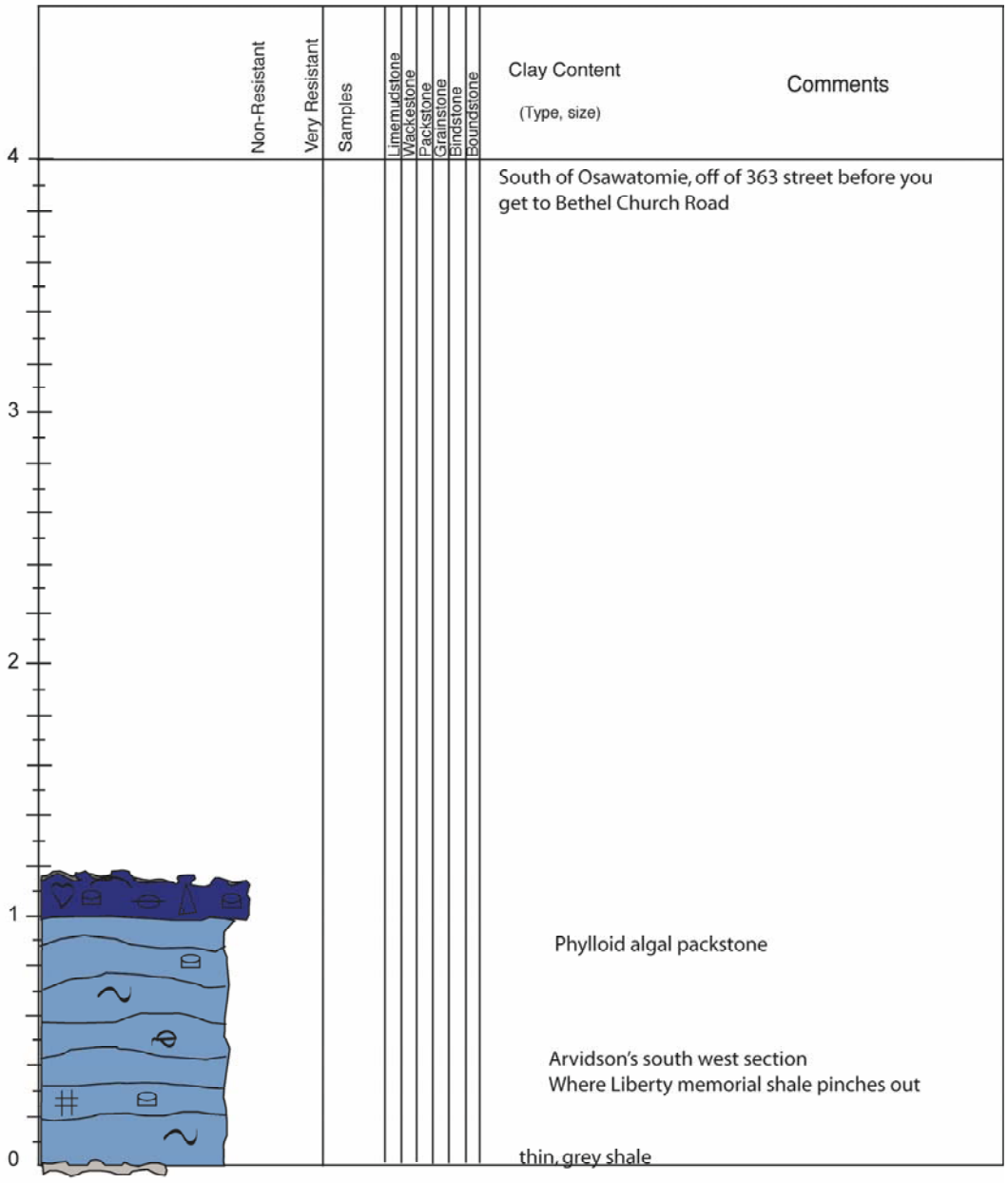

Section Name LO1 SE corner, sec.30, T16S, R25E Page____of_____
Location In Louisberg just west of main road through town--small car junk lot Date

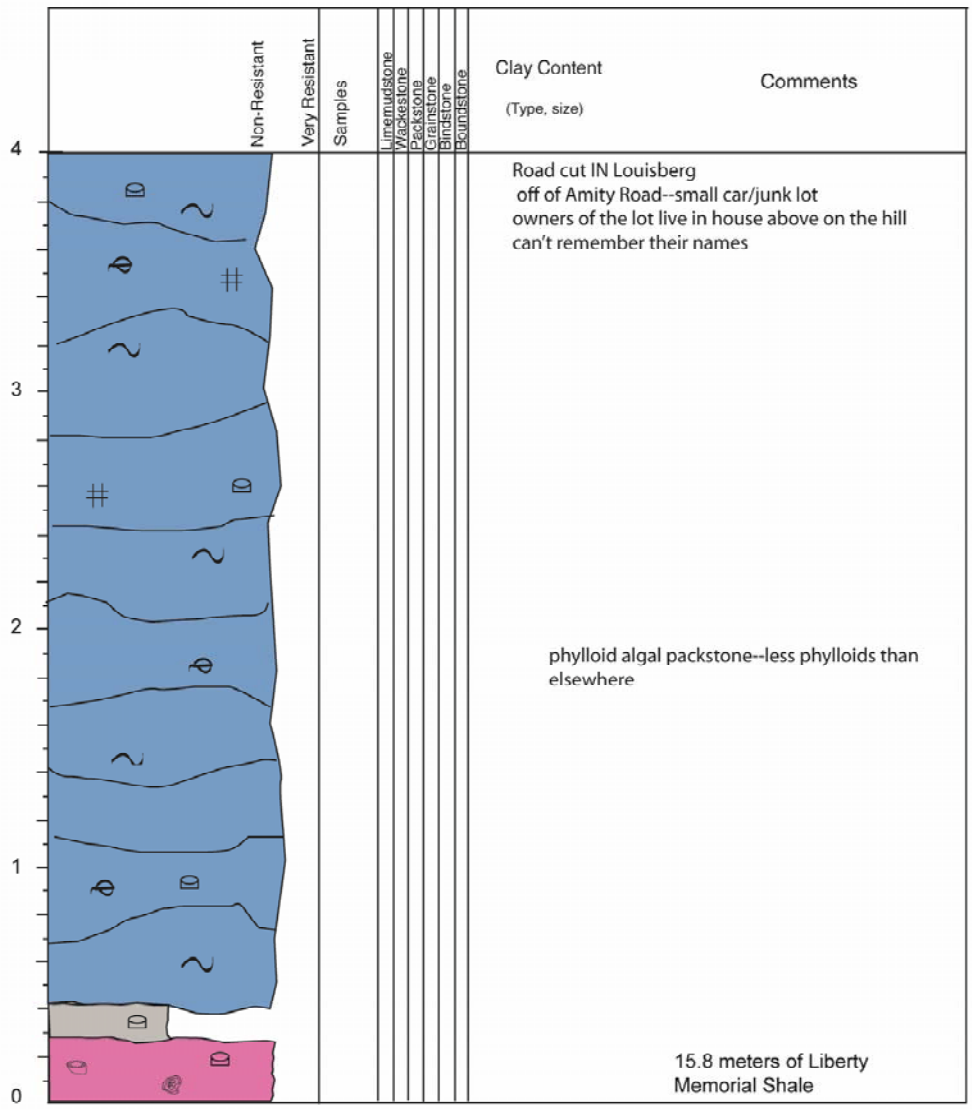

Section Name LO1_2 Page____of_____

Location In Louisberg just west of main road through town--small car junk lot

Date

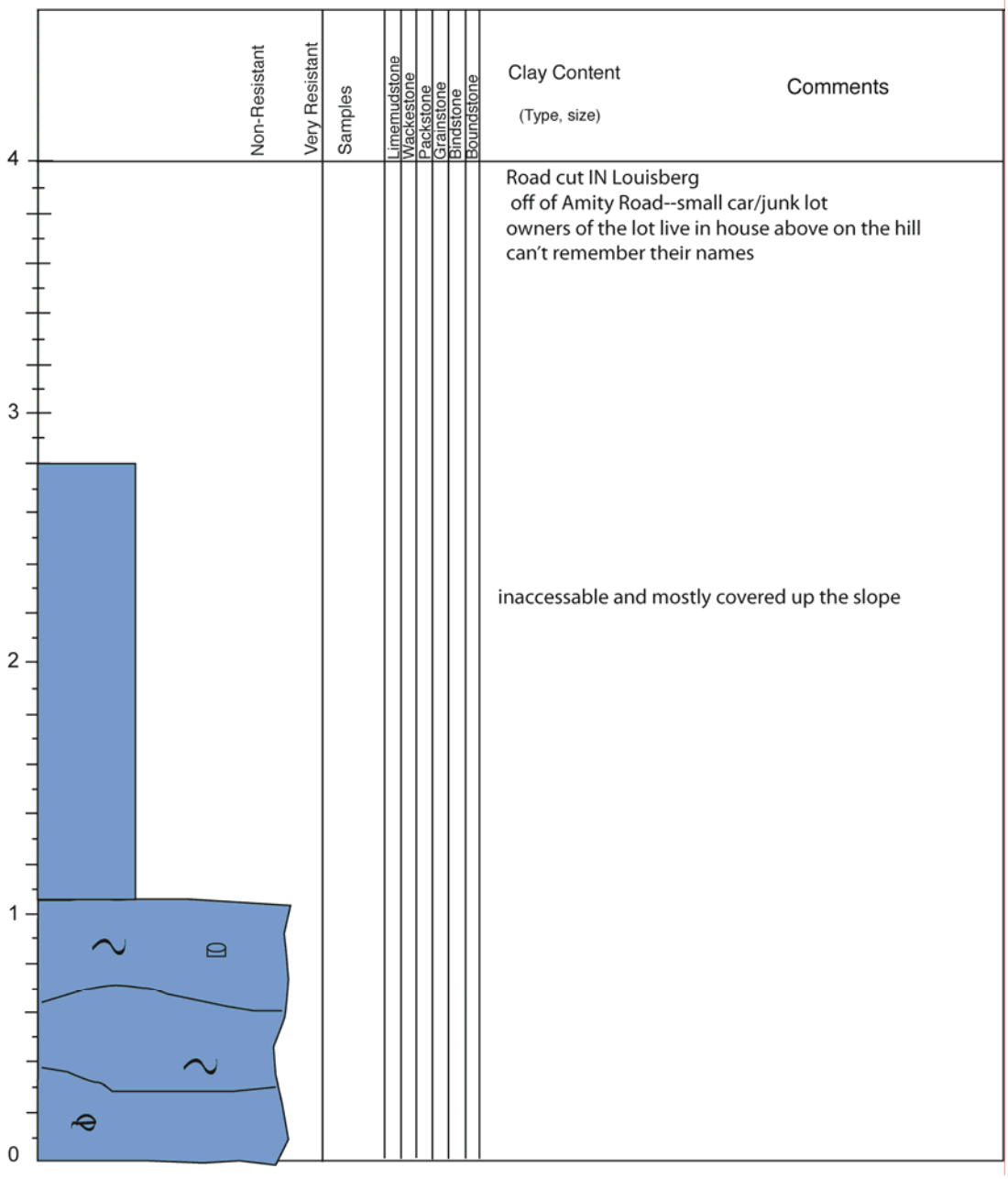

Section Name Loring Quarry--sub outcrop based on kdot thickness Page____of_____

Location N39.00824
W94.9223

Date

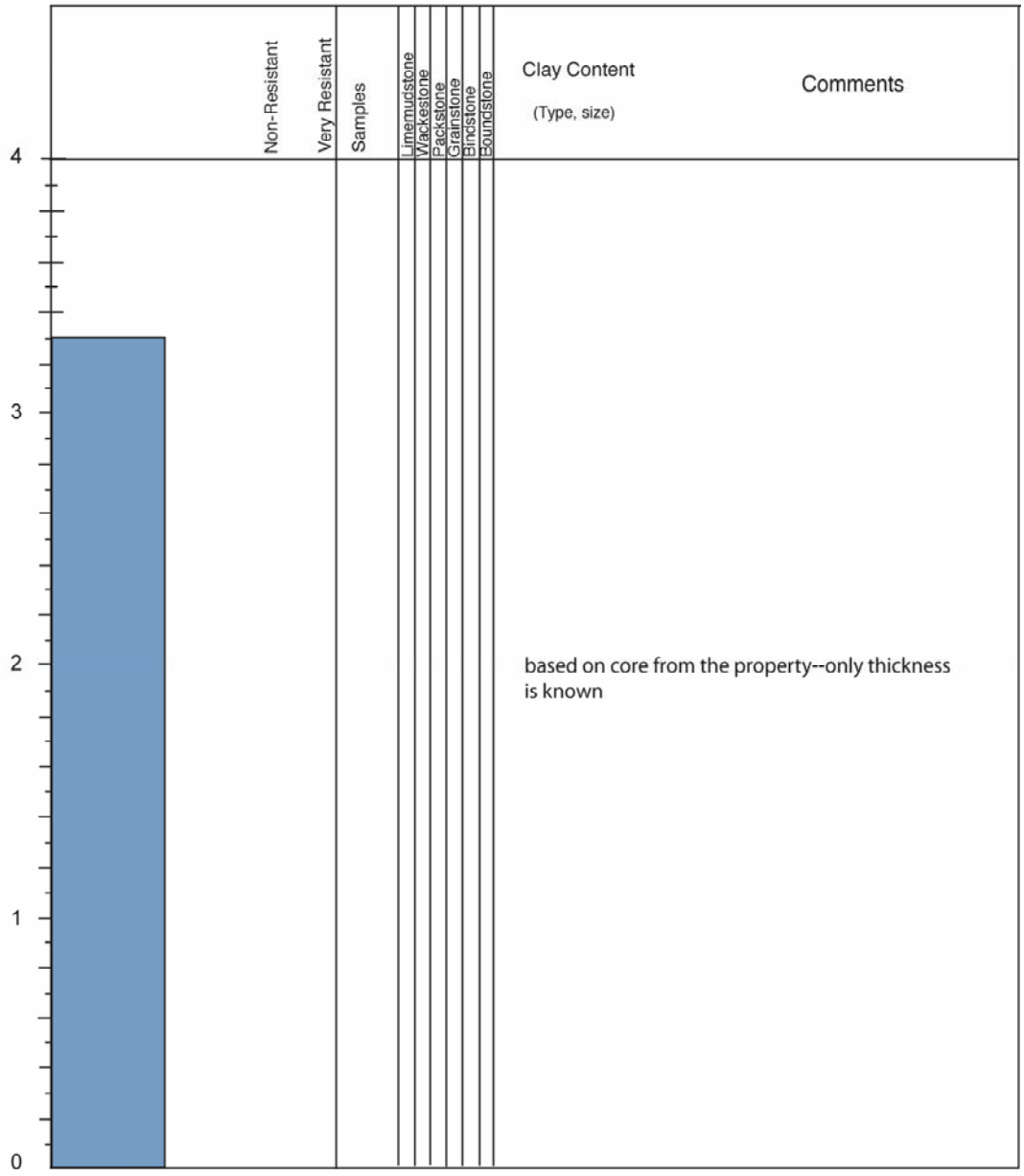

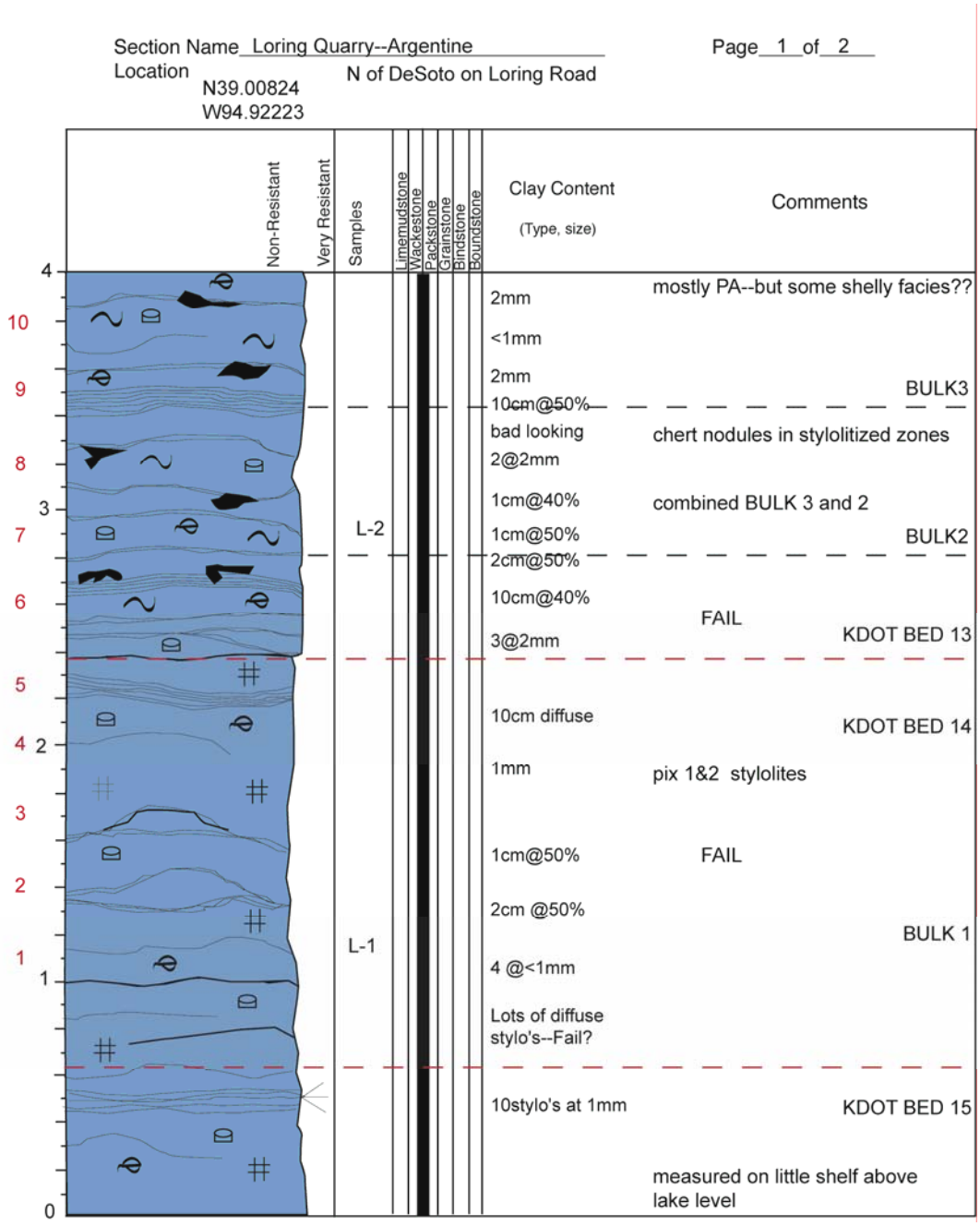
Section Name Loring Quarry--Argentine
Page 1 of 2
Location N of DeSoto on Loring Road
N39.00824
W94.92223
Non-Resistant
Very Resistant
Samples
Limemudstone
Wackestone
Packstone
Grainstone
Bindstone
Boundstone
Clay Content
(Type, size)
Comments
mostly PA--but some shelly facies??
2mm
<1mm
2mm
BULK3
10cm@50%
bad looking
chert nodules in stylolitized zones
2@2mm
1cm@40%
combined BULK 3 and 2
L-2
1cm@50%
BULK2
2cm@50%
10cm@40%
FAIL
3@2mm
KDOT BED 13
10cm diffuse
KDOT BED 14
1mm
pix 1&2 stylolites
1cm@50%
FAIL
2cm @50%
BULK 1
L-1
4 @<1mm
Lots of diffuse
stylo's--Fail?
10stylo's at 1mm
KDOT BED 15
measured on little shelf above
lake level

Section Name Loring Quarry--Argentine Page 2 of 2

Location N39.00824 W94.92223 N of DeSoto on Loring Road

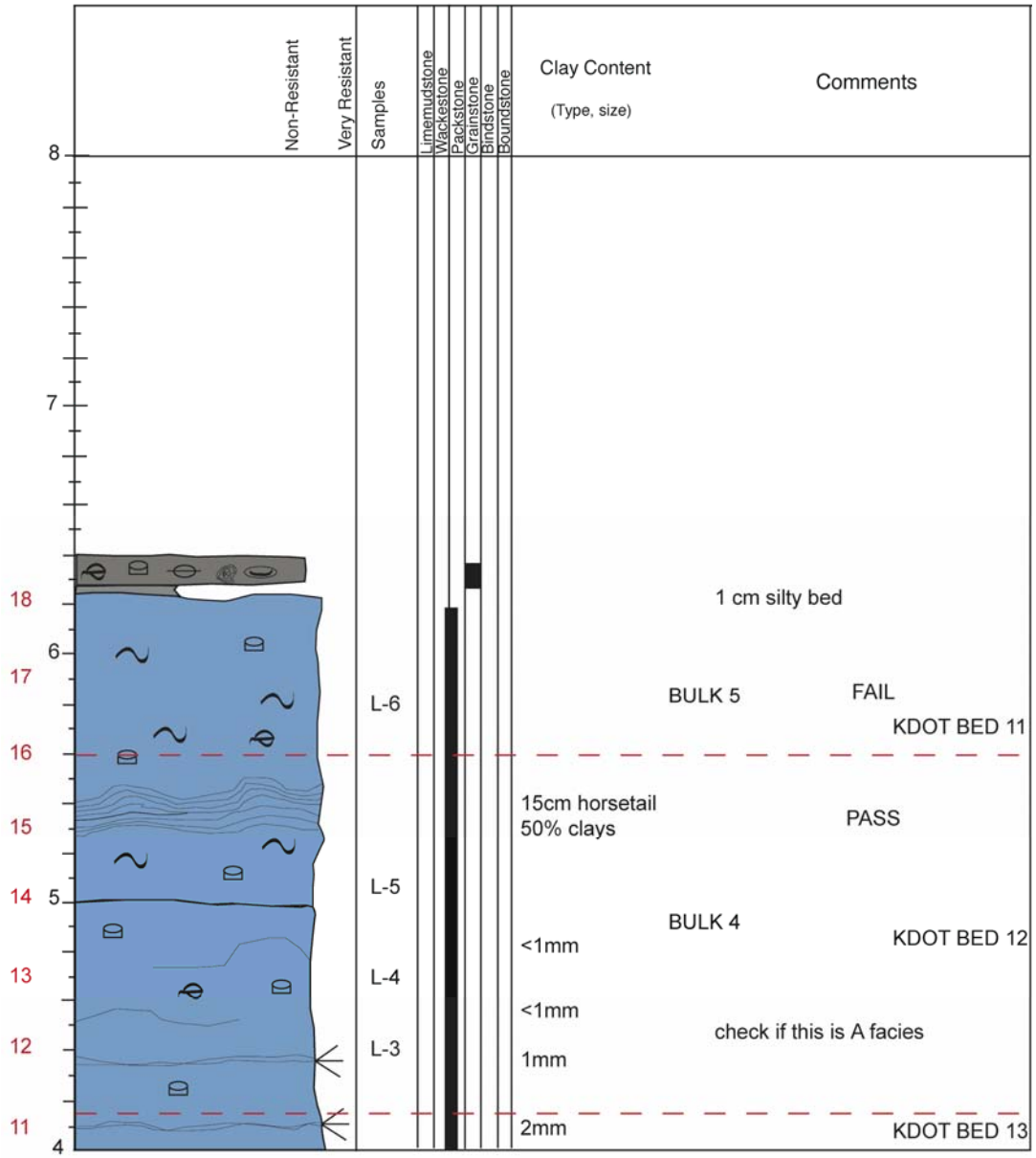

Section Name OBS--Outside SRC Bonner Springs quarry Page 1 of 3
Location N39.06857
W94.86062 Date

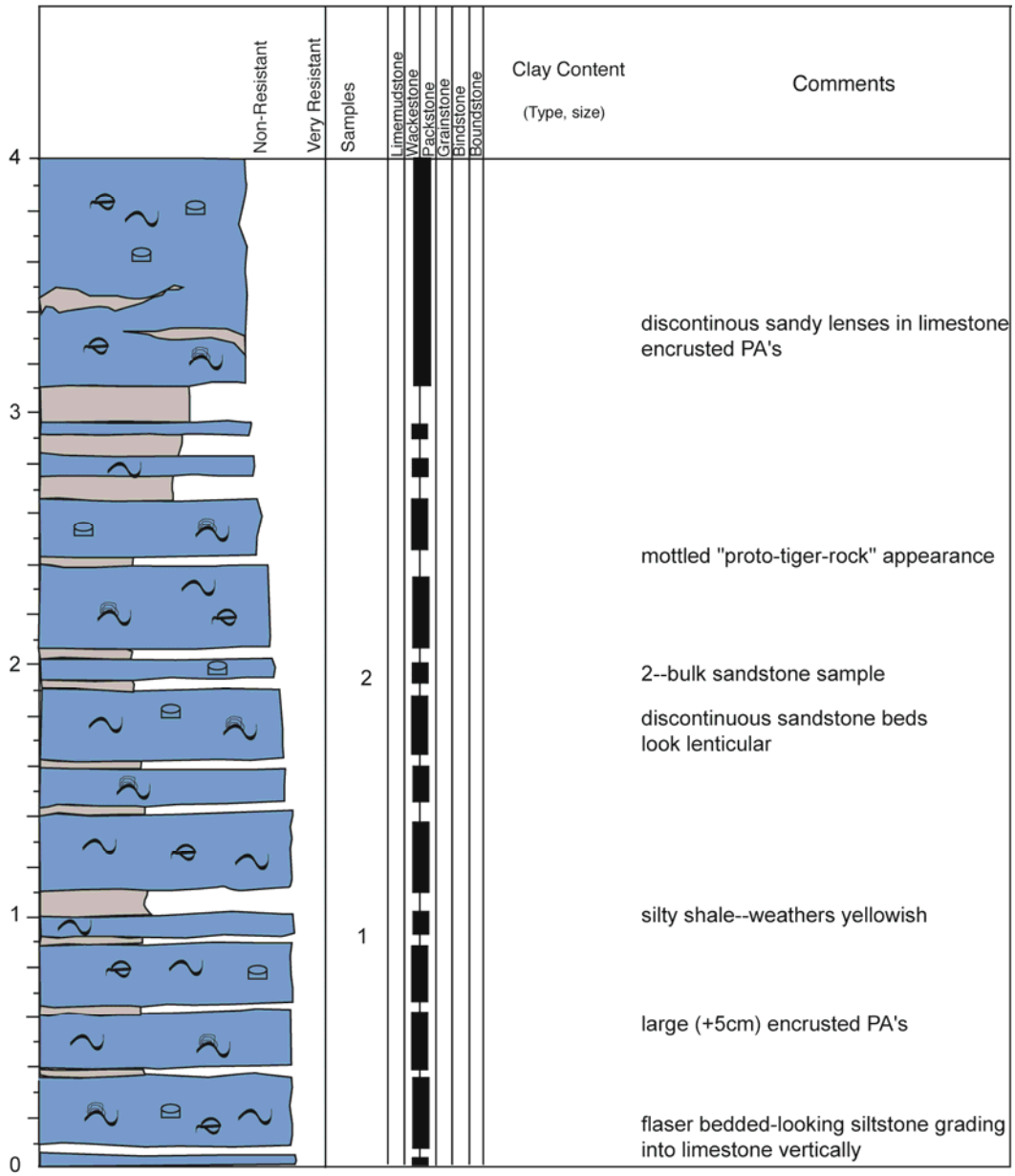

Section Name OBS--Outside SRC Bonner Springs quarry Page 2 of 3
Location N39.06857
W94.86062 Date

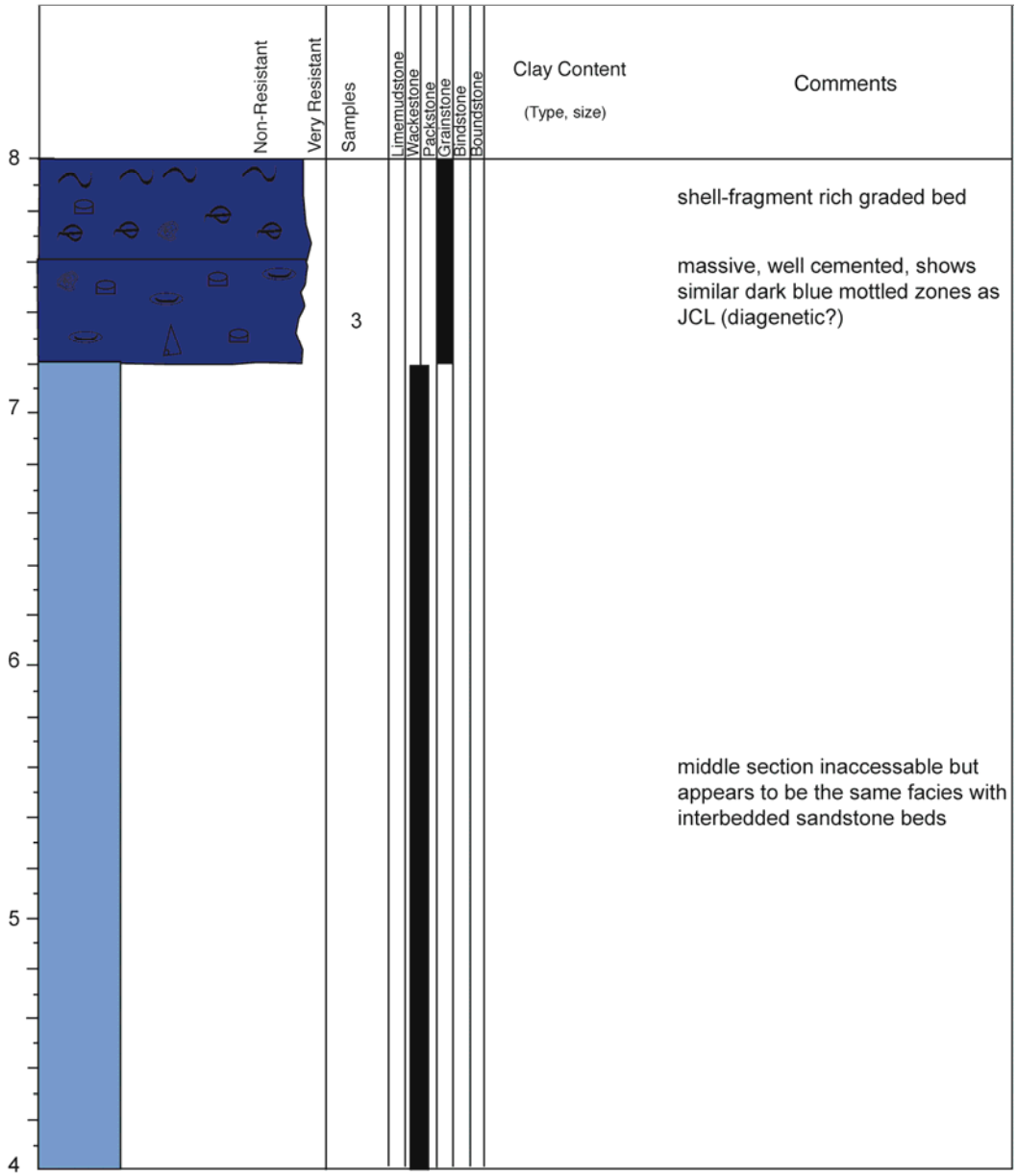

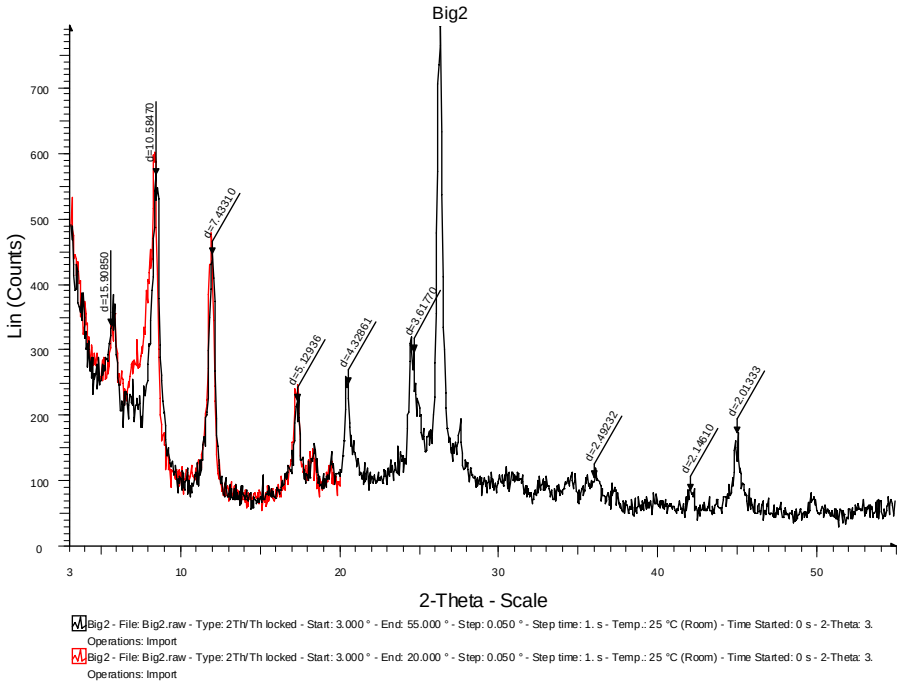
Big2
Lin (Counts)
2-Theta - Scale
d=10.59470
d=15.90850
d=7.43310
d=5.12936
d=4.32861
d=3.61770
d=2.49232
d=2.14610
d=2.01333
Big2 - File: Big2.raw - Type: 2Th/Th locked - Start: 3.000 ° - End: 55.000 ° - Step: 0.050 ° - Step time: 1. s - Temp.: 25 °C (Room) - Time Started: 0 s - 2-Theta: 3.
Operations: Import
Big2 - File: Big2.raw - Type: 2Th/Th locked - Start: 3.000 ° - End: 20.000 ° - Step: 0.050 ° - Step time: 1. s - Temp.: 25 °C (Room) - Time Started: 0 s - 2-Theta: 3.
Operations: Import

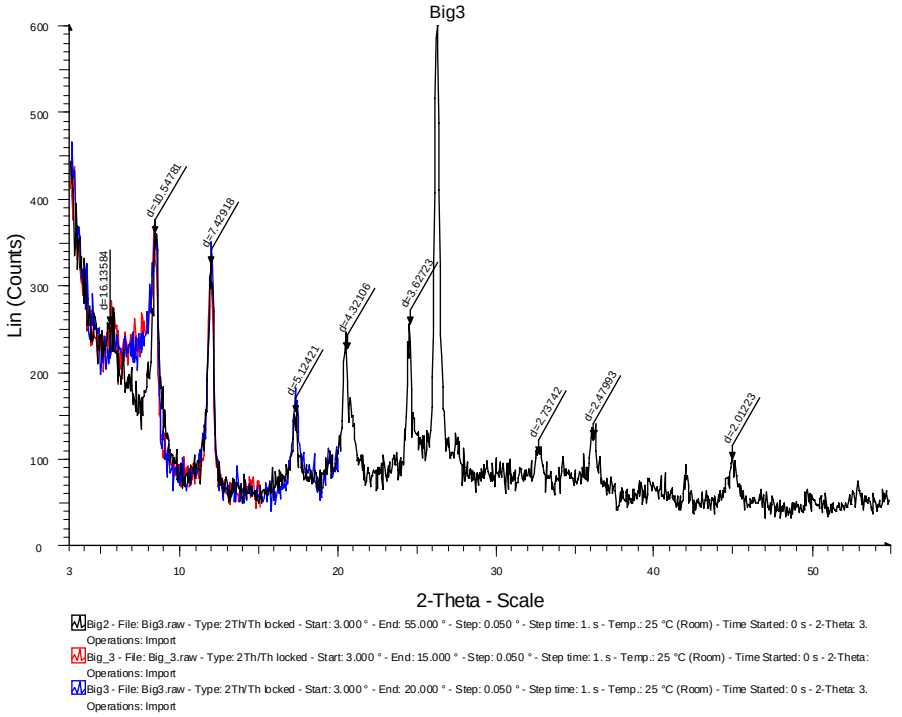
Big3
Lin (Counts)
2-Theta - Scale
d=16.13584
d=10.64778
d=7.42918
d=5.12421
d=4.32106
d=3.62723
d=2.73142
d=2.47893
d=2.01223
Big2 - File: Big3.raw - Type: 2Th/Th locked - Start: 3.000 ° - End: 55.000 ° - Step: 0.050 ° - Step time: 1. s - Temp.: 25 °C (Room) - Time Started: 0 s - 2-Theta: 3.
Operations: Import
Big_3 - File: Big_3.raw - Type: 2Th/Th locked - Start: 3.000 ° - End: 15.000 ° - Step: 0.050 ° - Step time: 1. s - Temp.: 25 °C (Room) - Time Started: 0 s - 2-Theta:
Operations: Import
Big3 - File: Big3.raw - Type: 2Th/Th locked - Start: 3.000 ° - End: 20.000 ° - Step: 0.050 ° - Step time: 1. s - Temp.: 25 °C (Room) - Time Started: 0 s - 2-Theta: 3.
Operations: Import

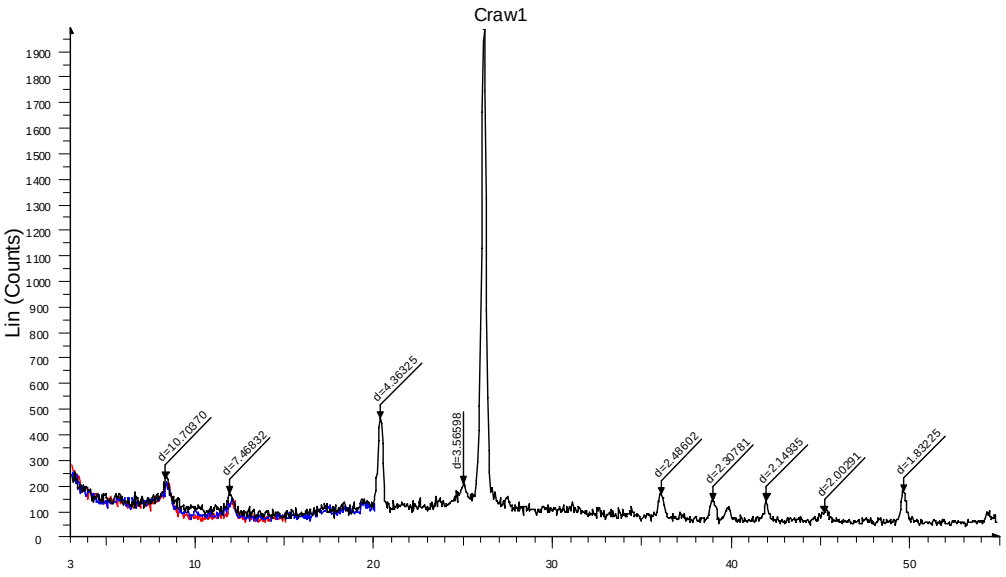

Craw1 - File: Craw1.raw - Type: 2Th/Th locked - Start: 3.000 ° - End: 55.000 ° - Step: 0.050 ° - Step time: 1. s - Temp.: 25 °C (Room) - Time Started: 0 s - 2-Theta: 3.000 ° - T
Operations: Import

Craw_1 - File: Craw_1.raw - Type: 2Th/Th locked - Start: 3.000 ° - End: 15.000 ° - Step: 0.050 ° - Step time: 1. s - Temp.: 25 °C (Room) - Time Started: 0 s - 2-Theta: 3.000 ° -
Operations: Import

HMCraw1 - File: Craw1.raw - Type: 2Th/Th locked - Start: 3.000 ° - End: 20.000 ° - Step: 0.050 ° - Step time: 1. s - Temp.: 25 °C (Room) - Time Started: 0 s - 2-Theta: 3.000 °
Operations: Import

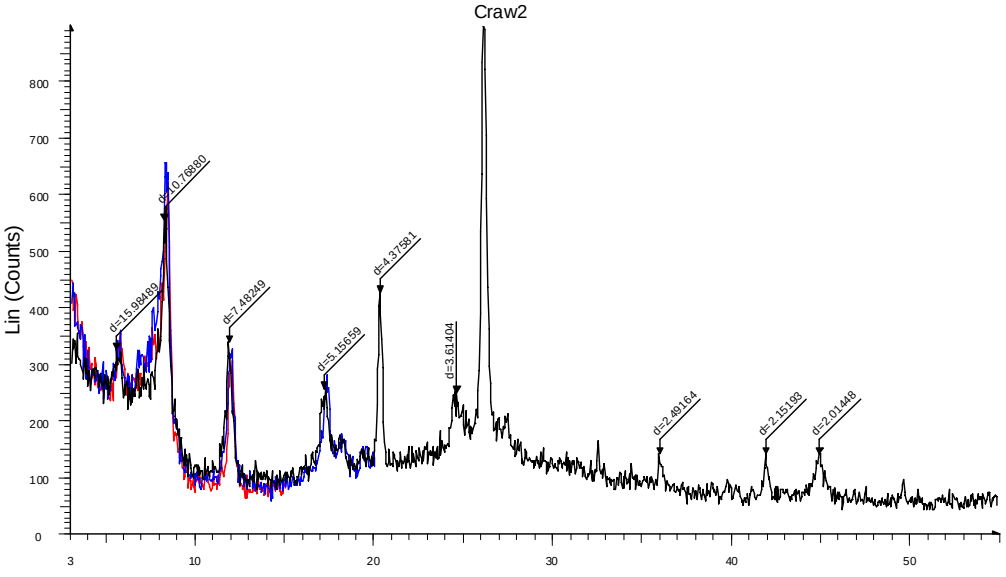

Craw2 - File: Craw2.raw - Type: 2Th/Th locked - Start: 3.000 ° - End: 55.000 ° - Step: 0.050 ° - Step time: 1. s - Temp.: 25 °C (Room) - Time Started: 0 s - 2-Theta: 3.000 ° - T
Operations: Import

Craw_2 - File: Craw_2.raw - Type: 2Th/Th locked - Start: 3.000 ° - End: 15.000 ° - Step: 0.050 ° - Step time: 1. s - Temp.: 25 °C (Room) - Time Started: 0 s - 2-Theta: 3.000 ° -
Operations: Import

Craw2 - File: Craw2.raw - Type: 2Th/Th locked - Start: 3.000 ° - End: 20.000 ° - Step: 0.050 ° - Step time: 1. s - Temp.: 25 °C (Room) - Time Started: 0 s - 2-Theta: 3.000 ° - T
Operations: Import

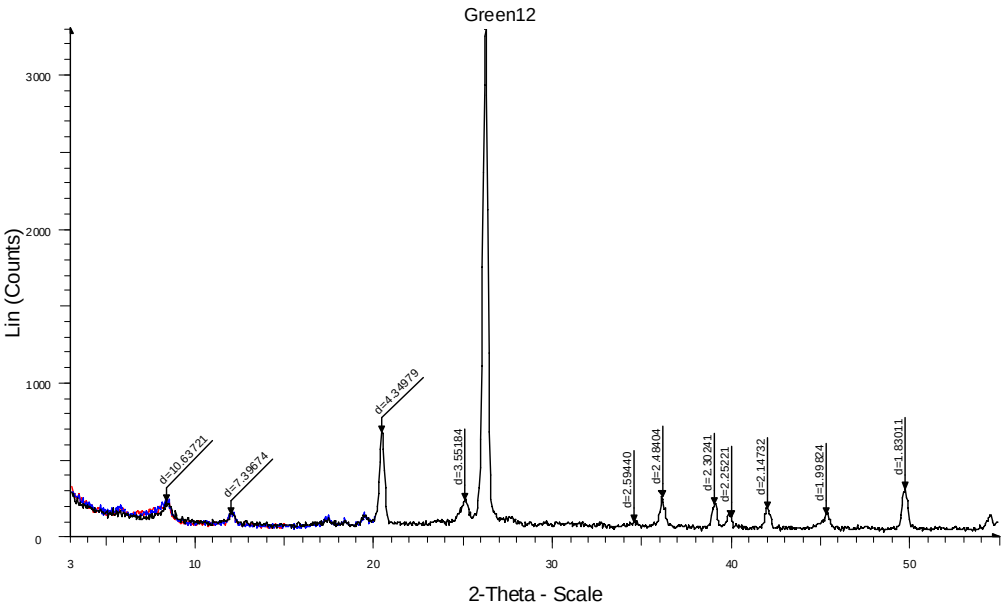

Green12 - File: Green12.raw - Type: 2Th/Th locked - Start: 3.000 ° - End: 55.000 ° - Step: 0.050 ° - Step time: 1. s - Temp.: 25 °C (Room) - Time Started: 0 s - 2-Theta: 3.000
Operations: Import
Green_12 - File: Green_12.raw - Type: 2Th/Th locked - Start: 3.000 ° - End: 15.000 ° - Step: 0.050 ° - Step time: 1. s - Temp.: 25 °C (Room) - Time Started: 0 s - 2-Theta: 3.00
Operations: Import
Green12 - File: Green12.raw - Type: 2Th/Th locked - Start: 3.000 ° - End: 20.000 ° - Step: 0.050 ° - Step time: 1. s - Temp.: 25 °C (Room) - Time Started: 0 s - 2-Theta: 3.000
Operations: Import

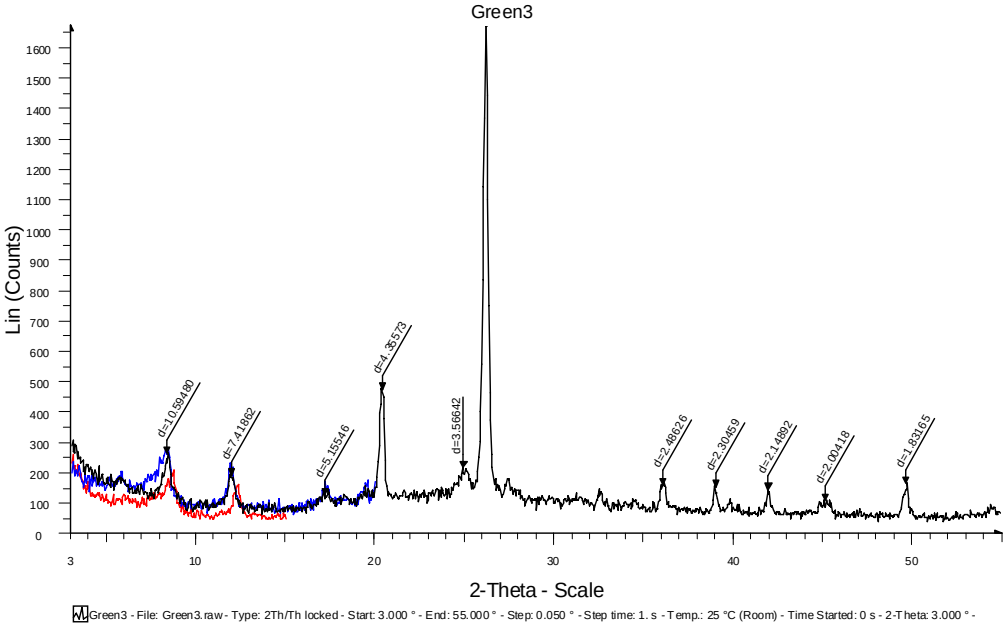

Green3 - File: Green3.raw - Type: 2Th/Th locked - Start: 3.000 ° - End: 55.000 ° - Step: 0.050 ° - Step time: 1. s - Temp.: 25 °C (Room) - Time Started: 0 s - 2-Theta: 3.000 ° -
Operations: Import
Green_3 - File: Green_3.raw - Type: 2Th/Th locked - Start: 3.000 ° - End: 15.000 ° - Step: 0.050 ° - Step time: 1. s - Temp.: 25 °C (Room) - Time Started: 0 s - 2-Theta: 3.000
Operations: Import
Green3 - File: Green3.raw - Type: 2Th/Th locked - Start: 3.000 ° - End: 20.000 ° - Step: 0.050 ° - Step time: 1. s - Temp.: 25 °C (Room) - Time Started: 0 s - 2-Theta: 3.000 ° -
Operations: Import

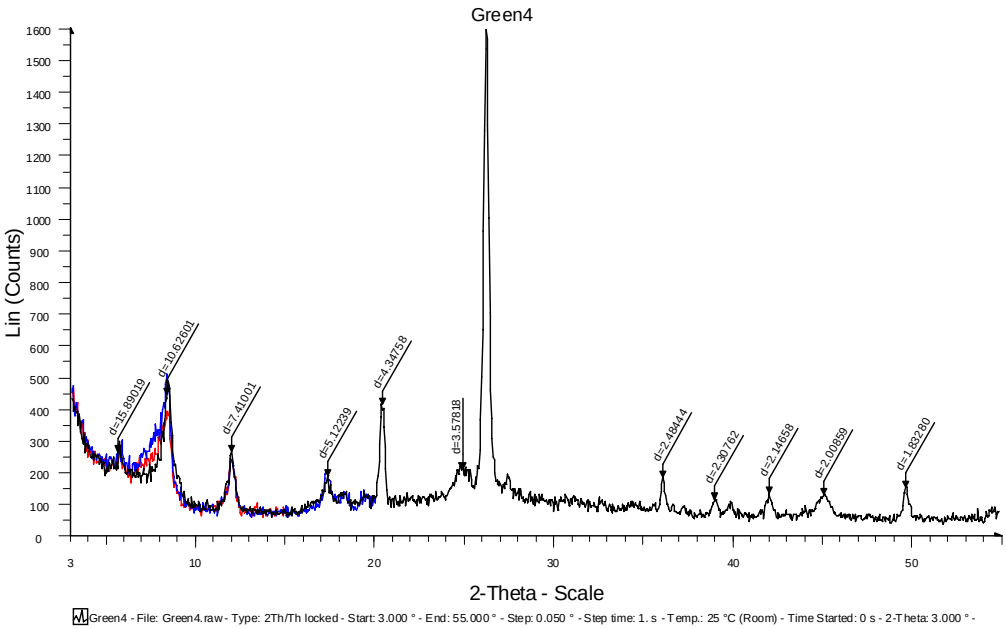
Green4
Lin (Counts)
2-Theta - Scale
d=15.89019
d=10.62601
d=7.41001
d=5.12239
d=4.34758
d=3.57818
d=2.48444
d=2.30762
d=2.14658
d=2.00859
d=1.89280
Green4 - File: Green4.raw - Type: 2Th/Th locked - Start: 3.000 ° - End: 55.000 ° - Step: 0.050 ° - Step time: 1. s - Temp.: 25 °C (Room) - Time Started: 0 s - 2-Theta: 3.000 ° - Operations: Import
Green_4 - File: Green_4.raw - Type: 2Th/Th locked - Start: 3.000 ° - End: 15.000 ° - Step: 0.050 ° - Step time: 1. s - Temp.: 25 °C (Room) - Time Started: 0 s - 2-Theta: 3.000 Operations: Import
Green4 - File: Green4.raw - Type: 2Th/Th locked - Start: 3.000 ° - End: 20.000 ° - Step: 0.050 ° - Step time: 1. s - Temp.: 25 °C (Room) - Time Started: 0 s - 2-Theta: 3.000 ° - Operations: Import

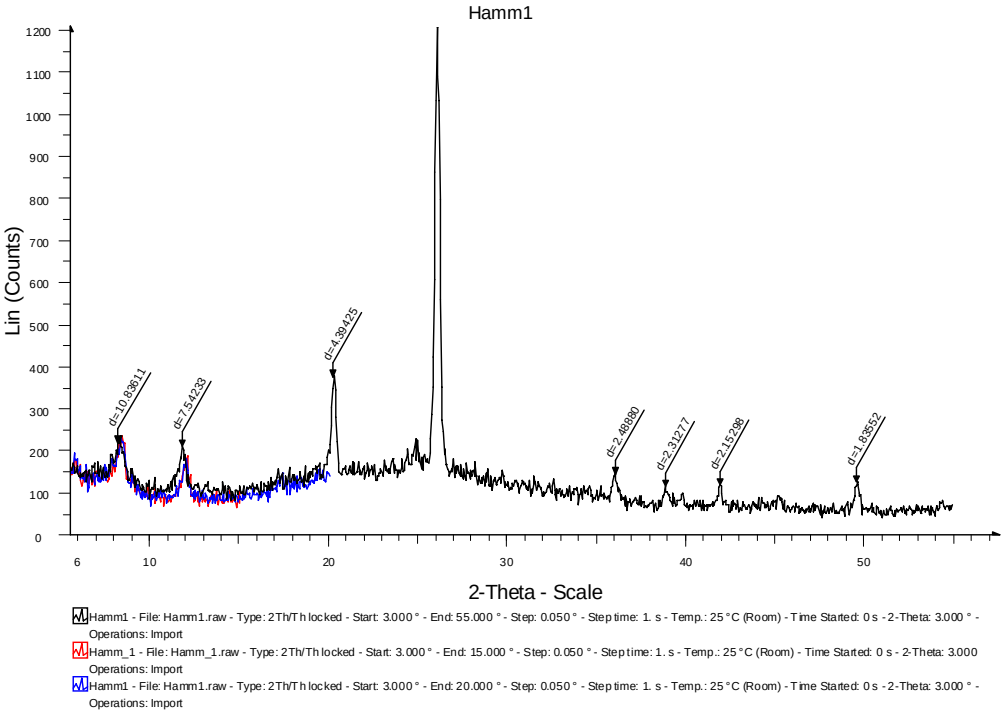
Hamm1
Lin (Counts)
2-Theta - Scale
d=10.83611
d=7.54233
d=4.39425
d=2.48880
d=2.31277
d=2.15298
d=1.85552
Hamm1 - File: Hamm1.raw - Type: 2Th/Th locked - Start: 3.000 ° - End: 55.000 ° - Step: 0.050 ° - Step time: 1. s - Temp.: 25 °C (Room) - Time Started: 0 s - 2-Theta: 3.000 ° - Operations: Import
Hamm_1 - File: Hamm_1.raw - Type: 2Th/Th locked - Start: 3.000 ° - End: 15.000 ° - Step: 0.050 ° - Step time: 1. s - Temp.: 25 °C (Room) - Time Started: 0 s - 2-Theta: 3.000 Operations: Import
Hamm1 - File: Hamm1.raw - Type: 2Th/Th locked - Start: 3.000 ° - End: 20.000 ° - Step: 0.050 ° - Step time: 1. s - Temp.: 25 °C (Room) - Time Started: 0 s - 2-Theta: 3.000 ° - Operations: Import

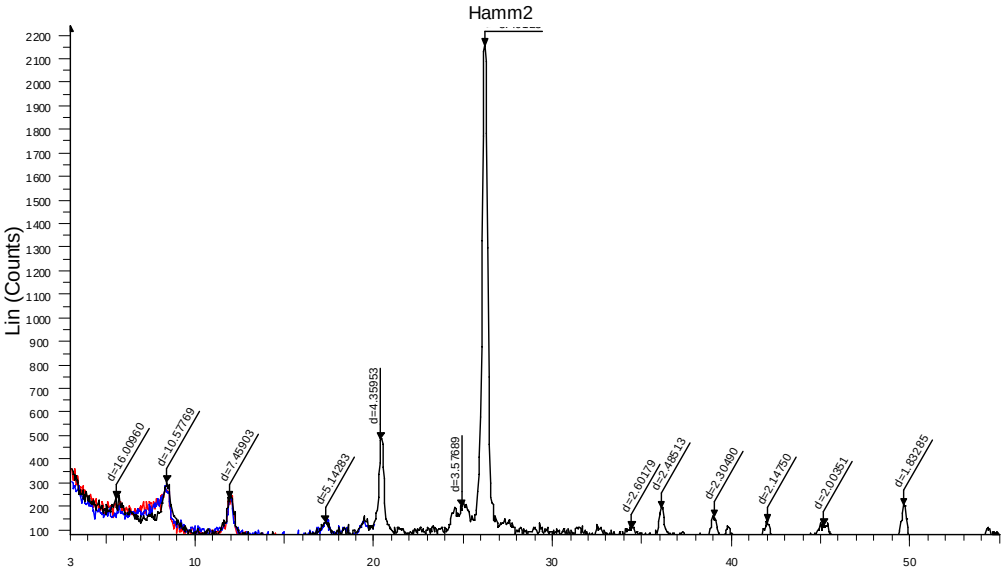

Hamm2 - File: Hamm2.raw - Type: 2Th/Th locked - Start: 3.000 ° - End: 55.000 ° - Step: 0.050 ° - Step time: 1. s - Temp.: 25 °C (Room) - Time Started: 0 s - 2-Theta: 3.000 ° - Operations: Import

Hamm_2 - File: Hamm_2.raw - Type: 2Th/Th locked - Start: 3.000 ° - End: 15.000 ° - Step: 0.050 ° - Step time: 1. s - Temp.: 25 °C (Room) - Time Started: 0 s - 2-Theta: 3.000 Operations: Import

Hamm2 - File: Hamm2.raw - Type: 2Th/Th locked - Start: 3.000 ° - End: 20.000 ° - Step: 0.050 ° - Step time: 1. s - Temp.: 25 °C (Room) - Time Started: 0 s - 2-Theta: 3.000 ° - Operations: Import

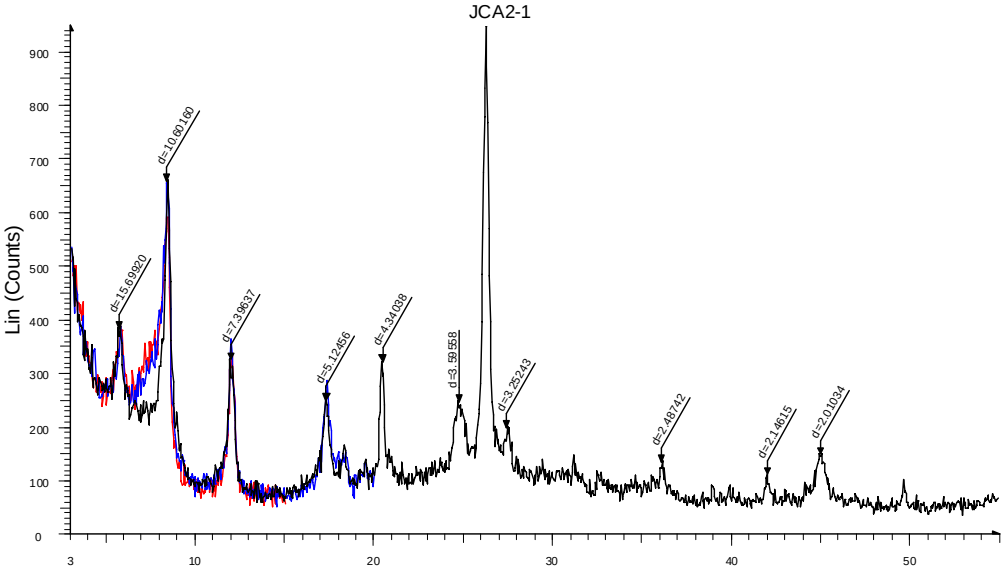

JCA2-1 - File: JCA2-1.raw - Type: 2Th/Th locked - Start: 3.000 ° - End: 55.000 ° - Step: 0.050 ° - Step time: 1. s - Temp.: 25 °C (Room) - Time Started: 0 s - 2-Theta: 3.000 ° - Operations: Import

JCA2_1 - File: JCA2_1.raw - Type: 2Th/Th locked - Start: 3.000 ° - End: 15.000 ° - Step: 0.050 ° - Step time: 1. s - Temp.: 25 °C (Room) - Time Started: 0 s - 2-Theta: 3.000 ° Operations: Import

JCA2-1 - File: JCA2_1.raw - Type: 2Th/Th locked - Start: 3.000 ° - End: 20.000 ° - Step: 0.050 ° - Step time: 1. s - Temp.: 25 °C (Room) - Time Started: 0 s - 2-Theta: 3.000 ° - Operations: Import

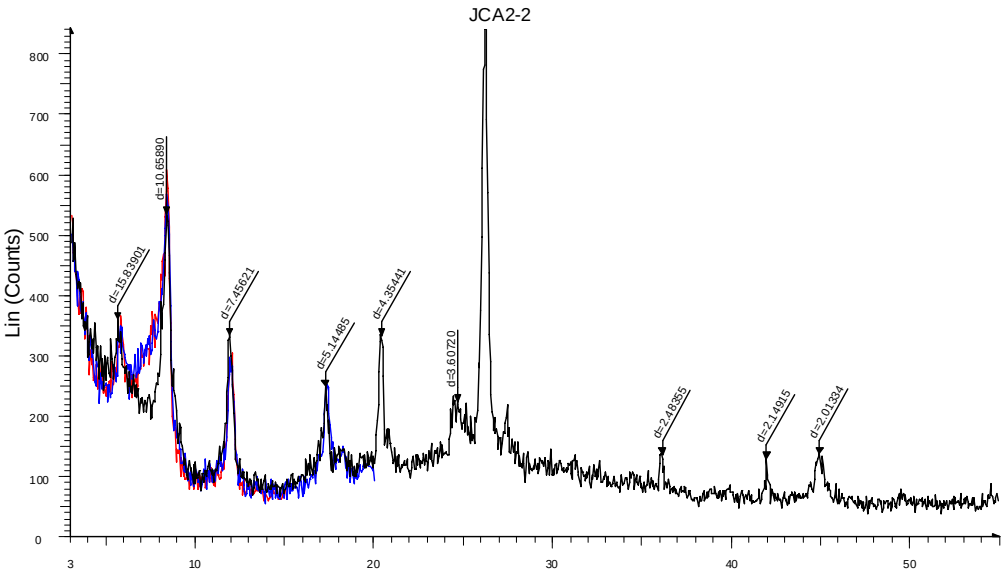
JCA2-2
Lin (Counts)
2-Theta - Scale
d=15.83901
d=10.65890
d=7.45621
d=5.14485
d=4.35441
d=3.60720
d=2.48355
d=2.14915
d=2.01334
JCA2-2 - File: JCA2-2.raw - Type: 2Th/Th locked - Start: 3.000 ° - End: 55.000 ° - Step: 0.050 ° - Step time: 1. s - Temp.: 25 °C (Room) - Time Started: 0 s - 2-Theta: 3.000 ° - Operations: Import
JCA 2_2 - File: JCA_2_2.raw - Type: 2Th/Th locked - Start: 3.000 ° - End: 15.000 ° - Step: 0.050 ° - Step time: 1. s - Temp.: 25 °C (Room) - Time Started: 0 s - 2-Theta: 3.000 Operations: Import
JCA2_2 - File: JCA2_2.raw - Type: 2Th/Th locked - Start: 3.000 ° - End: 20.000 ° - Step: 0.050 ° - Step time: 1. s - Temp.: 25 °C (Room) - Time Started: 0 s - 2-Theta: 3.000 ° Operations: Import

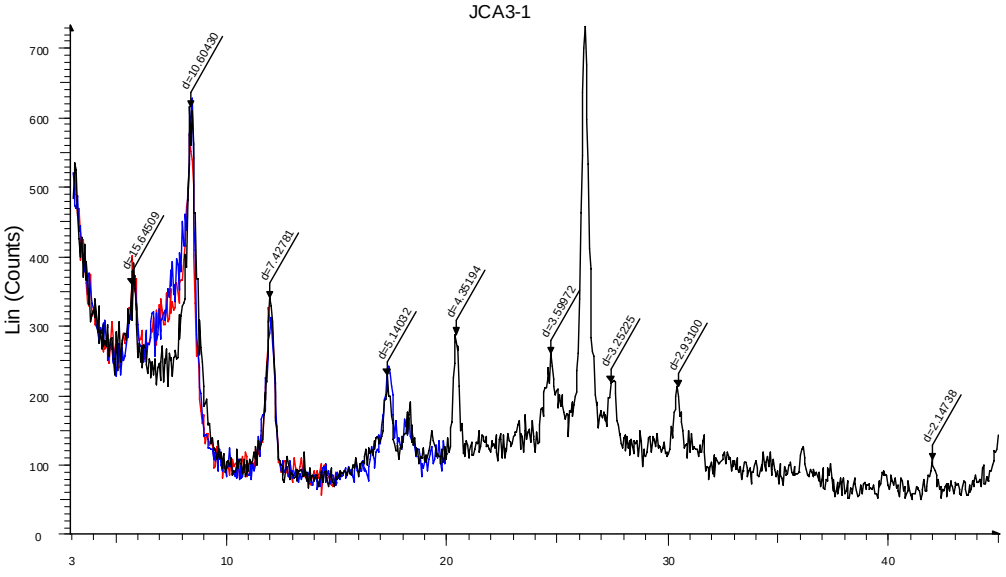
JCA3-1
Lin (Counts)
2-Theta - Scale
d=15.64509
d=10.60430
d=7.42781
d=5.14032
d=4.35194
d=3.59872
d=3.25225
d=2.93100
d=2.14738
JCA3-1 - File: JCA3_1.raw - Type: 2Th/Th locked - Start: 3.000 ° - End: 55.000 ° - Step: 0.050 ° - Step time: 1. s - Temp.: 25 °C (Room) - Time Started: 0 s - 2-Theta: 3.000 ° - Operations: Import
JCA_4_1 - File: JCA_3_1.raw - Type: 2Th/Th locked - Start: 3.000 ° - End: 15.000 ° - Step: 0.050 ° - Step time: 1. s - Temp.: 25 °C (Room) - Time Started: 0 s - 2-Theta: 3.000 Operations: Import
JCA3_1 - File: JCA3_1.raw - Type: 2Th/Th locked - Start: 3.000 ° - End: 20.000 ° - Step: 0.050 ° - Step time: 1. s - Temp.: 25 °C (Room) - Time Started: 0 s - 2-Theta: 3.000 ° Operations: Import

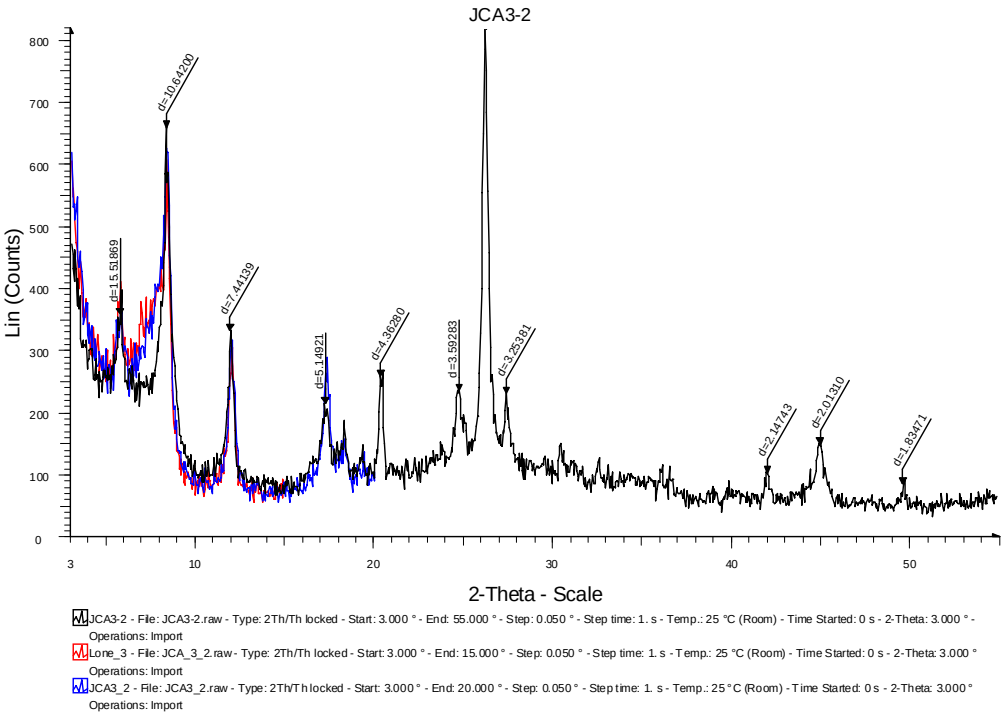
JCA3-2
Lin (Counts)
2-Theta - Scale
d=10.64209
d=15.51869
d=7.44139
d=5.14921
d=4.36280
d=3.59283
d=3.25381
d=2.14743
d=2.01310
d=1.83471
JCA3-2 - File: JCA3-2.raw - Type: 2Th/Th locked - Start: 3.000 ° - End: 55.000 ° - Step: 0.050 ° - Step time: 1. s - Temp.: 25 °C (Room) - Time Started: 0 s - 2-Theta: 3.000 ° - Operations: Import
Lone_3 - File: JCA_3_2.raw - Type: 2Th/Th locked - Start: 3.000 ° - End: 15.000 ° - Step: 0.050 ° - Step time: 1. s - Temp.: 25 °C (Room) - Time Started: 0 s - 2-Theta: 3.000 ° - Operations: Import
JCA3_2 - File: JCA3_2.raw - Type: 2Th/Th locked - Start: 3.000 ° - End: 20.000 ° - Step: 0.050 ° - Step time: 1. s - Temp.: 25 °C (Room) - Time Started: 0 s - 2-Theta: 3.000 ° - Operations: Import

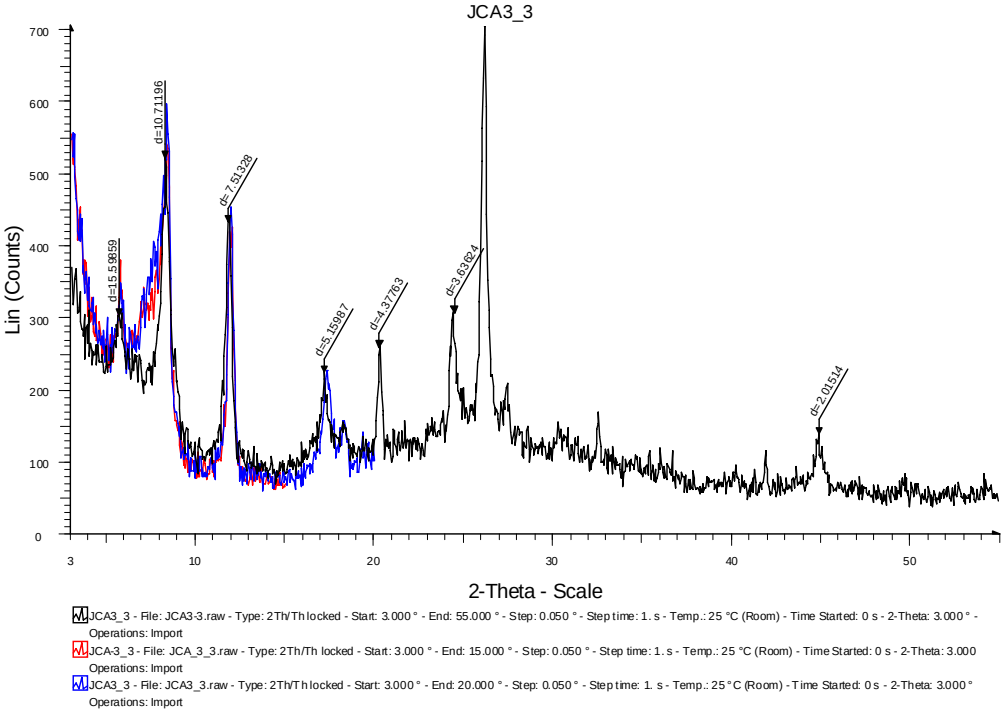
JCA3_3
Lin (Counts)
2-Theta - Scale
d=10.71196
d=15.59659
d=7.51328
d=5.15987
d=4.37763
d=3.63624
d=2.01514
JCA3_3 - File: JCA3-3.raw - Type: 2Th/Th locked - Start: 3.000 ° - End: 55.000 ° - Step: 0.050 ° - Step time: 1. s - Temp.: 25 °C (Room) - Time Started: 0 s - 2-Theta: 3.000 ° - Operations: Import
JCA-3_3 - File: JCA_3_3.raw - Type: 2Th/Th locked - Start: 3.000 ° - End: 15.000 ° - Step: 0.050 ° - Step time: 1. s - Temp.: 25 °C (Room) - Time Started: 0 s - 2-Theta: 3.000 ° - Operations: Import
JCA3_3 - File: JCA3_3.raw - Type: 2Th/Th locked - Start: 3.000 ° - End: 20.000 ° - Step: 0.050 ° - Step time: 1. s - Temp.: 25 °C (Room) - Time Started: 0 s - 2-Theta: 3.000 ° - Operations: Import

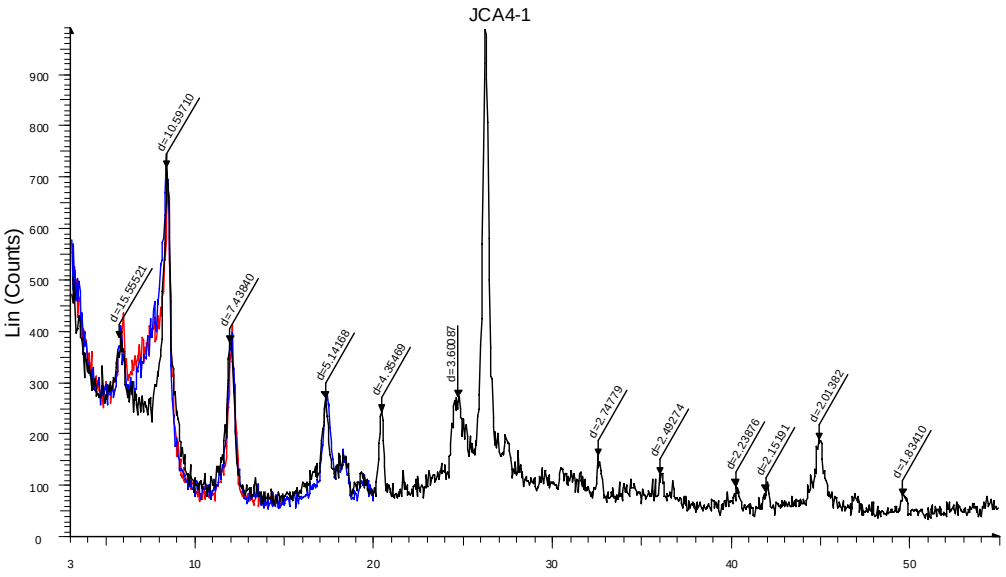
JCA4-1
Lin (Counts)
2-Theta - Scale
d=10.59710
d=15.55521
d=7.43940
d=5.14168
d=4.35469
d=3.60087
d=2.74779
d=2.49274
d=2.23876
d=2.15191
d=2.01382
d=1.83410
JCA4-1 - File: JCA4_1.raw - Type: 2Th/Th locked - Start: 3.000 ° - End: 55.000 ° - Step: 0.050 ° - Step time: 1. s - Temp.: 25 °C (Room) - Time Started: 0 s - 2-Theta: 3.000 ° - Operations: Import
JCA_4_1 - File: JCA_4_1.raw - Type: 2Th/Th locked - Start: 3.000 ° - End: 15.000 ° - Step: 0.050 ° - Step time: 1. s - Temp.: 25 °C (Room) - Time Started: 0 s - 2-Theta: 3.000 Operations: Import
JCA4_1 - File: JCA4-1.raw - Type: 2Th/Th locked - Start: 3.000 ° - End: 20.000 ° - Step: 0.050 ° - Step time: 1. s - Temp.: 25 °C (Room) - Time Started: 0 s - 2-Theta: 3.000 ° - Operations: Import

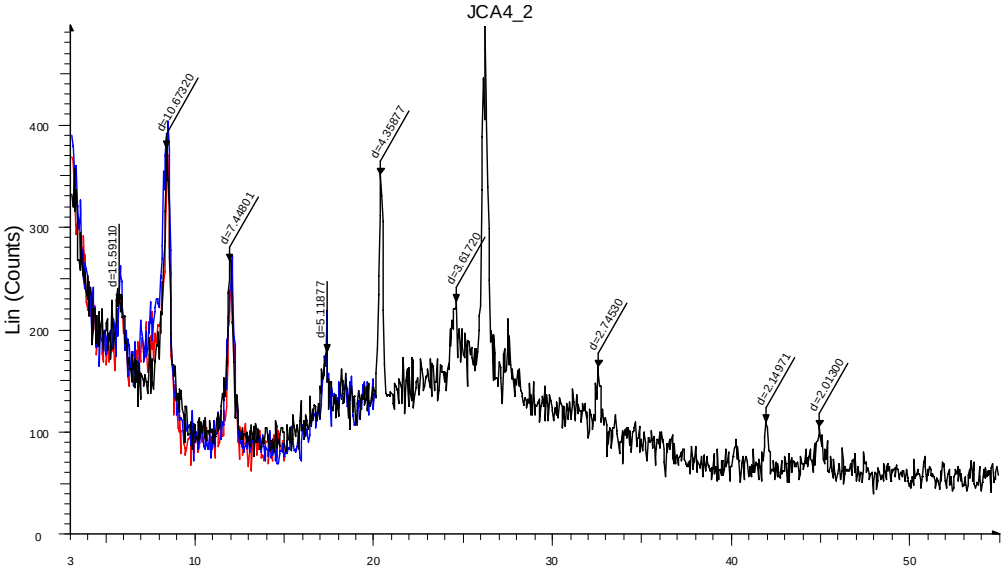
JCA4_2
Lin (Counts)
2-Theta - Scale
d=10.67320
d=15.59110
d=7.44801
d=5.11877
d=4.35877
d=3.61720
d=2.74530
d=2.14971
d=2.01300
JCA4_2 - File: JCA4-2.raw - Type: 2Th/Th locked - Start: 3.000 ° - End: 55.000 ° - Step: 0.050 ° - Step time: 1. s - Temp.: 25 °C (Room) - Time Started: 0 s - 2-Theta: 3.000 ° - Operations: Import
JCA_4_2 - File: JCA_4_2.raw - Type: 2Th/Th locked - Start: 3.000 ° - End: 15.000 ° - Step: 0.050 ° - Step time: 1. s - Temp.: 25 °C (Room) - Time Started: 0 s - 2-Theta: 3.000 Operations: Import
JCA4_2 - File: JCA4_2.raw - Type: 2Th/Th locked - Start: 3.000 ° - End: 20.000 ° - Step: 0.050 ° - Step time: 1. s - Temp.: 25 °C (Room) - Time Started: 0 s - 2-Theta: 3.000 ° - Operations: Import

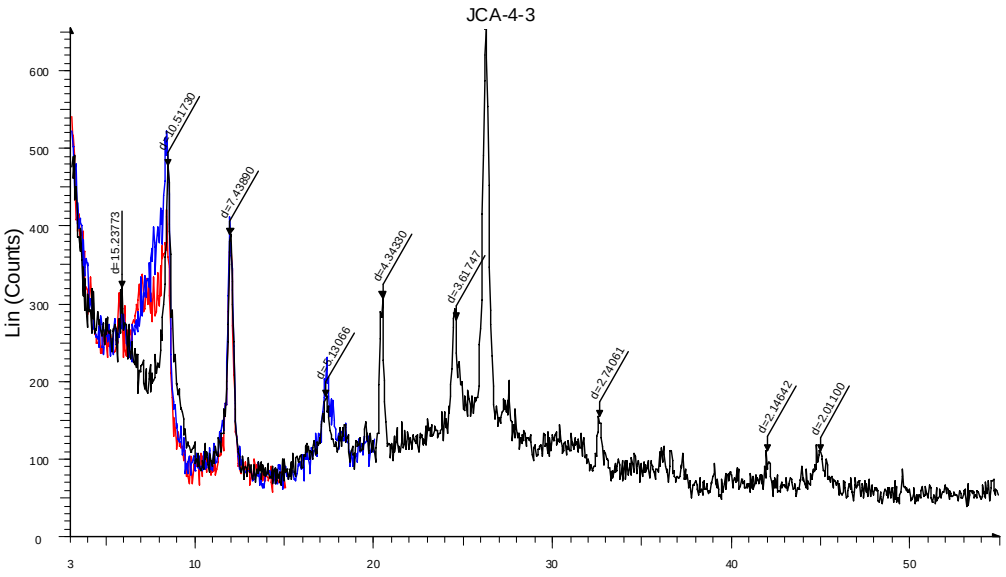

JCA-4-3 - File: JCA_4_3.raw - Type: 2Th/Th locked - Start: 3.000 ° - End: 55.000 ° - Step: 0.050 ° - Step time: 1. s - Temp.: 25 °C (Room) - Time Started: 0 s - 2-Theta: 3.000
Operations: Import

JCA-4_3 - File: JCA_4_3.raw - Type: 2Th/Th locked - Start: 3.000 ° - End: 15.000 ° - Step: 0.050 ° - Step time: 1. s - Temp.: 25 °C (Room) - Time Started: 0 s - 2-Theta: 3.000
Operations: Import

JCA4_3 - File: JCA4_3.raw - Type: 2Th/Th locked - Start: 3.000 ° - End: 20.000 ° - Step: 0.050 ° - Step time: 1. s - Temp.: 25 °C (Room) - Time Started: 0 s - 2-Theta: 3.000 °
Operations: Import

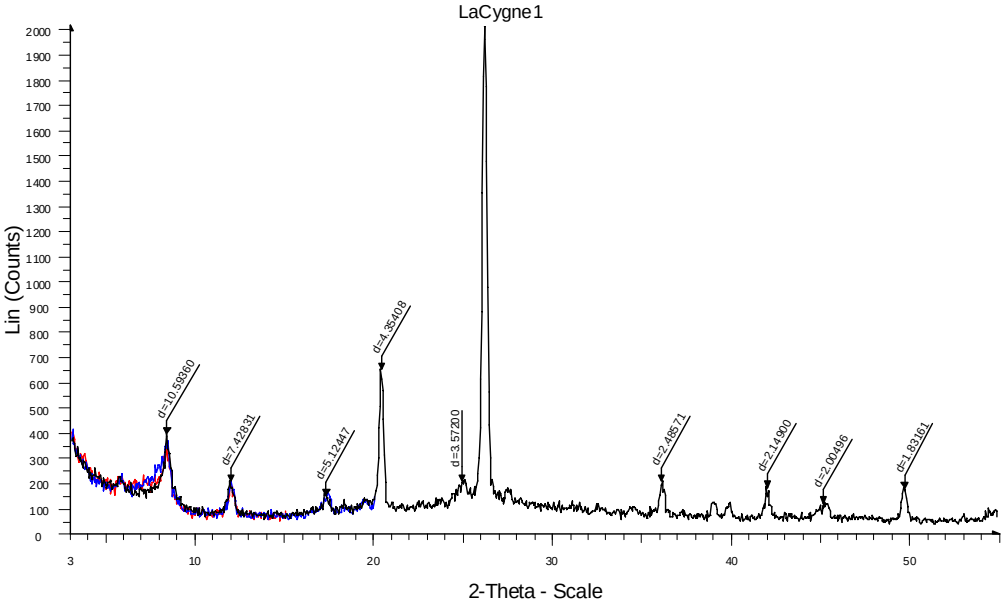

SunLFar1 - File: Lacy1.raw - Type: 2Th/Th locked - Start: 3.000 ° - End: 55.000 ° - Step: 0.050 ° - Step time: 1. s - Temp.: 25 °C (Room) - Time Started: 0 s - 2-Theta: 3.000 ° -
Operations: Import

Lacy_1 - File: Lacy_1.raw - Type: 2Th/Th locked - Start: 3.000 ° - End: 15.000 ° - Step: 0.050 ° - Step time: 1. s - Temp.: 25 °C (Room) - Time Started: 0 s - 2-Theta: 3.000 ° -
Operations: Import

lacy1 - File: Lacy1.raw - Type: 2Th/Th locked - Start: 3.000 ° - End: 20.000 ° - Step: 0.050 ° - Step time: 1. s - Temp.: 25 °C (Room) - Time Started: 0 s - 2-Theta: 3.000 ° - The
Operations: Import

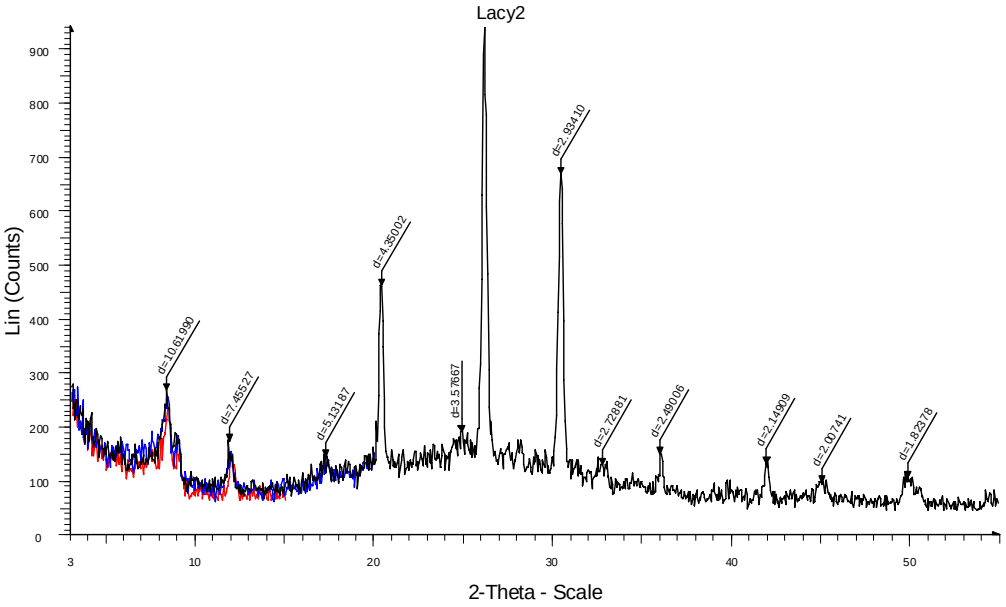

Lacy2 - File: Lacy2.raw - Type: 2Th/Th locked - Start: 3.000 ° - End: 55.000 ° - Step: 0.050 ° - Step time: 1. s - Temp.: 25 °C (Room) - Time Started: 0 s - 2-Theta: 3.000 ° - Th
Operations: Import
Lacy_2 - File: Lacy_2.raw - Type: 2Th/Th locked - Start: 3.000 ° - End: 15.000 ° - Step: 0.050 ° - Step time: 1. s - Temp.: 25 °C (Room) - Time Started: 0 s - 2-Theta: 3.000 ° -
Operations: Import
Lacy2 - File: Lacy2.raw - Type: 2Th/Th locked - Start: 3.000 ° - End: 20.000 ° - Step: 0.050 ° - Step time: 1. s - Temp.: 25 °C (Room) - Time Started: 0 s - 2-Theta: 3.000 ° - Th
Operations: Import

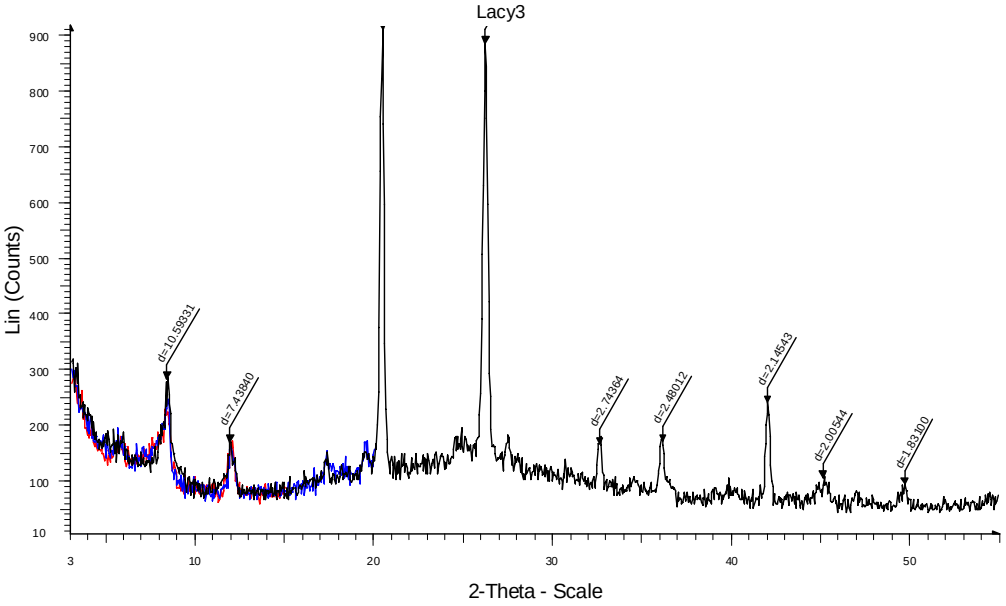

Lacy3 - File: Lacy3.raw - Type: 2Th/Th locked - Start: 3.000 ° - End: 55.000 ° - Step: 0.050 ° - Step time: 1. s - Temp.: 25 °C (Room) - Time Started: 0 s - 2-Theta: 3.000 ° - Th
Operations: Import
Lacy_3 - File: Lacy_3.raw - Type: 2Th/Th locked - Start: 3.000 ° - End: 15.000 ° - Step: 0.050 ° - Step time: 1. s - Temp.: 25 °C (Room) - Time Started: 0 s - 2-Theta: 3.000 ° -
Operations: Import
Lacy3 - File: Lacy3.raw - Type: 2Th/Th locked - Start: 3.000 ° - End: 20.000 ° - Step: 0.050 ° - Step time: 1. s - Temp.: 25 °C (Room) - Time Started: 0 s - 2-Theta: 3.000 ° - Th
Operations: Import

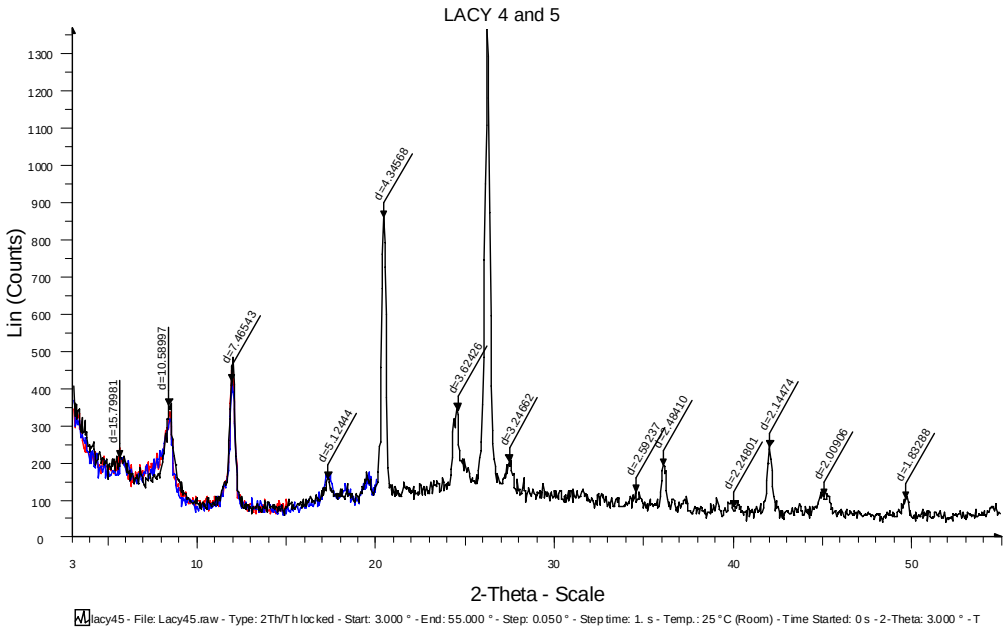
LACY 4 and 5
Lin (Counts)
2-Theta - Scale
d=15.79981
d=10.58997
d=7.46543
d=5.12444
d=4.34568
d=3.62426
d=3.24962
d=2.59237
d=2.48410
d=2.24801
d=2.14474
d=2.00906
d=1.83288
lacy45 - File: Lacy45.raw - Type: 2Th/Th locked - Start: 3.000 ° - End: 55.000 ° - Step: 0.050 ° - Step time: 1. s - Temp.: 25 °C (Room) - Time Started: 0 s - 2-Theta: 3.000 ° - T
Operations: Import
Lacy_45 - File: Lacy_45.raw - Type: 2Th/Th locked - Start: 3.000 ° - End: 15.000 ° - Step: 0.050 ° - Step time: 1. s - Temp.: 25 °C (Room) - Time Started: 0 s - 2-Theta: 3.000 °
Operations: Import
Lacy45 - File: Lacy45.raw - Type: 2Th/Th locked - Start: 3.000 ° - End: 20.000 ° - Step: 0.050 ° - Step time: 1. s - Temp.: 25 °C (Room) - Time Started: 0 s - 2-Theta: 3.000 ° -
Operations: Import

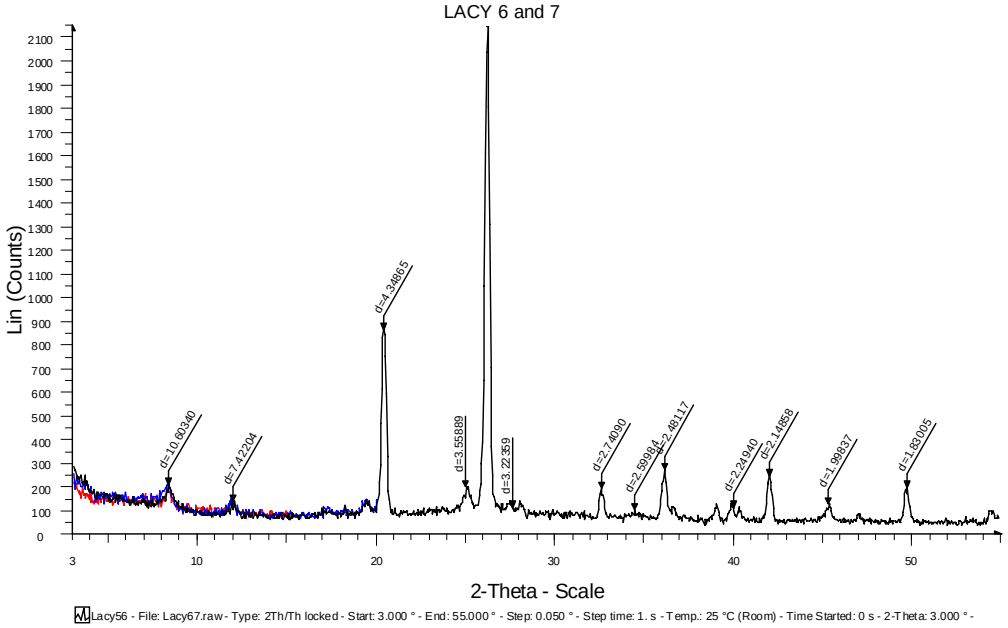
LACY 6 and 7
Lin (Counts)
2-Theta - Scale
d=10.60340
d=7.42204
d=4.34865
d=3.55689
d=3.22359
d=2.74090
d=2.59984
d=2.48117
d=2.24940
d=2.14858
d=1.98837
d=1.83005
Lacy56 - File: Lacy67.raw - Type: 2Th/Th locked - Start: 3.000 ° - End: 55.000 ° - Step: 0.050 ° - Step time: 1. s - Temp.: 25 °C (Room) - Time Started: 0 s - 2-Theta: 3.000 ° -
Operations: Import
Lacy_67 - File: Lacy_67.raw - Type: 2Th/Th locked - Start: 3.000 ° - End: 15.000 ° - Step: 0.050 ° - Step time: 1. s - Temp.: 25 °C (Room) - Time Started: 0 s - 2-Theta: 3.000 °
Operations: Import
Lacy67 - File: Lacy67.raw - Type: 2Th/Th locked - Start: 3.000 ° - End: 20.000 ° - Step: 0.050 ° - Step time: 1. s - Temp.: 25 °C (Room) - Time Started: 0 s - 2-Theta: 3.000 ° -
Operations: Import

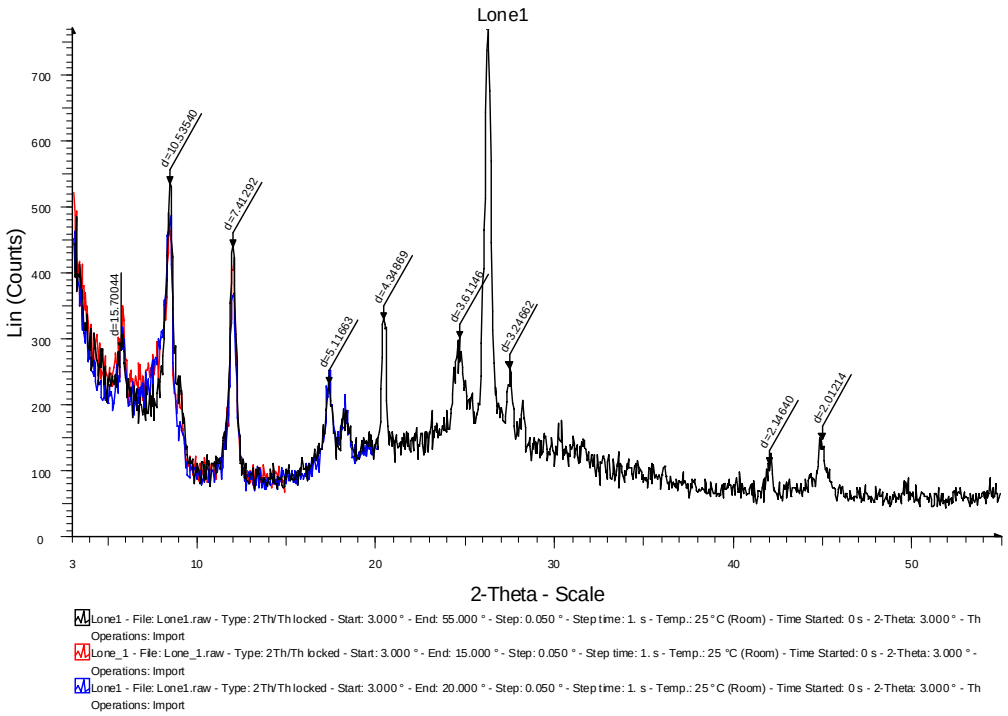
Lone1
Lin (Counts)
2-Theta - Scale
d=10.53540
d=7.41292
d=15.70044
d=5.11663
d=4.34869
d=3.61145
d=3.24662
d=2.14640
d=2.01214
Lone1 - File: Lone1.raw - Type: 2Th/Th locked - Start: 3.000 ° - End: 55.000 ° - Step: 0.050 ° - Step time: 1. s - Temp.: 25 °C (Room) - Time Started: 0 s - 2-Theta: 3.000 ° - Th
Operations: Import
Lone_1 - File: Lone_1.raw - Type: 2Th/Th locked - Start: 3.000 ° - End: 15.000 ° - Step: 0.050 ° - Step time: 1. s - Temp.: 25 °C (Room) - Time Started: 0 s - 2-Theta: 3.000 ° -
Operations: Import
Lone1 - File: Lone1.raw - Type: 2Th/Th locked - Start: 3.000 ° - End: 20.000 ° - Step: 0.050 ° - Step time: 1. s - Temp.: 25 °C (Room) - Time Started: 0 s - 2-Theta: 3.000 ° - Th
Operations: Import

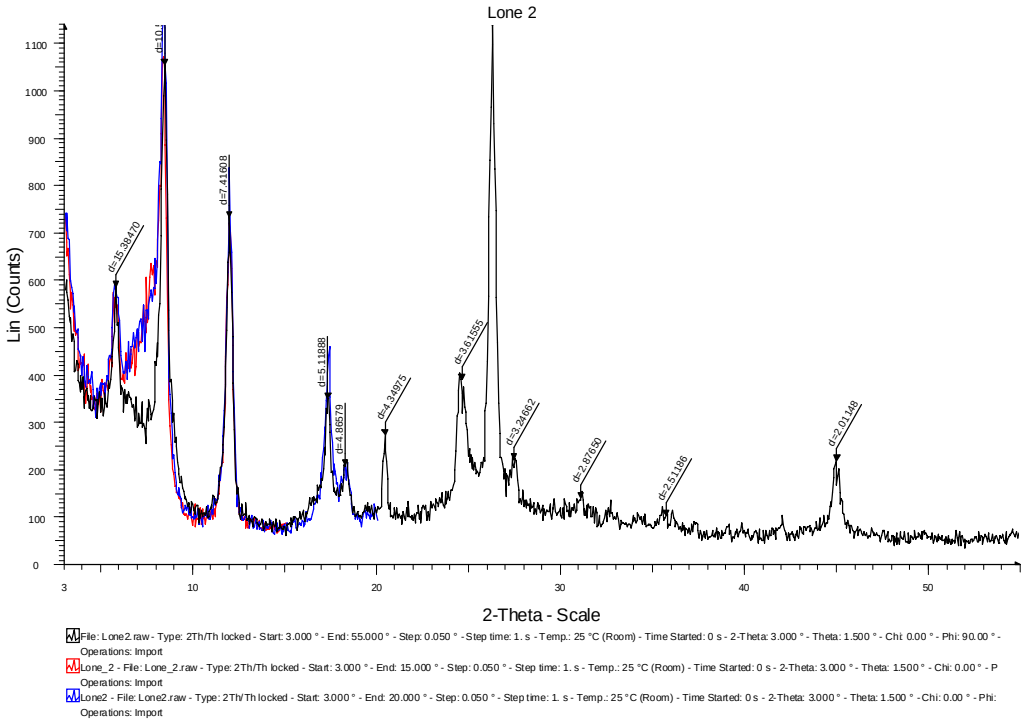
Lone 2
Lin (Counts)
2-Theta - Scale
d=15.38470
d=7.41608
d=5.11888
d=4.86679
d=4.34975
d=3.61655
d=3.34662
d=2.87659
d=2.51186
d=2.01148
File: Lone2.raw - Type: 2Th/Th locked - Start: 3.000 ° - End: 55.000 ° - Step: 0.050 ° - Step time: 1. s - Temp.: 25 °C (Room) - Time Started: 0 s - 2-Theta: 3.000 ° - Theta: 1.500 ° - Chi: 0.00 ° - Phi: 90.00 ° -
Operations: Import
Lone_2 - File: Lone_2.raw - Type: 2Th/Th locked - Start: 3.000 ° - End: 15.000 ° - Step: 0.050 ° - Step time: 1. s - Temp.: 25 °C (Room) - Time Started: 0 s - 2-Theta: 3.000 ° - Theta: 1.500 ° - Chi: 0.00 ° - P
Operations: Import
Lone2 - File: Lone2.raw - Type: 2Th/Th locked - Start: 3.000 ° - End: 20.000 ° - Step: 0.050 ° - Step time: 1. s - Temp.: 25 °C (Room) - Time Started: 0 s - 2-Theta: 3.000 ° - Theta: 1.500 ° - Chi: 0.00 ° - Phi:
Operations: Import

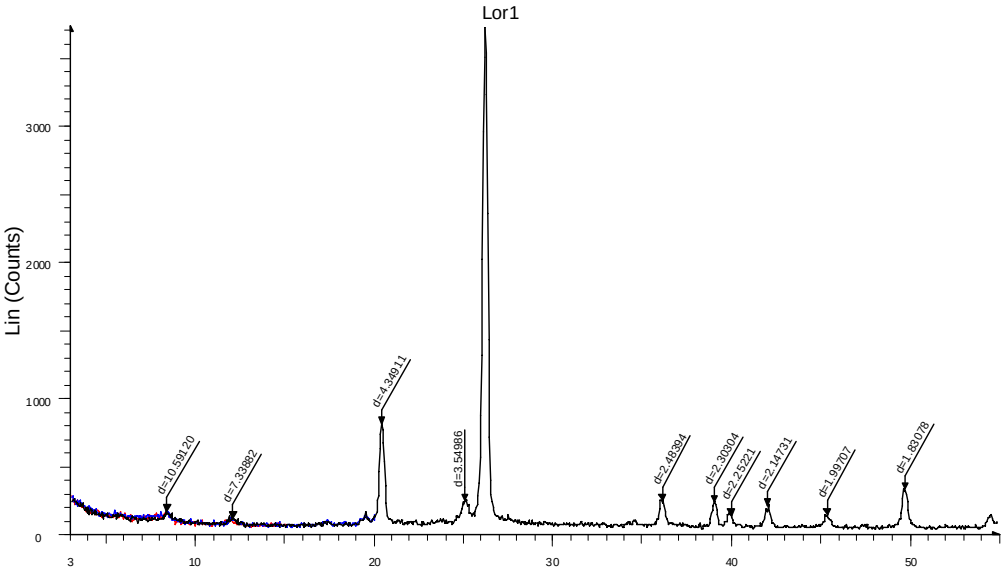

Lor1 - File: Lor1.raw - Type: 2Th/Th locked - Start: 3.000 ° - End: 55.000 ° - Step: 0.050 ° - Step time: 1. s - Temp.: 25 °C (Room) - Time Started: 0 s - 2-Theta: 3.000 ° - Theta:
Operations: Import

Lor_1 - File: Lor_1.raw - Type: 2Th/Th locked - Start: 3.000 ° - End: 15.000 ° - Step: 0.050 ° - Step time: 1. s - Temp.: 25 °C (Room) - Time Started: 0 s - 2-Theta: 3.000 ° - Th
Operations: Import

Lor1 - File: Lor1.raw - Type: 2Th/Th locked - Start: 3.000 ° - End: 20.000 ° - Step: 0.050 ° - Step time: 1. s - Temp.: 25 °C (Room) - Time Started: 0 s - 2-Theta: 3.000 ° - Theta:
Operations: Import

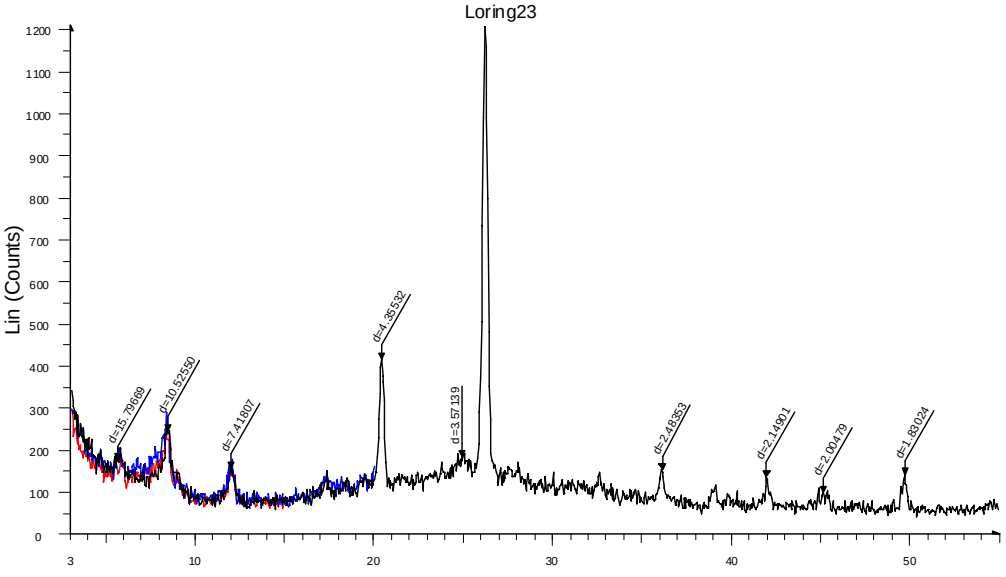

Loring23 - File: Loring23.raw - Type: 2Th/Th locked - Start: 3.000 ° - End: 55.000 ° - Step: 0.050 ° - Step time: 1. s - Temp.: 25 °C (Room) - Time Started: 0 s - 2-Theta: 3.000
Operations: Import

Lor_2&3 - File: Lor_23.raw - Type: 2Th/Th locked - Start: 3.000 ° - End: 15.000 ° - Step: 0.050 ° - Step time: 1. s - Temp.: 25 °C (Room) - Time Started: 0 s - 2-Theta: 3.000 ° -
Operations: Import

Loring23 - File: Loring23.raw - Type: 2Th/Th locked - Start: 3.000 ° - End: 20.000 ° - Step: 0.050 ° - Step time: 1. s - Temp.: 25 °C (Room) - Time Started: 0 s - 2-Theta: 3.000
Operations: Import

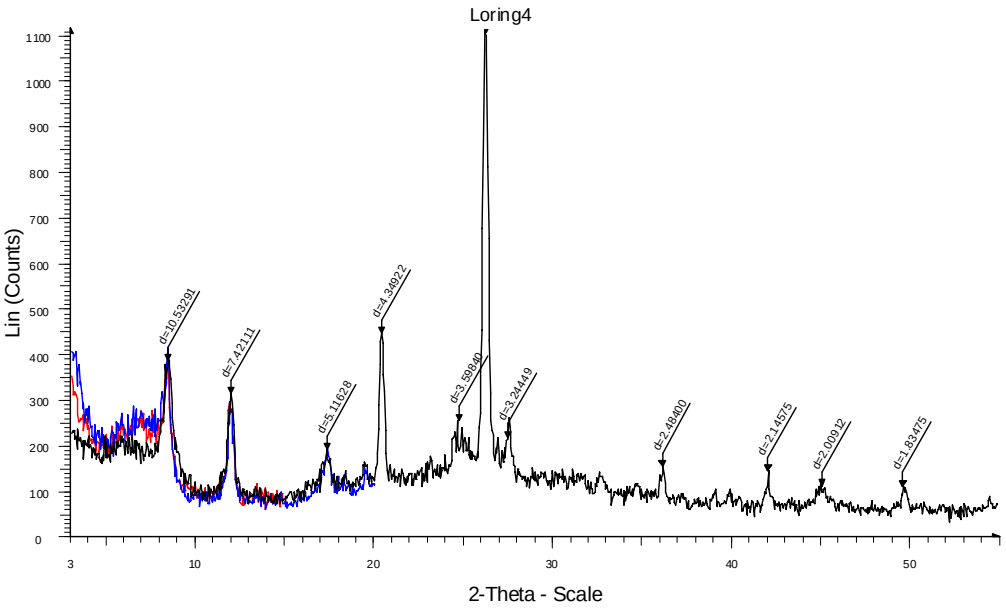
Loring4
Lin (Counts)
2-Theta - Scale
d=10.53291
d=7.42111
d=5.11628
d=4.34922
d=3.59840
d=3.24449
d=2.48400
d=2.14575
d=2.00912
d=1.83475
Loring4 - File: Loring4.raw - Type: 2Th/Th locked - Start: 3.000 ° - End: 55.000 ° - Step: 0.050 ° - Step time: 1. s - Temp.: 25 °C (Room) - Time Started: 0 s - 2-Theta: 3.000 ° - Operations: Import
Lor4_dry - File: Lor4_dry.raw - Type: 2Th/Th locked - Start: 3.000 ° - End: 15.000 ° - Step: 0.050 ° - Step time: 1. s - Temp.: 25 °C (Room) - Time Started: 0 s - 2-Theta: 3.000 Operations: Import
Loring4 - File: Loring4.raw - Type: 2Th/Th locked - Start: 3.000 ° - End: 20.000 ° - Step: 0.050 ° - Step time: 1. s - Temp.: 25 °C (Room) - Time Started: 0 s - 2-Theta: 3.000 ° - Operations: Import

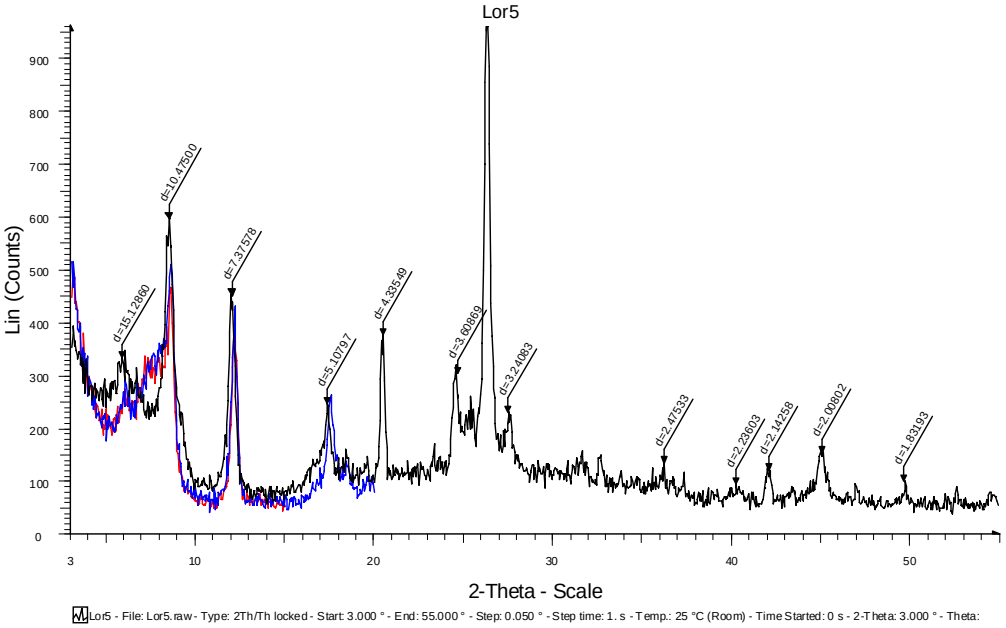
Lor5
Lin (Counts)
2-Theta - Scale
d=15.12860
d=10.47500
d=7.37578
d=5.10797
d=4.39549
d=3.60869
d=3.24093
d=2.47533
d=2.29603
d=2.14258
d=2.00802
d=1.83193
Lor5 - File: Lor5.raw - Type: 2Th/Th locked - Start: 3.000 ° - End: 55.000 ° - Step: 0.050 ° - Step time: 1. s - Temp.: 25 °C (Room) - Time Started: 0 s - 2-Theta: 3.000 ° - Theta: Operations: Import
Lor_5 - File: Lor_5.raw - Type: 2Th/Th locked - Start: 3.000 ° - End: 15.000 ° - Step: 0.050 ° - Step time: 1. s - Temp.: 25 °C (Room) - Time Started: 0 s - 2-Theta: 3.000 ° - Th Operations: Import
Lor5 - File: Lor5.raw - Type: 2Th/Th locked - Start: 3.000 ° - End: 20.000 ° - Step: 0.050 ° - Step time: 1. s - Temp.: 25 °C (Room) - Time Started: 0 s - 2-Theta: 3.000 ° - Theta: Operations: Import

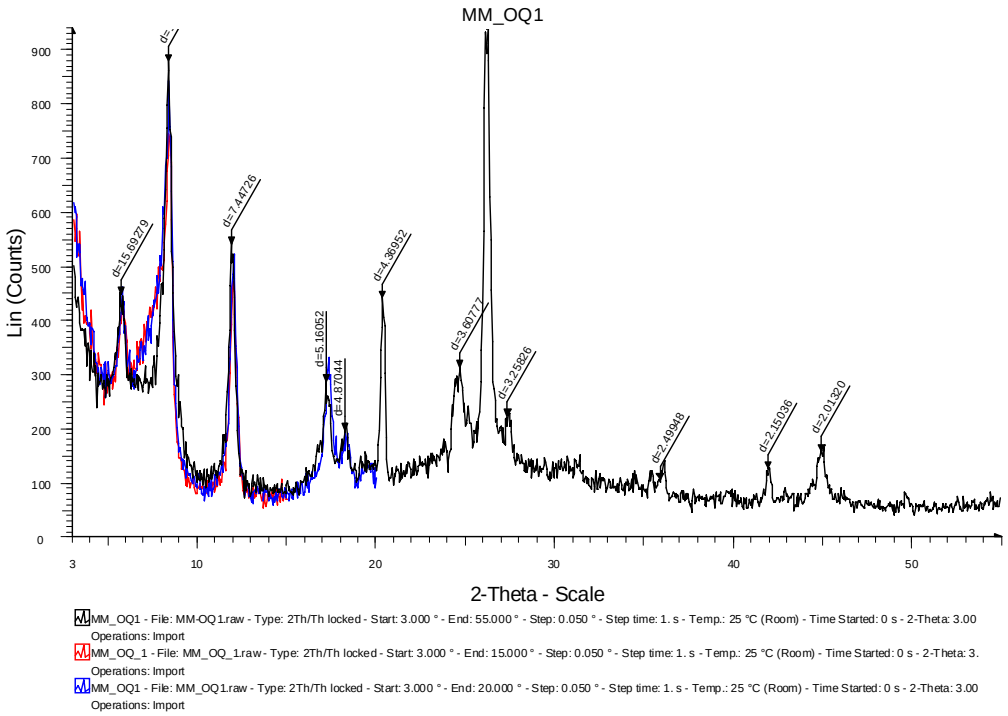
MM_OQ1
Lin (Counts)
2-Theta - Scale
d=15.69279
d=7.44726
d=5.16052
d=4.87044
d=4.36952
d=3.60777
d=3.25826
d=2.49948
d=2.15036
d=2.01320
MM_OQ1 - File: MM-OQ1.raw - Type: 2Th/Th locked - Start: 3.000 ° - End: 55.000 ° - Step: 0.050 ° - Step time: 1. s - Temp.: 25 °C (Room) - Time Started: 0 s - 2-Theta: 3.00
Operations: Import
MM_OQ_1 - File: MM_OQ_1.raw - Type: 2Th/Th locked - Start: 3.000 ° - End: 15.000 ° - Step: 0.050 ° - Step time: 1. s - Temp.: 25 °C (Room) - Time Started: 0 s - 2-Theta: 3.
Operations: Import
MM_OQ1 - File: MM_OQ1.raw - Type: 2Th/Th locked - Start: 3.000 ° - End: 20.000 ° - Step: 0.050 ° - Step time: 1. s - Temp.: 25 °C (Room) - Time Started: 0 s - 2-Theta: 3.00
Operations: Import

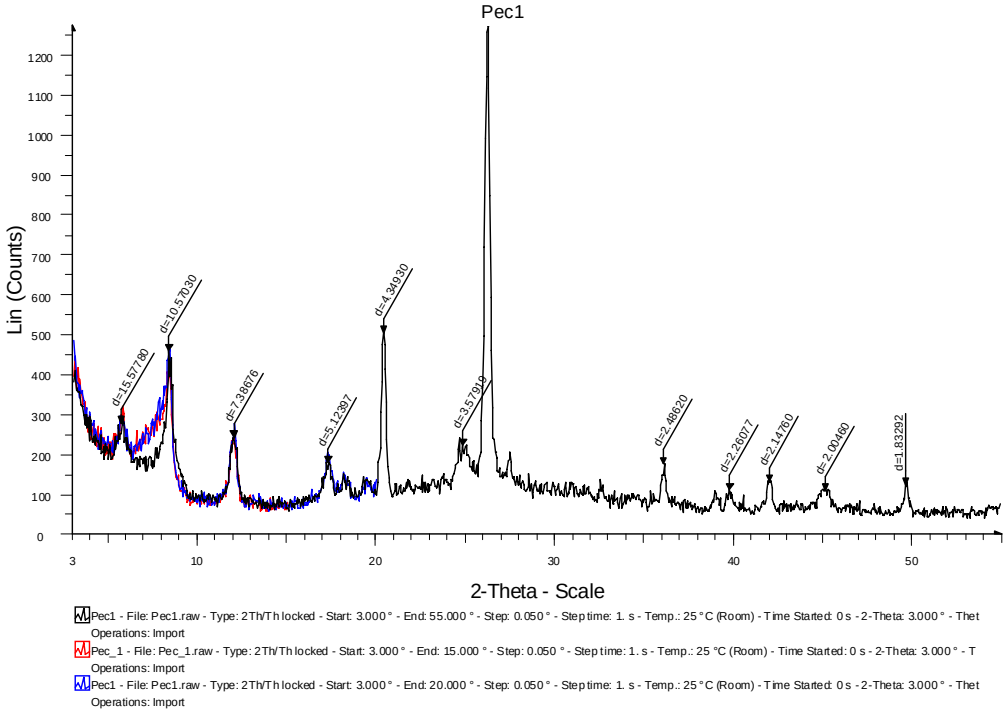
Pec1
Lin (Counts)
2-Theta - Scale
d=15.57780
d=10.57030
d=7.38676
d=5.12397
d=4.34930
d=3.57910
d=2.48620
d=2.26077
d=2.14760
d=2.00480
d=1.83292
Pec1 - File: Pec1.raw - Type: 2Th/Th locked - Start: 3.000 ° - End: 55.000 ° - Step: 0.050 ° - Step time: 1. s - Temp.: 25 °C (Room) - Time Started: 0 s - 2-Theta: 3.000 ° - Thet
Operations: Import
Pec_1 - File: Pec_1.raw - Type: 2Th/Th locked - Start: 3.000 ° - End: 15.000 ° - Step: 0.050 ° - Step time: 1. s - Temp.: 25 °C (Room) - Time Started: 0 s - 2-Theta: 3.000 ° - T
Operations: Import
Pec1 - File: Pec1.raw - Type: 2Th/Th locked - Start: 3.000 ° - End: 20.000 ° - Step: 0.050 ° - Step time: 1. s - Temp.: 25 °C (Room) - Time Started: 0 s - 2-Theta: 3.000 ° - Thet
Operations: Import

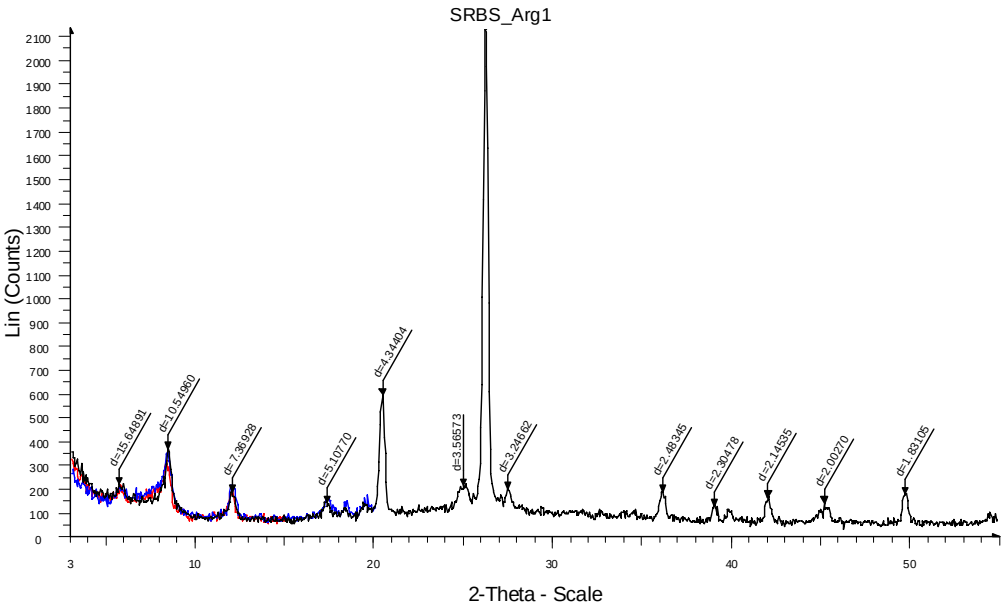
SRBS_Arg1
Lin (Counts)
2-Theta - Scale
d=15.64891
d=10.54960
d=7.36928
d=5.10770
d=4.34404
d=3.56573
d=3.24662
d=2.48345
d=2.30478
d=2.14535
d=2.00270
d=1.83105
SRBS_Arg1 - File: SRBS_Arg1.raw - Type: 2Th/Th locked - Start: 3.000 ° - End: 55.000 ° - Step: 0.050 ° - Step time: 1. s - Temp.: 25 °C (Room) - Time Started: 0 s - 2-Theta:
Operations: Import
Craw_2 - File: SRBS_Arg_1.raw - Type: 2Th/Th locked - Start: 3.000 ° - End: 15.000 ° - Step: 0.050 ° - Step time: 1. s - Temp.: 25 °C (Room) - Time Started: 0 s - 2-Theta: 3.0
Operations: Import
SRBS_Arg1 - File: SRBS_Arg1.raw - Type: 2Th/Th locked - Start: 3.000 ° - End: 20.000 ° - Step: 0.050 ° - Step time: 1. s - Temp.: 25 °C (Room) - Time Started: 0 s - 2-Theta:
Operations: Import

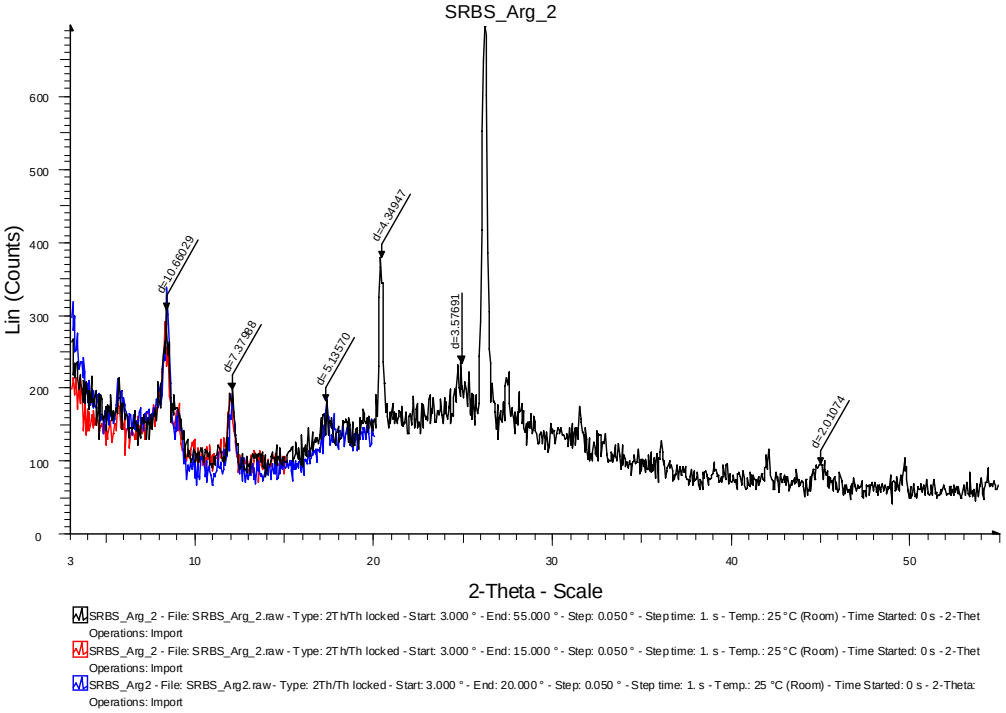
SRBS_Arg_2
Lin (Counts)
2-Theta - Scale
d=10.66029
d=7.37988
d=5.33570
d=4.34947
d=3.57691
d=2.01074
SRBS_Arg_2 - File: SRBS_Arg_2.raw - Type: 2Th/Th locked - Start: 3.000 ° - End: 55.000 ° - Step: 0.050 ° - Step time: 1. s - Temp.: 25 °C (Room) - Time Started: 0 s - 2-Thet
Operations: Import
SRBS_Arg_2 - File: SRBS_Arg_2.raw - Type: 2Th/Th locked - Start: 3.000 ° - End: 15.000 ° - Step: 0.050 ° - Step time: 1. s - Temp.: 25 °C (Room) - Time Started: 0 s - 2-Thet
Operations: Import
SRBS_Arg2 - File: SRBS_Arg2.raw - Type: 2Th/Th locked - Start: 3.000 ° - End: 20.000 ° - Step: 0.050 ° - Step time: 1. s - Temp.: 25 °C (Room) - Time Started: 0 s - 2-Theta:
Operations: Import

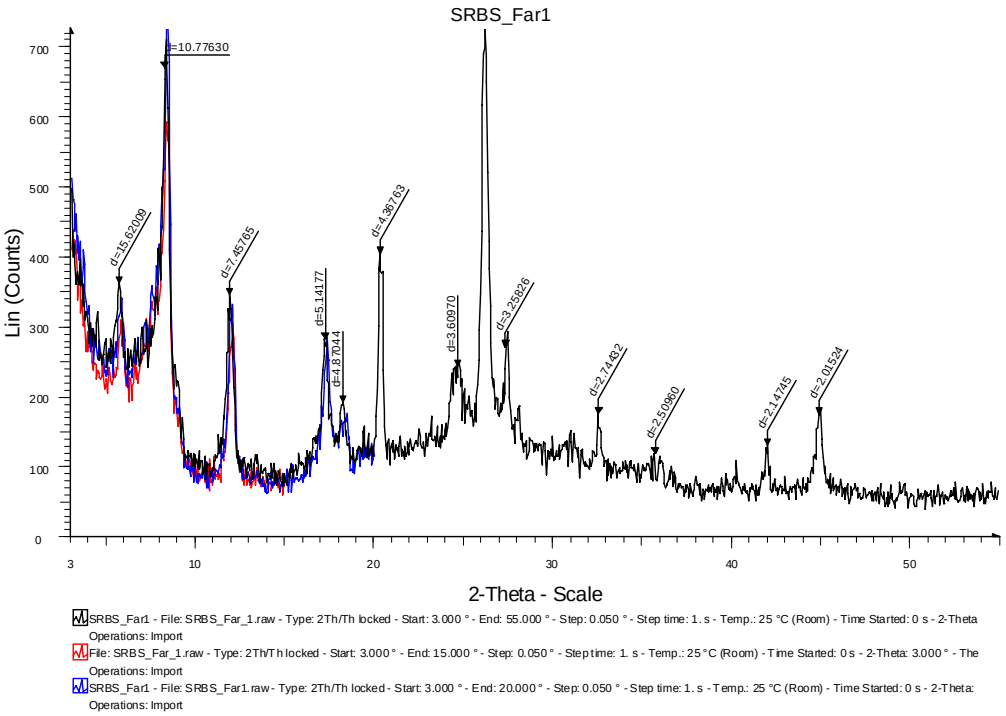
SRBS_Far1
d=10.77630
d=15.62009
d=7.45765
d=5.14177
d=4.87044
d=4.38763
d=3.60970
d=3.25826
d=2.74432
d=2.50960
d=2.14745
d=2.01524
Lin (Counts)
2-Theta - Scale
SRBS_Far1 - File: SRBS_Far_1.raw - Type: 2Th/Th locked - Start: 3.000 ° - End: 55.000 ° - Step: 0.050 ° - Step time: 1. s - Temp.: 25 °C (Room) - Time Started: 0 s - 2-Theta
Operations: Import
File: SRBS_Far_1.raw - Type: 2Th/Th locked - Start: 3.000 ° - End: 15.000 ° - Step: 0.050 ° - Step time: 1. s - Temp.: 25 °C (Room) - Time Started: 0 s - 2-Theta: 3.000 ° - The
Operations: Import
SRBS_Far1 - File: SRBS_Far1.raw - Type: 2Th/Th locked - Start: 3.000 ° - End: 20.000 ° - Step: 0.050 ° - Step time: 1. s - Temp.: 25 °C (Room) - Time Started: 0 s - 2-Theta:
Operations: Import

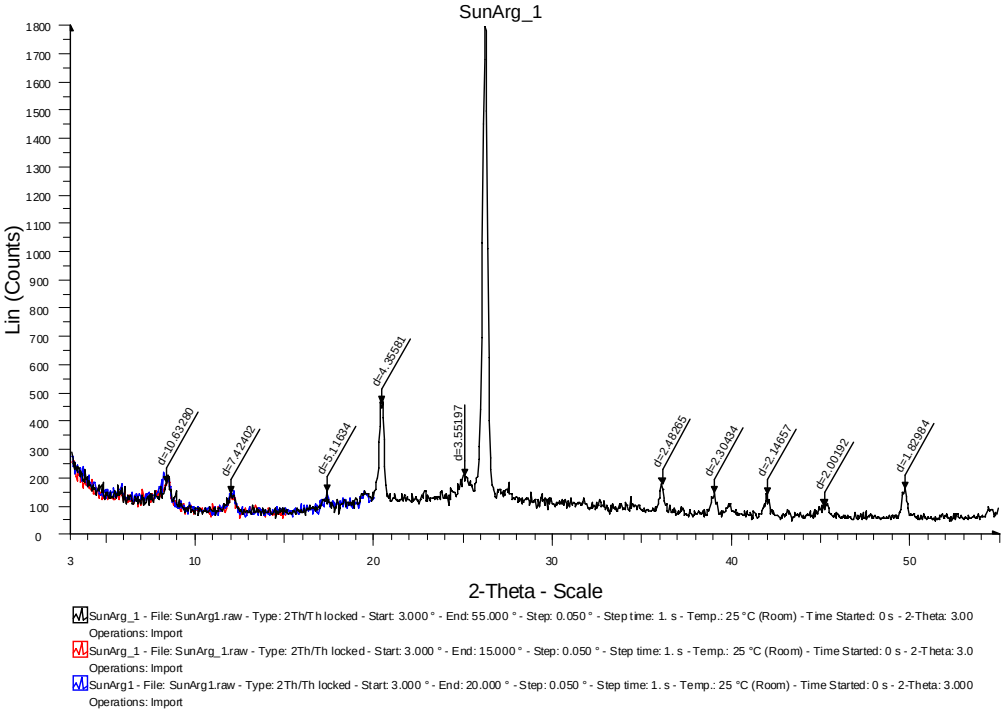
SunArg_1
d=10.63280
d=7.42402
d=5.11624
d=4.35681
d=3.55197
d=2.48265
d=2.30434
d=2.14657
d=2.00192
d=1.82984
Lin (Counts)
2-Theta - Scale
SunArg_1 - File: SunArg1.raw - Type: 2Th/Th locked - Start: 3.000 ° - End: 55.000 ° - Step: 0.050 ° - Step time: 1. s - Temp.: 25 °C (Room) - Time Started: 0 s - 2-Theta: 3.00
Operations: Import
SunArg_1 - File: SunArg_1.raw - Type: 2Th/Th locked - Start: 3.000 ° - End: 15.000 ° - Step: 0.050 ° - Step time: 1. s - Temp.: 25 °C (Room) - Time Started: 0 s - 2-Theta: 3.0
Operations: Import
SunArg1 - File: SunArg1.raw - Type: 2Th/Th locked - Start: 3.000 ° - End: 20.000 ° - Step: 0.050 ° - Step time: 1. s - Temp.: 25 °C (Room) - Time Started: 0 s - 2-Theta: 3.000
Operations: Import

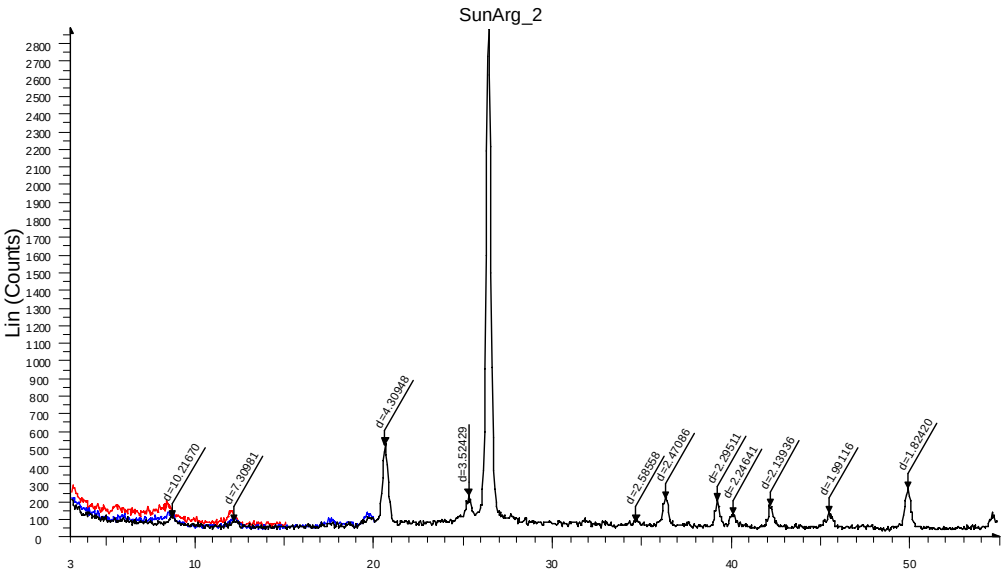

SunArg_2 - File: SunArg_2.raw - Type: 2Th/Th locked - Start: 3.000 ° - End: 55.000 ° - Step: 0.050 ° - Step time: 1. s - Temp.: 25 °C (Room) - Time Started: 0 s - 2-Theta: 3.0
Operations: Import

Sun_Arg_2 - File: Sun_Arg_2.raw - Type: 2Th/Th locked - Start: 3.000 ° - End: 15.000 ° - Step: 0.050 ° - Step time: 1. s - Temp.: 25 °C (Room) - Time Started: 0 s - 2-Theta: 3
Operations: Import

SunArg2 - File: SunArg2.raw - Type: 2Th/Th locked - Start: 3.000 ° - End: 20.000 ° - Step: 0.050 ° - Step time: 1. s - Temp.: 25 °C (Room) - Time Started: 0 s - 2-Theta: 3.000
Operations: Import

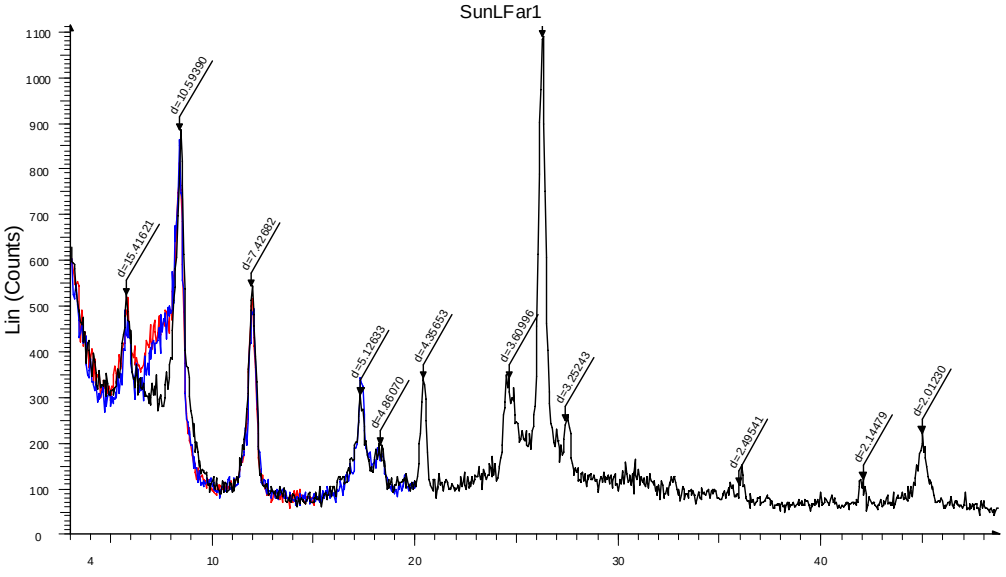

SunLFar1 - File: Sun_LFar1.raw - Type: 2Th/Th locked - Start: 3.000 ° - End: 55.000 ° - Step: 0.050 ° - Step time: 1. s - Temp.: 25 °C (Room) - Time Started: 0 s - 2-Theta: 3.0
Operations: Import

Sun_LFar_1 - File: Sun_LFar_1.raw - Type: 2Th/Th locked - Start: 3.000 ° - End: 15.000 ° - Step: 0.050 ° - Step time: 1. s - Temp.: 25 °C (Room) - Time Started: 0 s - 2-Theta:
Operations: Import

SunLFar1 - File: SunLFar1.raw - Type: 2Th/Th locked - Start: 3.000 ° - End: 20.000 ° - Step: 0.050 ° - Step time: 1. s - Temp.: 25 °C (Room) - Time Started: 0 s - 2-Theta: 3.00
Operations: Import

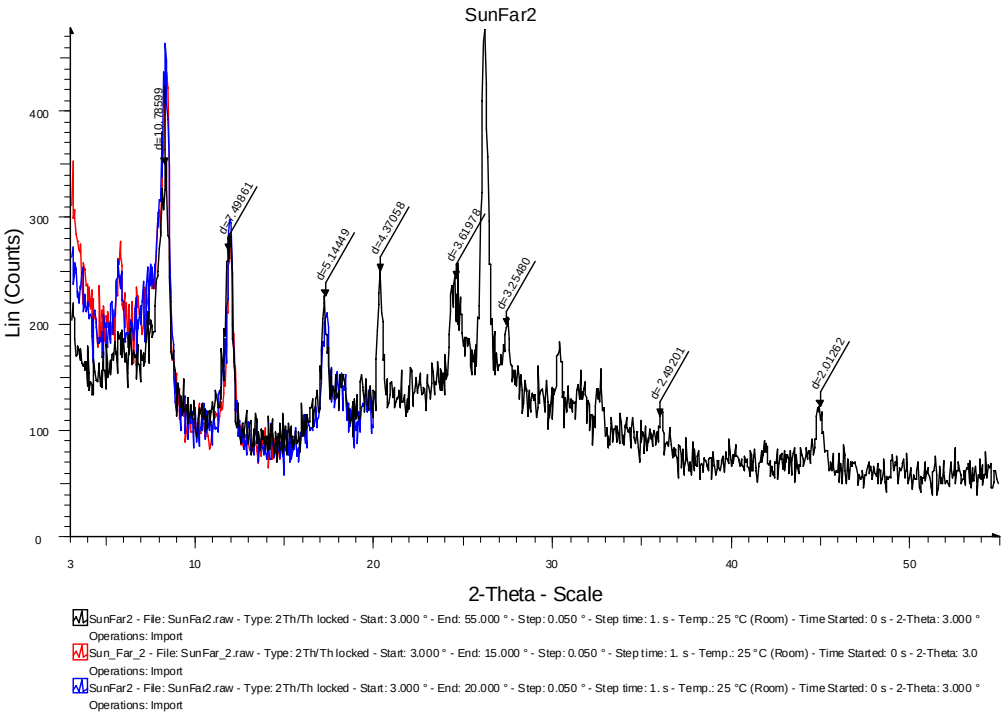

SunFar2 - File: SunFar2.raw - Type: 2Th/Th locked - Start: 3.000 ° - End: 55.000 ° - Step: 0.050 ° - Step time: 1. s - Temp.: 25 °C (Room) - Time Started: 0 s - 2-Theta: 3.000 °
Operations: Import

Sun_Far_2 - File: SunFar_2.raw - Type: 2Th/Th locked - Start: 3.000 ° - End: 15.000 ° - Step: 0.050 ° - Step time: 1. s - Temp.: 25 °C (Room) - Time Started: 0 s - 2-Theta: 3.0
Operations: Import

SunFar2 - File: SunFar2.raw - Type: 2Th/Th locked - Start: 3.000 ° - End: 20.000 ° - Step: 0.050 ° - Step time: 1. s - Temp.: 25 °C (Room) - Time Started: 0 s - 2-Theta: 3.000 °
Operations: Import

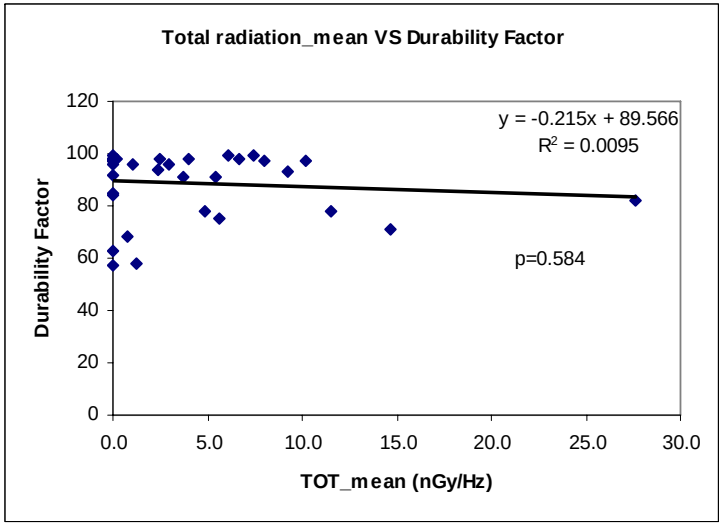
Total radiation_mean VS Durability Factor
y = -0.215x + 89.566
R2 = 0.0095
p=0.584
Durability Factor
TOT_mean (nGy/Hz)
0
20
40
60
80
100
120
0.0
5.0
10.0
15.0
20.0
25.0
30.0

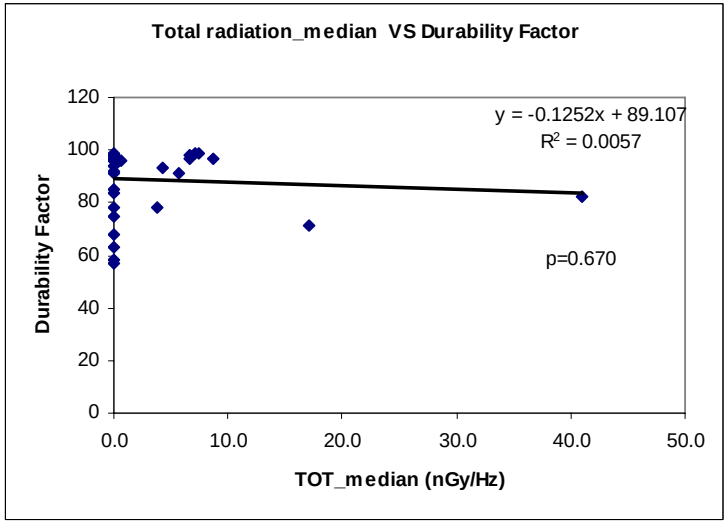
Total radiation_median VS Durability Factor
y = -0.1252x + 89.107
R2 = 0.0057
p=0.670
Durability Factor
TOT_median (nGy/Hz)
0
20
40
60
80
100
120
0.0
10.0
20.0
30.0
40.0
50.0

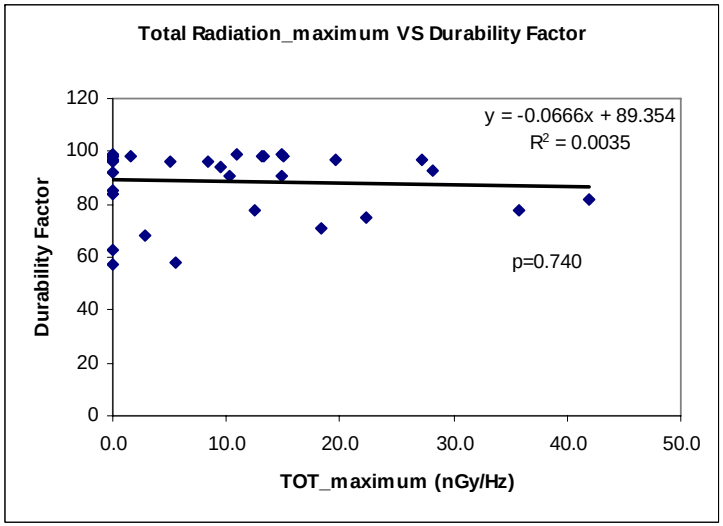
Total Radiation_maximum VS Durability Factor
y = -0.0666x + 89.354
R2 = 0.0035
p=0.740
Durability Factor
TOT_maximum (nGy/Hz)
0
20
40
60
80
100
120
0.0
10.0
20.0
30.0
40.0
50.0

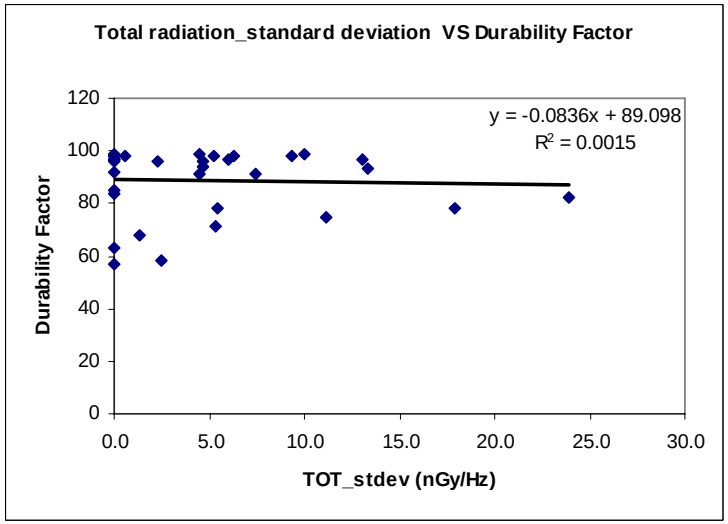
Total radiation_standard deviation VS Durability Factor
y = -0.0836x + 89.098
R2 = 0.0015
Durability Factor
TOT_stdev (nGy/Hz)
0
20
40
60
80
100
120
0.0
5.0
10.0
15.0
20.0
25.0
30.0

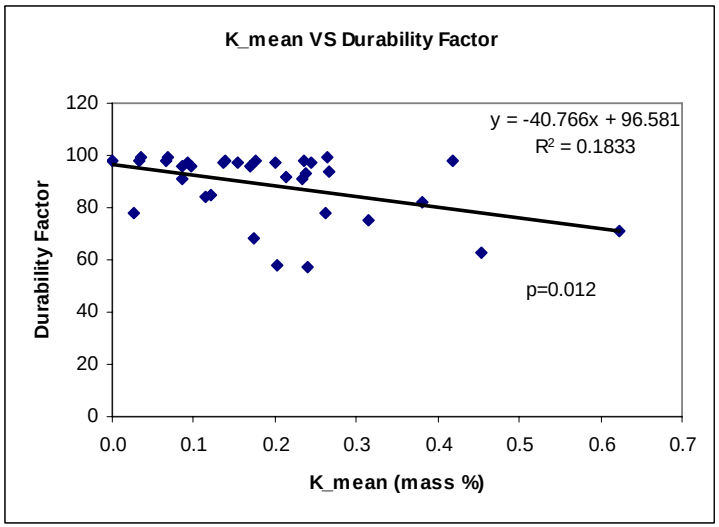
K_mean VS Durability Factor
y = -40.766x + 96.581
R² = 0.1833
p=0.012
Durability Factor
K_mean (mass %)
0
20
40
60
80
100
120
0.0
0.1
0.2
0.3
0.4
0.5
0.6
0.7

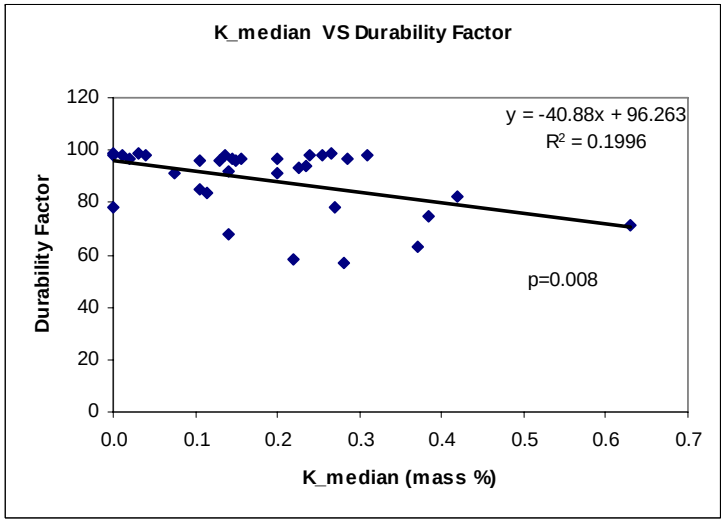
K_median VS Durability Factor
y = -40.88x + 96.263
R² = 0.1996
p=0.008
Durability Factor
K_median (mass %)
0
20
40
60
80
100
120
0.0
0.1
0.2
0.3
0.4
0.5
0.6
0.7

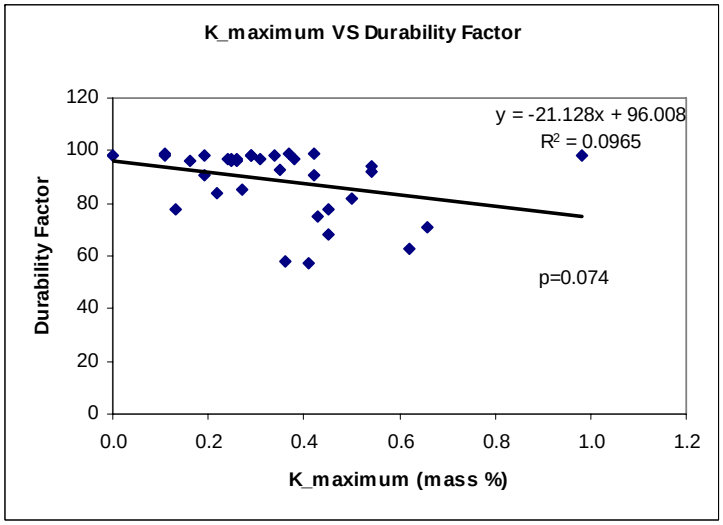
K_maximum VS Durability Factor
y = -21.128x + 96.008
R² = 0.0965
p=0.074
Durability Factor
K_maximum (mass %)
0
20
40
60
80
100
120
0.0
0.2
0.4
0.6
0.8
1.0
1.2

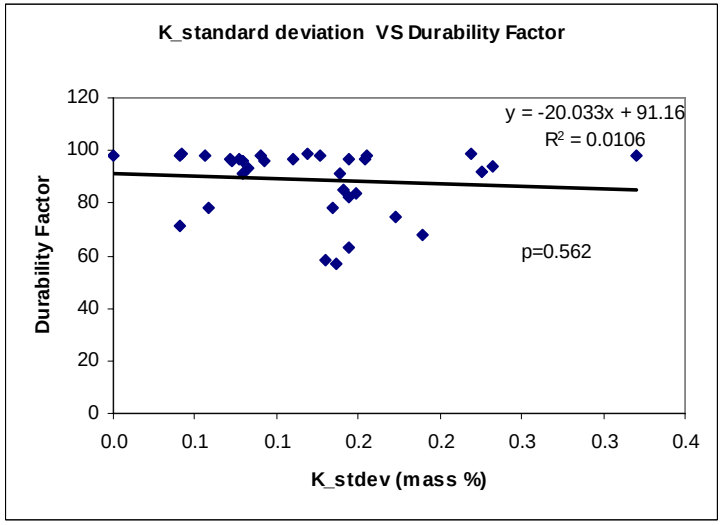
K_standard deviation VS Durability Factor
y = -20.033x + 91.16
R² = 0.0106
p=0.562
Durability Factor
K_stdev (mass %)
0
20
40
60
80
100
120
0.0
0.1
0.1
0.2
0.2
0.3
0.3
0.4

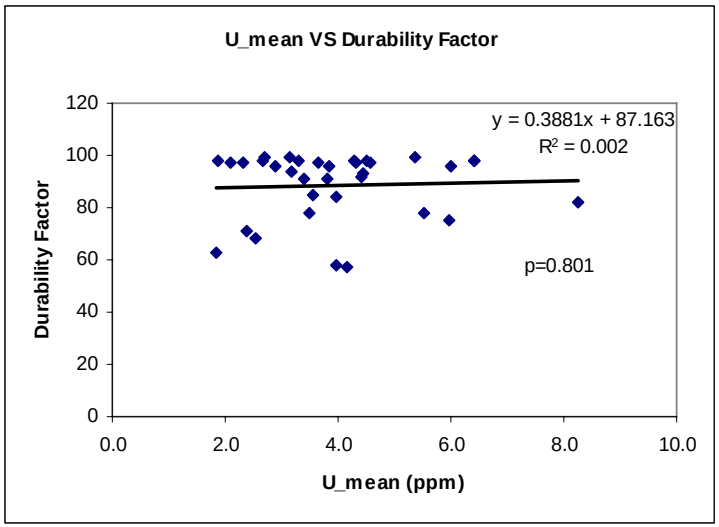
U_mean VS Durability Factor
y = 0.3881x + 87.163
R² = 0.002
p=0.801
Durability Factor
U_mean (ppm)
0
20
40
60
80
100
120
0.0
2.0
4.0
6.0
8.0
10.0

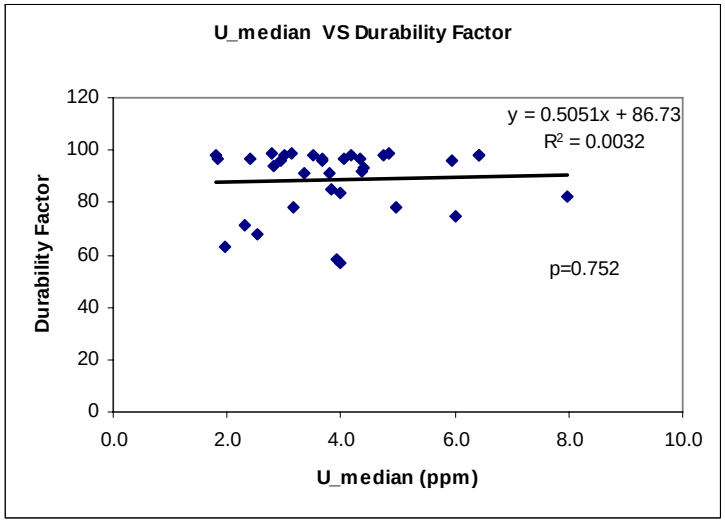
U_median VS Durability Factor
y = 0.5051x + 86.73
R² = 0.0032
p=0.752
Durability Factor
U_median (ppm)
0
20
40
60
80
100
120
0.0
2.0
4.0
6.0
8.0
10.0

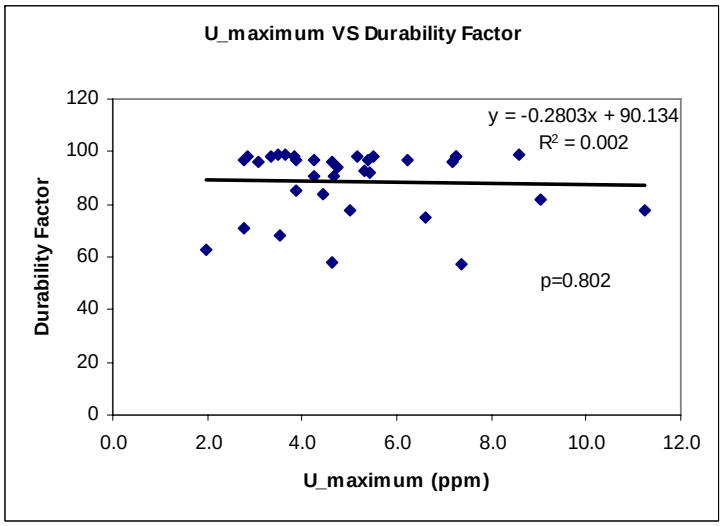
U_maximum VS Durability Factor
y = -0.2803x + 90.134
R² = 0.002
p=0.802
Durability Factor
U_maximum (ppm)
0
20
40
60
80
100
120
0.0
2.0
4.0
6.0
8.0
10.0
12.0

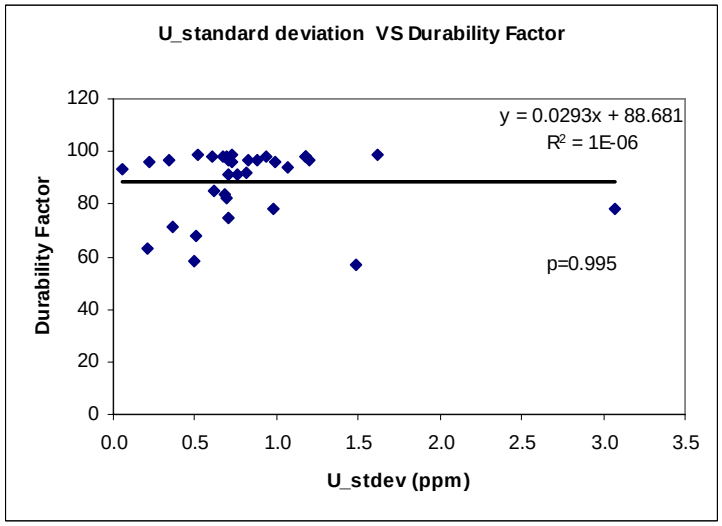
U_standard deviation VS Durability Factor
y = 0.0293x + 88.681
R² = 1E-06
p=0.995
Durability Factor
U_stdev (ppm)
0
20
40
60
80
100
120
0.0
0.5
1.0
1.5
2.0
2.5
3.0
3.5

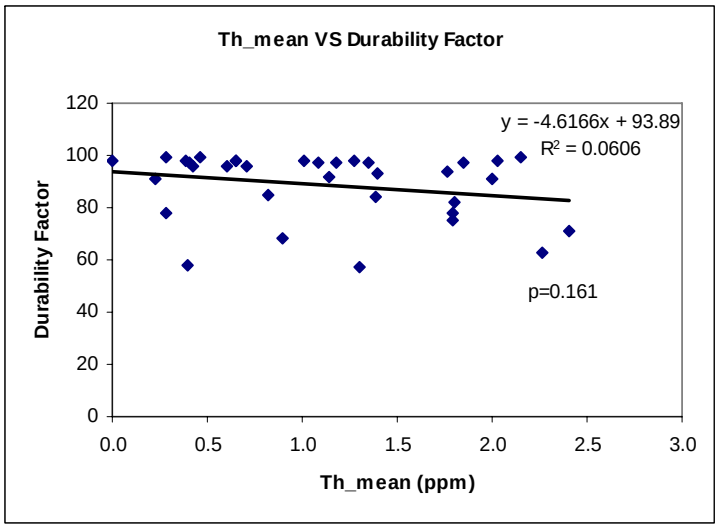
Th_mean VS Durability Factor
y = -4.6166x + 93.89
R² = 0.0606
p=0.161
Durability Factor
Th_mean (ppm)
0
20
40
60
80
100
120
0.0
0.5
1.0
1.5
2.0
2.5
3.0

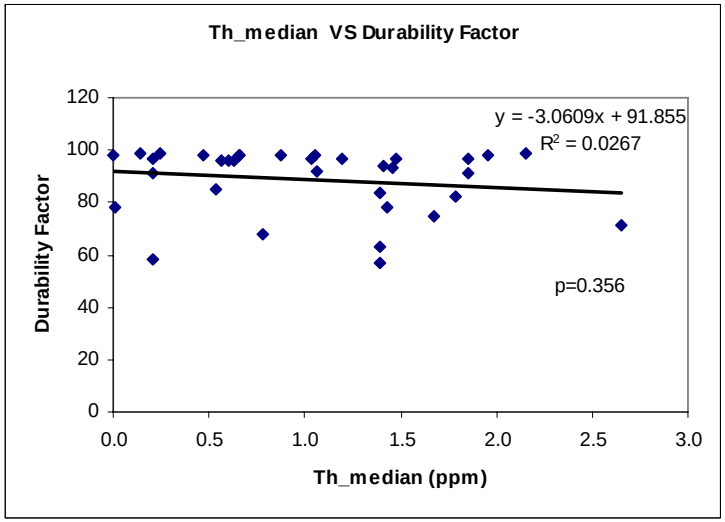
Th_median VS Durability Factor
y = -3.0609x + 91.855
R² = 0.0267
p=0.356
Durability Factor
Th_median (ppm)
0
20
40
60
80
100
120
0.0
0.5
1.0
1.5
2.0
2.5
3.0

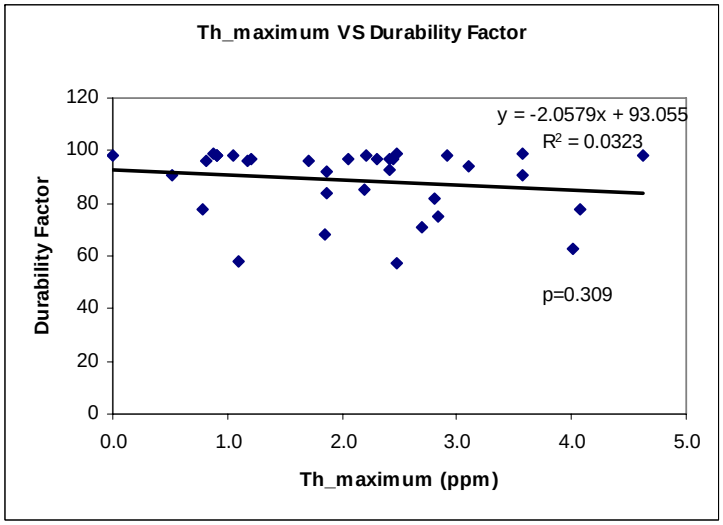
Th_maximum VS Durability Factor
y = -2.0579x + 93.055
R² = 0.0323
p=0.309
Durability Factor
Th_maximum (ppm)
0
20
40
60
80
100
120
0.0
1.0
2.0
3.0
4.0
5.0

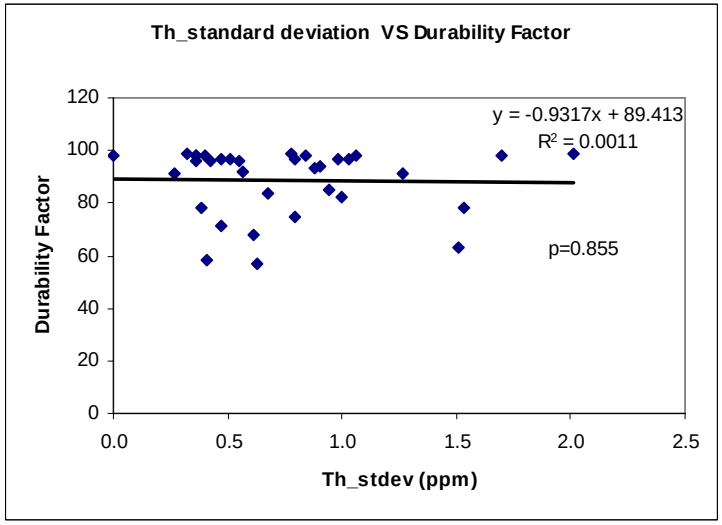
Th_standard deviation VS Durability Factor
y = -0.9317x + 89.413
R² = 0.0011
p=0.855
Durability Factor
Th_stdev (ppm)
0
20
40
60
80
100
120
0.0
0.5
1.0
1.5
2.0
2.5

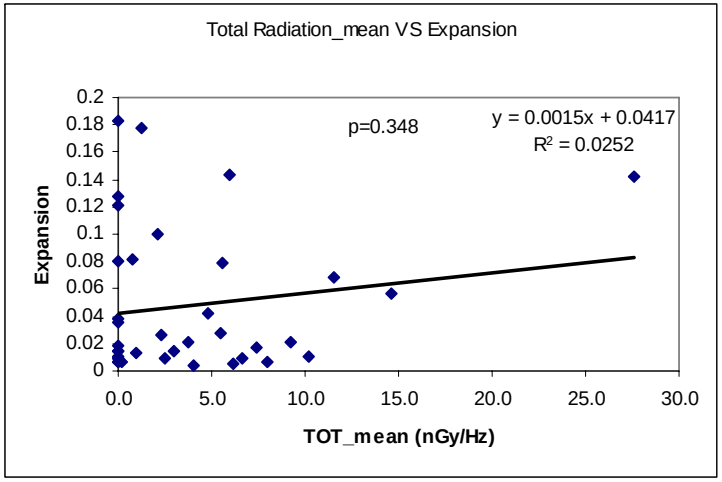
Total Radiation_mean VS Expansion
p=0.348
y = 0.0015x + 0.0417
R² = 0.0252
Expansion
TOT_mean (nGy/Hz)

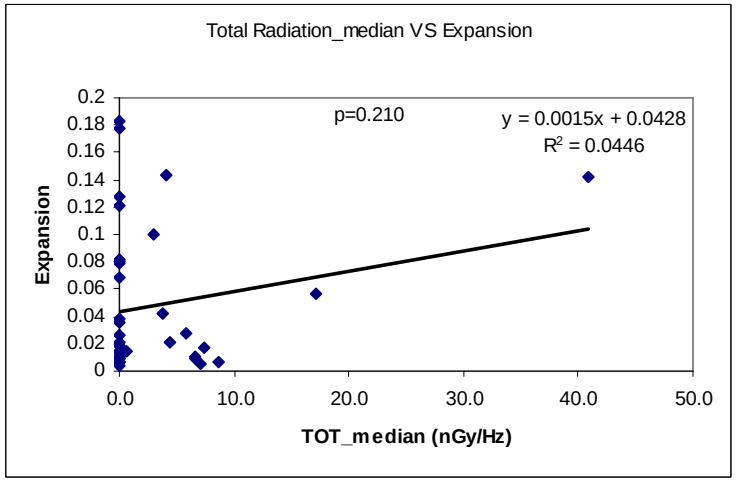
Total Radiation_median VS Expansion
p=0.210
y = 0.0015x + 0.0428
R² = 0.0446
Expansion
TOT_median (nGy/Hz)

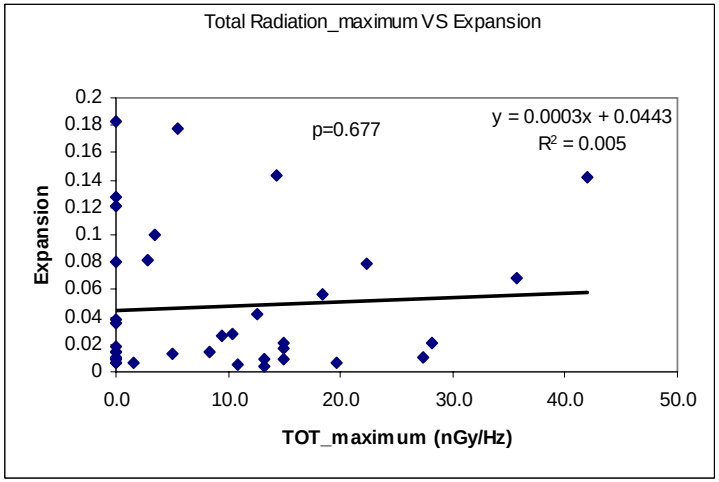
Total Radiation_maximum VS Expansion
p=0.677
y = 0.0003x + 0.0443
R² = 0.005
Expansion
TOT_maximum (nGy/Hz)

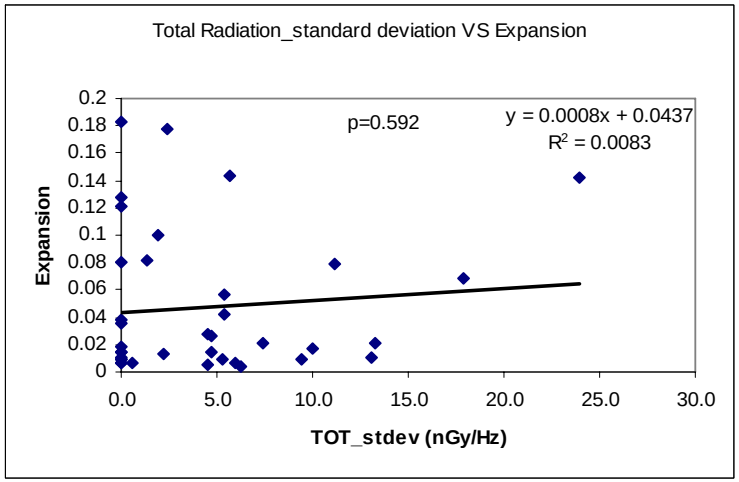
Total Radiation_standard deviation VS Expansion
p=0.592
y = 0.0008x + 0.0437
R² = 0.0083
Expansion
TOT_stdev (nGy/Hz)

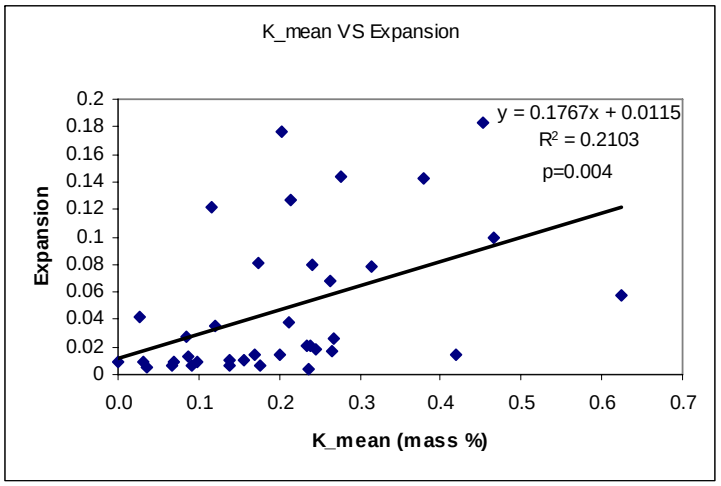
K_mean VS Expansion
y = 0.1767x + 0.0115
R² = 0.2103
p=0.004
Expansion
K_mean (mass %)

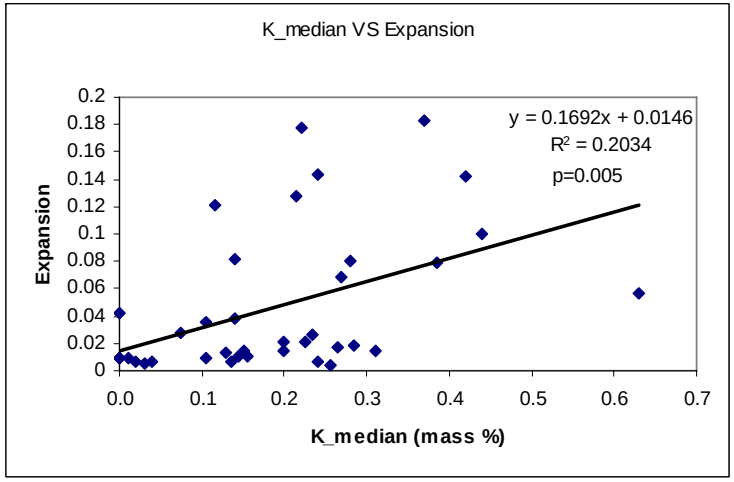
K_median VS Expansion
y = 0.1692x + 0.0146
R² = 0.2034
p=0.005
Expansion
K_median (mass %)

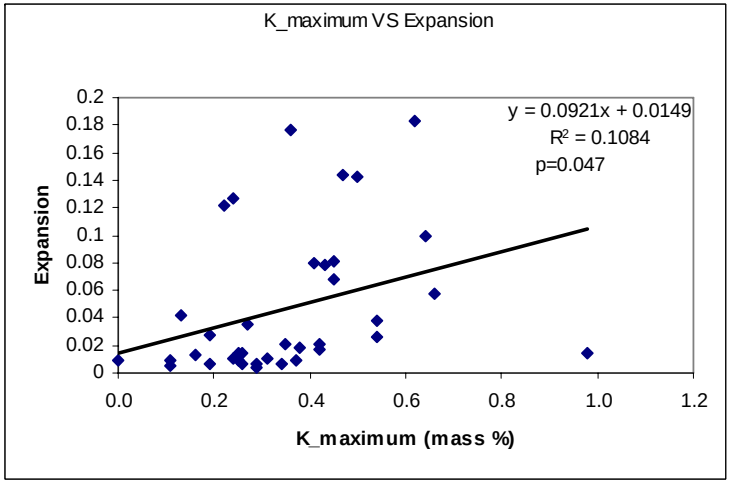
K_maximum VS Expansion
y = 0.0921x + 0.0149
R² = 0.1084
p=0.047
Expansion
K_maximum (mass %)

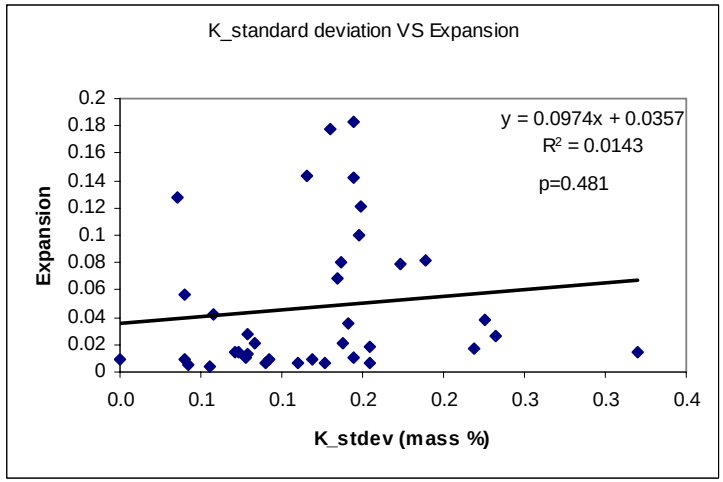
K_standard deviation VS Expansion
y = 0.0974x + 0.0357
R² = 0.0143
p=0.481
Expansion
K_stdev (mass %)

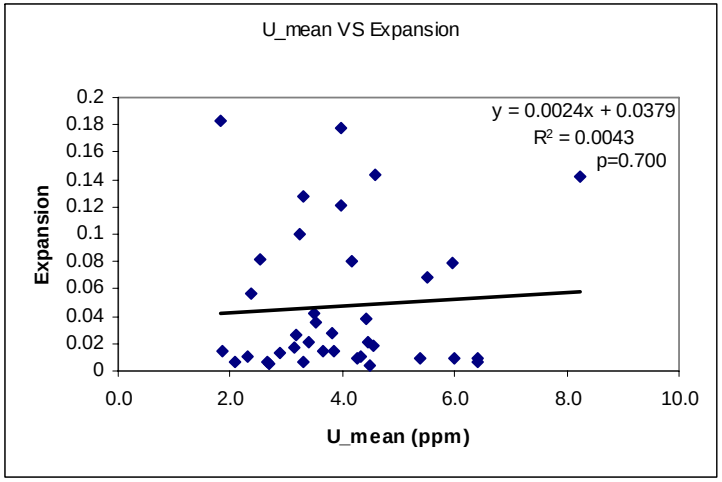
U_mean VS Expansion
y = 0.0024x + 0.0379
R² = 0.0043
p=0.700
Expansion
U_mean (ppm)

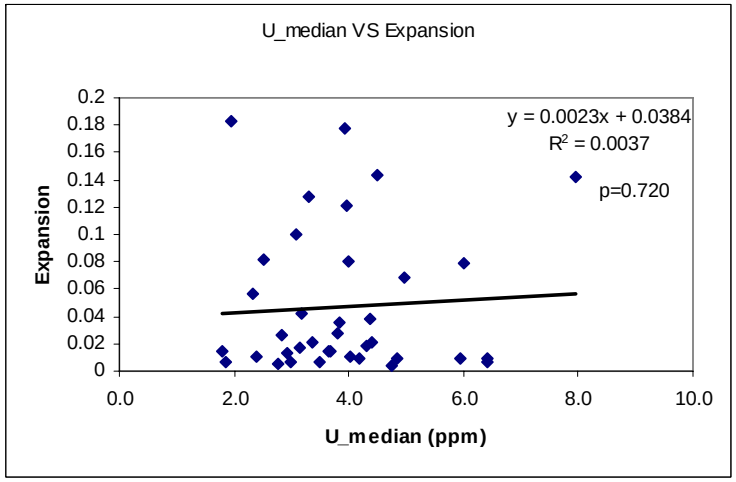
U_median VS Expansion
y = 0.0023x + 0.0384
R² = 0.0037
p=0.720
Expansion
U_median (ppm)

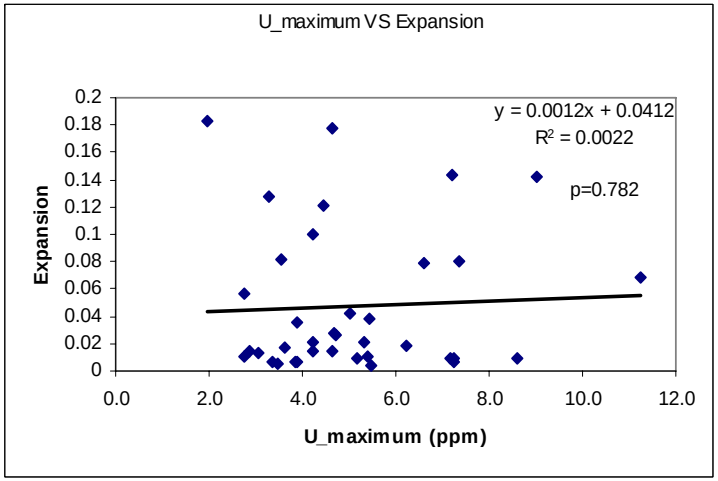
U_maximum VS Expansion
y = 0.0012x + 0.0412
R² = 0.0022
p=0.782
Expansion
U_maximum (ppm)

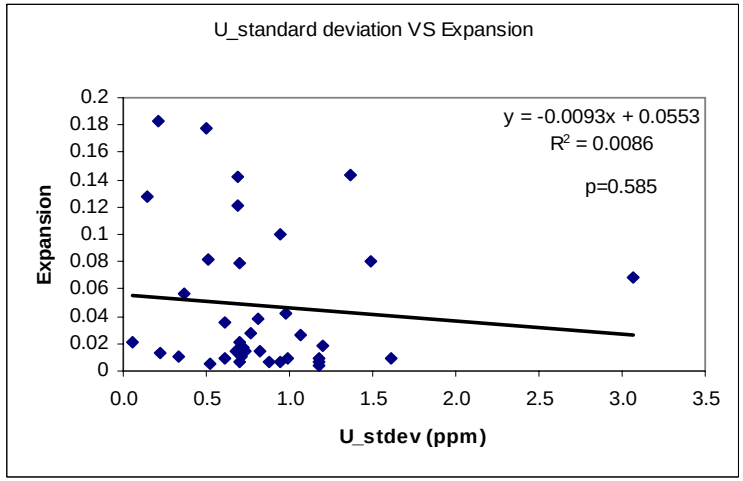
U_standard deviation VS Expansion
y = -0.0093x + 0.0553
R² = 0.0086
p=0.585
Expansion
U_stdev (ppm)

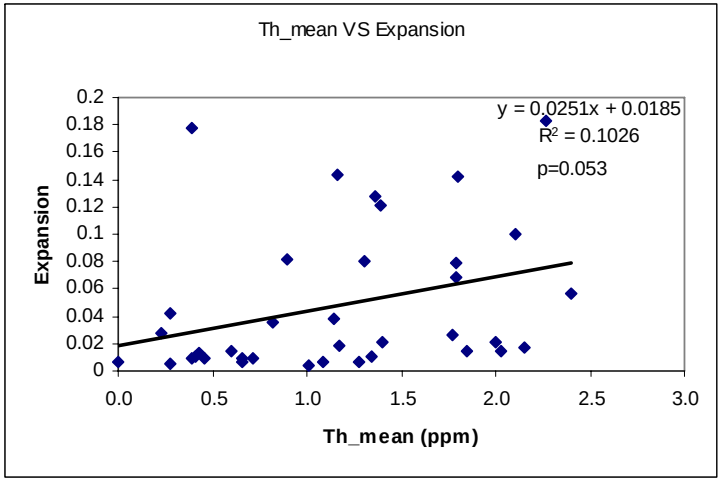
Th_mean VS Expansion
y = 0.0251x + 0.0185
R² = 0.1026
p=0.053
Expansion
Th_mean (ppm)

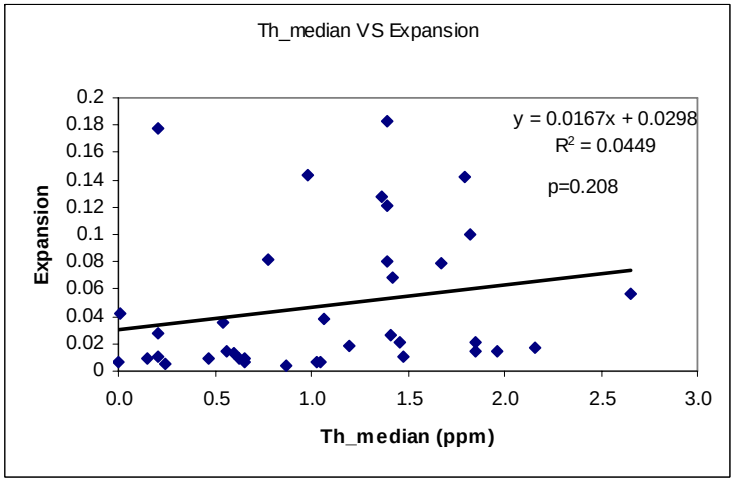
Th_median VS Expansion
y = 0.0167x + 0.0298
R² = 0.0449
p=0.208
Expansion
Th_median (ppm)

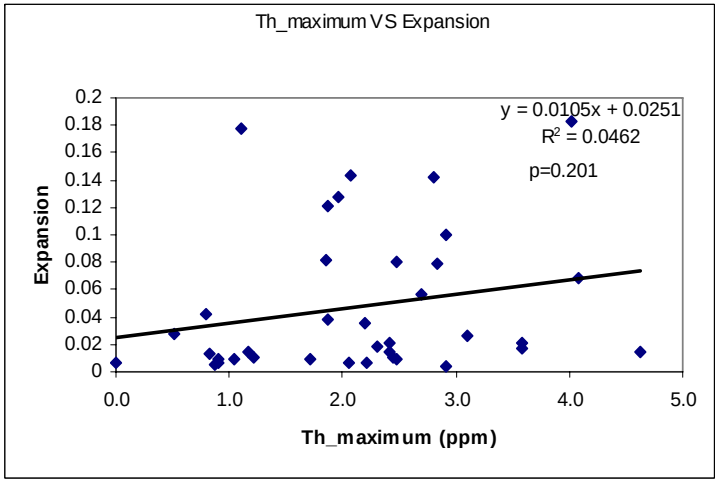
Th_maximum VS Expansion
y = 0.0105x + 0.0251
R² = 0.0462
p=0.201
Expansion
Th_maximum (ppm)

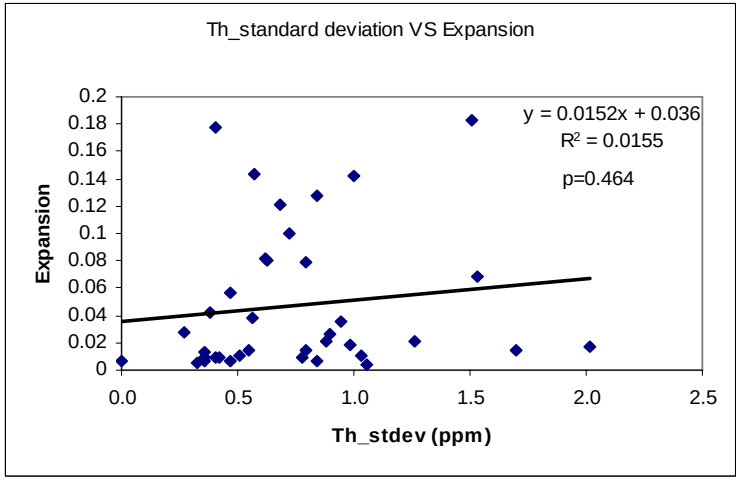
Th_standard deviation VS Expansion
y = 0.0152x + 0.036
R² = 0.0155
p=0.464
Expansion
Th_stdev (ppm)

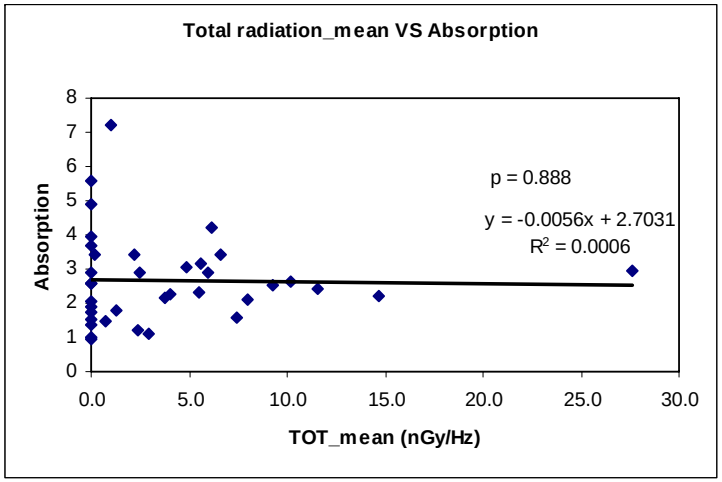
Total radiation_mean VS Absorption
Absorption
TOT_mean (nGy/Hz)
p = 0.888
y = -0.0056x + 2.7031
R2 = 0.0006

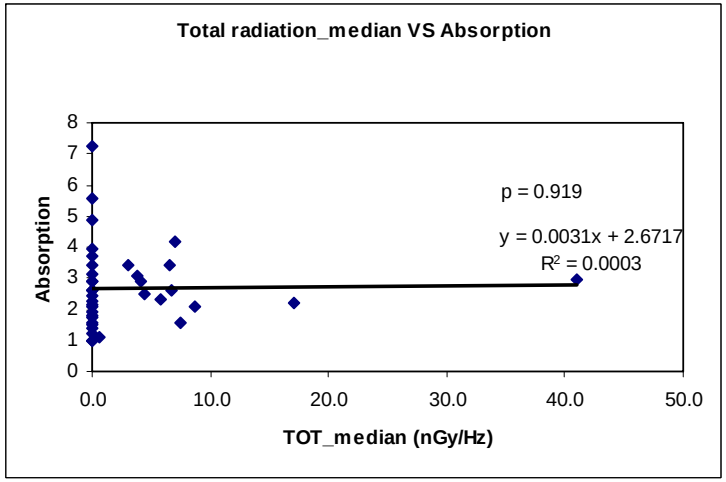
Total radiation_median VS Absorption
Absorption
TOT_median (nGy/Hz)
p = 0.919
y = 0.0031x + 2.6717
R2 = 0.0003

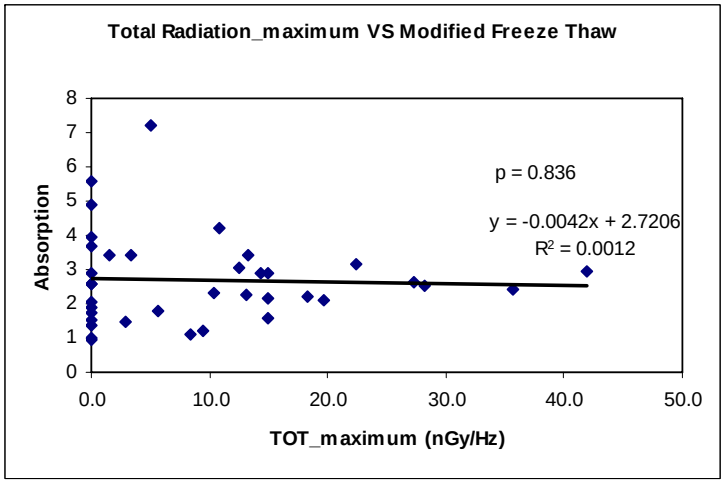
Total Radiation_maximum VS Modified Freeze Thaw
Absorption
TOT_maximum (nGy/Hz)
p = 0.836
y = -0.0042x + 2.7206
R2 = 0.0012

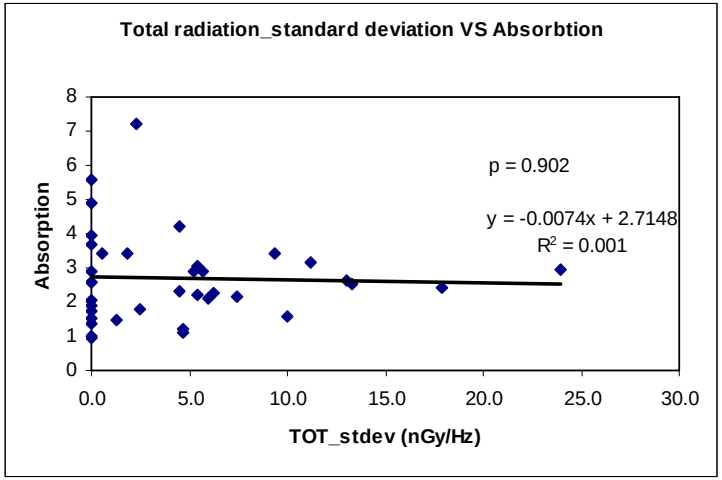
Total radiation_standard deviation VS Absorbtion
Absorption
TOT_stdev (nGy/Hz)
p = 0.902
y = -0.0074x + 2.7148
R2 = 0.001

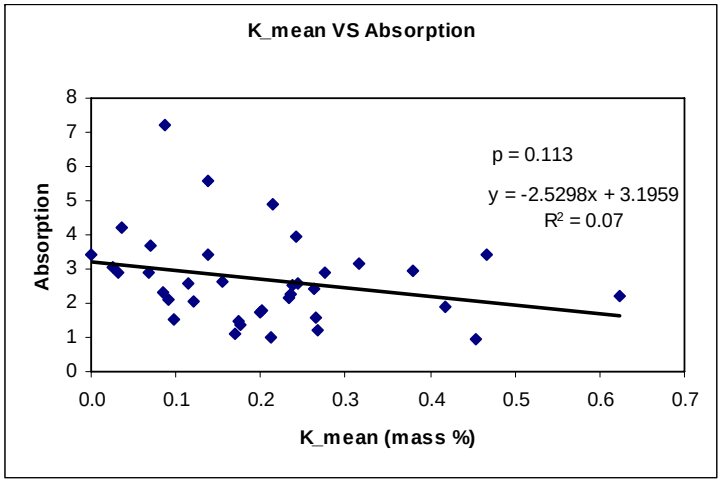
K_mean VS Absorption
Absorption
K_mean (mass %)
p = 0.113
y = -2.5298x + 3.1959
R² = 0.07

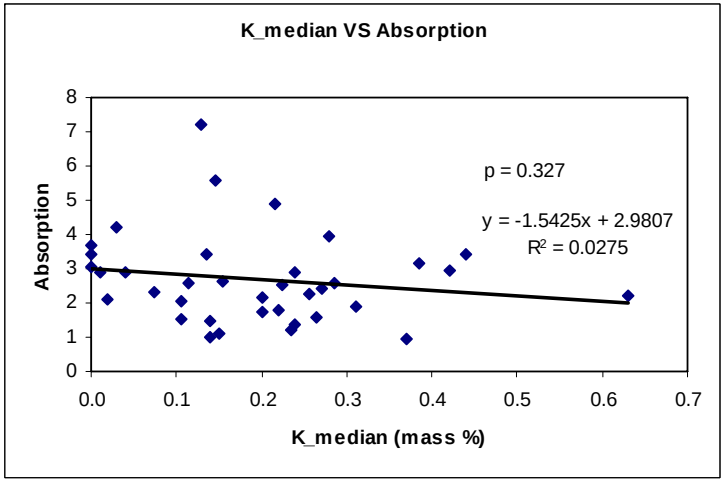
K_median VS Absorption
Absorption
K_median (mass %)
p = 0.327
y = -1.5425x + 2.9807
R² = 0.0275

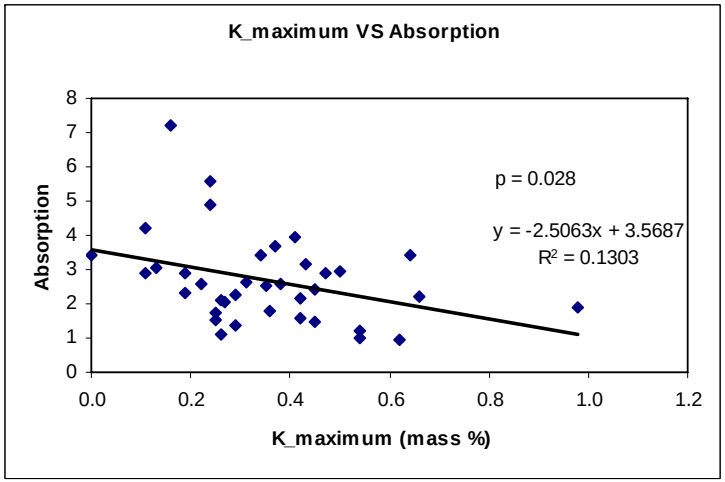
K_maximum VS Absorption
Absorption
K_maximum (mass %)
p = 0.028
y = -2.5063x + 3.5687
R² = 0.1303

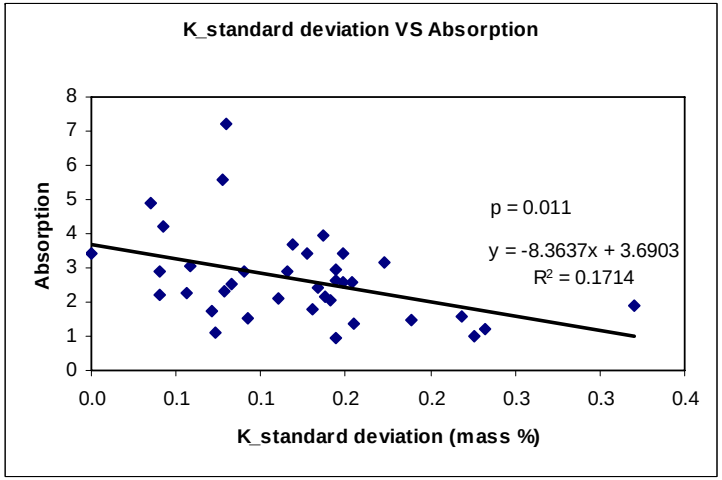
K_standard deviation VS Absorption
Absorption
K_standard deviation (mass %)
p = 0.011
y = -8.3637x + 3.6903
R² = 0.1714

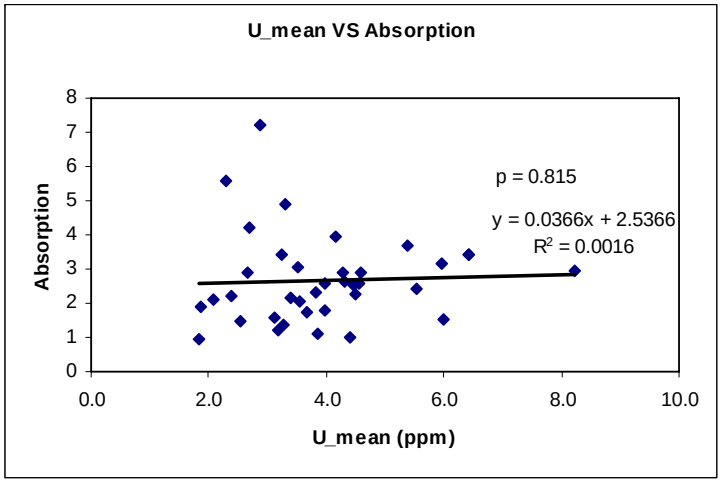
U_mean VS Absorption
Absorption
U_mean (ppm)
p = 0.815
y = 0.0366x + 2.5366
R2 = 0.0016
0
1
2
3
4
5
6
7
8
0.0
2.0
4.0
6.0
8.0
10.0

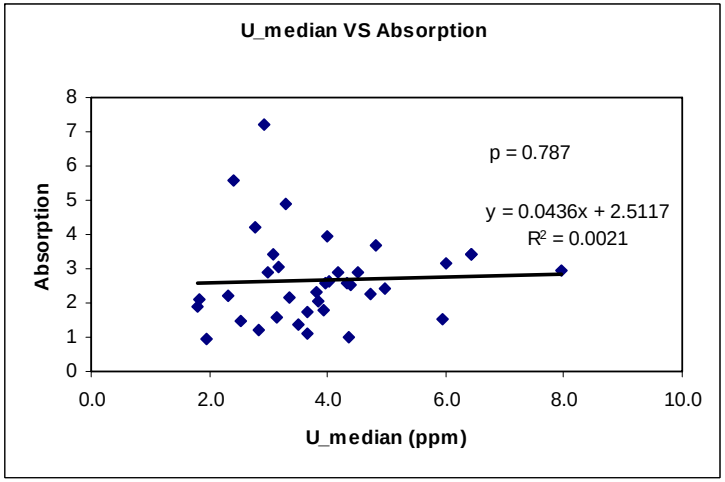
U_median VS Absorption
Absorption
U_median (ppm)
p = 0.787
y = 0.0436x + 2.5117
R2 = 0.0021
0
1
2
3
4
5
6
7
8
0.0
2.0
4.0
6.0
8.0
10.0

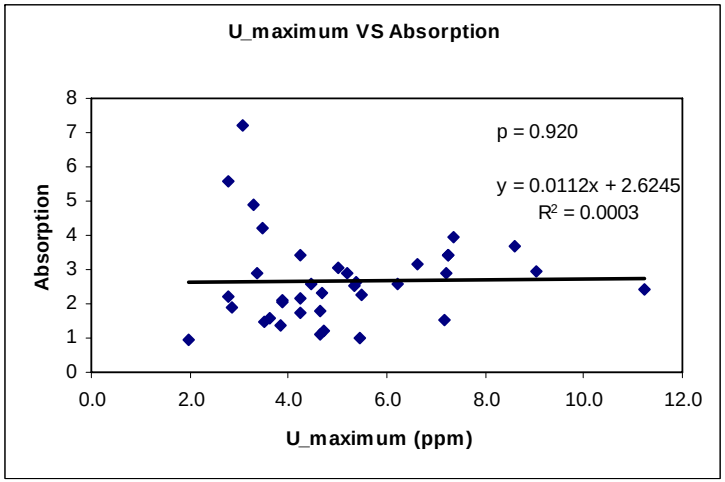
U_maximum VS Absorption
Absorption
U_maximum (ppm)
p = 0.920
y = 0.0112x + 2.6245
R2 = 0.0003
0
1
2
3
4
5
6
7
8
0.0
2.0
4.0
6.0
8.0
10.0
12.0

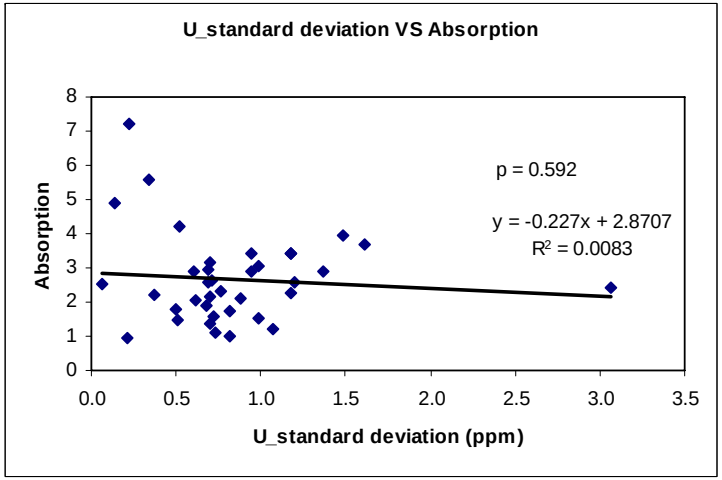
U_standard deviation VS Absorption
Absorption
U_standard deviation (ppm)
p = 0.592
y = -0.227x + 2.8707
R2 = 0.0083
0
1
2
3
4
5
6
7
8
0.0
0.5
1.0
1.5
2.0
2.5
3.0
3.5

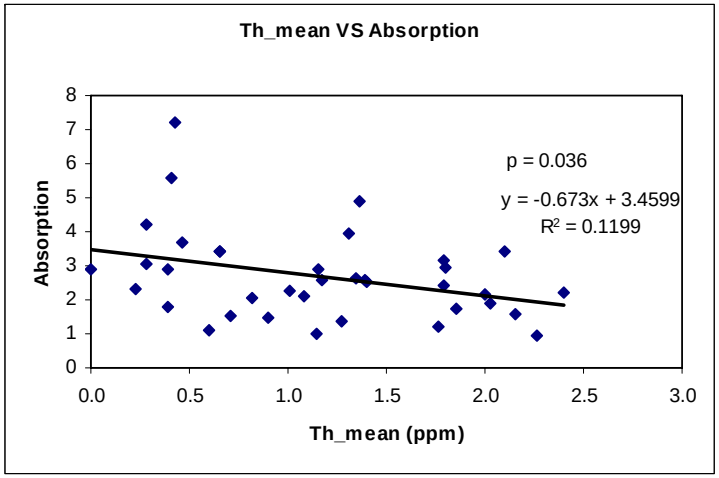
Th_mean VS Absorption
Absorption
Th_mean (ppm)
p = 0.036
y = -0.673x + 3.4599
R² = 0.1199

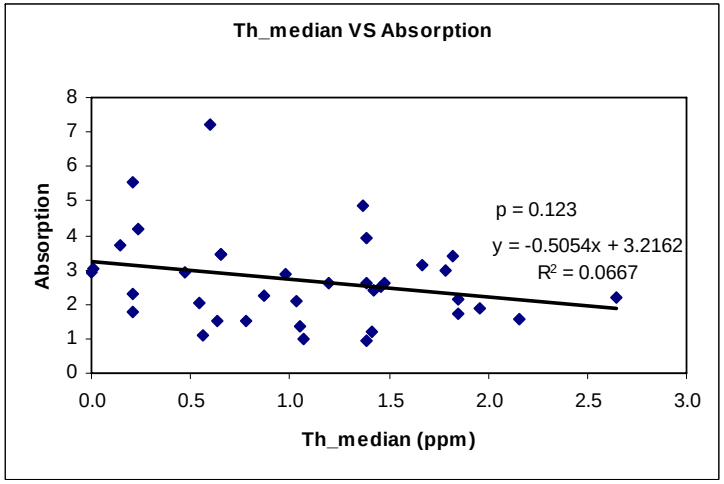
Th_median VS Absorption
Absorption
Th_median (ppm)
p = 0.123
y = -0.5054x + 3.2162
R² = 0.0667

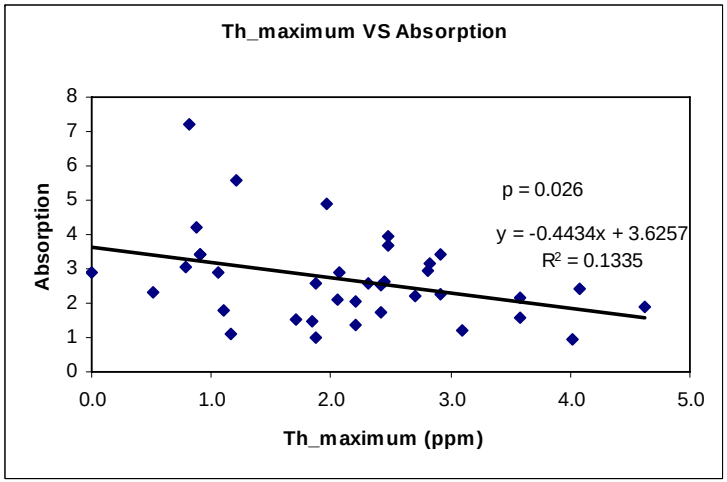
Th_maximum VS Absorption
Absorption
Th_maximum (ppm)
p = 0.026
y = -0.4434x + 3.6257
R² = 0.1335

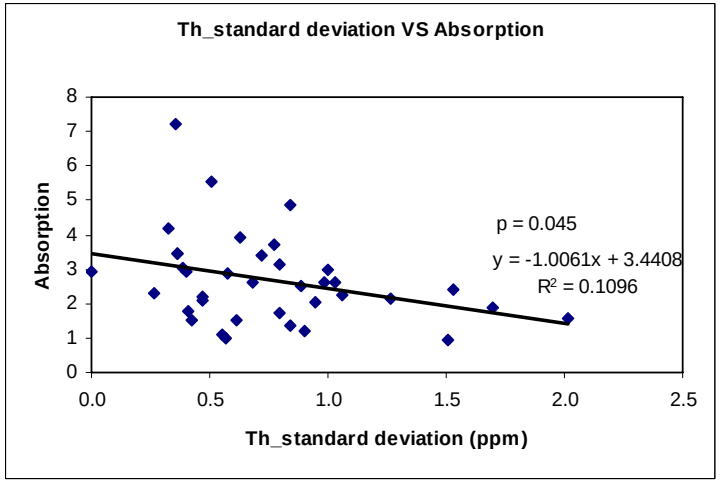
Th_standard deviation VS Absorption
Absorption
Th_standard deviation (ppm)
p = 0.045
y = -1.0061x + 3.4408
R² = 0.1096

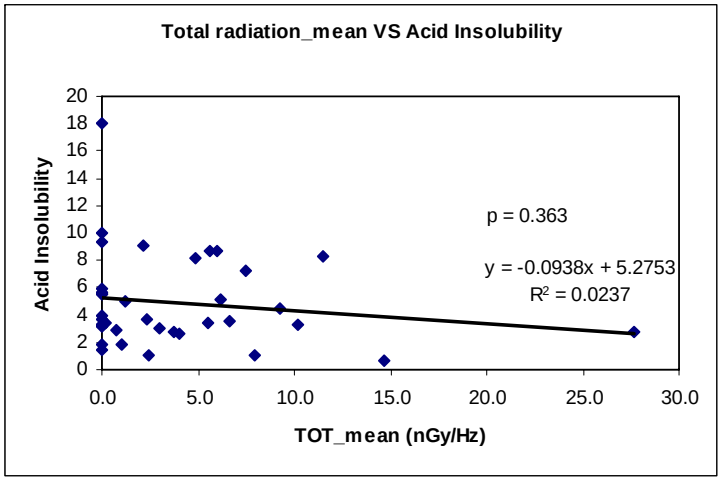
Total radiation_mean VS Acid Insolubility
Acid Insolubility
TOT_mean (nGy/Hz)
p = 0.363
y = -0.0938x + 5.2753
R² = 0.0237

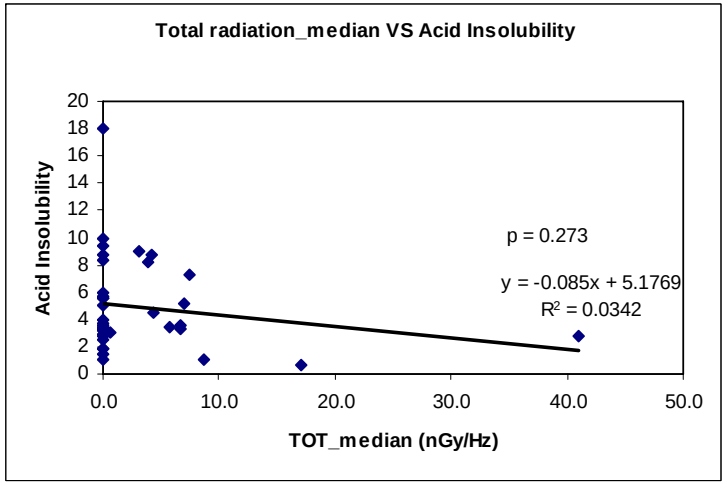
Total radiation_median VS Acid Insolubility
Acid Insolubility
TOT_median (nGy/Hz)
p = 0.273
y = -0.085x + 5.1769
R² = 0.0342

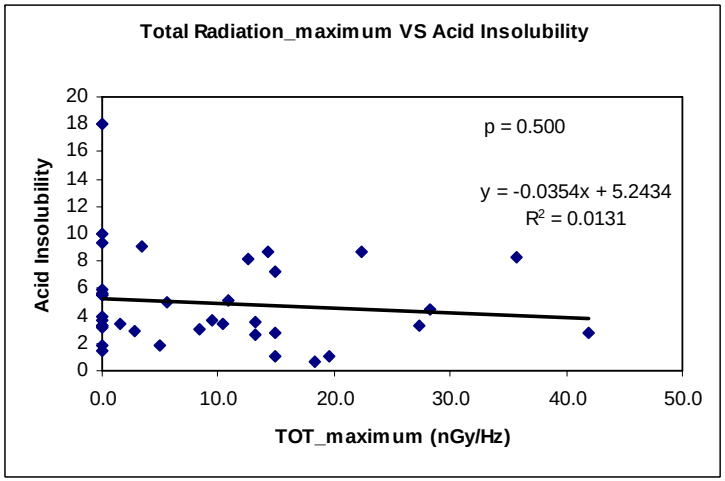
Total Radiation_maximum VS Acid Insolubility
Acid Insolubility
TOT_maximum (nGy/Hz)
p = 0.500
y = -0.0354x + 5.2434
R² = 0.0131

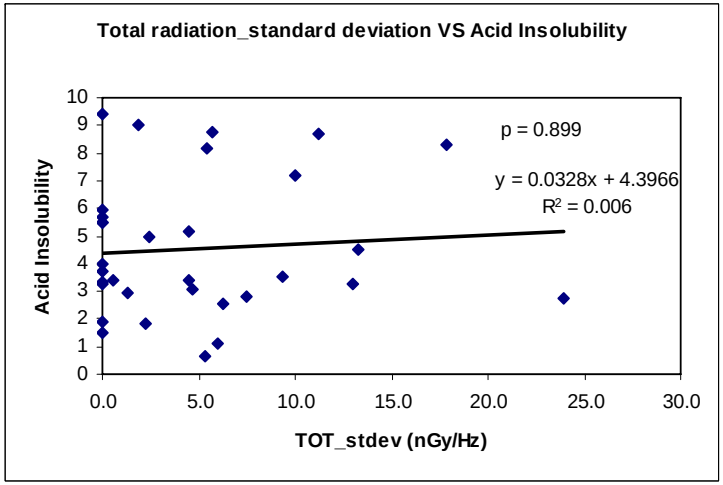
Total radiation_standard deviation VS Acid Insolubility
Acid Insolubility
TOT_stdev (nGy/Hz)
p = 0.899
y = 0.0328x + 4.3966
R² = 0.006

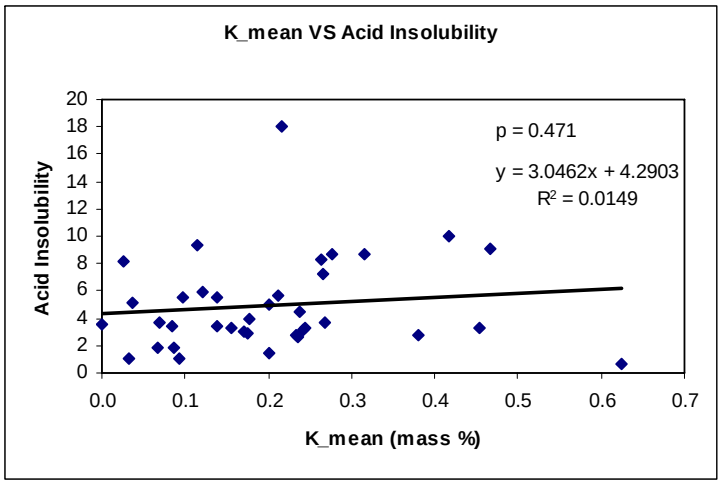
K_mean VS Acid Insolubility
Acid Insolubility
K_mean (mass %)
p = 0.471
y = 3.0462x + 4.2903
R² = 0.0149

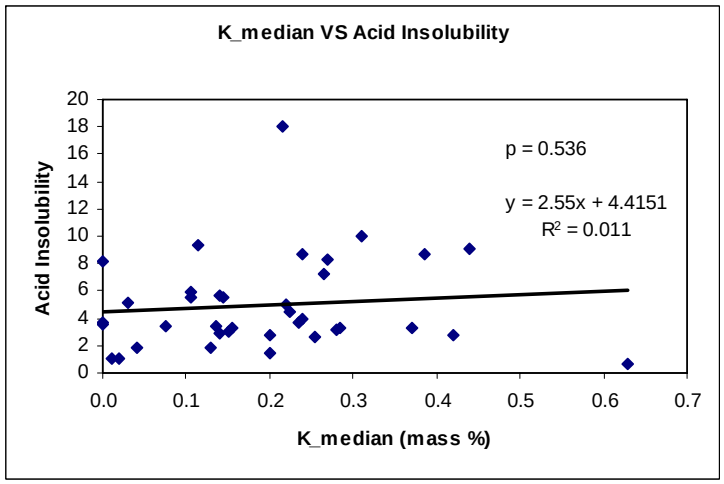
K_median VS Acid Insolubility
Acid Insolubility
K_median (mass %)
p = 0.536
y = 2.55x + 4.4151
R² = 0.011

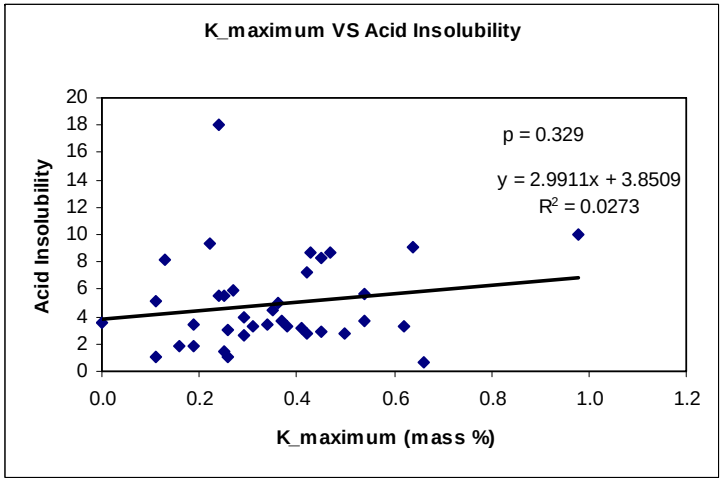
K_maximum VS Acid Insolubility
Acid Insolubility
K_maximum (mass %)
p = 0.329
y = 2.9911x + 3.8509
R² = 0.0273

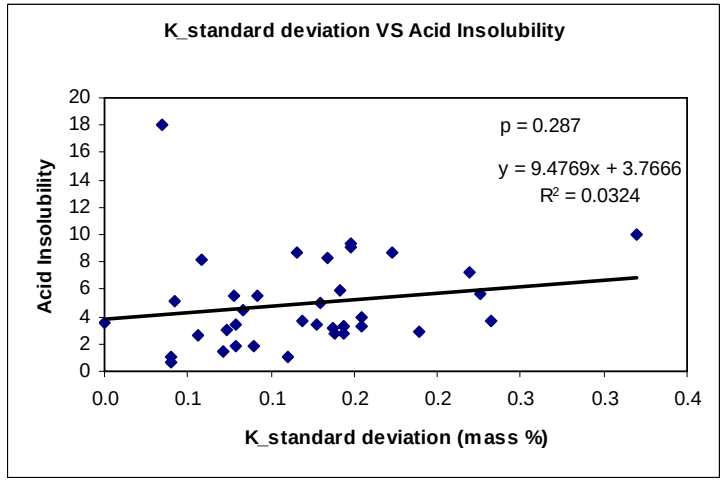
K_standard deviation VS Acid Insolubility
Acid Insolubility
K_standard deviation (mass %)
p = 0.287
y = 9.4769x + 3.7666
R² = 0.0324

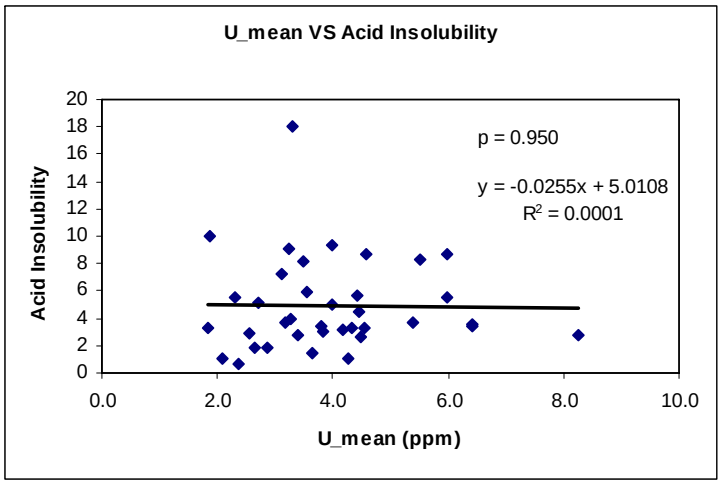
U_mean VS Acid Insolubility
Acid Insolubility
U_mean (ppm)
p = 0.950
y = -0.0255x + 5.0108
R2 = 0.0001

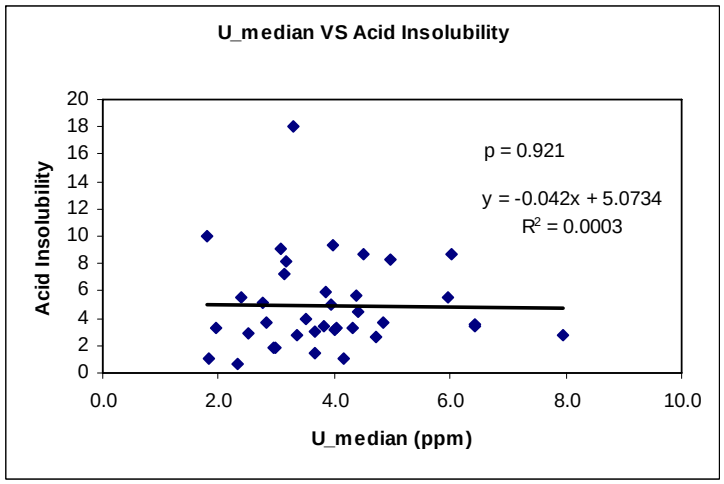
U_median VS Acid Insolubility
Acid Insolubility
U_median (ppm)
p = 0.921
y = -0.042x + 5.0734
R2 = 0.0003

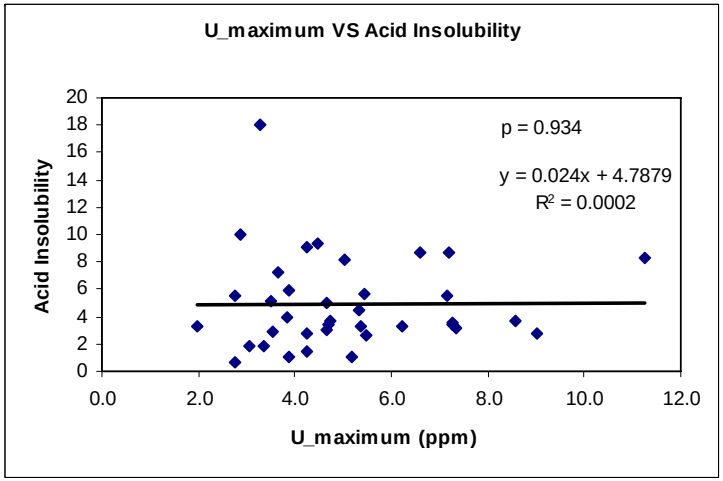
U_maximum VS Acid Insolubility
Acid Insolubility
U_maximum (ppm)
p = 0.934
y = 0.024x + 4.7879
R2 = 0.0002

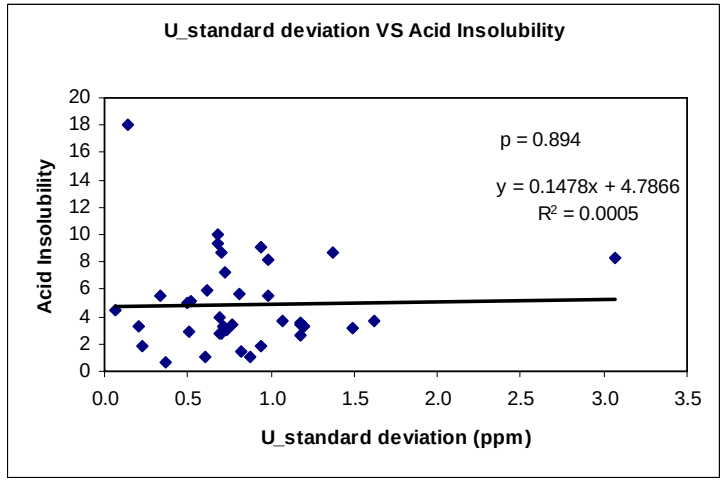
U_standard deviation VS Acid Insolubility
Acid Insolubility
U_standard deviation (ppm)
p = 0.894
y = 0.1478x + 4.7866
R2 = 0.0005

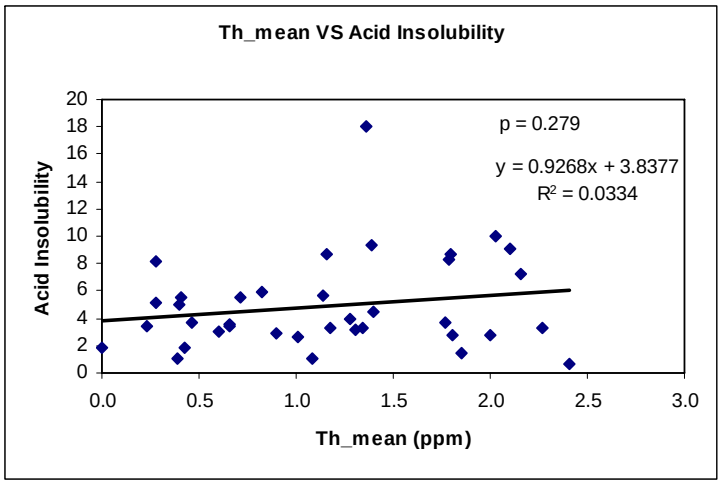
Th_mean VS Acid Insolubility
p = 0.279
y = 0.9268x + 3.8377
R² = 0.0334
Acid Insolubility
Th_mean (ppm)

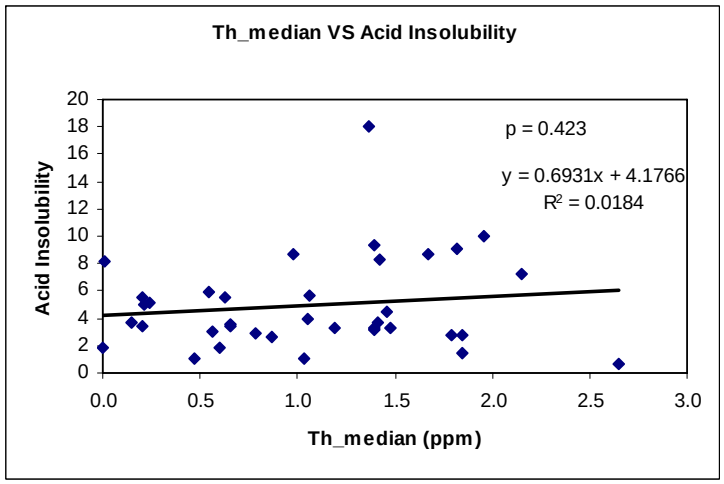
Th_median VS Acid Insolubility
p = 0.423
y = 0.6931x + 4.1766
R² = 0.0184
Acid Insolubility
Th_median (ppm)

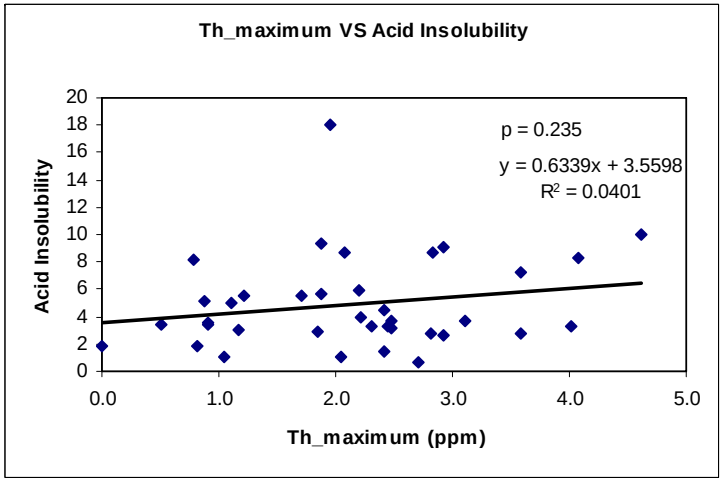
Th_maximum VS Acid Insolubility
p = 0.235
y = 0.6339x + 3.5598
R² = 0.0401
Acid Insolubility
Th_maximum (ppm)

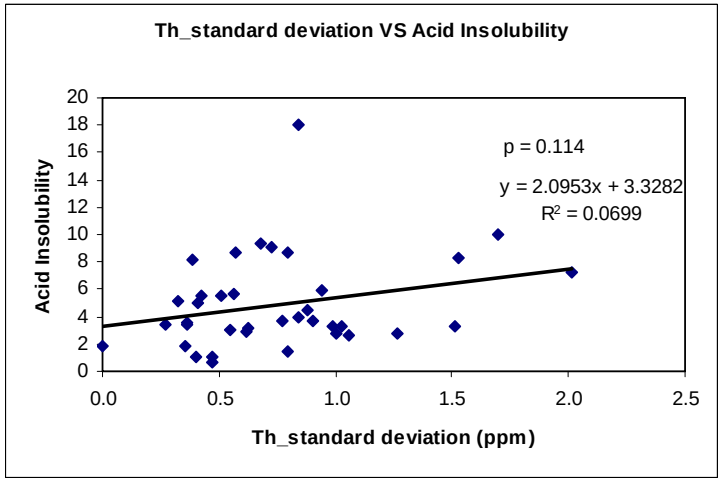
Th_standard deviation VS Acid Insolubility
p = 0.114
y = 2.0953x + 3.3282
R² = 0.0699
Acid Insolubility
Th_standard deviation (ppm)

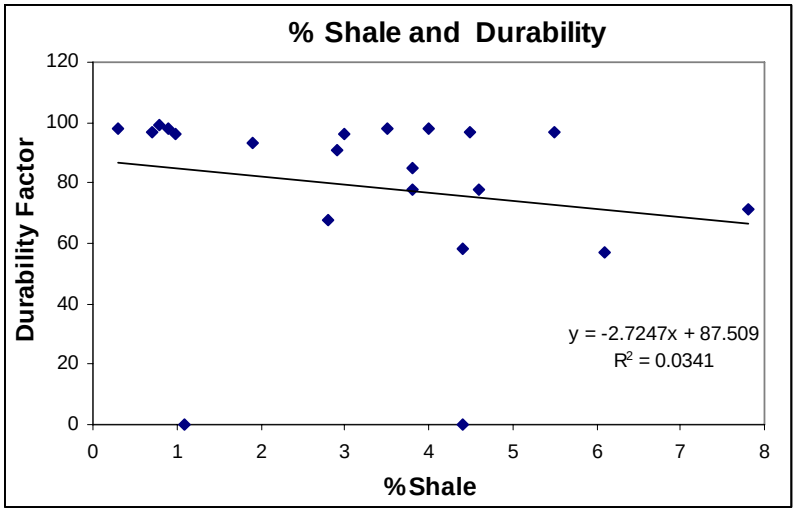
% Shale and Durability
Durability Factor
%Shale
y = -2.7247x + 87.509
R² = 0.0341

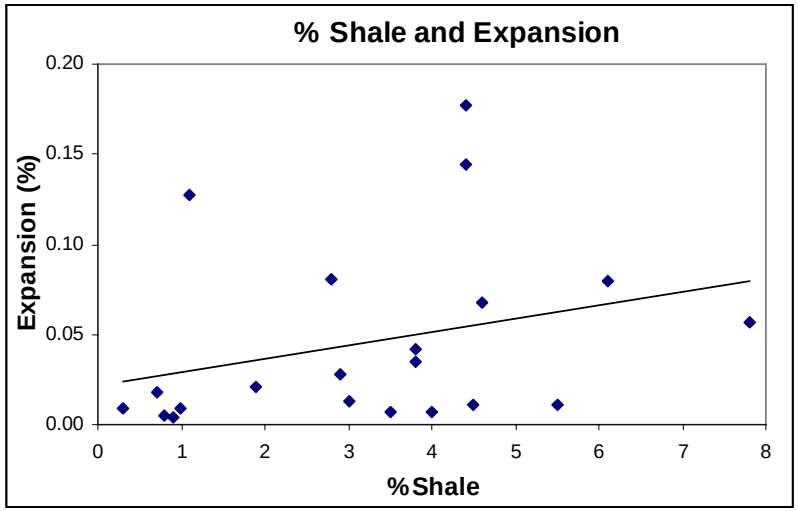
% Shale and Expansion
Expansion (%)
%Shale

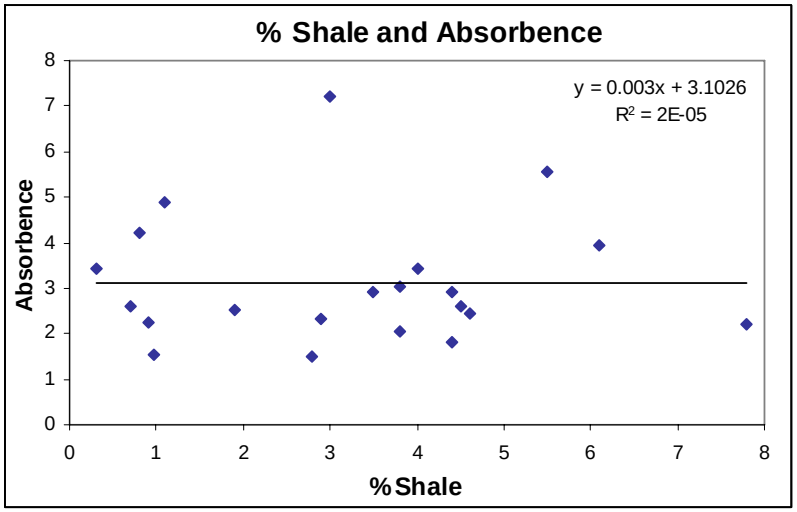
% Shale and Absorbence
Absorbence
%Shale
y = 0.003x + 3.1026
R² = 2E-05

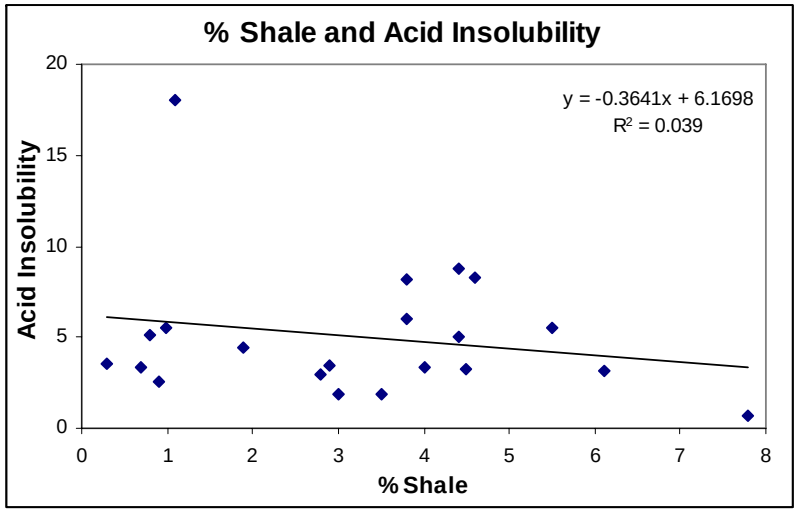
% Shale and Acid Insolubility
Acid Insolubility
%Shale
y = -0.3641x + 6.1698
R² = 0.039

Chi-square output tables of the association between pass/fail designation and:

1) Number of Clays Present
2) Major Clay

P_F		MajClay chlorite	illite	ill_chl	
Fail	Observed	0	15	6	21
	Expected	0.57	15.89	4.54	
	Cell Chi-Sq	0.57	0.05	0.47	
Pass	Observed	1	13	2	16
	Expected	0.43	12.11	3.46	
	Cell Chi-Sq	0.74	0.07	0.62	
		1	28	8	37

Overall Chi-Square 2.51
P-Value 0.2846
Degrees of Freedom 2
CAUTION: 2 cell(s) have expected values less than 1.0
Cases Included 37 Missing Cases 0

3) Smectite presence

P_F		smectite 0	1	
Fail	Observed	14	7	21
	Expected	13.62	7.38	
	Cell Chi-Sq	0.01	0.02	
Pass	Observed	10	6	16
	Expected	10.38	5.62	
	Cell Chi-Sq	0.01	0.03	
		24	13	37

Overall Chi-Square 0.07
P-Value 0.7925
Degrees of Freedom 1
Cases Included 37 Missing Cases 0

4) Kaolinite presence

P_F		kaolinite 0	1	
Fail	Observed	15	6	21
	Expected	16.46	4.54	
	Cell Chi-Sq	0.13	0.47	
Pass	Observed	14	2	16
	Expected	12.54	3.46	
	Cell Chi-Sq	0.17	0.62	
		29	8	37

Overall Chi-Square 1.38
P-Value 0.2394
Degrees of Freedom 1
CAUTION: 2 cell(s) have expected values less than 5.0
Cases Included 37 Missing Cases 0

Winterset Limestone

Section Name Ashgrove Aggregate-LaCygne Quarry Page 1 of 1

Location N38.38345
W94.61563

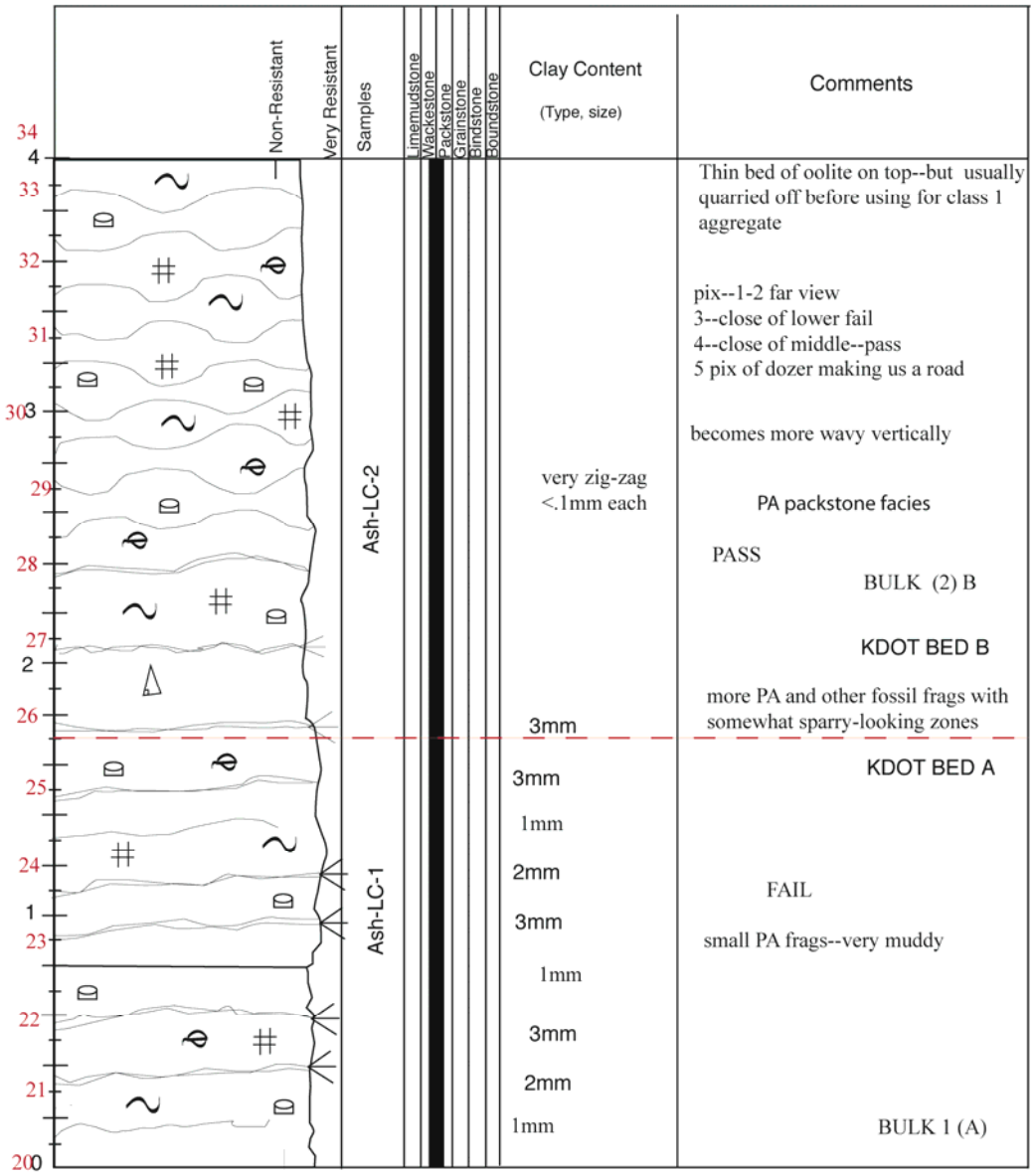

Bethany Falls Limestone--All Pass

Section Name Ashgrove Aggregates--LaCygne quarry Page 1 of 1

Location N38.38345
W94.61563

BETHANY FALLS LIMESTONE

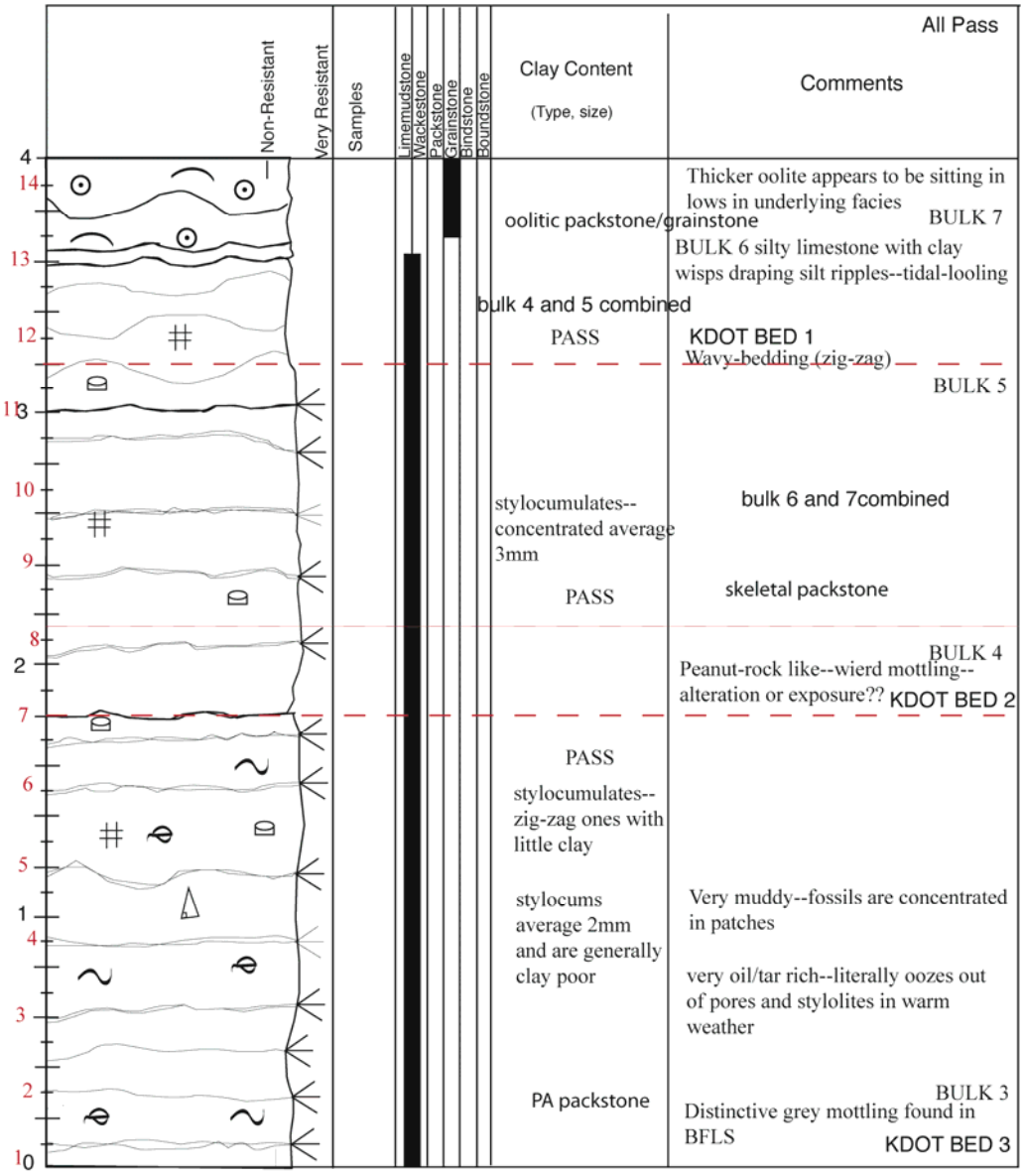

Section Name Martin Marietta Big Springs Quarry Page 1 of 1

Location N38.99009 W95.48541 Ervine Creek Limestone

KDOT 1-089-05 SN county Kansas

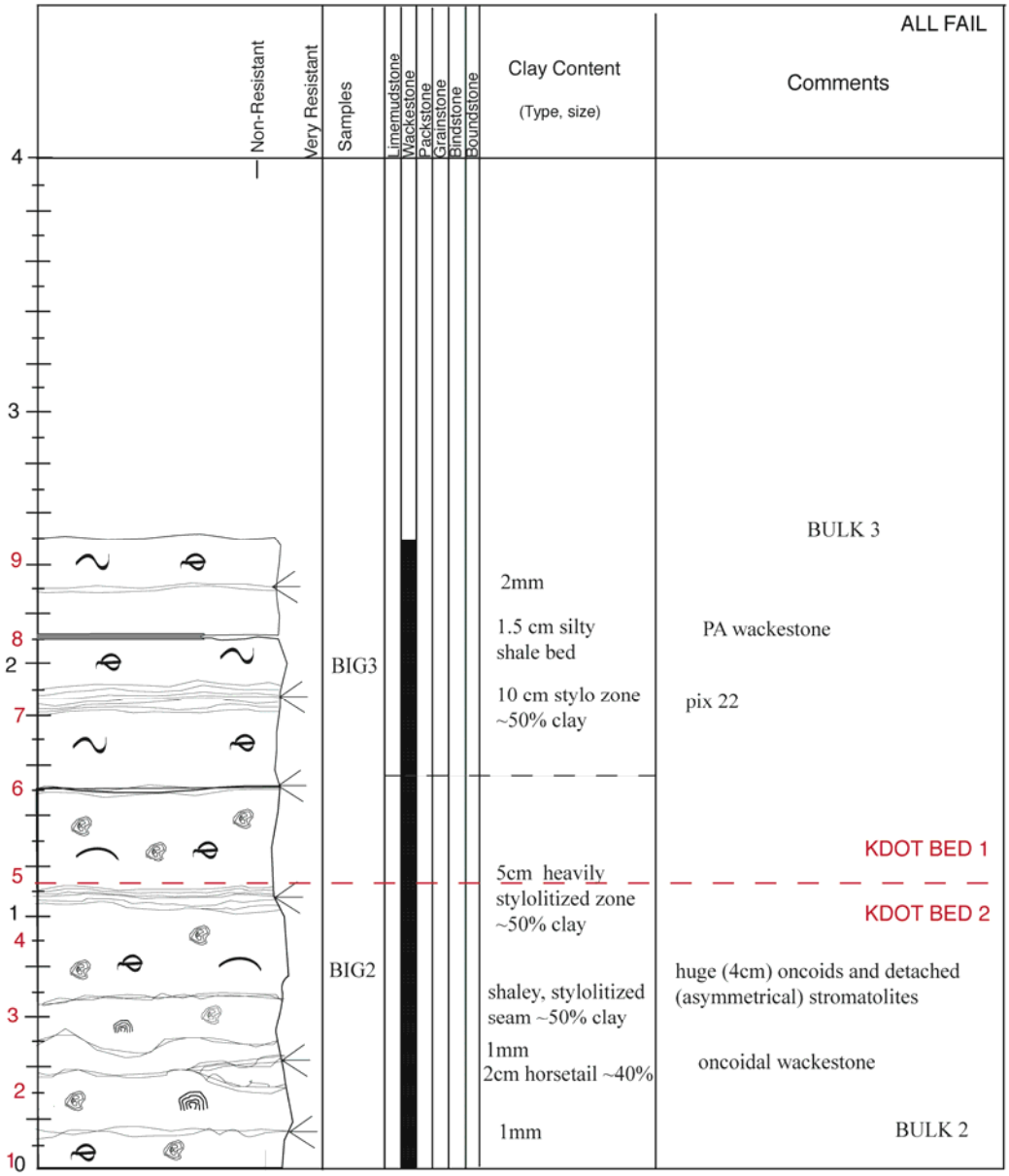

Section Name Martin Marietta--Greenwood Quarry Page 1 of 1

Location N38.81906
W94.32461

Bethany Falls Limestone

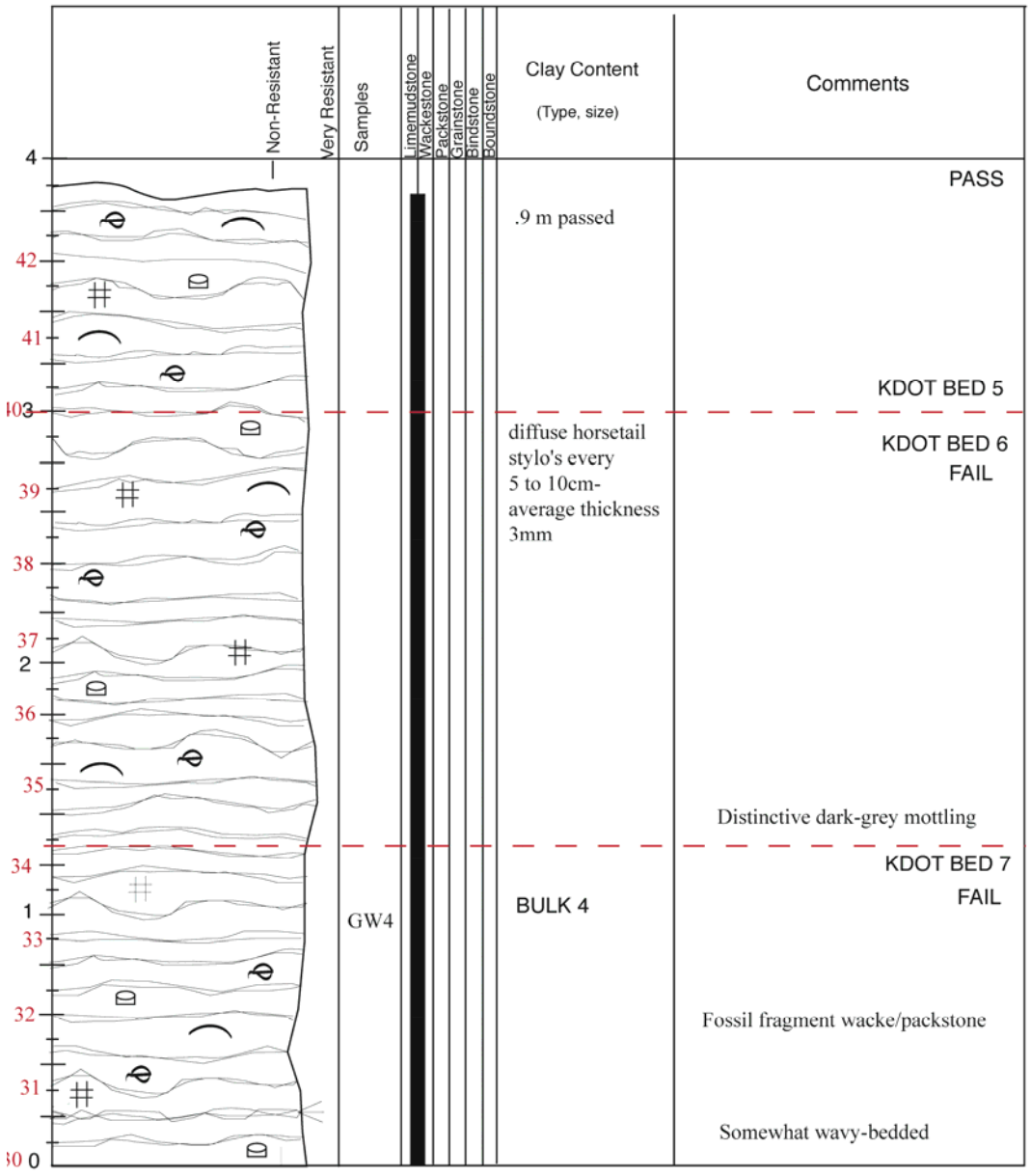

Winterset Limestone

Section Name Martin Marietta--Greenwood Quarry 2 Page 1 of 1

Location N38.81738
W94.32499

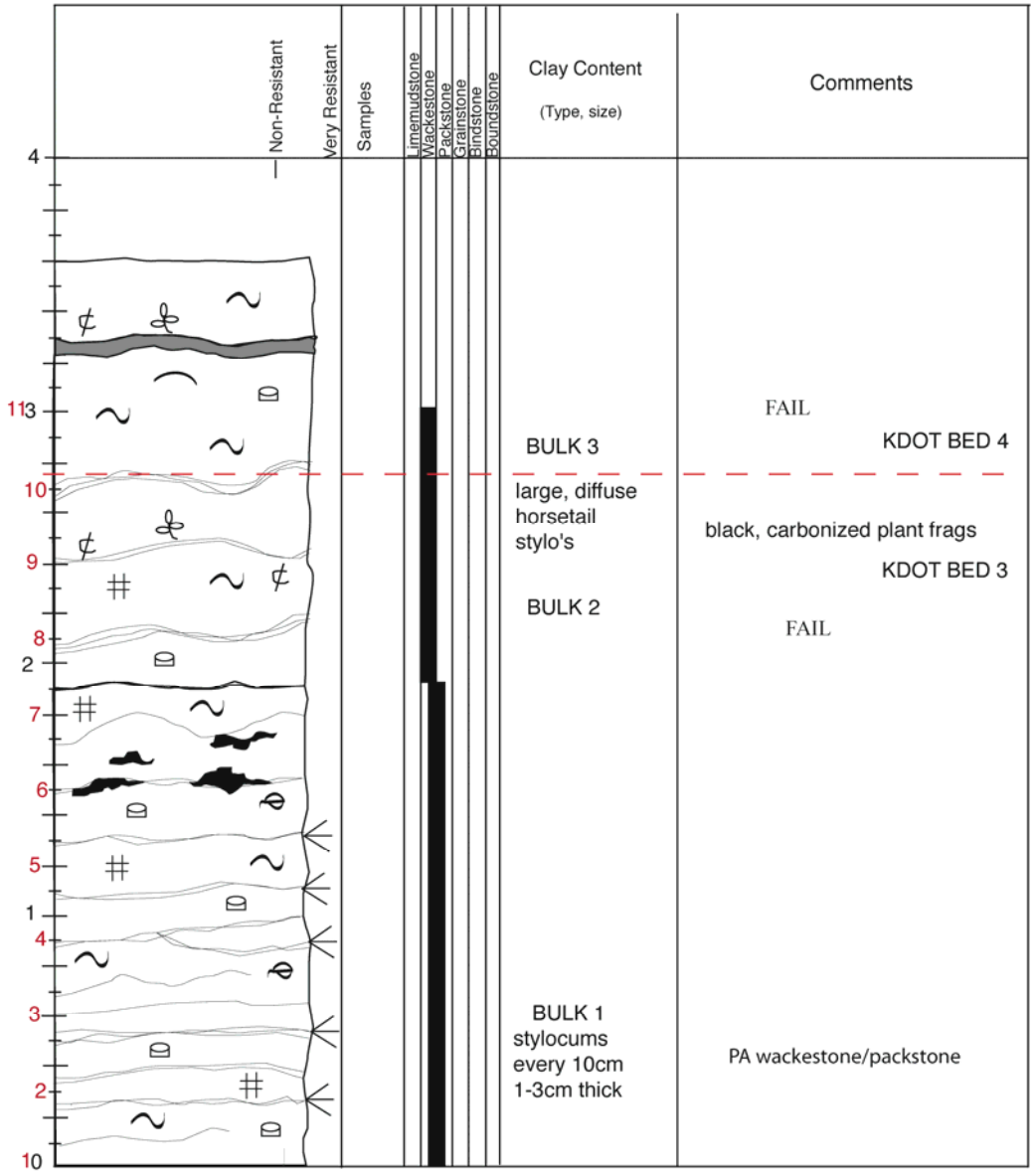

Plattsmouth Limestone

Section Name Hamm-Lawrence Quarry

Page 1 of 1

Location N39.04273
W95.25574

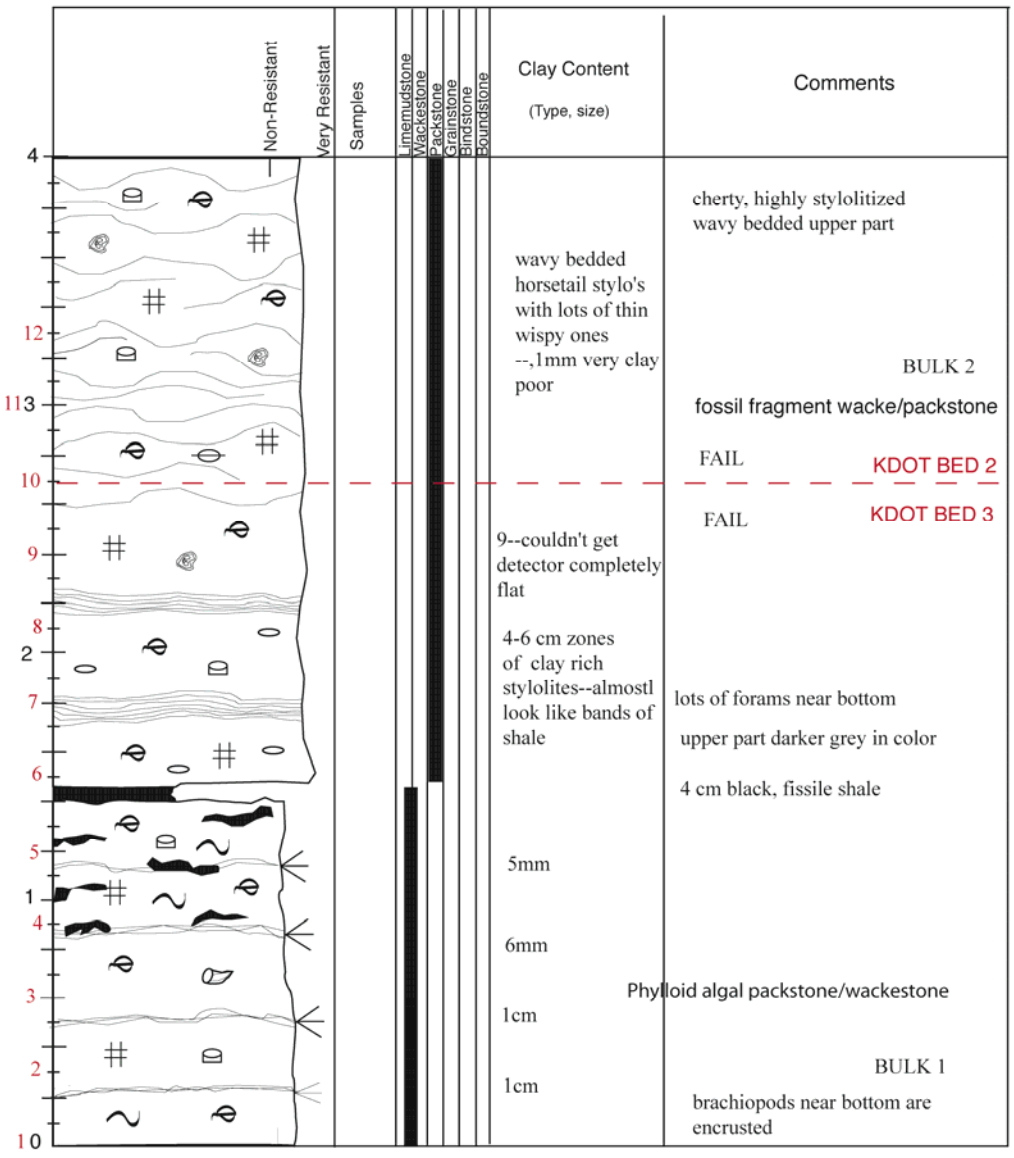

Lower Farley

Section Name Hunt Midwest--Sunflower Quarry Page 1 of 1

Location N38.93888
W94.9741

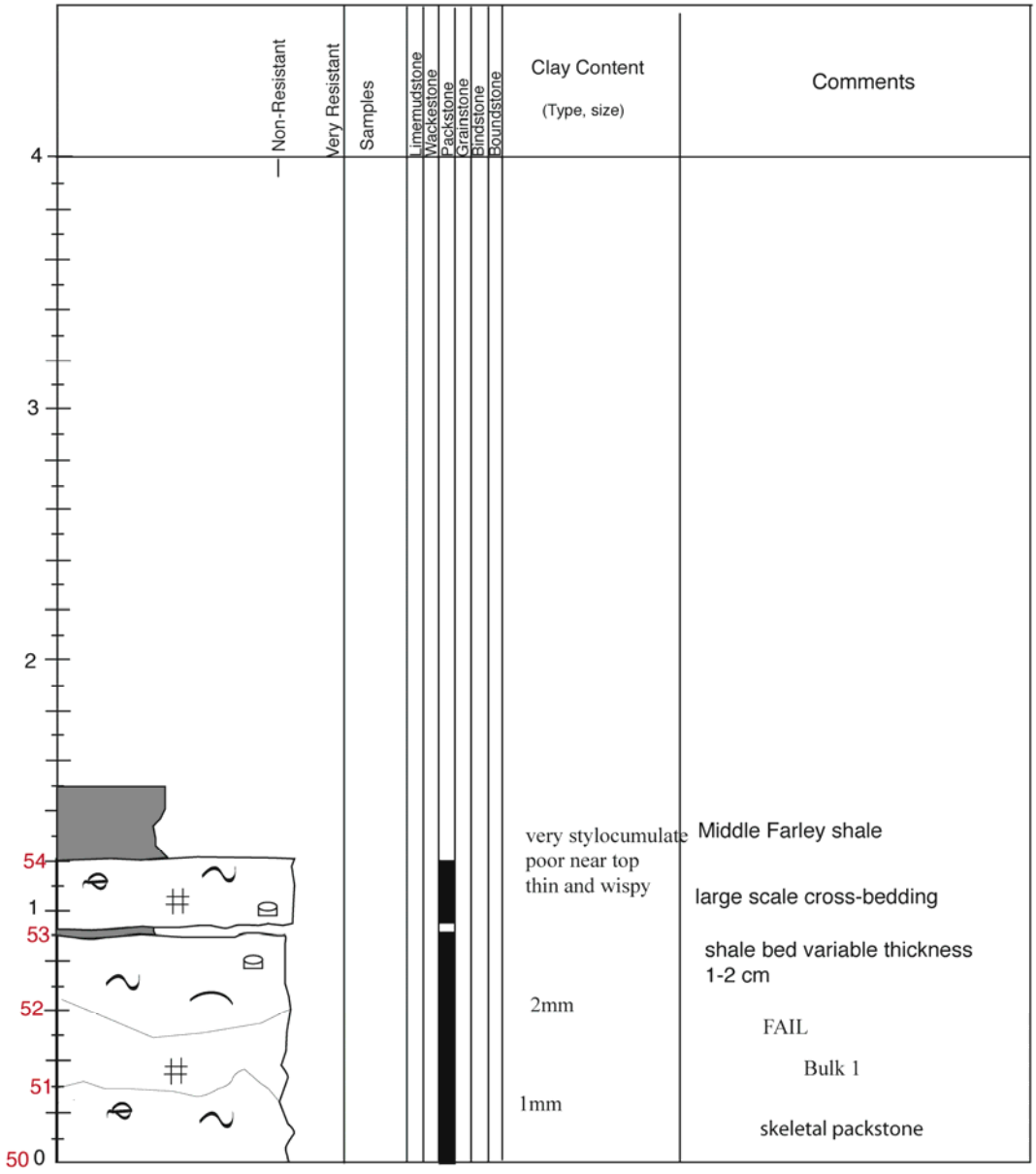

Section Name Hunt Midwest--Sunflower Page 1 of 1

Location N38.93888 W94.9741 Upper Farley Limestone

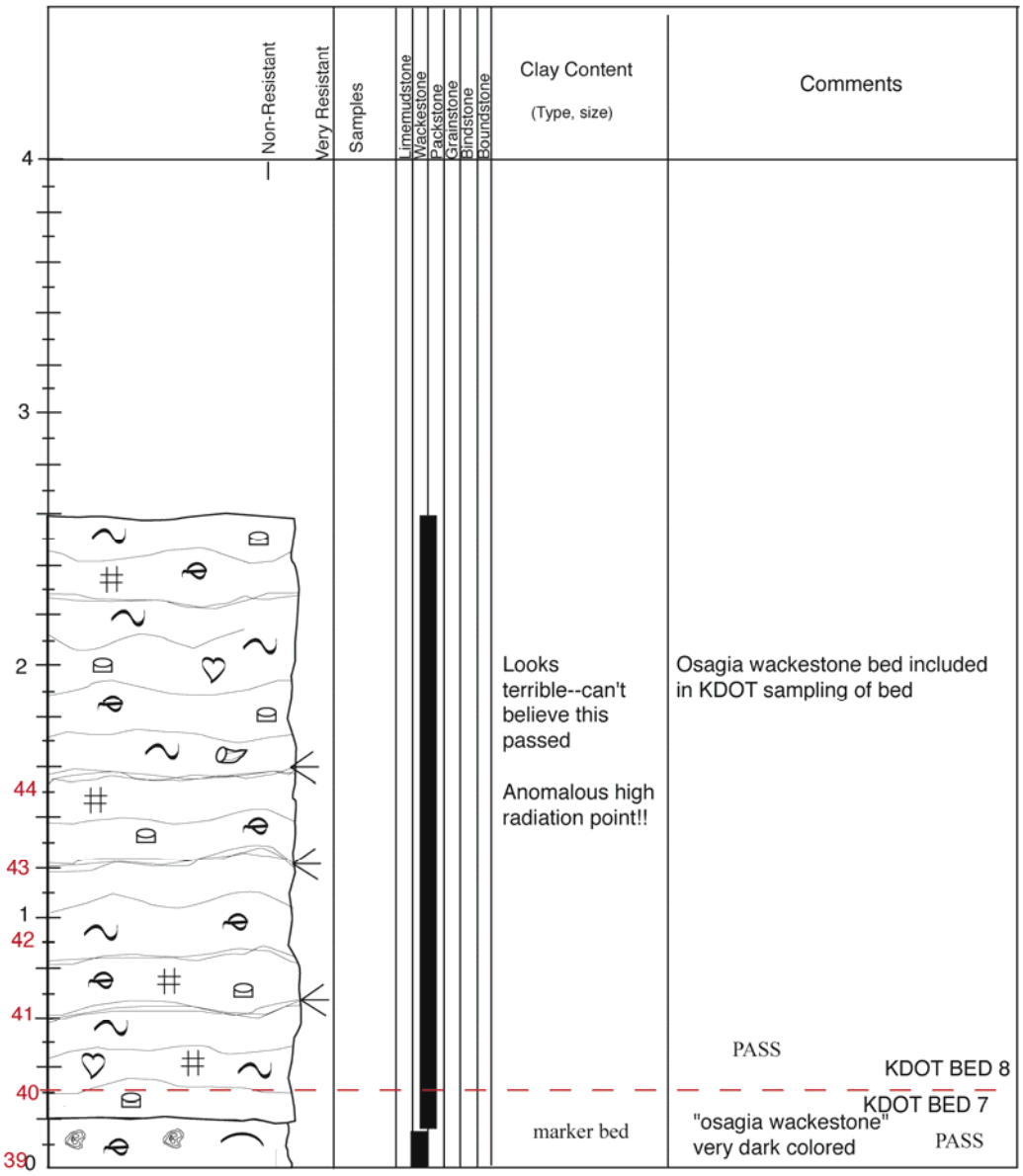

Section Name Johnson County Aggregate/Ashgrove 2 Page 1 of 1

Location N38.84861
W94.85795

Stoner Limestone

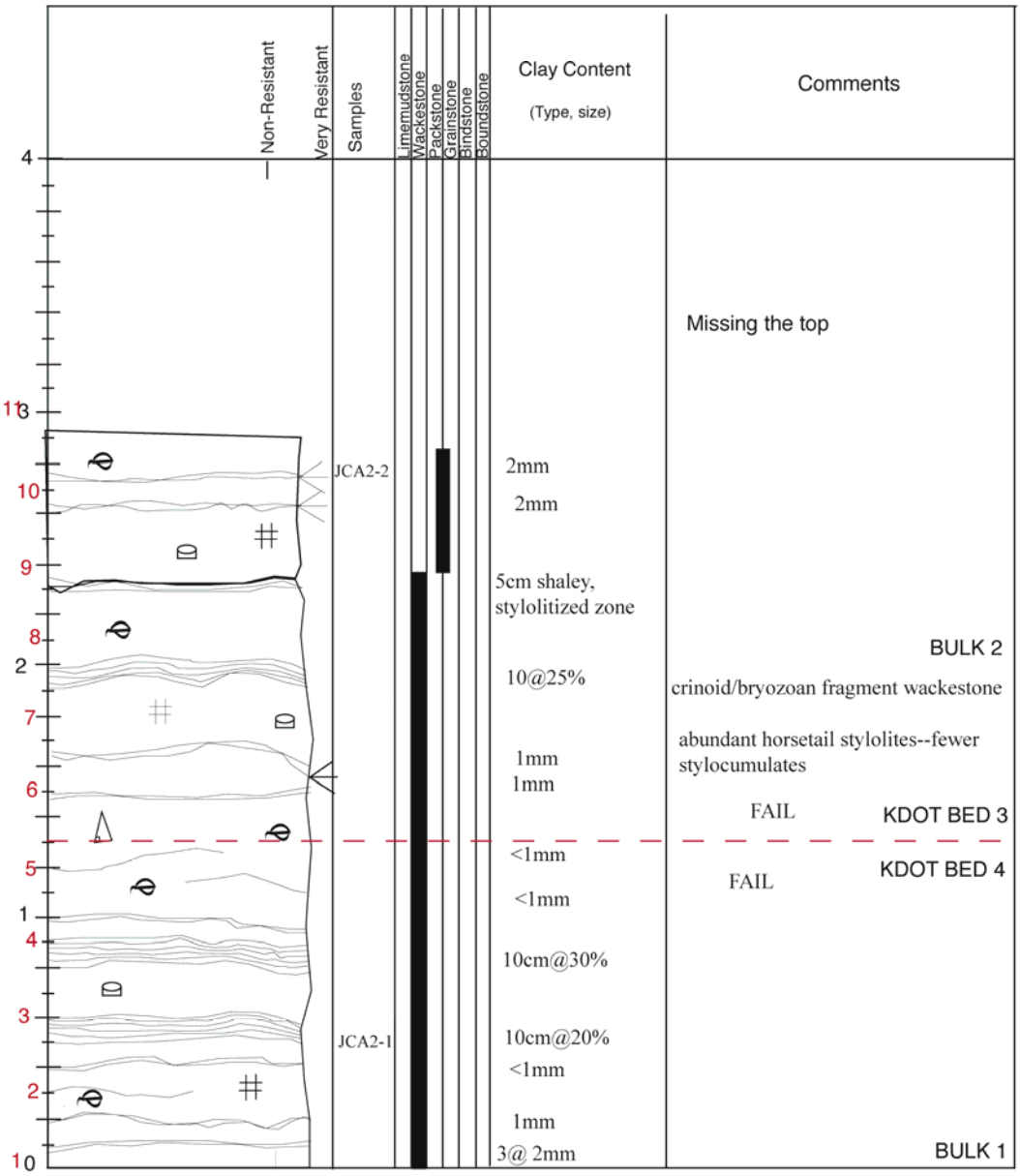

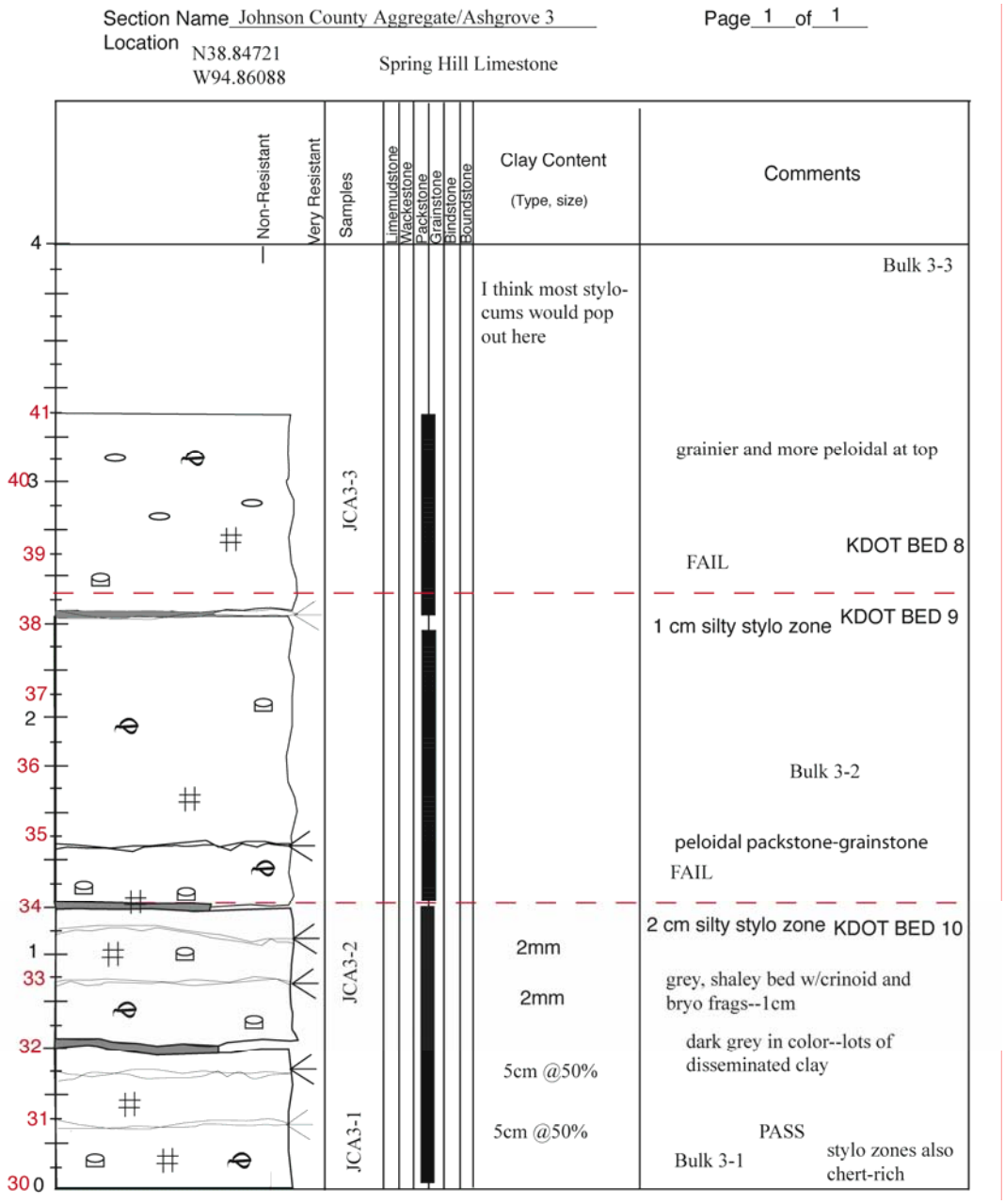
Section Name Johnson County Aggregate/Ashgrove 3
Page 1 of 1
Location N38.84721
W94.86088
Spring Hill Limestone
Non-Resistant
Very Resistant
Samples
Limemudstone
Wackestone
Packstone
Grainstone
Bindstone
Boundstone
Clay Content
(Type, size)
Comments
4
41
40
39
38
37
36
35
34
33
32
31
30
3
2
1
0
JCA3-3
JCA3-2
JCA3-1
I think most stylo-cums would pop out here
Bulk 3-3
grainier and more peloidal at top
FAIL
KDOT BED 8
1 cm silty stylo zone
KDOT BED 9
Bulk 3-2
peloidal packstone-grainstone
FAIL
2 cm silty stylo zone
KDOT BED 10
2mm
2mm
grey, shaley bed w/crinoid and bryo frags--1cm
dark grey in color--lots of disseminated clay
5cm @50%
5cm @50%
PASS
Bulk 3-1
stylo zones also chert-rich

Section Name Johnson County Aggregate 4 Page____of_____

Location N38.84781
W94.86104

Captian Creek Limestone

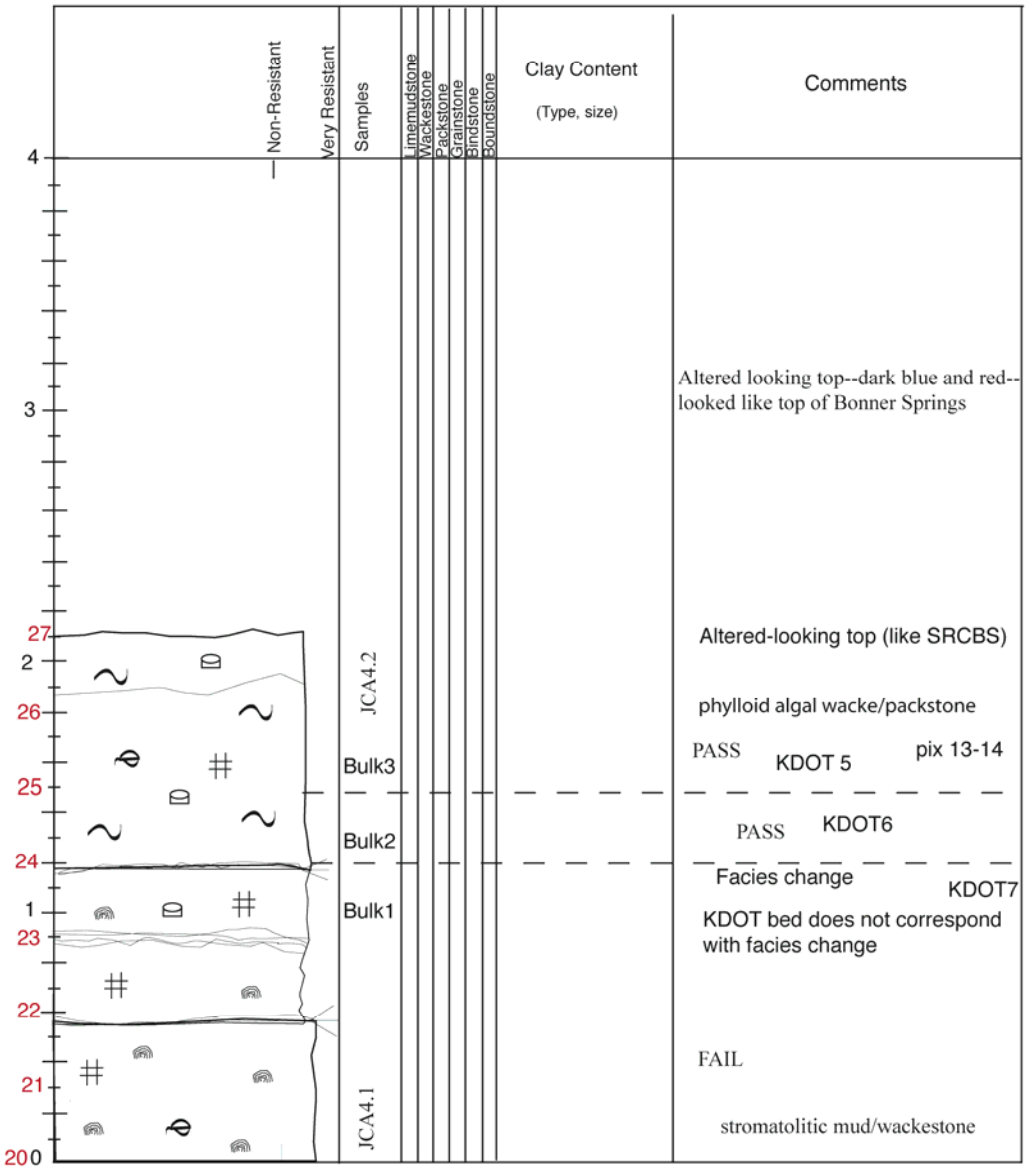

Section Name MM-Peculiar--small ledge Page 1 of 1

Location N38.73583
W94.50439

Bethany Falls Limestone

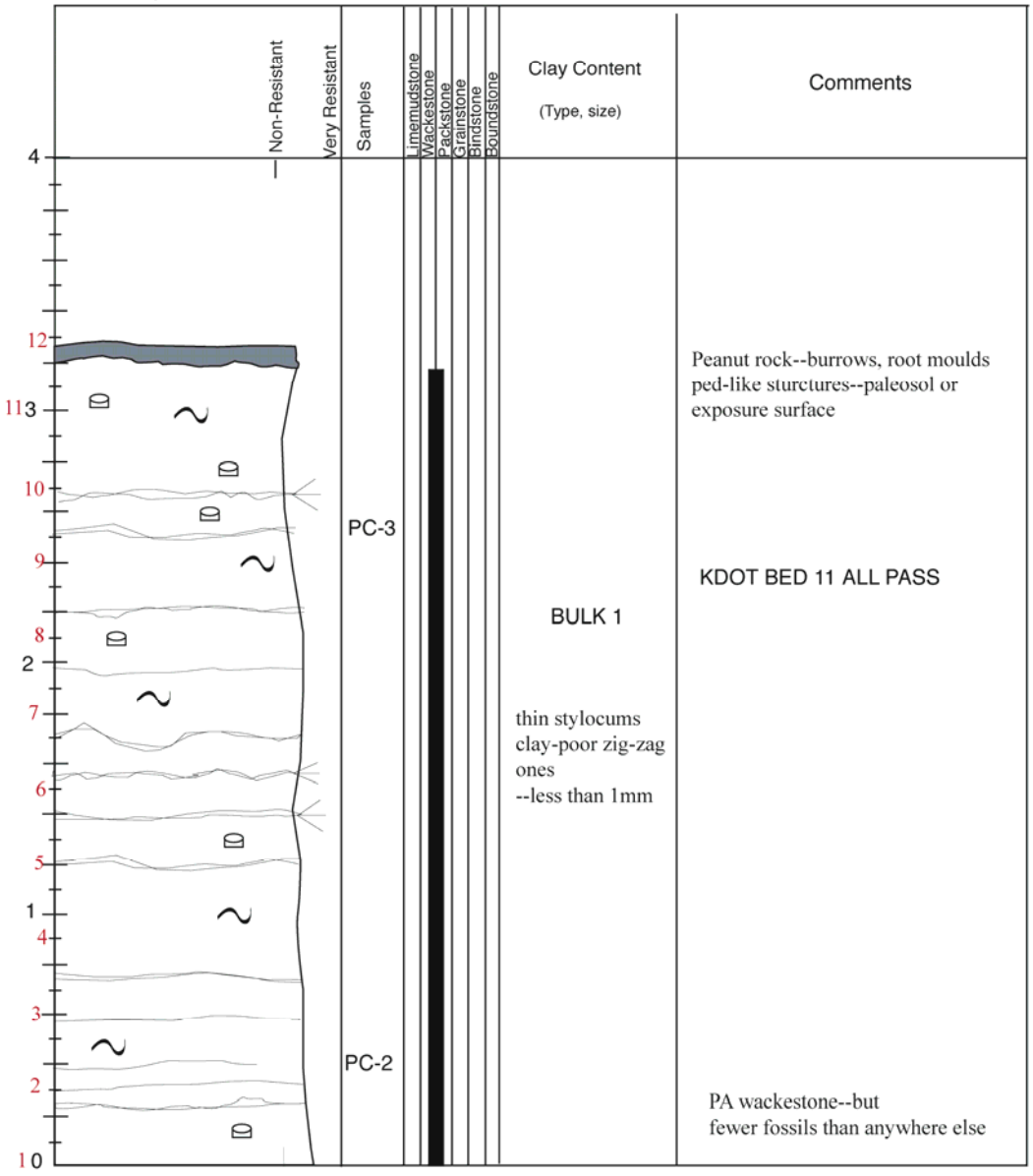

Section Name Martin Marietta Ottawa Quarry 2 Page 1 of 1

Location N38.65432 W95.25733 Stoner Limestone

KDOT 4-030-02 Franklin County

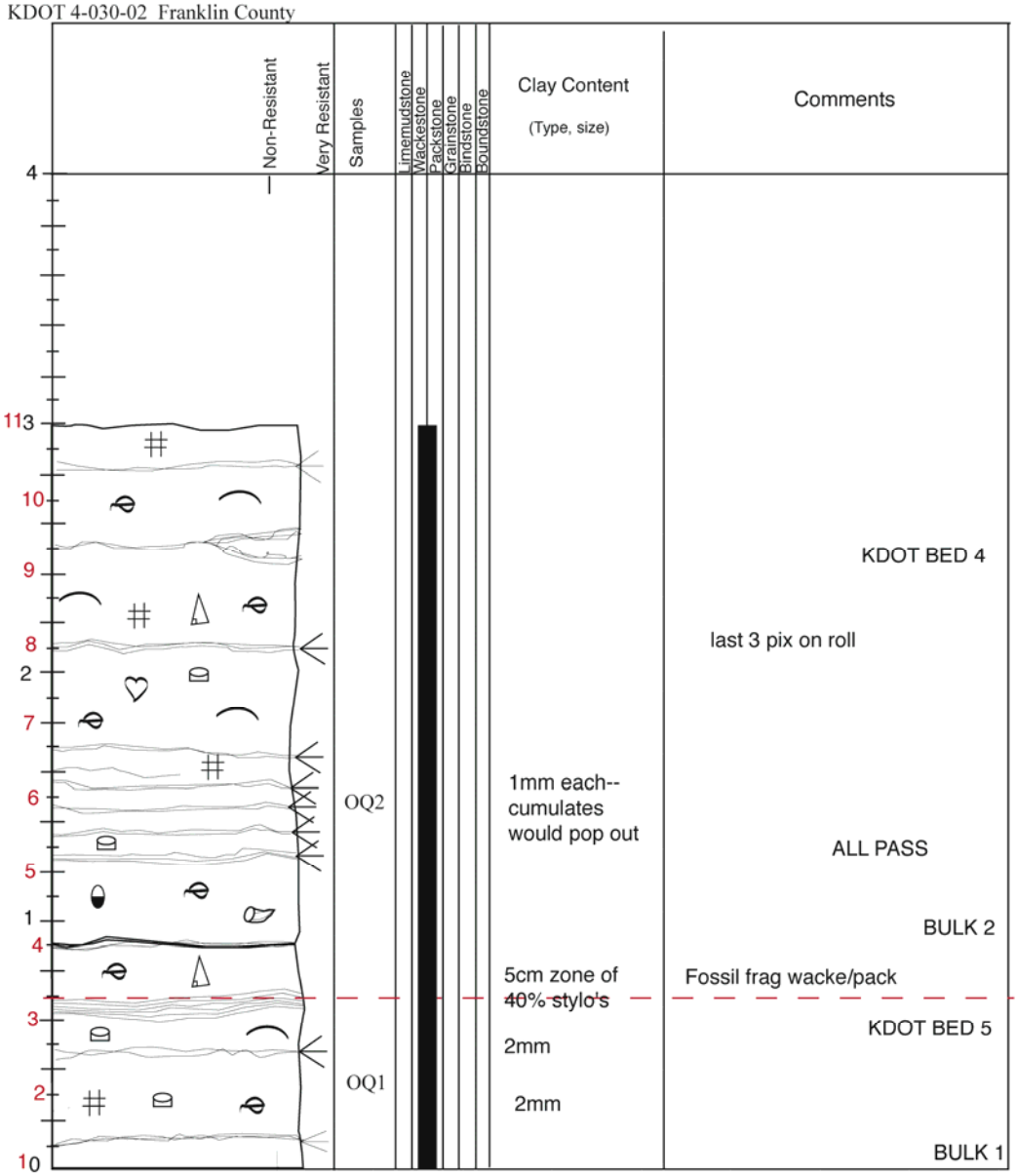

Section Name SRC_BS Farley--upper

Page 1 of 1

Location Shawnee rock company in JCL N39.07367 W94.89730

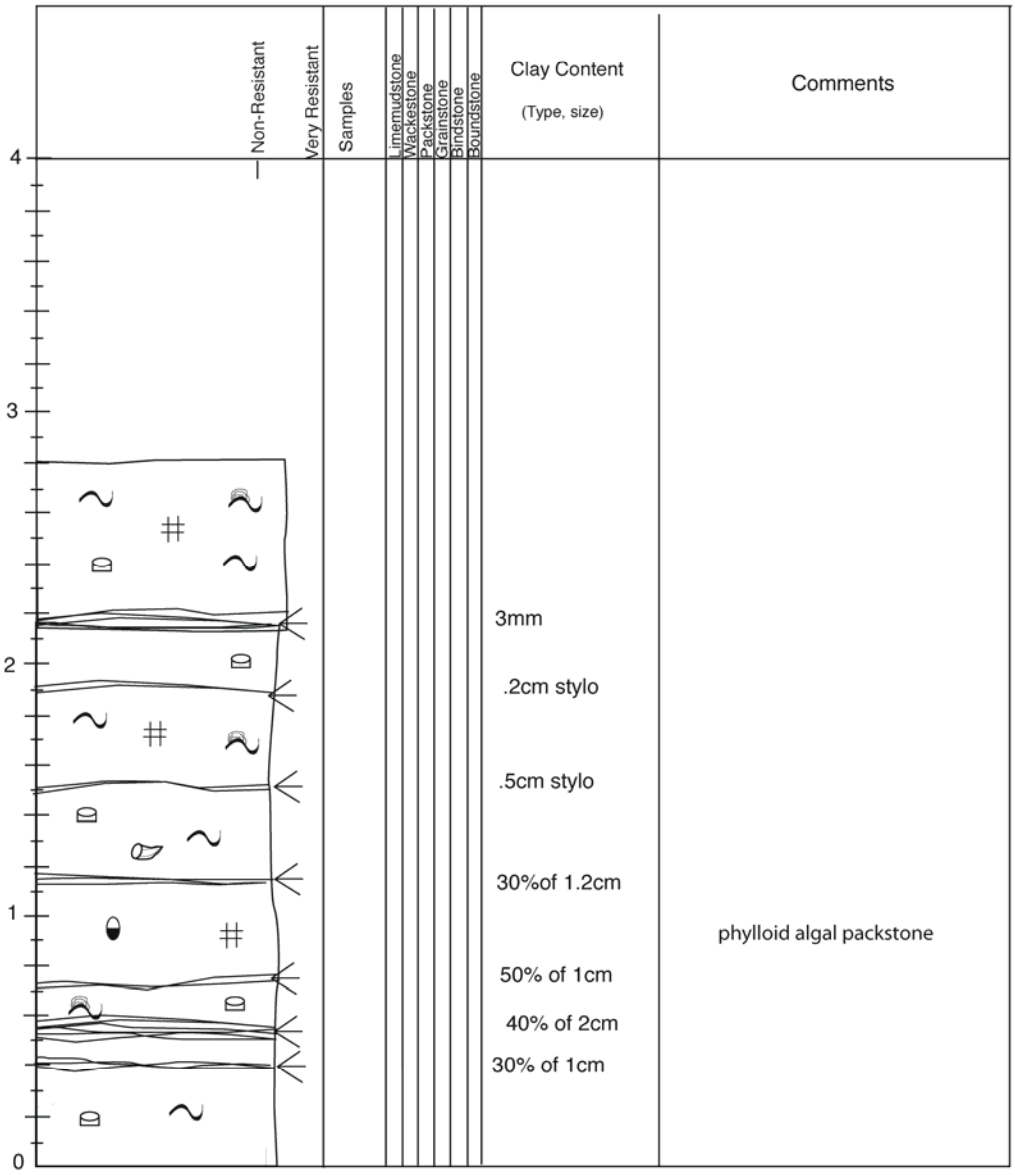

K - TRAN

KANSAS TRANSPORTATION RESEARCH
AND
NEW - DEVELOPMENTS PROGRAM

A COOPERATIVE TRANSPORTATION RESEARCH PROGRAM BETWEEN:

KANSAS DEPARTMENT OF TRANSPORTATION

THE UNIVERSITY OF KANSAS

KANSAS STATE UNIVERSITY